UNIVERSITI TEKNOLOGI MARA

DESIGN AND SYNTHESIS β-CARBOLINE INDOLE HYBRID: SYNTHETIC, BIOLOGICAL AND *IN SILICO* STUDIES

SITI ZAFIRAH BINTI ZULKIFLI

PhD

August 2026

UNIVERSITI TEKNOLOGI MARA

DESIGN AND SYNTHESIS β-CARBOLINE INDOLE HYBRID: SYNTHETIC, BIOLOGICAL AND *IN SILICO* STUDIES

SITI ZAFIRAH BINTI ZULKIFLI

Thesis submitted in fulfilment
of the requirements for the degree of
Doctor of Philosophy
(Science)

Faculty of Applied Sciences

August 2026

CONFIRMATION BY PANEL OF EXAMINERS

I certify that a Panel of Examiners has met on 21st May 2026 to conduct the final examination of Siti Zafirah binti Zulkifli on her Doctor of Philosophy thesis entitled "Design and Synthesis β-Carboline Indole Hybrid: Synthetic, Biological and *In Silico* Studies" in accordance with Universiti Teknologi MARA Act 1976 (Akta 173). The Panel of Examiners recommends that the student be awarded the relevant degree. The Panel of Examiners was as follows:

Nor Suhaila Mohamad Hanapi, PhD
Associate Professor
Faculty of Applied Sciences
Universiti Teknologi MARA
(Chairman)

Mohd Tajudin Mohd Ali, PhD
Associate Professor
Faculty of Applied Sciences
Universiti Teknologi MARA
(Internal Examiner)

Shafida Abd Hamid, PhD
Professor
Kulliyyah of Science
International Islamic University Malaysia
(External Examiner)

PROF DR HJH ZURAEDA BINTI IBRAHIM
Dean
Institute of Postgraduate Studies
Universiti Teknologi MARA
Date: 20 August 2026

AUTHOR'S DECLARATION

I declare that the work in this thesis was carried out in accordance with the regulations of Universiti Teknologi MARA. It is original and is the results of my own work, unless otherwise indicated or acknowledged as referenced work. This thesis has not been submitted to any other academic institution or non-academic institution for any degree or qualification.

I, hereby, acknowledge that I have been supplied with the Academic Rules and Regulations for Postgraduate, Universiti Teknologi MARA, regulating the conduct of my study and research.

Name of Student	:	Siti Zafirah binti Zulkifli
Student I.D. No	:	2023344455
Programme	:	Doctor of Philosophy (Science) -AS950
Faculty	:	Applied Sciences
Thesis Title	:	Design and Synthesis β-Carboline Indole Hybrid: Synthetic, Biological and *In Silico* Studies
Signature of Student	:	
Date	:	August 2026

ABSTRACT

Hyrtiosulawesine (**1**) is a marine alkaloid isolated from *Hyrtio erectus* and *H. reticulatus* and has been reported to possess various bioactivities. Due to its significant bioactivity and the limited supply from natural sources, synthetic approaches have been explored. While successful, the earlier synthetic routes were lengthy and afforded poor overall yields. Therefore, this study reports a streamlined three-step synthetic route comprising of Friedel-Crafts acylation mediated by tin (IV) chloride ($SnCl_4$) and acetyl chloride, a subsequent iodine-mediated multicoupled-domino reaction, and a final demethylation using boron tribromide (BBr_3) with an overall yield of 28%. Meanwhile, additional *O*-acylation using benzoyl chloride in the presence of potassium hydroxide (KOH), and *N*-alkylation using various alkyl halides under KOH-mediated basic conditions to yield the corresponding derivatives. The antimalarial activity of hyrtiosulawesine and its derivatives were evaluated using the *Plasmodium* lactate dehydrogenase (pLDH) assay, while their anticancer potential was assessed through cytotoxicity assays against breast (MDA-MB-231) and colon (HT-29) cancer cell lines. In addition, *in silico* molecular docking, molecular dynamics simulation, and ADMET analyses were conducted to virtually screen three active compounds against *Plasmodium falciparum* lactate dehydrogenase (*Pf*LDH). A total of 30 known compounds, 10 new compounds, and several new and known intermediates were successfully synthesized. Intermediate **53** showed the lowest IC_{50} value (5.44 ± 0.48 μM) in the *Pf*LDH, reflecting its moderate activity. Whilst the cytotoxicity results revealed compound **110** as the most active against MDA-MB-231 (IC_{50}=26 ± 4.00), while compound **106** showed the highest activity against HT-29 cells (IC_{50}=35 ± 4.00). Compounds **53**, **113,** and **114** show good binding affinity within the *Pf*LDH active site through molecular docking. Compound **53** remained highly stable with minimal conformational flexibility within the enzyme's active site during the first 60 ns of the trajectory, explaining its notable biological potency (5 μM). These findings highlight the pharmacological relevance of hyrtiosulawesine derivatives and provide a foundation for further optimization toward therapeutic development for antimalarial and anticancer.

ACKNOWLEDGEMENT

In the name of Allah, The Most Gracious, and The Most Merciful.

Alhamdulillah, all praise and thanks are due to Allah, the Most Gracious and Most Merciful, for giving me the strength, patience, and clarity to embark on and complete this PhD journey. It is truly by His mercy and guidance that this milestone has been reached.

First and foremost, I would like to express my deepest gratitude to my supervisor, Assoc. Prof. Dr. Noor Hidayah Pungot. Her invaluable guidance, unwavering support, and faith in my abilities have been a constant source of encouragement throughout this research. I am also sincerely grateful to my co-supervisors, Dr. Nor Akmalazura Jani and Dr. Nurasyikin Hamzah, whose thoughtful input and generous expertise greatly enriched this study. Their encouragement and understanding have been instrumental in keeping me on course. Special thanks go to Cik Nurhainis, Dr Syahrul Imran, and Dr. Hanis for their valuable help with the antimalarial, anticancer assays, molecular docking, and molecular dynamics studies. Their contributions were essential in bridging the experimental and computational aspects of this research.

My heartfelt appreciation goes to my mother, Her endless prayers, unconditional love, and steadfast belief in me have been my unwavering foundation. To my siblings Hilman, Hazim, Wana, Aisyah, and Hanif, thank you for your constant support and your sacrifices mean more than words can ever express. To my dear nephews and nieces, Eryna, Ammar, Idrees, Ameena, Abu, Maryam and Hadeef, your joyful laughter and innocence have been a bright light in my darkest moments.

I would also like to sincerely thank the staff and fellow researchers at the Institute of Science (IOS). To my lab mates, thank you for your camaraderie, your shared struggles, and the laughter that made the long lab hours more bearable.

Lastly, to my closest friends Nabilah, Fatin, Afiqah, and Kem, your friendship, presence, and encouragement through every high and low have been priceless. I will always cherish the memories we created and wish you nothing but success and happiness in your own journeys. This achievement does not belong to me alone. It belongs to every person who believed in me, lifted me up, and journeyed alongside me. May Allah bless you all abundantly.

Thank you.

TABLE OF CONTENT

		Page
AUTHOR'S DECLARATION		**ii**
CONFIRMATION BY PANEL OF EXAMINERS		**iii**
ABSTRACT		**iv**
ACKNOWLEDGEMENT		**v**
TABLE OF CONTENT		**vi**
LIST OF TABLES		**x**
LIST OF FIGURES		**xi**
LIST OF ABBREVIATIONS		**xiv**
CHAPTER 1: INTRODUCTION		**1**
1.1	Plant Secondary Metabolites in Future Drug Discovery	1
1.2	Classification of Alkaloids	3
1.3	Indole Substituted β-Carboline	4
1.4	Discovery of Hyrtiosulawesine	6
1.5	Synthetic Approach to Synthesize Hyrtiosulawesine and Its Derivatives	7
1.6	Research Problem	8
1.7	Significance of Study	9
1.8	Objective of Study	9
1.9	Scope and Limitation	10
CHAPTER 2: LITERATURE REVIEW		**12**
2.1	Synthesis of β-Carboline Bearing Indole	12
2.1.1	Classical Pictet-Spengler Condensation Approaches to Indole-Substituted-β-Carbolines	13
2.1.2	Friedel-Crafts Hydroxyalkylation Approaches to Indole-Substituted-β-Carbolines	19

2.1.3 Hybridization of β-Carboline and Indole Cores via Amide Coupling 20
2.2 Discovery and Previous Synthesis of Hyrtiosulawesine 25
2.3 Biological Activities of Hyrtiosulawesine 28
2.3.1 Antimalarial Activity 29
2.3.2 Anticancer Activity 30
2.4 Other Biological Activities of Hyrtiosulawesine and its Derivatives 31
2.4.1 Antioxidant 32
2.4.2 Cytotoxicity 33
2.4.3 Antimicrobial 35
2.4.4 Antiplasmodial 36
2.4.5 Antiproliferative 36
2.4.6 Antiphospholipase A_2 37
2.4.7 Antiacetylcholinesterase 38
2.4.8 Antidiabetic 38
2.4.9 Anti-inflammatory 36
2.5 *In silico* Analysis of Hyrtiosulawesine Derivatives
2.5.1 Molecular Docking 39
2.5.2 Molecular Dynamics (MD) Simulation 42

CHAPTER 3: METHODOLOGY 44
3.1 Research Framework 44
3.2 General Experimental Procedure 45
3.2.1 Melting Points 45
3.2.2 Infrared Spectra (IR) 45
3.2.3 Chromatography Mass Spectroscopy (GC-MS) 45
3.2.4 Liquid Chromatography Mass Spectroscopy (LC-MS) 45
3.2.5 Nuclear Magnetic resonance (NMR) 46
3.3 General Procedure for the Synthesis and Characterization of Compounds 46
3.3.1 O-Acylation of 5-Hydroyxindole 46
3.3.2 *N*-Alkylation of Indole 51
3.3.3 Synthesis of 5-Substituted-3-acetylindole 55

3.3.4 Multicoupled Domino Reaction 70
3.3.5 Demethylation of (5-methoxy-1H-indol-3-yl)(6-methoxy-9H-pyrido[3,4-b]indol-1-yl)methanone, **53**, to Produce Hyrtiosulawesine, **1** 94
3.4 *In vitro* Antimalarial Assay 95
3.4.1 Reagents and Biological Materials 95
3.4.2 Inhibition of *Pf*LDH Activity by The Selected Compounds 96
3.5 Cytotoxicity Assay 96
3.5.1 Cell Culture 96
3.5.2 Determination of cell growth inhibition 96
3.6 *In silico* Study
3.6.1 Molecular Docking 97
3.6.1.1 Structural Protein Preparation 97
3.6.1.2 Ligand Preparation 98
3.6.1.3 Defining Grid Box for Docking 98
3.6.1.4 Molecular Docking Using Auto Dock Vina 98
3.6.2 Molecular Dynamic Simulation 99
3.6.3 ADMET Analysis 100

CHAPTER 4: RESULTS AND DISCUSSIONS 101
4.1 General Overview 101
4.2 Total Synthesis of Hyrtiosulawesine
4.2.1 Formation of 5-Hydroxy-3-acetylindole via Friedel-Crafts Acylation 101
4.2.2 Formation of 5-Methoxy-3-acetylindole *via* Friedel-Crafts Acylation 103
4.2.3 Formation of (5-methoxy-1H-indol-3-yl)(6-methoxy-9H-pyrido[3,4b]indol-1-yl)methanone, 53 via Multicouple Domino Reaction 107
4.2.4 Formation of Hyrtiosulawesine via Demethylation 110
4.3 Synthesis of Hyrtiosulawesine's Derivatives 114
4.3.1 *O*-Acylation of Indole at C-5 Position 114
4.3.2 *N*-Alkylation of Indole 117

4.3.3 Friedel-Crafts Acylation of *N*- and 5-Substituted Indole 119
4.3.4 Formation of Hyrtiosulawesine Derivatives via Multicouple Domi Reaction 122
4.4 Biological Activity of Hyrtiosulawesine and its Derivatives 124
4.4.1 Antimalarial Activity 124
4.4.2 Cytotoxicity Activity 133
4.5 *In silico* Analysis 137
4.5.1 Molecular Docking 137
4.5.2 Molecular Dynamic Simulation 141
4.5.3 ADMET Analysis 148

CHAPTER 5: CONCLUSION AND RECOMMENDATION 152
5.1 Synthesis, Bioactivity and Computational Studies of Hyrtiosulawesine and its Derivatives 152
5.1.1 Total Synthesis of Hyrtiosulawesine and Its Derivatives 152
5.1.2 Biological Activities and *in silico* Studies 154
5.2 Recommendation for Future Study 155

REFERENCES 156
APPENDICES 168
AUTHOR'S PROFILE 178

LIST OF TABLES

Tables	Title	Page
Table 4.1	Optimization of the Friedel-Crafts Acylation Reaction of 5-Methoxyindole (**36d**)	104
Table 4.2	Optimization of the Domino Reaction of 5-methoxy-3-acetylindole (**89**)	109
Table 4.3	Optimization of Demethylation Reaction to Afford **1**	111
Table 4.4	Comparison of ^{1}H and ^{13}C NMR Data of Hyrtiosulawesine with Reported Study	111
Table 4.5	*O*-Acylation of 5-Hydroxyindole (**2**)	116
Table 4.6	*N*-alkylation of Indole (**36a**)	118
Table 4.7	Friedel-Crafts Acylation of substituted Indole	121
Table 4.8	Domino Reactions of Hydrosulawesine Derivatives	123
Table 4.9	Percentage Inhibition (%) of *Pf*LDH by Hyrtiosulawesine Derivatives Screened at 1 μM Concentration.	126
Table 4.10	Antimalarial Activity against *Pf*LDH of Selected Hyrtiosulawesine's Derivatives	132
Table 4.11	Summary of Structure-Activity Relationships (SAR) For Hyrtiosulawesine Derivatives Against *Pf*LDH	133
Table 4.12	Cytotoxic IC_{50} (μM) of Tested Compounds in Breast and Colon Cancer Cells	134
Table 4.13	Molecular Docking Results of Hyrtiosulawesine and Its Derivatives	137
Table 4.14	Assessment of Drug-Likeness Based on Lipinski's Rules of Compounds **53, 113** and **114**	149
Table 4.15	ADMET Profiling Enlisting Absorption, Distribution, Metabolism and Toxicity Related Drug-likeness Parameters of Selected Compound **53**, **113** And **114**	150

LIST OF FIGURES

Figures	Title	Page
Figure 1.1	Chemical Structures of Selected Plant-derived Drugs	2
Figure 1.2	Classification of Alkaloids Based on Their Biosynthetic Precursors	4
Figure 1.3	Structure of β-Carboline	5
Figure 1.4	Structure of Hyrtiosulawesine, **1**	6
Figure 2.1	Derivative Indole and Benzaldehyde	21
Figure 2.2	Modified Structure of β-Carboline	25
Figure 2.3	Global Status of Indigenous Malaria Transmission (World Health Organization, 2023)	29
Figure 2.4	Dynamic Schematic of The Recreation of Oxygen Species (ROS) Formation and Their Overall Breakage Human Physiology (Hong *et al.,* 2024)	32
Figure 2.5	Chemical Structure of Compound **1** and **15b**	32
Figure 2.6	Chemical Structure of Compound **40f, 40m, 40n** and **47c**	32
Figure 2.7	Chemical Structure of Compound **9**	35
Figure 2.8	Chemical Structure of Compound **15a**	36
Figure 2.9	Chemical Structure of Compound **20c**, **20d**, **21b** and **25b**	37
Figure 2.10	Schematic Diagram of Protein-Ligand Interactions (Dnyandev *et al.,* 2021)	40
Figure 2.11	Binding Interactions between 1-Substituted Tetrahydro-β-Carbolines Compound within Their Active Site of (A) Phosphoethanolamine Methyltransferase (PMT); (B) Falcipain-2 (FP2); (C) Falcipain-3 (FP3); (D) Lactate Dehydrogenase (LDH); and (E) Malate Dehydrogenase (MDH) within 4 Å (Jaromin e*t al.,* 2021)	41
Figure 2.12	Ligand RMSD of 10 Hits Preselected Against *Pf*Hsp90 (Wang *et al.,* 2016)	43

Figure 3.1	Research Framework for the Synthesis, Biological Evaluation, and Computational Analysis of Hyrtiosulawesine and Its Derivatives	44
Figure 3.2	Crystal Structure of *Plasmodium falciparum* Lactate Dehydrogenase (PDB 1U4S)	99
Figure 4.1	^{1}H NMR Spectrum of Hyrtiosulawesine	112
Figure 4.2	APT-NMR Spectrum of Hyrtiosulawesine	113
Figure 4.3	Comparison of ^{1}H NMR Spectrum between (a) *N*-Alkylation Using Potassium Hydroxide Base and (B) *N*-Alkylation Using Nah Base	119
Figure 4.4	Schematic Illustration of Competitive Inhibition of *Pf*ldh. An Inhibitor (e.g., Chloroquine) Competes with NADH at the Active Site of *Pf*ldh, Impairing NADH-Dependent Conversion of Lactate to Pyruvate. This Inhibition Interrupts ATP Production, Leading to the Accumulation of Toxic Haematin. Inhibited Polymerization into Haemozoin Ultimately Causes Parasite Death. (Dey *et al.,* 2022)	125
Figure 4.5	Percentage of *Pf*LDH Inhibition of Different Compounds. Compound **114** Shows the Highest Inhibition at 39.1% of *Pf*LDH	131
Figure 4.6	Superposition of Naphthalene-2,6-Disulfonic Acid (Pink) as Bound and Redocked Native Ligand (Yellow) with RMSD Value of 0.069	137
Figure 4.7	3D Representation Showing the Docking Poses of Ligands **53** (magenta), **113** (red) and **114** (green) Docked at Protein Active Site and 2D Interactions of (b) Compound **53**, (c) Compound **113** and (d) Compound **114**	140
Figure 4.8	Protein (blue)-Ligand (red) RMSD of Derivative **53**	141
Figure 4.9	(a) Protein-Ligand Contacts Illustrating Ligand Movement and (b) Detailed Protein Interactions with the Ligand of Compound **53**	142
Figure 4.10	(a) Ligand Interaction with RMSD, Rg, MoISA, SASA and PSA, (b) Ligand Torsion Profile of Compound **53**	144

Figure 4.11	Snapshots of Compound **53** Ligand Movement and Protein-Ligand Interactions: (a) Ligand Position within the Active Site During the First 60 ns and (b) Ligand Position After 60 ns	144
Figure 4.12	Protein (blue)-Ligand (red) RMSD of (a) Compound **113** and (b) Compound **114**	145
Figure 4.13	(a) Ligand Interaction with RMSD, Rg, Moisa, SASA and PSA, (b) Ligand Torsion Profile and (c) Protein-Ligand Contacts of Compound **113**	146
Figure 4.14	(a) Ligand Interaction with RMSD, Rg, MoISA, SASA and PSA, (b) Ligand Torsion Profile of Compound **114**	147

LIST OF ABBREVIATIONS

Abbreviations

%	Percentage
ºC	Degree Celcius
IC_{50}	Inhibition Concentration at 50%
µM	Micromolar
^1H	Proton
APT	Attached Proton Test
$CDCl_3$	Deuterated Chloroform
CD_3OD	Deuterated Methanol
CH_2Cl_2	Chloroform
DMSO	Dimethyl Sulfoxide
DDQ	2,3-Dichloro-5,6-Dicyano-1,4-Benzoquinone
h	Hour
Hz	Hertz
mg	Milligram
mmol	Millimole
min	Minute (S)
mL	Millilitre (S)
ppm	Parts Per Million
p-TsOH	*Para*-Toluenesulfonic Acid
rt	Room Temperature
TFA	Trifluoroacetic Acid
THF	Tetrahydrofuran
UV	Ultra-Violet

CHAPTER 1
INTRODUCTION

1.1 Plant Secondary Metabolites in Future Drug Discovery

Natural products are chemical compounds or substances isolated from living organism such as plants, animals, and microorganisms. They are manufactured as primary metabolites involved in the production of their food or biosynthesized as secondary metabolites for protection, competition, and species interactions (David & Gordon, 2012). Secondary metabolites have made significant contributions to being used as a remedy in treating a variety of diseases and ailments. In addition, secondary metabolites are also important in some ecological processes. This includes pollinator attraction, seed dispersal, defense against pathogens, herbivores, and environmental stressors (Clemensen *et al.,*2020; Takshak & Agrawal, 2018).

Nowadays, much attention has been directed towards the secondary metabolites of plant extract due to its major role as primary health care in developing countries. Over 80% of the global population currently relies on traditional medicines, including herbal remedies, as an alternative medicine (WHO, 2025). This is because this traditional medicine has been identified as the most affordable, safe, and accessible treatment, particularly in impoverished communities. As a result, multiple herbs have been exploited to treat a wide range of illnesses. For instance, *Centella asiatica* known as 'pegaga' in Malaysia, is one of the popular medicinal plants that can help to cure people having epilepsy, hyperglycemic, tumor, ulcer, and lepra (Gohil *et al.,*2010). Hence, plants remained seen as the basis of modern medicine thus necessitate the researcher to explore more novel lead compounds.

Many natural resources plants were successfully marketed as medications in pharmaceutical applications today. Morphine (Figure 1.1), is the first marketed drugs by Merck in 1826, help to reduce pain by interrupting the way nerves signal pain between the brain and the body (Murphy, 2023). Aspirin, the first semi synthetic drugs derived from salicin which was isolated from *Salix alba* to reduce inflammation, swelling, pain, and fever (Veeresham, 2012). This led to the isolation of the commercial drugs such as cocaine, codeine, digitoxin, quinine and pilocarpine. More modern

examples are paclitaxel from *Taxus brevifolia* for lung, ovarian, and breast cancer, artemisinin from *Artemisia annua* used against multidrug-resistant malaria, and silymarin from *Silybum marianum*, for liver disease (Veeresham, 2012). Epidiolex, containing cannabidiol (CBD) isolated from *Cannabis sativa*, which received FDA approval in 2018 for the treatment of seizures associated with two rare forms of epilepsy, Lennox-Gastaut syndrome and Dravet syndrome (FDA, 2018).

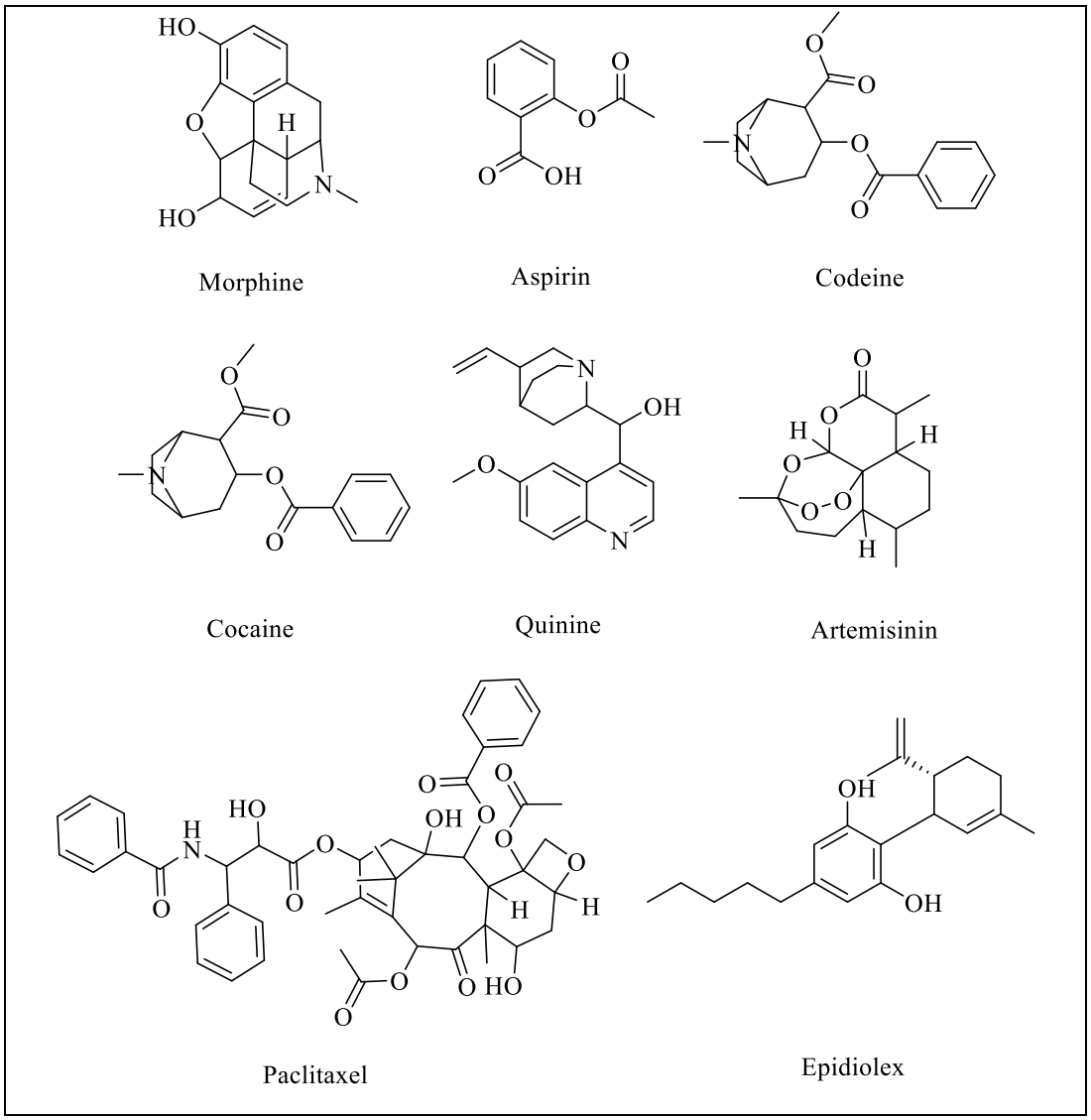

Figure 1.1 Chemical Structures of Selected Plant-derived Drugs

Although natural products play a vital role in drug discovery, they have limitations such as low drug activity, high structural complexity, unfavorable physicochemical and pharmacokinetic properties, and significant toxicity (Sun *et al.,*2022). Despite these challenges, ongoing research continues to fully realize the therapeutic potential of these substances while addressing their drawbacks. Therefore,

synthetic approaches allow researchers to design compounds focusing on the structural modification and optimization of compounds, so that it can lead to the development of molecules with improved efficacy and selectivity. To better understand these developments, it is essential to explore the different classes of plant secondary metabolites, particularly alkaloid since it has long served as a rich source of biologically active compounds.

1.2 Classification of Alkaloids

Natural products are made up of various groups of compounds particularly alkaloids, tannins, flavonoids, and phenolic compounds (Chioccio *et al.,*2021). In ancient times, alkaloids were known as a major source of drugs for therapeutic purposes. Galanthamine, the first alkaloid isolated in 1951 from *Galanthus woronoii* (Amaryllidaceae), provides an effective indicative treatment for Alzheimer's patients and slows the progression of the diseases (Lim *et al*, 2024). In addition, morphine and codeine (opioid) which isolated from *Papaver somniferum* are widely used in pharmaceutical today as analgesic, anti-pain, cough suppressants, and diarrhea relievers (Singu & Verbeeck, 2021).

Alkaloids are large and structurally diverse groups of nitrogen-containing natural products. They are commonly classified according to the amino acid that contributes both the nitrogen atom and the core scaffold of the alkaloid skeleton (Chioccio *et al.,*2021). As depicted in Figure 1.2, the subdivision of alkaloids can be made into groups based on amino acid precursors of ornithine, lysine, nicotinic acid, tyrosine, tryptophan, anthranilic acid, histidine, and purine. For instance, tryptamine and indole are derived from the amino acid tryptophan, tropane from ornithine, while benzylisoquinoline alkaloids derive from tyrosine, and purine alkaloids from purine (Bhambhani *et al.,*2021).

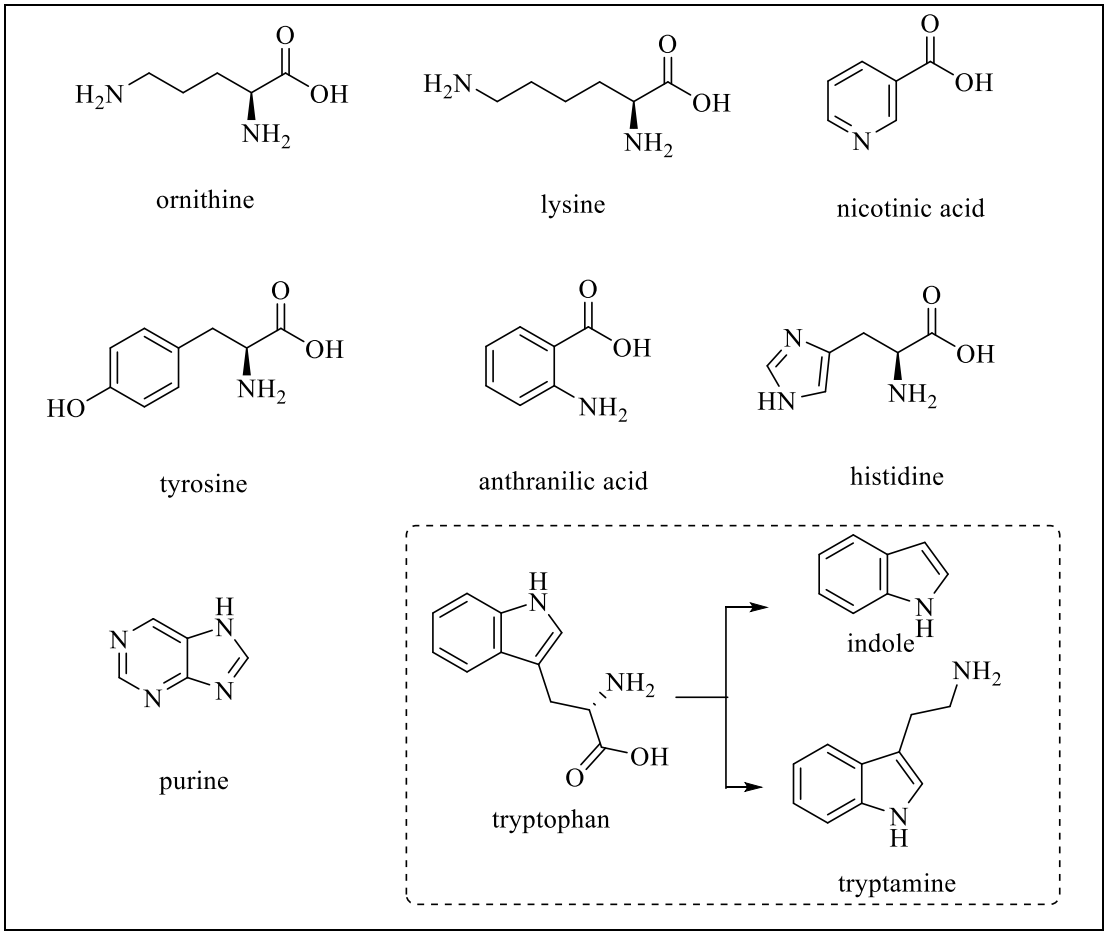

Figure 1.2 Classification of Alkaloids Based on Their Biosynthetic Precursors

However, not all alkaloids are derived from an amino acid core but sometimes can arise by amination of another type of substrate such as acetate derived, phenylalanine derived, a terpene or a steroid. Examples are pyridine and terpenoid types which do not originally rise from amino acid, but through alternative polyketide pathway, terpenoid (isoprenoid) pathway and mixed or modified pathways (Bhambhani *et al.,*2021; Lin *et al.,*2022).

1.3 Indole Substituted β-Carboline

Indole is an alkaloid derived from tryptophan, a bicyclic structure consisting of a benzene ring fused to a pyrrole ring. The presence of a pyrrole ring confers pharmacological activity on indole (Saruengkhanphasit *et al.,*2025). The β-carboline ring system, on the other hand, is a subgroup of indole alkaloids which includes a benzene ring fused to a pyridine ring, forming a tricyclic structure. It is a naturally heterocyclic compounds with a diverse range of biological activities (Rajput *et*

*al.,*2022). In β-carboline system, unsaturated members are known as fully aromatic β-carbolines (βCs), whereas the partially or completely saturated ones are known as dihydro-β-carbolines (DHβCs) and tetrahydro-β-carbolines (THβCs), respectively (Cao *et al.,*2007). As illustrated in Figure 1.3, the rings are identified as A, B and C, and classified according to the degree of saturation (fully saturated: 1,2,3,4-tetrahydro; partially saturated: 3,4-dihydro; and unsaturated β-carbolines) and the position of the N-atom in the C-ring as α-, β-, γ or δ-carbolines.

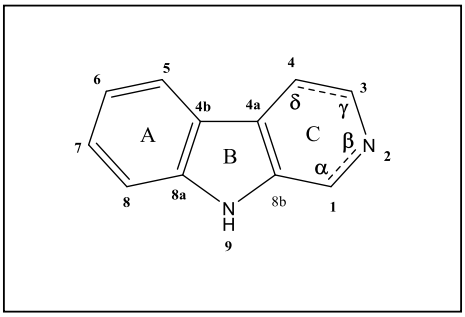

Figure 1.3 Structure of β-Carboline

Pictet-Spengler condensation reactions were commonly used to synthesize β-carboline scaffolds. The reaction fuses β-arylethylamine with aldehyde and α-keto acid, to yield a ring closure of tetrahydro-β-carbolines (THβCs) (Stoeckigt *et al.,*2011). The desired β-carboline framework is further promoted by an oxidative dehydrogenation reaction. Advanced research on these compounds has resulted in the identification of various analogues containing different substituents on the indole ring in the tricyclic compounds, especially C-1, C-6, and C-7 positions (Kushwaha *et al.,*2023). Substitution at the C-1 position of β-carboline structure is the most common since it is the only atom in the ring system that does not belong to arylethylamine, the amino acid precursor for the biosynthesis of these class compounds (Liew *et al.,*2014).

Alkaloids of indole substituted β-carboline are commonly reported to exhibit a wide range of biological activities including effects on the central nervous system, cytotoxicity towards cancer cell lines, and antimalarial properties (Liew *et al.,*2014). As the antimalarial and antitumor effects of these alkaloids are well documented, all analogues were also evaluated against *Plasmodium falciparum* and human tumor cell lines. Furthermore, various derivatives of indole β-carboline with important biological activities which include anticancer, antituberculosis, antileishmanial, antifungal, antiproliferative, antimalarial, antimetastatic and anti-chollinergic activity are clearly

established (Kovvuri *et al.,*2018). Intrigued by its biological properties, we set out to create a concise and applicable synthetic approach towards new derivatives of indole-β-carboline of hyrtiosulawesine.

1.4 Discovery of Hyrtiosulawesine

Hyrtiosulawesine (Figure 1.4) is a bioactive compound, primarily isolated from Indonesia marine sponges of *Hyrtios erectus* and *Hyrtios reticulatus* in 2002 (Salmoun *et al.,*2002). Following that, in 2012, this compound was extracted from *Alocasia macrorrhiza* and demonstrated antiproliferative activity against human nasopharyngeal carcinoma epithelial cells (Zhu *et al.,*2012). Hyrtiosulawesine was then found from other natural resources including a marine sponge of *Ircinia sp*. and from the roots of *Aristolochia cordigera,* which is a member of the birthwort family (Abdjul *et al.,*2015; Periera *et al.,*2017).

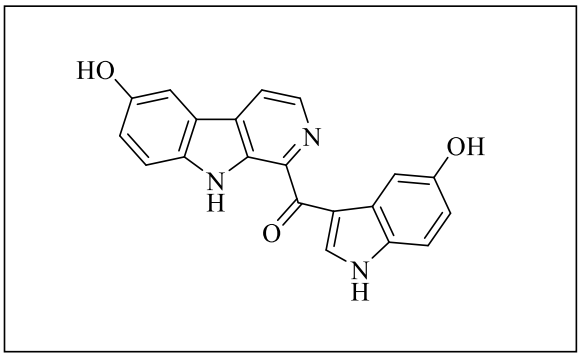

Figure 1.4 Structure of Hyrtiosulawesine, **1**

This alkaloid was further evaluated and showed various pharmacological effects such as antidiabetic, anti-inflammatory, antioxidant, antiphospholipase, antiplasmodial, and cytotoxicity (Liew *et al.,*2014; Sauleau *et al.,*2006; Ha *et al.,*2002). Due to their remarkable biological activities, Zhang *et al.* (2010) first attempted to investigate how to synthesize this valuable molecule for future purposes. With skeleton of β-carboline connecting to indole, its synthetic route with the modified eight steps oxidation reaction were established *via* Pictet-Spengler condensation reaction. After four years of research, Liew and the team developed a new four step synthetic strategy for the preparation of hyrtiosulawesine (Liew *et al*., 2014).

1.5 Synthetic Approach to Synthesize Hyrtiosulawesine and Its Derivatives

The total synthesis or semi-synthesis of secondary metabolites were often done by the researchers due to low abundance of its natural form. This is because it is difficult to isolate the active compound directly from plants or marine organisms as it can be time-consuming, expensive, and environmentally unsustainable. Besides, synthetic chemistry will allow scalable production, structural modification, and structure-activity relationship (SAR) studies to optimize drug properties such as solubility, potency, and selectivity.

Pictet-Spengler reactions, formyl-β-carboline routes, and biocatalytic oxidations are commonly used to synthesize β-carboline frameworks like hyrtiosulawesine. The introduction of flow chemistry, biocatalysis, and late-stage functionalization allows for efficient and environmentally friendly synthesis of diverse analogues. This modern synthesis not only reproduces natural scaffolds but also tailors their structure to enhance pharmacological properties. Through total synthesis, researchers can now generate hyrtiosulawesine derivatives with improved antimalarial potency and lower toxicity, bridging chemistry with computational and biological evaluation. The total synthesis of hyrtiosulawesine and its derivatives were attempted with synthetic analysis which outline in Scheme 1.1.

The synthetic strategy commenced with the Friedel–Crafts acylation of 5-hydroxyindole (**2**) using various Lewis acids to afford 5-hydroxy-3-acetylindole (**3**). Subsequent Kornblum oxidation of **3** with iodine and dimethyl sulfoxide (DMSO) yielded the key intermediate, indole-3-glyoxal (**4**). A Pictet–Spengler condensation between **4** and serotonin (**5**) in the presence of *p*-toluenesulfonic acid (*p*-TsOH) then furnished the target natural product, hyrtiosulawesine (**1**). Reaction conditions, including temperature, reaction time, and reagent choice, were systematically varied to optimize the yields of intermediates and the final product.

To expand the chemical diversity, a library of hyrtiosulawesine derivatives was synthesized by employing indole precursors bearing different substituents at the C-5 position of the aromatic ring were selected. The modifications on the scaffolds were attempted to investigate how different substituents affect biological activity through selective *O*-acylation and *N*-alkylation reactions. Subsequent multicoupled domino reactions enabled the efficient construction of β-carboline frameworks with varied R_1, R_2, and R_3 substituents.

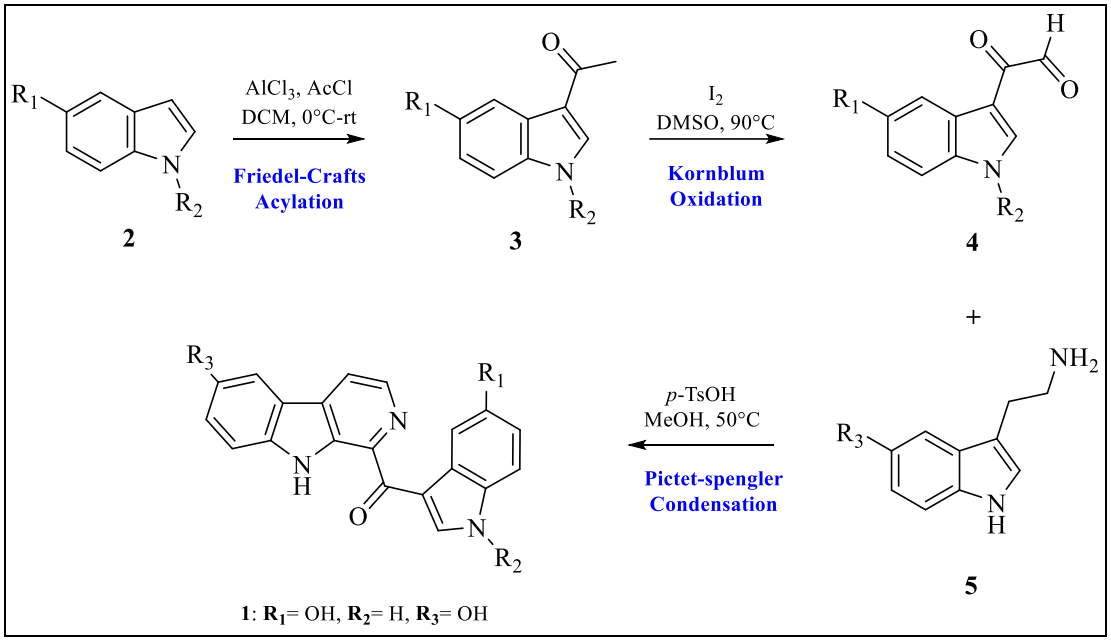

Scheme 1.1 Proposed Synthetic Route of Hyrtiosulawesine and Its Derivatives

1.6 Research Problem

Marine alkaloid such as hyrtiosulawesine have been recognized to exhibit diverse pharmacological properties, including antimalarial and anticancer activity (Liew *et al.,* 2014). Despite having interesting biological activities, its eight steps synthesis is lengthy and gives a very low yield. Besides, the urgency of this research is underscored by current global health challenges due to malaria continuing to develop a resistance towards the current antimalarial drugs. Nevertheless, effective *Pf*LDH inhibitors with clear therapeutic potential remain underexplored, and many reported inhibitors are still at the early discovery or preclinical evaluation stage rather than being established as clinically used antimalarial drugs. This crisis demands the discovery of novel compound with distinct mechanisms of action to overcome treatment failures.

In addition, cancer remains one of the leading causes of mortality globally, emphasizing the need to identify novel cytotoxic agents that can serve as potential leads for future chemotherapeutic development. The anticancer potential of hyrtiosulawesine derivatives has not been extensively explored. Moreover, systematic investigations into its structure-activity relationships (SARs), mechanistic insights, and computational studies are scarce, leaving significant gaps in understanding its therapeutic potential. Addressing these challenges requires not only the development of shorter and more efficient synthetic strategies to access hyrtiosulawesine and its derivatives, but also

comprehensive *in vitro* and *in silico* evaluations to clarify their biological activities, binding interactions, and drug-likeness properties.

1.7 Significance of Study

The significance of this study is to synthesize the natural alkaloid hyrtiosulawesine and its derivatives, using a short synthetic route for both antimalarial and cytotoxicity screening. By introducing new chemical compounds, this helps to address the challenge of *Plasmodium* drug resistance by offering structurally unique molecules with alternative mechanisms of action. Additionally, through structural modification and optimization, biological efficacy was enhanced by increasing potency and selectivity. Furthermore, computational analysis of molecular docking and dynamics provide key structural insights that allow for the rational, evidence-based design of potent antimalarial medicines. Besides, by shortening the synthetic pathway with better percent yield will facilitate and accelerate bioactivity screening, so that the real potential of the compounds can be discovered.

Importantly, this research highlights the β-carboline-indole hybrid as a privileged scaffold in medicinal chemistry. By creating unique structural modifications, this study introduces novel molecules to combat *Plasmodium* drug resistance via alternative mechanisms of action. Furthermore, this scaffold holds significant relevance in oncology. The β-carboline-indole core is a promising chemotype for new chemotherapeutic development, driven by its potential to induce apoptosis and modulate key cancer-related signalling pathways. Finally, integrating computational molecular docking provides critical structural insights, offering an evidence-based foundation for the rational design of both next-generation antimalarial and anticancer agents.

1.8 Objective of Study

This study embarks on the following specific objectives:

(a) To synthesize and characterize hyrtiosulawesine and 40 derivatives using Friedel-crafts acylation, multicoupled domino, demethylation, *O*-acylation and *N*-alkylation reactions.

(b) To screen the synthesized compounds against *Plasmodium falciparum* lactate dehydrogenase (*Pf*LDH) and cancer cell lines to identify promising lead scaffolds for further therapeutic optimization.

(c) To perform virtual screening for antimalarial activity on hyrtiosulawesine and its derivatives using *in silico* molecular docking analysis, molecular dynamic simulation and *in silico* ADMET analysis against *Plasmodium falciparum* lactate dehydrogenase (*Pf*LDH).

1.9 Scope and Limitation

The scope of the study is to synthesize and characterize the hyrtiosulawesine using a three-step synthetic route including Friedel-crafts acylation, multicoupled domino and demethylation reactions with 5-methoxindole as starting materials, along with the preparation of forty derivatives. In parallel, all compounds were evaluated for their biological potential through *in vitro* enzymatic antimalarial assays targeting *Plasmodium falciparum* lactate dehydrogenase (*Pf*LDH). Hyrtiosulawesine and derivatives were also evaluated for potential anticancer activity against breast cancer cells (MDA-MB-231), and colon cancer cells (HT-29) through MTT cytotoxicity assay. To complement the experimental studies, *in silico*, including molecular docking, molecular dynamics simulations, and ADME predictions were employed to analyze binding interactions, stability within the *Pf*LDH active site, and drug-likeness properties. This integrative approach enables the identification of key structural features responsible for enhanced pharmacological activity and provides valuable insights into the mechanistic basis of action for hyrtiosulawesine derivatives.

The limitation of this project is that the derivatives encounter challenges such as yield limitations, complex reaction conditions, and instability of intermediates, which limited the number of analogues successfully obtained. Due to yield constraints, only a few derivatives were screened for cytotoxicity activity. Comprehensive synthesis, analysis, and biological evaluations demand time, resources, and expertise, potentially limiting the number of derivatives synthesized or tested against *Pf*LDH protein. Finally, although molecular docking and molecular dynamics simulations offered valuable mechanistic insights, these computational predictions require experimental validation and may not fully capture the complexity of in vivo biological systems. The molecular dynamics simulations were constrained by a simulation

timescale of 100 ns, which is sufficient for observing local structural fluctuations but may not capture larger-scale, slower conformational transitions or unbinding kinetics that occur over microsecond to millisecond intervals.

CHAPTER 2
LITERATURE REVIEW

2.1 Synthesis of β-Carboline Bearing Indole

β-Carboline is a heterocyclic molecule made up of pyridine and indole rings and is reported to exhibit various biological activities and pharmacological effects. Researchers are exploring a synthetic pathway based on β-carbolines to generate novel medications and advance organic chemistry due to their potential medicinal benefits.

β-Carboline can be synthesized *via* several processes. One of the most commonly technique is Pictet-Spengler reaction which converts tryptamine derivatives and aldehydes into tetrahydro-β-carboline and is the most often used technique for preparing β-carboline (Szabó *et al.,* 2021). The desired β-carboline framework is further promoted by an oxidative dehydrogenation reaction. Another commonly employed method for preparing β-carbolines is the Bischler-Napieralski reaction (Love, 1996). Like the Pictet-Spengler reaction, tryptophan or tryptamine derivatives are the usual starting materials for this reaction. Acylation of the exocyclic amine followed by treatment with any of several dehydrating agents (phosphorus pentoxide and phosphorus oxychloride) results in cyclization to give dihydro-β-carbolines. These compounds are then treated with an oxidant to provide β-carbolines. However, the reaction of Bischler-Napieralski often necessitates harsher reaction conditions involving high temperatures and potentially toxic reagents compared to Pictet-Spengler (Li, 2009).

Advanced research on β-carbolines based compounds has resulted in the identification of various analogues containing different substituents on the indole ring in the tricyclic compounds, especially C-1, C-6, and C-7 positions (Kushwaha *et al.,* 2023). Substitution at the C-1 position of β-carboline structure is the most common since it is the only atom in the ring system that does not belong to arylethylamine, the amino acid precursor for the biosynthesis of these class compounds (Liew *et al.,* 2014). Understanding these synthetic routes and substitution patterns is crucial for guiding the rational modification of the β-carboline core and enhanced pharmacological activities.

2.1.1 Classical Pictet-Spengler Condensation Approaches to Indole-Substituted-β-Carbolines

Eudistomin U is one of the indole-substituted β-carbolines which was primarily isolated from Caribbean *Lissoclinum fragile* and reported to have antibacterial, antimalarial, and anticancer properties (Serdyuk & Kolodina, 2018). Due to its interesting bioactivity, a synthetic route for synthesizing this compound has been discovered. Compound **9** was synthesized using Pictet-Spengler condensation and oxidation strategy. The reaction started with tryptamine **6** or tryptophan with indole-3-carboxaldehyde **7**. The imine formation was achieved by heating toluene or MeOH and subsequent solvent removal facilitated the intramolecular cyclization. Ring closure **8** was then attained by the addition of CH_2Cl_2/TFA (Liew *et al.,* 2014).

As a result, the intermediate, 1,2,3,4-tetrahydro-β-carboline **8** was formed and further oxidation using 2,3-dichloro-5,6-dicyano-1,4-benzoquinone (DDQ) in THF has facilitated dehydrogenation process, yielded eudistomin U as shown in Scheme 2.1. This sequence effectively illustrates the classical Pictet–Spengler cyclization followed by oxidative aromatization to yield the desired natural product.

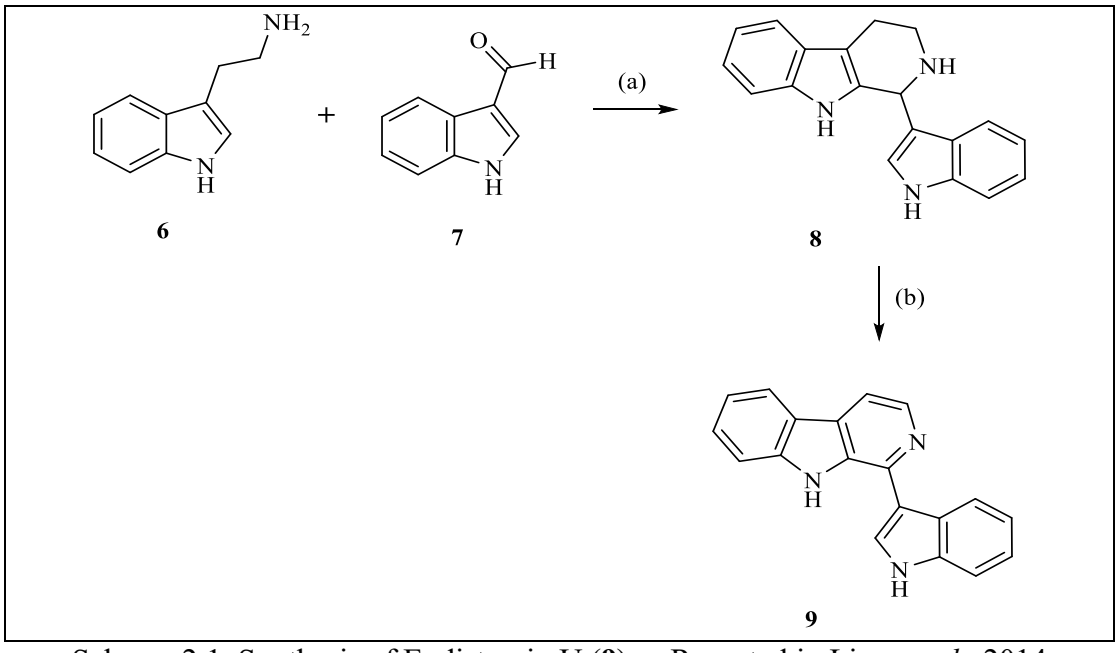

Scheme 2.1. Synthesis of Eudistomin U (**9**) as Reported in Liew *et al.,* 2014

Reagents and Condition: (a) toluene or MeOH, reflux, 1-72 h, CH_2Cl_2, TFA, rt, 16-24 h, 76%, (b) DDQ, THF, CH_2Cl_2, rt, 50 min-24 h, 40%.

Having successfully developed the method, the same condition was used to produce analogues of **9** using different starting material of *L*-tryptophan methyl ester **10**. This led to an intermediate 1,2,3,4-tetrahydro-β-carboline **11**, and subsequent oxidation with LiOH in THF and water (3:1) gave an ester **12a**. A deprotection step of compound **12a** finally resulted in the formation of an acid **12b** (Scheme 2.2). The choice of dehydrogenation reagent is the fundamental difference with compound **9**. LiOH is a moderate base, whereas DDQ's higher oxidizing capabilities generate side reactions such as oxidative demethylation or decarboxylation of the methyl ester group.

Since the conditions are mildly basic, it will promote hydrolysis of the methyl ester and facilitate the dehydrogenation of tetrahydro-β-carboline intermediate to form the fully aromatic β-carboline core. The hydroxide ions of the basic will extract protons from the nitrogen and benzylic positions. This enables the formation of fully aromatized β-carboline, especially in the presence of dissolved oxygen. This base-induced dehydrogenation is favored because LiOH provides sufficient basicity without over-oxidizing the sensitive indole moiety.

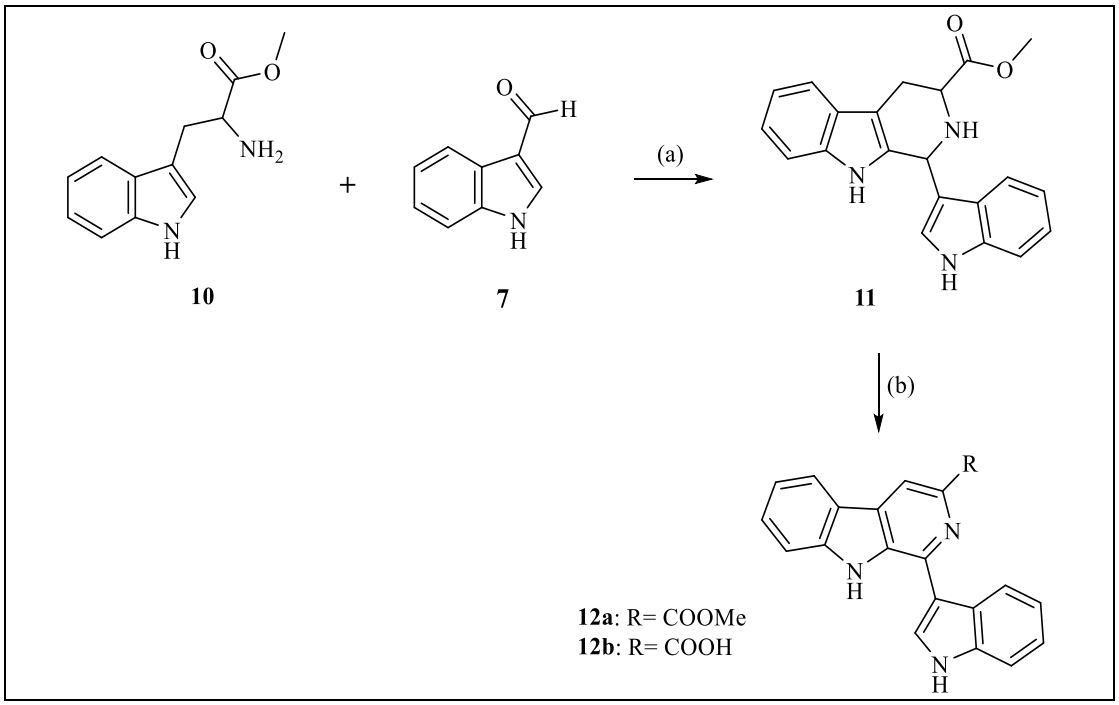

Scheme 2.2. Synthesis of Eudistomin U Derivative (**12a** and **12b**) as Reported in Liew *et al.,* 2014.

Reagents and Condition: (a) toluene or MeOH, reflux, 1-72 h, CH_2Cl_2, TFA, rt, 16-24 h, 36-76%, (b) LiOH, THF/H_2O (3:1), reflux, 13 h, 96%.

The formation of methyl ether analogue **15a** was achieved by substituting the amine component of 5-methoxytryptamine **13** in place of tryptamine through condensation reaction. Upon subjecting to oxidation reaction and subsequently to a meticulous deprotection of **15a**, a phenol compound **15b** was obtained (Scheme 2.3). The reaction was initiated at -78°C to minimize side reactions and was gradually warmed to room temperature over two hours. The successful conversion of **15a** to **15b** reveals the efficiency of the BBr_3-mediated demethylation under mild conditions, providing access to the free phenol analogue for subsequent biological evaluation (Scheme 2.3).

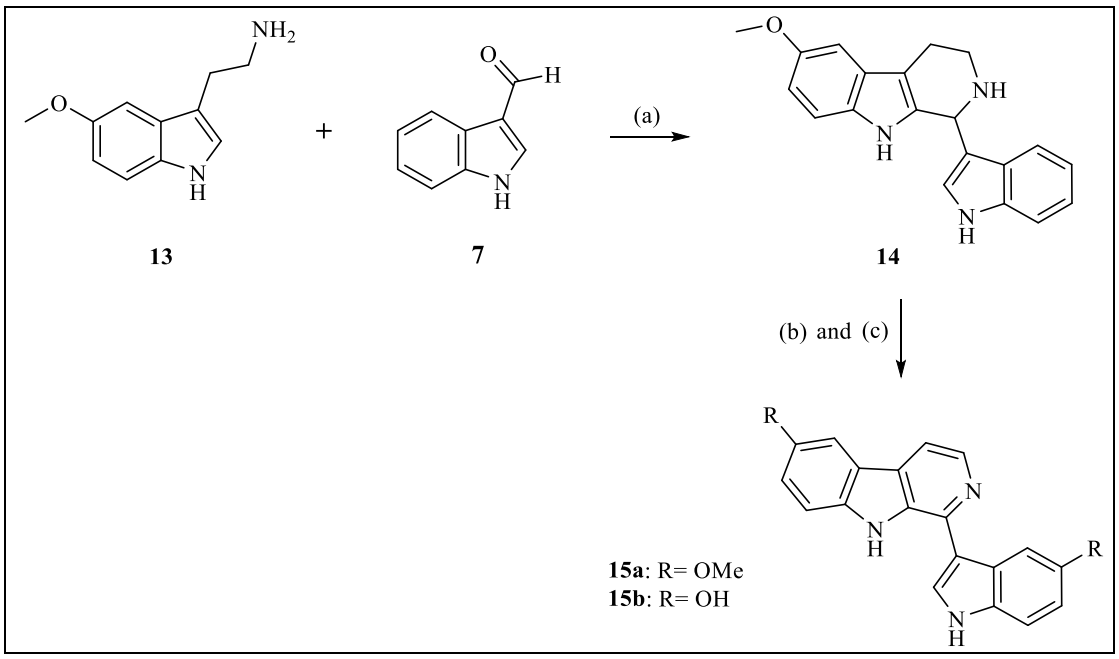

Scheme 2.3. Synthesis of Eudistomin U Derivatives (**15a** and **15b**) as reported in Liew *et al.,* 2014.

Reagents and Condition: (a) toluene or MeOH, reflux, 1-72 h, CH_2Cl_2, TFA, rt, 16-24 h, 73%, (b) DDQ, THF, CH_2Cl_2, rt, 50 min-24 h. (c) BBr_3, CH_2Cl_2, N_2, -78°C to rt, 2 h, 45-31%.

Another indole ring attached to β-carboline with a carbonyl group at the C-1 position was successfully discovered in 2014 by using glyoxal as the reagent. According to Zhang *et al.* (2011), β-carboline bearing indole substituents can be directly synthesized without the use of the two-step reaction of condensation and oxidation as reported by Liew *et al.* (2014). Pityriacitrin **18**, a dehydrogenated β-carboline was formed directly by adding indole-3-glyoxal **17** into a mixture of *p*-toluenesulfonic acid (p-TsOH) and *L*-tryptophan **16** in methanol, illustrated in Scheme

2.4. In this reaction, *p*-TsOH acts as acid catalyst for protonation process. The process occurs smoothly in methanol since protic solvent will stabilize intermediates and supports proton transfer during the reaction.

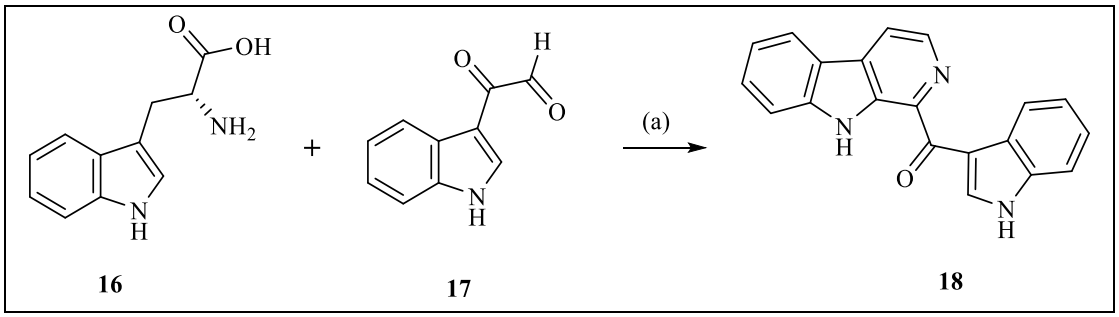

Scheme 2.4. Synthesis of Pityriacitrin (**18**) as Reported in Zhang *et al.,* 2011.

Reagents and Condition: (a) *p*-TsOH, MeOH, 50°C, 2 h, 27%.

A successful reaction has led to synthesis of pityriacitrin derivatives with different substituents at C-6 and C-5′ which resulted in the formation of compound **20a** to **20g** (20-29%). Even so, the isolation of compounds **20c** and **20d** unintentionally gave rise to another derivative of pityriacitrin called pityriacitrin B **21a** and derivatives of **21b** and **21c** (23-27%). The structure has an additional carboxylic acid at C-3 of the β-carboline framework as shown in Schemes 2.5.

Having successfully developed the method for pityriacitrin, Zhang and his team designed derivatives with various amide substitutes on the C-3 skeleton, depicted in Scheme 2.6. By using the same starting material (*L*-tryptophan) and reagents, the corresponding diastereoisomeric mixture 1,2,3,4-tetrahydro-β-carboline-3-carboxylic acid **22** was produced with a condition of 1% H_2SO_4 in water at room temperature in high yield. In this synthesis, dehydrogenation and decarboxylation in Pictet-Spengler cyclization was not observed. This is due to the mild reaction conditions, lower temperature and lower acidity of acids. This is important so that the tryptophan easily dissolved and not lead to many side reactions. Further esterification with methanol in the presence of $SOCl_2$ led to methyl 1,2,3,4-tetrahydro-β-carboline-3-carboxylate **23** in a significant yield (95%).

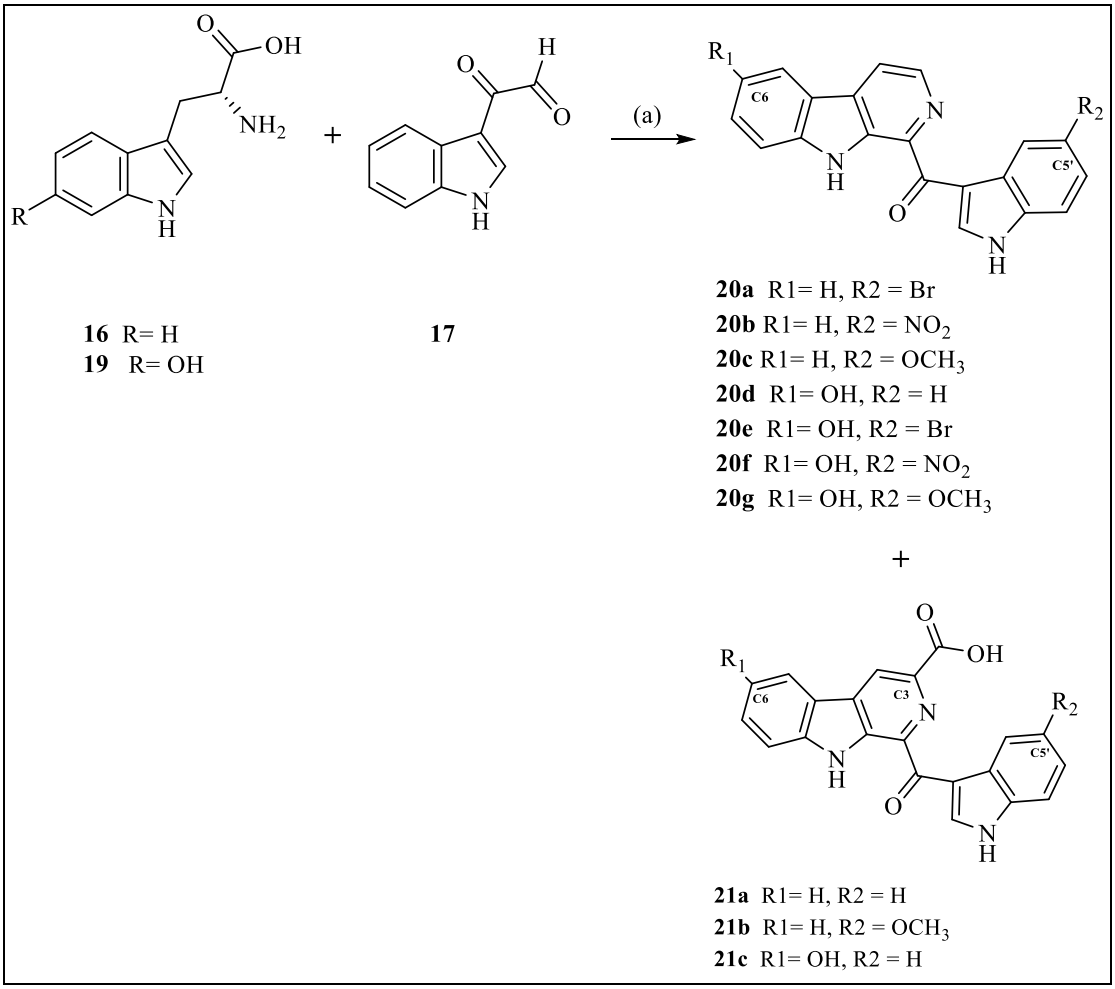

Scheme 2.5. Synthesis of Pityriacitrin Derivatives (**20a-20g**, **21a-21c**) as Reported in Zhang *et al.,* 2011.

Reagents and Condition: (a) *p*-TsOH, MeOH, 50°C, 2 h, 25-29%.

The intermediate esters of **23** were further dehydrogenated using the most commonly reported reagent from previous studies which are Pd/C, elemental sulphur, DDQ, and $Pb(OAc)_4$. Unfortunately, dehydrogenation with either DDQ in refluxing THF or Pd/C at 200°C and even with $Pb(OAc)_4$ in glacial acetic acid gave poor yields of 10-15%. Nevertheless, the problems were overcome by using sulphur in refluxing xylene to produce 1-substituted β-carboline-3-carboxylates (**24a** and **24b**), in improved yields of 71% and 70%, respectively. Consequently, to avoid dimerization of carboline, a large excess of various alkyl diamine and milder reaction temperatures were employed. This strategy was successful since the amidation of compounds **24a** and **24b** with alkyl diamine afforded high yields of compounds **25a** to **25k**, as illustrated in Scheme 2.6.

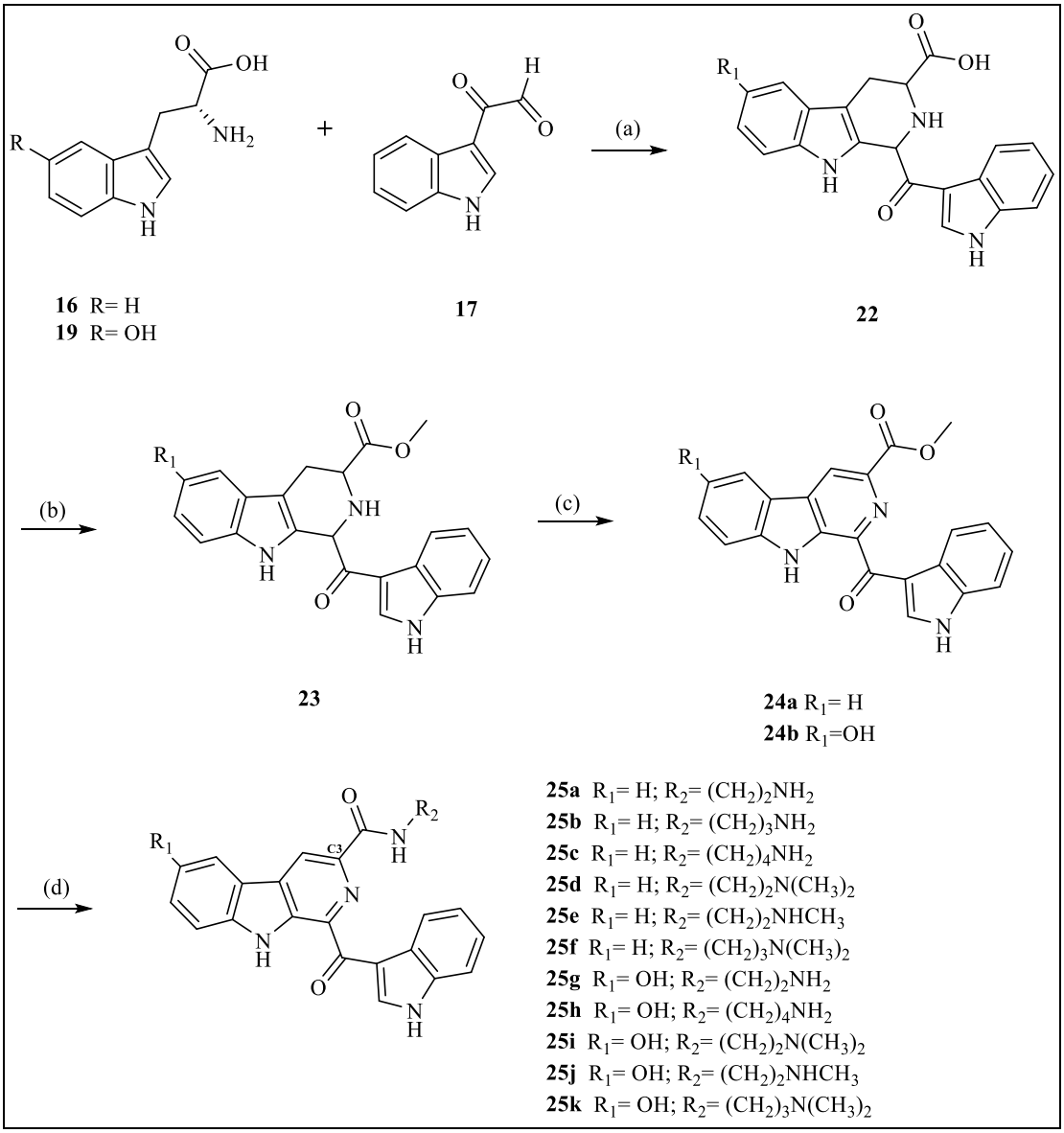

Scheme 2.6. Synthesis of Pityriacitrin Amide Derivatives (**25a-25k**) as Reported in Zhang *et al.,* 2011.

Reagents and Condition: (a) H_2SO_4/H_2O (1/100, v/v), rt, 10 h, (b) $SOCl_2$, methanol, rt, 12 h, 95%, (c) S, Xylene, reflux, 6 h, 70-71%, (d) alkyl diamine, rt, 6 h, 80-98%.

The method proposes by Zhang *et al.,* 2011 provides a direct and efficient route to the β-carboline skeleton and illustrates a concise synthesis of pityriacitrin from readily available starting materials. This study illustrates how selected substituents on both reactants influence the reagent usage, product distribution and structure. Besides, it represents a versatile synthetic pathway of pityriacitrin and its analogues while expanding the potential for further exploration towards β-carboline derivatives.

2.1.2 Friedel-Crafts Hydroxyalkylation Approaches to Indole-Substituted-β-Carbolines

Trigonostemine A-D and trigonostemine G were isolated from *Trigonostemon filipes* Chang & Mo and *Trigonostemon lii* Chang. Like hyrtiosulawesine, trigonostemone species was found to have a cytotoxic effect (Wang *et al.,* 2017) and in additional to trigonostemine G, it was reported to have anti-acetylcholinesterase activity (Szabó *et al.,* 2021). The first total synthesis of trigonostemine G **30a** (Scheme 2.7) was investigated by Szabó *et al.* (2019), where the reaction started with derivatives of β-carboline aldehydes **26a-c** and protected indole under slightly alkaline condition, yielded hydroxy compounds **28a-c**. The choice of lightly basic medium was critical to promote nucleophilic addition while preventing undesirable side reactions.

The compounds were further oxidized using activated MnO_2 in boiling 1,4-dioxane gave ketone intermediates **29a-c** prior to the deprotected step with caesium fluoride (CsF) in acetonitrile to provide **30a** and its isomer derivative (5-hydroxy-1H-indol-3-yl)(6-methoxy-9H-b-carbolin-1-yl) methanone **30b** as well as dimethoxy trigonostemine G **30c**. Mechanistically, MnO_2 acts as a selective oxidant for benzylic alcohols, facilitating the transformation of the hydroxyl group into a carbonyl function without over-oxidation or cleavage of sensitive heteroaromatic rings. The use of boiling 1,4-dioxane not only ensured sufficient solubility of the substrates but also provided the high temperature required to drive the oxidation to completion.

To achieve the target product, deprotection step was accomplished by treating **29a–c** with caesium fluoride (CsF). CsF was selected in these conditions to form cleavage of Si-N bonding due to CsF has strong affinity towards silicon. In summary, this investigation emphasizes a chemoselective synthetic approach for trigonostemine G and its analogues *via* base-promoted condensation, MnO_2 oxidation, and fluoride-induced deprotection. Also, the use of protecting TBS chemical to control the reactivity of C-C bond formation.

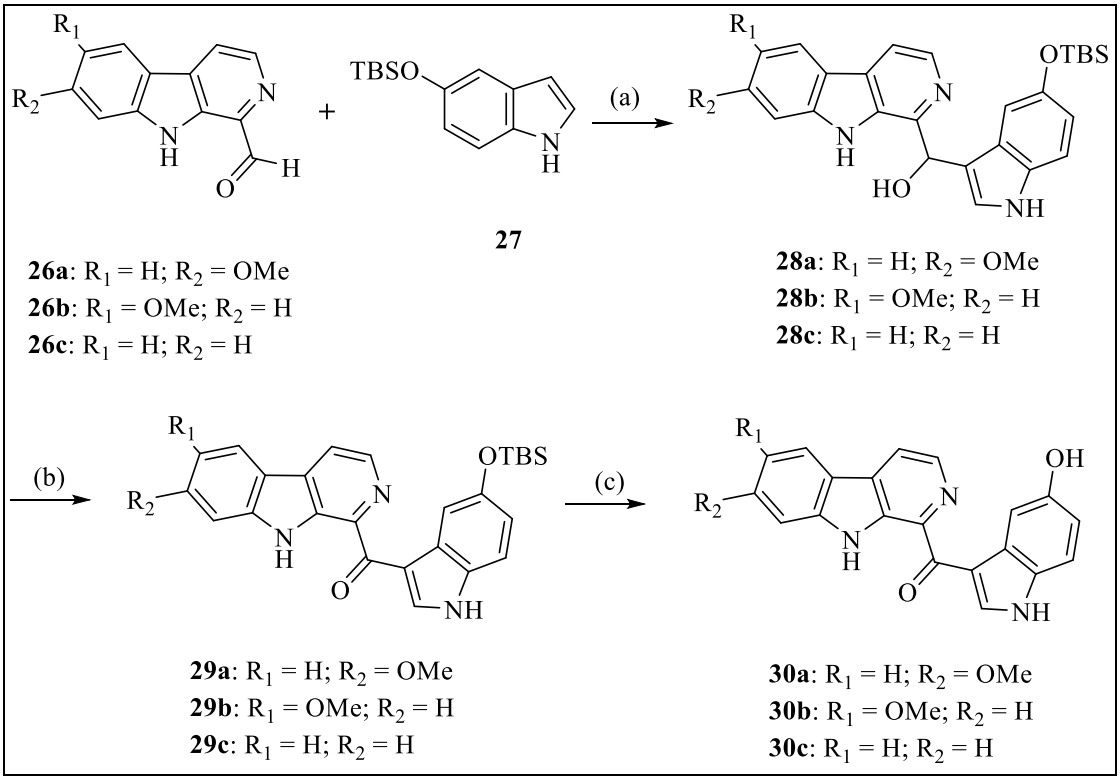

Scheme 2.7. Synthesis of Trigonostemine G (**30a**) and Its Derivatives (**30b** and **30c**) as Reported in Szabó *et al.,* 2021.

Reagents and conditions: (a) NaOH, H_2O, CH_2Cl_2, MeOH, rt, 48 h, 37-45%, (b) MnO_2, 1,4-dioxane, reflux, 0.5 h, 98-99%, (c) CsF, MeCN, 0°C to rt, 24 h, 34-39%.

2.1.3 Hybridization of β-Carboline and Indole Cores via Amide Coupling

Since β-carboline bearing indole provides good biological activity, a modified synthesis of glyoxamide linked β-carboline-indole conjugates was investigated to enhance the bioactivity. In the formation of **40a-y**, a multi-step synthetic route was employed. Two main components of β-carboline amines **36a-d** and indole-3-glyoxalyl chlorides **39a-i** were required to be initially prepared (Soni *et al.,* 2023). The synthesis of **38a-d** started with *L*-tryptophan **16** as starting material which was esterified with methanol in the presence of thionyl chloride ($SOCl_2$) for six hour. This will activate the carboxylic acid toward nucleophilic substitution, providing a xsuitable intermediate to produce methyl tryptophanate **10**. Due to the amine functionality of ester **10**, it was then subjected to Pictet-Spengler condensation reaction with different aromatic aldehydes **31a-d** (Figure 2.1) to generate tetrahydro-β-carboline esters **32a-d**. Those saturated esters were then aromatized using oxidizing agent $KMnO_4$ to obtain 1-aryl-β-carboline esters **33a-d**. This oxidizing agent helps alcohol or benzylic groups turn into carbonyl

compounds. Then, $LiAlH_4$ reduces those compounds to yield corresponding amines or alcohols.

The alcohols of **34a-d** were treated with diphenylphosphoryl azide (DPPA) in the presence of 1,8-diazabicyclo[5.4.0]undec-7-ene (DBU) to acquire azides **35a-d**. The reagent, DPPA/DBU followed by triphenylphosphine (TPP) reduction enabled the generation of amine intermediates (**37a-d**) under mild, high-yielding conditions. Simultaneously, commercially available indoles **36a-d** were reacted with different alkyl halides in the presence of a base to procure *N*-alkylated indoles **38a-g**. Subsequently, these indoles (including -NH indoles) were treated with an excess of oxalyl chloride to obtain indole-3-glyoxalyl chlorides **39a-i**, which were then utilized in the amine coupling reaction without purification due to low air stability. These acid chlorides were reacted with β-carboline amines **36a-d** using EDC-HOBt to obtain the designed products **40a-y** in acceptable yields.

In general, the chosen of reagents can carefully manage the selectivity of oxidation, reduction, and coupling steps. This is needed to put together this structurally diverse library of β-carboline-indole conjugates.

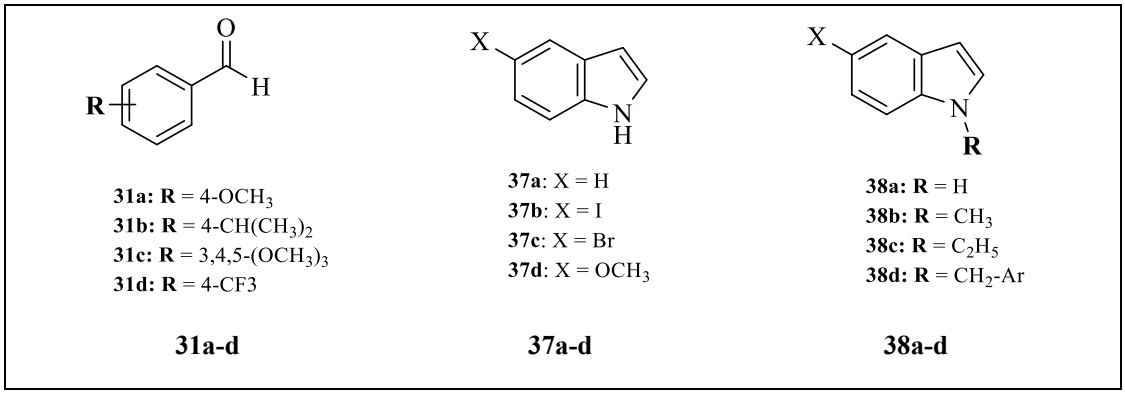

Figure 2.1 Derivative Indole and Benzaldehyde

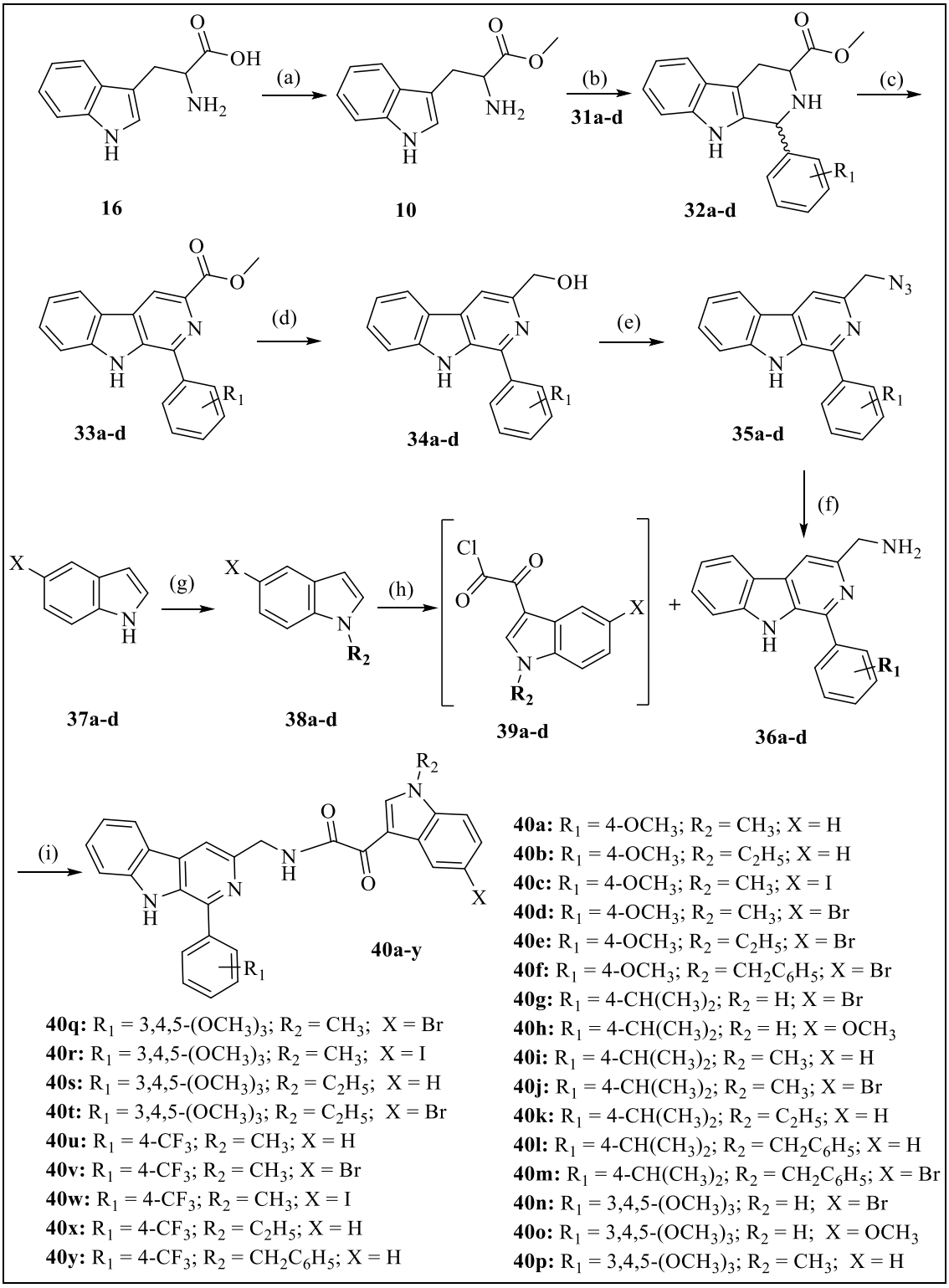

Scheme 2.8. Synthesis of Glyoxamide Linked β-Carboline-Indole (**40a-40y**) as Reported in Soni *et al.,* 2023.

Reagents and conditions: (a) $SOCl_2$, MeOH, 0 °C to rt, 6h, 98%, (b) 5% TFA, CH_2Cl_2, 0 °C to rt, 8 h, R^2-X, rt, 4h, 75-94%, (c) $KMnO_4$, THF, rt, 12h, 62-74%, (d) $LiAlH_4$, dry THF, 0 °C to rt, 2 h, 85-96%, (e) DPPA, DBU, THF, rt, 12 h, 74-83%, (f) TPP, CN: H_2O (1:1), rt, 12 h, 72-80%,(g) oxalyl chloride, N_2, Diethylether, 0 °C, 2 h, (h) R^2-X, Cs_2CO_3, DMF, rt, 0.5–2h, 84-97%, (i) EDC.HCl, HOBt, DIPEA, THF,0 °C to rt, 12-15 h, 68-88%.

The synthesis of thiadiazolo-carboxamide bridged β-carboline-indole is depicted in Scheme 2.9. Five steps reactions were established based on the study by Tokala *et al.* (2020). Modified indoles with thiodiazole **43a–c** was attained by esterification of the starting material, indole-2-acid **41** with $SOCl_2$ in methanol at room temperature for 4 h. Subsequently, compound **42** was alkylated using different alkyl halides at the N-1 position to yield alkylated indole-2-esters **43a-c**, which then hydrolyzed further to their respective alkylated indole-2-acids **44a-c**. These intermediates served as key scaffolds for coupling with the thiadiazole hydrazine derivatives (**45a-c**).

A $POCl_3$ was chosen because it efficiently promotes cyclodehydration and ring formation under controlled conditions. Compounds **47a-k** was achieved by acid–amine coupling between previously modified β-carboline **46a-f** and indole **45a–c** in moderate yields. Finally, an amide coupling between compounds **45a-c** and **46a-f** was carried out using EDC/HOBt in dichloromethane, affording the final thiadiazolyl-carboxamide bridged β-carboline-indole hybrids **(47a–k)** in good yields.

In summary, this multi-step sequence effectively integrates the β-carboline and indole cores *via* a thiadiazole-carboxamide linkage, demonstrating a strategic synthetic approach to construct the complex structure of heterocyclic frameworks.

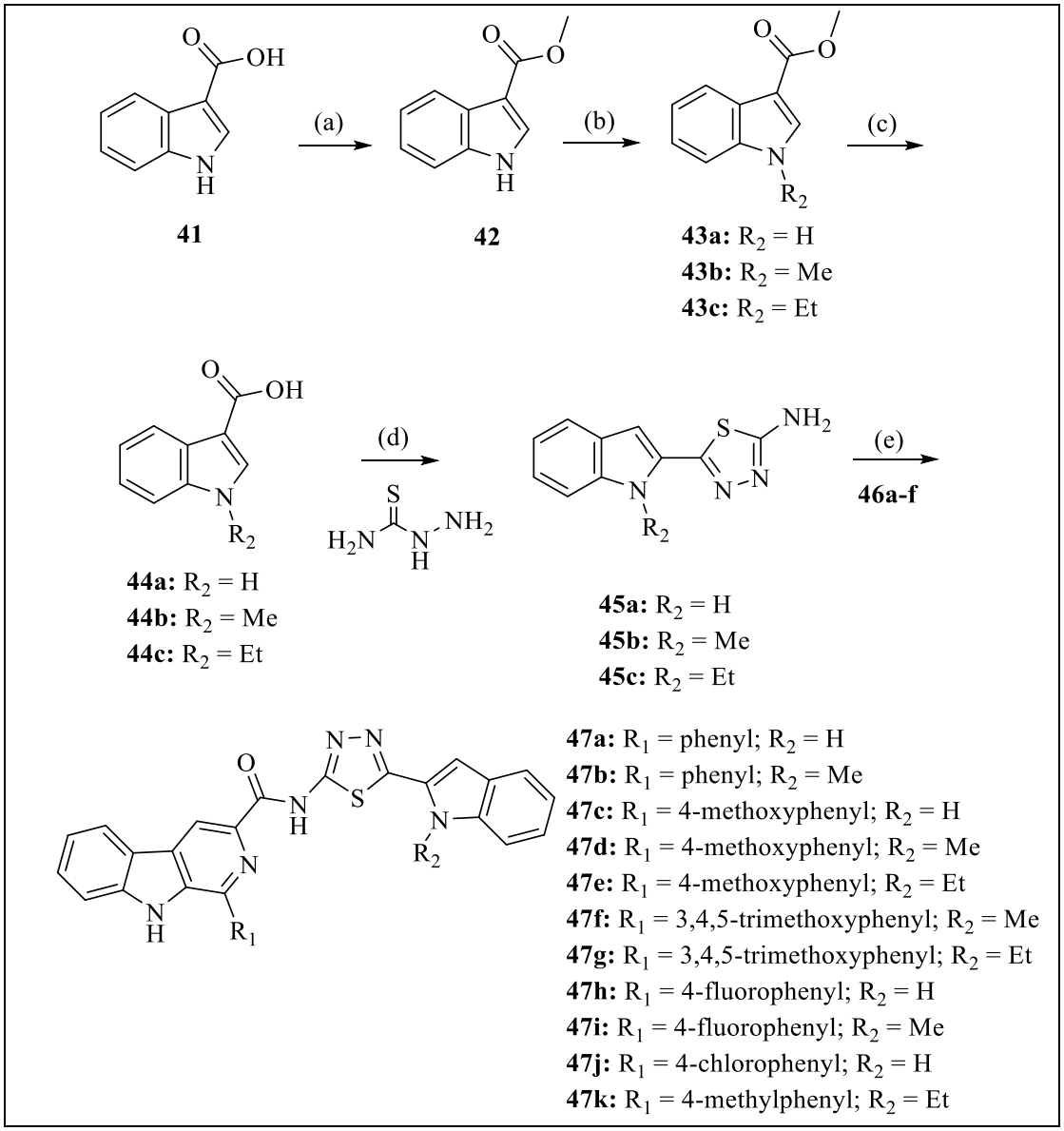

Scheme 2.9. Synthesis of Thiadiazolo-Carboxamide Bridged β-Carboline-Indole (**47a-47k**) as Reported in Tokala *et al.,* 2020.

Reagents and conditions: (a) $SOCl_2$, MeOH, rt, 4 h, 90%, (b) NaH, DMF, 0°C to rt, 0.5 h, R_2-X, rt, 4 h, 80-90%, (c) NaOH, EtOH, reflux, 2 h, 75-80%, (d) $POCl_3$, reflux, 0.5 h, 60-65%, (e) EDC, HOBt, CH_2Cl_2, rt, 12 h, 72-85%.

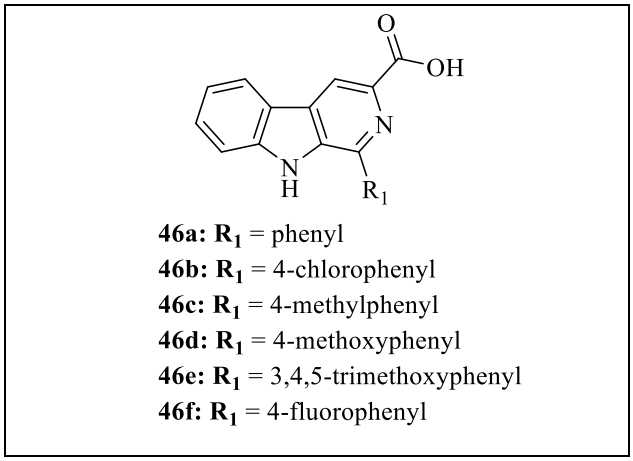

Figure 2.2 Modified Structure of β-Carboline

2.2 Discovery and Previous Synthesis of Hyrtiosulawesine

Hyrtiosulawesine, **1** is another indole ring attached to β-carboline with hydroxy substituents on C-6 and C-5′ framework. It was isolated and characterized by marine sponges *Hyrtios erectus* and *Hyrtios reticulatus* in 2002. Since this compound is good for antimalarial, cytotoxicity, and anti-phospholipase A_2, Zhang *et al.* (2010) were tempted to investigate its synthetic route with the modified one-pot oxidation reaction.

The target compound was initially synthesized from 5-methoxyindole **36d** with oxalyl chloride in an anhydrous ether at 0-5°C for an hour to afford compound **49**. As to form 5-methoxyindole-3-glyoxal **49**, compound **48** was treated with tributyltin in anhydrous ethyl acetate at 0°C condition. Tributyltin hydride acts as a radical reducing agent which will donate a hydrogen atom (H·) to radicals to afford the corresponding indole glyoxal intermediates.

Parallel to this, compound **36d** (β-carboline precursor) underwent a Vilsmeier–Haack reaction using $POCl_3$ and DMF, producing the corresponding aldehyde (**50**) in an excellent yield of 98%. In this process, aldehyde moiety is effectively installed onto electron-rich heteroaromatic systems, particularly on the β-carboline ring. Further condensation with nitromethane based on the classic Henry reaction afforded vinyl nitro compound **51** in 92% yield. The Henry reaction is crucial to generates a highly functionalized nitroalkene intermediate, which can later be selectively reduced to access the desired amine functionalities.

Reducing compound **51** with $NaBH_4$ at room temperature yielded compound **52** which was then reduced further by H_2 in the presence of Pd/C in methanol to afford 5-

methoxy tryptamine **13**. Treating **13** with the intermediate compound **49** in acetic acid directly generated derivative of the target compound **53**, similar to investigation of Zhang *et al.,* 2011. The final deprotection step successfully yielded hyrtiosulawesine in the presence of BBr_3 in CH_2Cl_2, as shown in Scheme 2.10.

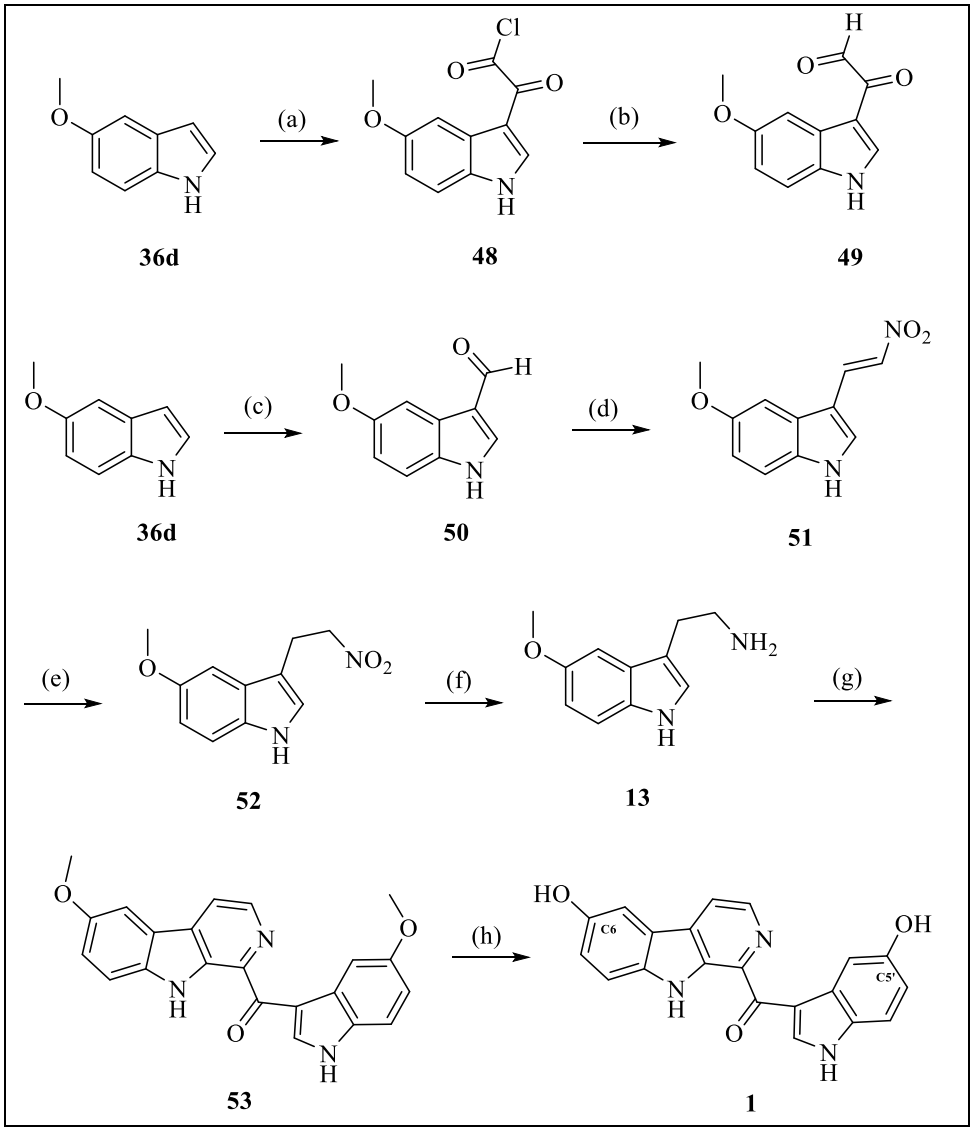

Scheme 2.10. Synthesis of hyrtiosulawesine (**1**) as Reported in Zhang *et al.,* 2010.

Reagents and conditions: (a) $C_2O_2Cl_2$, Et_2O, 0-5 °C, 1 h, 91%, (b) Bu_3SnH, EtOAc, rt, 2 h, 67%, (c) $POCl_3$, DMF, NaOH, 98%, (d) CH_3NO_2, CH_3COONH_4, benzene, reflux, 92%, (e) $NaBH_4$, THF, MeOH, rt, 98%, (f) Pd, C, H_2, 99%, (g) **49**, AcOH, 90 °C, 40%, (h) BBr_3, CH_2Cl_2, -78 °C to rt, 95%.

In general, this synthetic sequence not only afford to hyrtiosulawesine production, but it also showed some important synthetic principles: selective aldehyde introduction through the Vilsmeier-Haack and tributyltin-mediated formylation,

efficient carbon-carbon bond construction through the Henry reaction, and strategic protection-deprotection steps to control chemoselectivity. By successfully reproducing the natural product compounds, the synthesis paved the way for further structural analogues to be generated, enabling structure–activity relationship (SAR) studies to optimize its antimalarial, cytotoxic, and anti-inflammatory properties.

After four years later, Liew and co-workers described a three steps synthetic strategy for the preparation of hyrtiosulawesine. The starting material of 5-methoxytryptamine **13** was reacted with *N*-Boc-indole-3-acetaldehyde **54** under acidic conditions (5% HOAc) afforded 1,2,3,4-tetrahydro-β-carboline **55** in 37% yield. The use of acetic acid serves not only to promote the condensation reaction but also to facilitate the deprotection of the Boc group. Subsequent conversion was the pyridine ring oxidation, achieved using the oxidant of 2,3-dichloro-5,6-dicyano-1,4-benzoquinone (DDQ) without concomitant oxidation of the doubly benzylic methylene group. The final deprotection step of hyrtiosulawesine was achieved in the presence of BBr_3 in CH_2Cl_2. This strategy decreased the number of steps, but overall yields were average and still had protection and deprotection steps.

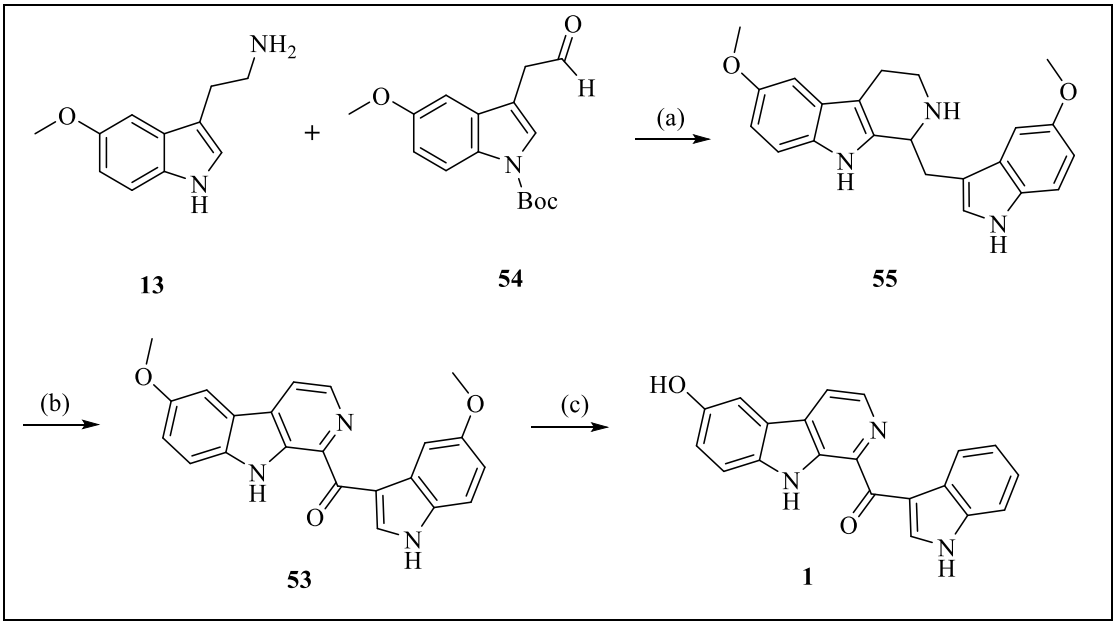

Scheme 2.11. Synthesis of Hyrtiosulawesine (**1**) as Reported in Liew *et al.,* 2014.

Reagents and conditions: (a) 5 or 10% HOAc/H_2O, reflux, 1.5-5 h, 77%, (b) DDQ, CH_2Cl_2/H_2O, rt, 30-90 min, 25%, (c) BBr_3, CH_2Cl_2, N_2, -78°C, 40 min, rt, 3 h, 87%.

Beyond hyrtiosulawesine, thiadiazolo-carboxamide and glyoxamide functional groups on indole have emerged as bulky connected groups in several reported

compounds. These structural modifications add synthetic complexity and molecular mass, increasing the barrier to molecule development and decreasing permeability of the membrane, which may jeopardize drug-likeness. In order to overcome these difficulties, this study puts forward a simplified three-step synthesis to combine the indole moiety with a β-carboline core at the C-1 position. Such reduced strategy is aimed at promoting greater synthetic facile, providing the ability to formulate compounds quickly. This will improve pharmacological capacity by reducing the total mass size of a molecule.

2.3 Biological Activities of Hyrtiosulawesine

Hyrtiosulawesine have been reported to exhibit a wide range of pharmacological effects. However, this literature review focuses primarily on its potential as an antimalarial agent and its cytotoxic effects against specific cell lines, which directly align with the core objectives of this study.

2.3.1 Antimalarial Activity

Malaria remains a colossal global health menace, especially ravaging developing nations with its most devastating toll in sub-Saharan Africa, where countless children under the age of five succumb to this relentless scourge. The crisis has deteriorated over time as the parasites evolve and develop resistance to current antimalarial treatments and medicine often cannot be afforded. Since 2020, the malaria cases keep inclines not only sub-Saharan Africa, but this endemic also extend to South Asia, South America, and India (Figure 2.3).

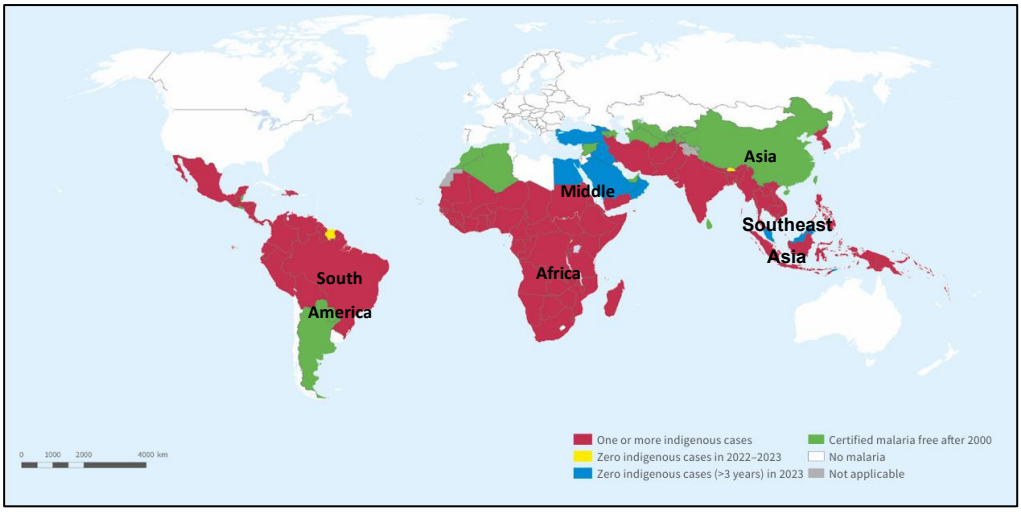

Figure 2.3 Global Status of Indigenous Malaria Transmission (World Health Organization, 2023)

The transmission of the malaria significantly influenced by climatic factors, particularly in area with a great temperature, humidity, and rainfall, in tropical and subtropical regions. According to WHO, Malaysia had zero indigenous cases caused by human *Plasmodium* species for the sixth consecutive year in 2023, while Saudi Arabia and Timor-Leste had their third straight year, bringing the malaria epidemic to an end. Cabo Verde and Belize were confirmed malaria-free in 2023, after four years of no malaria cases. Egypt has been proclaimed malaria-free in 2024.

Malaria is mostly caused by human plasmodium parasites, specifically *Plasmodium falciparum*, *Plasmodium vivax*, *Plasmodium ovale*, and *Plasmodium malariae*. These species are the major contribution to this endemic. Of these, *P. falciparum* is the most concerned as it is the most likely to induce severe cases of illness in humans and cause higher mortality rate (World Health Organization, 2014). As reported, *P. falciparum* has caused 86.6% of cases in Africa, 70.9% in Central America, 20.8% in South America, and 4.8% in Asia. The accumulation of *P. falciparum* in tissues, together with the up regulation of cytokines and other toxic chemicals as well as the absence or late administration of effective antimalarial medication, are the critical reasons why *P. falciparum* can cause extreme fatality. While this species shows zero cases in Malaysia, the identification of novel active compounds is still crucial for addressing infections in other affected regions.

The urgent need for antimalarial medications is critical. For decades, thousands of natural bioactive compounds were tested to determine the prime antimalarial medications. However, the long approach to clinical stage may fail due to their toxicity,

bioavailability, and a few other side effects, causing them to not be qualified as viable drugs candidates. Chemical synthesis with a focus on structural alterations was also carried out to produce a powerful medication. For example, artesunate is derived from artemisinin, chlorquine from quinine, and atovaquone from ubiquinone. All of these are currently available antimalarial medications that have been semi-synthesized from natural compounds to enhanced efficacy and potency. Hyrtiosulawesine (**1**) demonstrated inhibitory activity with IC_{50} values of 1 µM and 5 µM against chloroquine-resistant strain (FcB1) of *P. falciparum* (Liew *et al.,* 2014).

Provided that the main thrust of this research was to look at hyrtiosulawesine and its derivatives as potential antimalarial agents through *Pf*LDH inhibition, a secondary screening was done in cancer models to further explore the pharmacological landscape of these molecules. MDA-MB-231 triple-negative breast cancer cells and HT-29 colorectal adenocarcinoma cells were selected to represent aggressive tumor types that are clinically relevant. This screening against human cell lines complements insights related to cytotoxicity, selectivity, as well as scaffold versatility and enhances the interest in antimalarial studies.

2.3.2 Anticancer Activity

Cancer is the plague of the 21st century and a global emergency. This disease is thought to have millions of cases worldwide (Chikkara & Parang, 2012). As highlighted by Matthews *et al.* (2022), this perilous, shape-shifting malignancy arises from the disruption of normal cellular mitosis. It has become so common that colon cancer is now one of the most feared diseases, affecting 10.0% of the entire population. Specifically, it was stated that out of the 1.9 million new cases in 2020, 10% were newly diagnosed. Additionally, lung cancer (11.7%) and breast cancer (11.4%) contributed to 23.1% of new cases combined with GLOBOCAN statistics (Sung *et al.,* 2021). The sudden increase in cancer rates is mainly attributed to technological progress, along with major shifts in lifestyle and dietary habits influenced by the global food industry, particularly the agriculture, fisheries, and livestock sectors (Eala *et al.,* 2022).

The increasing rate of cancer patients has made it imperative to develop effective treatments for this progressively formidable disease, and one way to address this challenge is by creating new compounds with strong, aggressive anticancer properties (Chikkara & Parang, 2012; Manzari-Tavakoli *et al.* 2024). As noted by

Muhammad *et al.* in 2022, a diverse range of natural resources has been explored and has demonstrated potential in cancer treatment. Additionally, due to the exceptionally low toxicity of these natural resources to healthy cells, these compounds are anticipated to be highly beneficial in therapeutic applications, contributing to the advancement of modern anticancer drugs and enhancing antibiotic development (Cragg & Pezzuto, 2016; Najmi *et al.,* 2022). Apart from the diterpenoid described, the β-carboline alkaloid has also been reported to be very promising with a plethora of pharmacological effects (Tshikhudo *et al.,* 2024). Hyrtiosulawesine was reported to display good cytotoxic effects towards HepG2 cell line with IC_{50} value of 19.3 µmol/L (Wang *et al.,* 2013). These compounds are known to cause apoptosis, prevent cell proliferation, and are strong inhibitors to some of the most essential signalling pathways, placing them right in the centre of the combat against cancer (Zhao *et al.,* 2023).

β-carbolines, a subclass of indole alkaloids, are produced by various species worldwide and play an important role in drug discovery and development (Dzobo, 2022). Aside from showing antimalarial properties, understanding that hyrtiosulawesine was built with indole and β-carboline as the major skeleton, anticancer activity was also assessed. As a result, it is hoped that the efficacy and selectivity of derivatives of these compounds in anticancer medications will be increased, hence improving the therapeutic effect and patient prognosis (Sharifi-Rad *et al.,* 2019).

2.4 Other Biological Activities of Hyrtiosulawesine and its Derivatives

Some of the synthesized and isolated compounds described in previous sections were demonstrated to have various pharmacological effects. These include antioxidants, antimicrobial, cytotoxicity, anti-phospholipase A_2, antiproliferative, antiplasmodial, anti-inflammatory, and antidiabetic properties. All additional details regarding their biological activities have been elaborated upon in this section.

2.4.1 Antioxidant

The imbalance in the formation of reactive oxygen species (ROS) and the body need to overcome them by providing antioxidants, leads to the manifestation of oxidative stress (Olufunmilayo *et al.,* 2023). As illustrated in Figure 2.4, the ROS is normally produced by endogenous systems, and the formation may occur due to

exposure to various physiochemical conditions or pathological states (Gharu, 2022). Excessive levels of free radicals in the body can impair insulin signaling and the pancreatic cell leading to type 2 diabetes (Asmat *et al.,* 2016). Besides, increased oxidative stress in adipose tissue can also contribute to the malfunction of adipocytes and cause obesity (Manna & Jain, 2015). Other chronic pathologies will emerge such as infertility, pulmonary, cardiovascular, and neurodegenerative disorders (Taviano *et al.,* 2018). Hence, adopting external sources of antioxidants from natural products and synthetic origins can assist in mitigating the harmful effects of oxidative stress these deleterious effects.

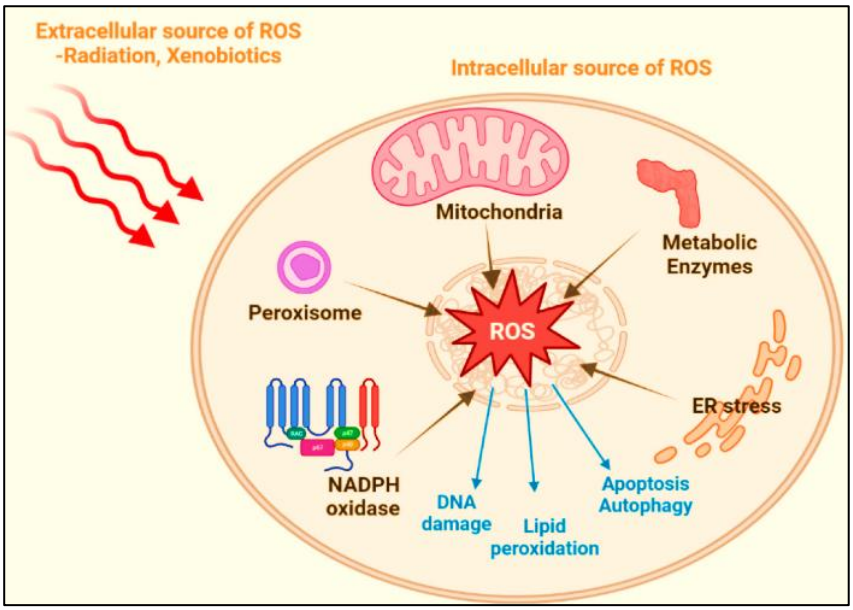

Figure 2.4 Dynamic Schematic of the Recreation of Oxygen Species (ROS) Formation and Their Overall Breakage Human Physiology (Hong *et al.,* 2024)

As reported by Liew *et al.* (2014), hyrtiosulawesine, **1** and derivative **15b** exhibited antioxidant properties by using a qualitative DPPH TLC assay. In this study, the antioxidant activity was quantified using an ORAC assay against ascorbic acid. Both compounds displayed significant activity and surpassed vitamin C (ORAC value of **1** = 6.23, **15b** = 5.66, positive control= 0.48). The presence of the phenolic hydroxyl group is believed to be responsible for this biological activity as illustrated in Figure 2.5.

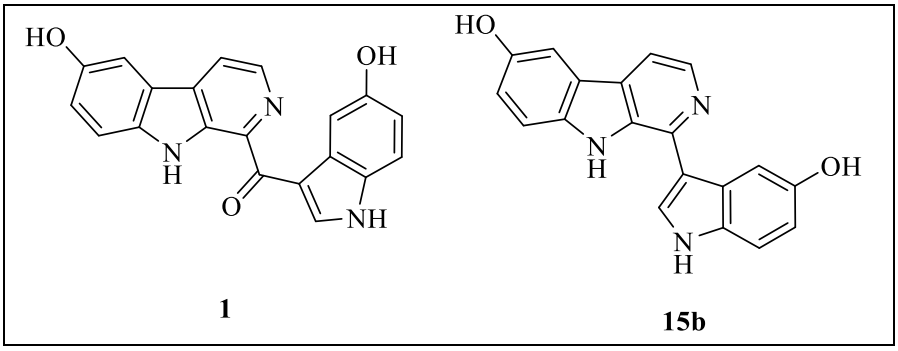

Figure 2.5 Chemical Structure of Compound **1** and **15b**

2.4.2 Cytotoxicity

Cell cytotoxicity assays are primarily used to screen the response of the cells against a drug or any chemical agent (Adan *et al.,* 2016). They are commonly used in the pharmaceutical industry to determine the effects of newly developed agents on cells. Researchers employ different types of assays to evaluate the efficacy of developed therapeutics that mainly target cancer cells. There are a variety of methods for detecting the cytotoxic effects of different compounds and measuring cellular viability (Adan *et al.,* 2016). One of them is the MTT assay, which was used to access the cytotoxicity activity against compound **30c.** From the result, **30c** was found to have weak cytotoxicity against K562 tumour cell lines with IC_{50} value of 39.6 μM (Wang *et al.* 2017).

As illustrated in previous sections, β-carboline-indole was modified with thiadiazolo-carboxamide bridge to improve its bioactivity (Tokala *et al.,* 2020). The resulting compounds, **47a–k**, exhibited significant cytotoxicity against all the tested cancer cell lines (A549, MDA-MB-231, BT-474, HCT-116, HL-60, and THP-1). Compound **47c** was found to have the highest cytotoxic effect against A549 cell line with IC_{50} value of 2.82±0.10 μM and was followed by THP-1 (IC_{50} = 3.18 μM) and HL-60 (IC_{50} = 3.83 μM). Moreover, in both breast cancer cell lines (MDA-MB-231 and BT-474), **47c** displayed a potent activity with IC_{50} values of 3.28 and 4.09 μM and a value of 4.78 μM in colon cancer cell (HCT-116). In contrast, compound **47c** was the only compound exhibiting cytotoxic activity against BEAS-2B, with an IC_{50} value of 71.25 μM (weak activity). Compounds **47a**, **47f**, **47h**, and **47j** on the other hand expressed good activity in all tested cell lines with IC_{50} less than 10 μM. Besides,

compounds **47b**, **47d**, **47i**, and **47k** demonstrated reasonable *in vitro* cytotoxicity on A549 and MDA-MB-231 cell lines with IC_{50} values less than 10 µM.

In addition to thiadiazolo-carboxamide bridge, Soni *et al.* (2023) investigated and provided another 25 compounds of glyoxamide linked β-carboline-indole and tested for their cytotoxicity effect. The MTT assay was performed on all the derivatives on human cancer cell lines such as colon cancer (HCT116), lung cancer (A549), melanoma (SKMEL-28), breast cancer (MCF-7) as well as normal rat kidney cell line (NRK52E). Based on the results, compounds **40f** and **40n** exhibited good cytotoxicity against MCF-7 cells with an IC_{50} values of 6.47 and 9.56 µM, respectively. Compound **40n** was discovered to have the highest activity against A549 cells with IC_{50} value of 3.84 µM compared to **40m**, **40o**, and **40x** with IC_{50} values of 6.89, 8.05, and 8.23 µM. Furthermore, compounds **40o**, **40u**, **40v**, and **40x** demonstrated promising cytotoxicity against HCT116 with IC_{50} values of 5.65, 7.69, 6.74, and 6.03 µM, respectively. Compound **40n**, **40u**, **40v**, and **40x** also displayed significant cytotoxicity on SK-MEL-28 with IC_{50} values of 9.56, 5.50, 4.52, and 4.37 µM. In addition, compound **40x** provided significant activity against normal kidney cell lines with IC_{50} value 33.61 µM.

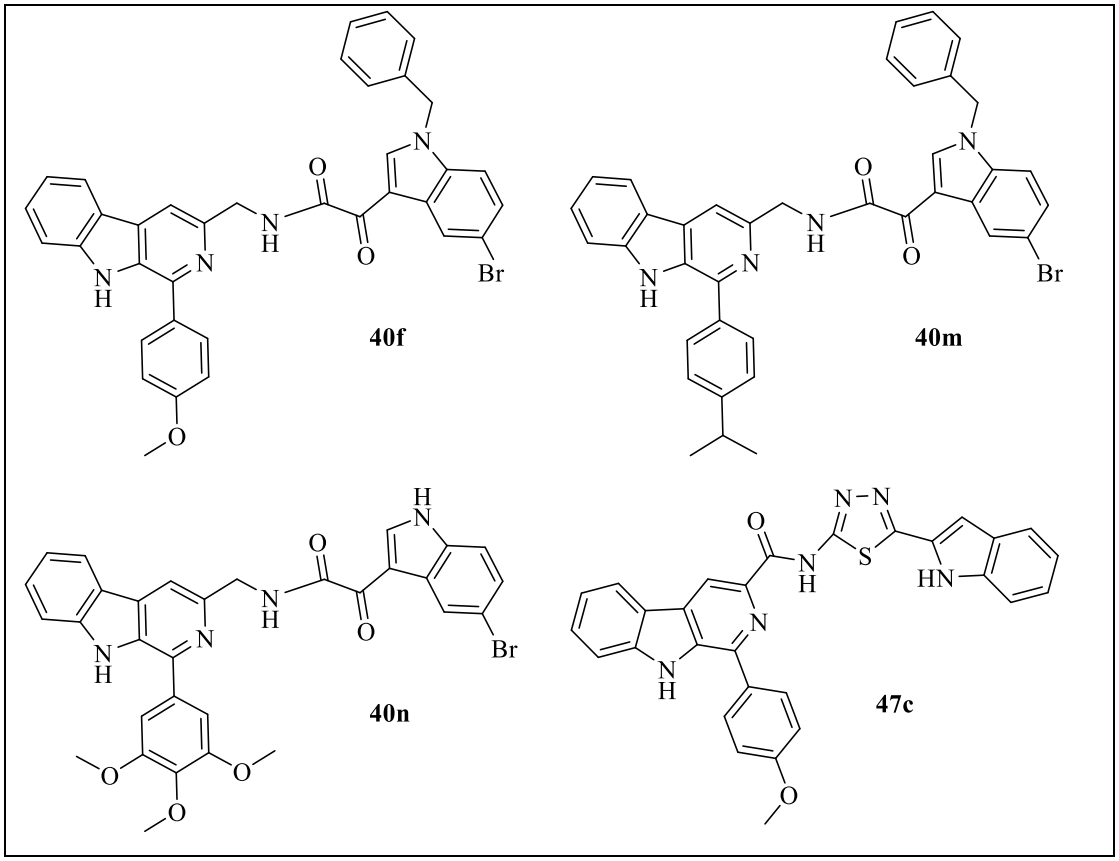

Figure 2.6 Chemical Structure of Compound **40f, 40m, 40n** and **47c**

2.4.3 Antimicrobial

Indole substituted β-carboline compounds were also documented to have antimicrobial activity. In 2014, a more detailed biological profile of **9** was described. Gram-positive bacteria (*Streptococcus pyogenes*, *Staphylococcus aureus*, and *Mycobacterium smegmatis*) were observed to be more susceptible to the treatment than Gram-negative bacteria, with IC_{50} value of 3.4, 6.4, and 3.6 µg/mL, respectively (Roggero *et al.,* 2014). These results demonstrated that indole–β-carboline scaffolds can disrupt bacterial viability at low micromolar concentrations, highlighting their promise as antimicrobial leads.

The difference in susceptibility between Gram-positive and Gram-negative strains is consistent with well-established bacterial physiology. According to Richter and Hergenrother (2019), Gram-positive bacteria are more vulnerable because they possess only a single lipid membrane, whereas Gram-negative bacteria have two. The additional outer membrane in Gram-negative bacteria contains lipopolysaccharides (LPS), which make it difficult for most small molecules to penetrate without assistance from channel proteins known as porins.

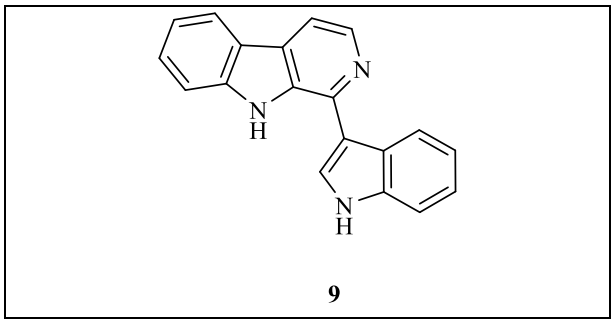

9

Figure 2.7 Chemical Structure of Compound **9**

2.4.4 Antiplasmodial

Malaria is a human infectious disease that is caused by protozoa of the genus *Plasmodium* that kills over 1 million people per year which continues to be a global health problem (Escala *et al.,* 2023). A total of 360 antiplasmodial agents of natural products including alkaloids were discovered to be effective in the treatment of malaria infections (Nogueira & Lopes, 2011). Decarbonyl eudistomin U analogues of **15a** and

15b demonstrated antimalarial effect against chloroquine-resistant strain (FcB1) of *P. falciparum* with IC_{50} 4.7 µM and 11.0 µM. In the assay, chloroquinone was used as a positive control and displayed IC_{50} = 61.8±6.2 nM.

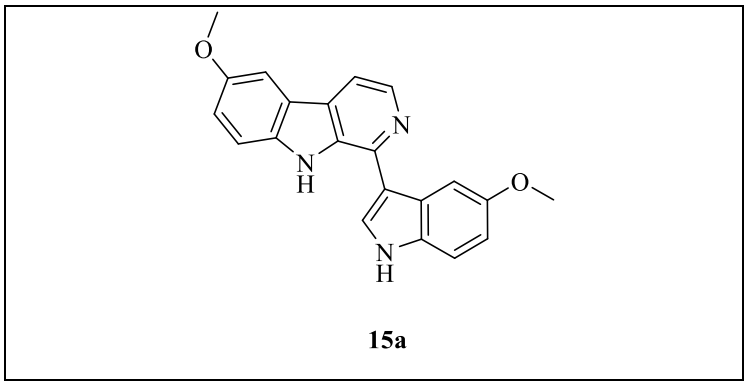

15a

Figure 2.8 Chemical Structure of Compound **15a**

2.4.5 Antiproliferative

Differ from cytotoxicity mechanism as describe from 2.3.2 sections, antiproliferative activity refers to a compound's ability to inhibit rapid cell growth (Malta *et al.,* 2013). This means that the abnormal cells are not allowed to multiply rapidly. The American Cancer Society's Cancer Facts & Figures 2025 report estimates significant case and death numbers within the US separately, reinforcing the continuing global cancer challenge (American Cancer Society, 2025). Due to such concerns, the use of botanicals to treat many diseases including cancer has become more sensible.

A study by Zhang *et al.* (2011), pityriacitrin analogs has shown a significant antiproliferative effect on cell lines of breast cancer for MCF-7, MDA-231, and PC3. The cause of such notable activity is attributed to the occurrence of the carboxyl group present at the C-3 position of the β-carboline moiety. As observed, compounds **20c** and **20d** have potent antiproliferative activity against MCF-7 and MDA-231, followed by derivatives **21a** and **21b** against MCF-7. The bromo substituents in compound **20e** and the nitro substituents in compound **20b** and the 6-hydroxy, 5'-methoxy, 5'-bromo, and 5'-nitro double substitutions in compounds **20e-20g** resulted in weak antiproliferative activity. Since the C-3 and C-6 positions on the β-carboline skeleton are crucial in antiproliferative activity, the structure was further developed. Pityriacitrin amide analogues **25b-25e** and **25i-25k** was more active, whose IC_{50} ranged from 1.33 to 4.36 µM against MDA-MB-231 cell line.

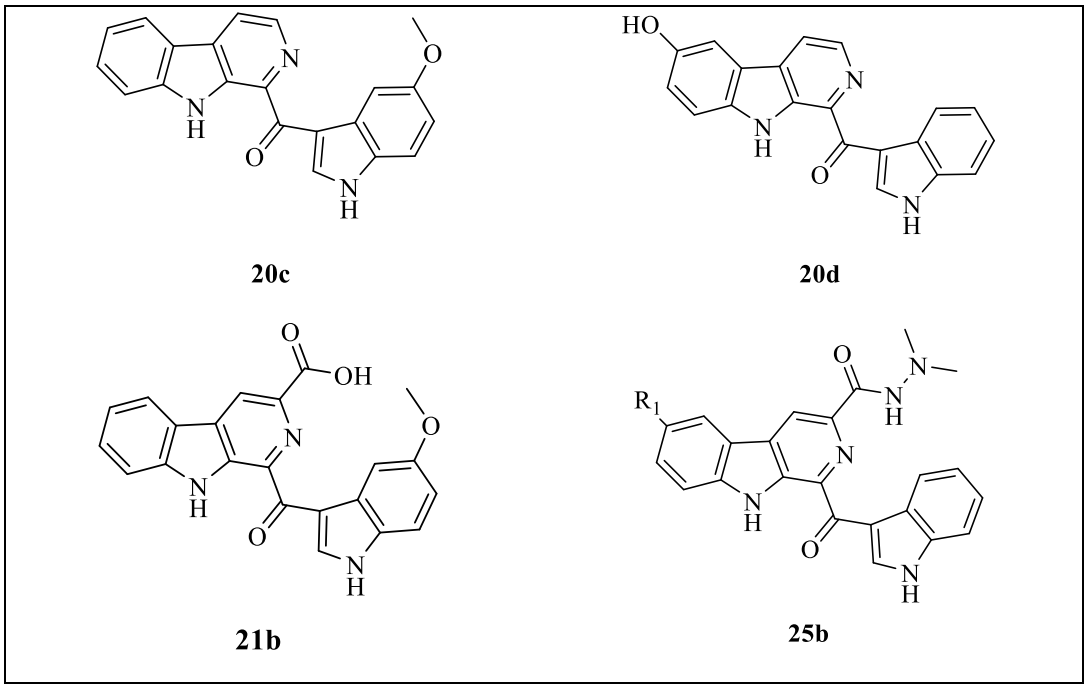

Figure 2.9 Chemical Structure of Compound **20c**, **20d**, **21b** and **25b**

2.4.6 Antiphospholipase A_2

Excessive Phospholipase A_2 enzymes can result in the formation of free fatty acids and arachidonic acid which cause the development of metabolic disorders such as obesity, diabetes, hyperlipidaemia, and fatty liver diseases (Murakami *et al.,* 2023).

The PLA_2 enzyme is also found in all groups of venomous snakes and is involved in the envenomation process (Xiao *et al.,* 2017). It may lead to coagulation problems, haemorrhage, inflammation, neuromuscular weakness, and pain (Harris & Scott-Davey, 2013). According to Dennis *et al.* (2011), various venomous species have quite varied poisonous effects. As noted, compounds **1**, **21a**, and **15a** show an anti-phospholipase A_2 activity. **1** has previously been reported to inhibit *Crotalus adamentus* (snake) venom PLA_2 with IC_{50} 14 µM (Sauleau *et al.,* 2006). In addition, alkaloids **21a** and **15a** showed weak inhibition ofphospholipase A_2 (IC_{50} =171 and 131 µM) against bee venom (*Apis mellifera*) enzyme (Liew *et al.,* 2014).

2.4.7 Antiacetylcholinesterase

Acetylcholinesterase is an enzyme that has the main role of catalyzing and facilitating the degradation of a neurotransmitter named acetylcholine (Lazarevic-Pasti *et al.,* 2017). However, the excessive of production of acetylcholine may have its effect on the central nervous system, raising health issues such as confusion, insomnia, and respiratory depression (Ailioaie *et al.,* 2023). Thus, trigonostemine G **30c**, a natural resource compound of β-carboline bearing indole was tested and found to have moderate inhibitory activity against AChE with an inhibition ratio of 31.6% (Tacrine= 51.7%) (Wang *et al.,* 2017).

2.4.8 Antidiabetic

α-Glucosidase has a role in the digestion of carbohydrates, starting with breaking them into small parts of sugar, glucose, later to be absorbed in the bloodstream (Mihaylova *et al.,* 2021). α-Glucosidase inhibitors compete with these enzymes in the body and slow down the digestion of complex carbohydrates (Kashtoh & Baek, 2022). In addition to its antioxidant, cytotoxic, antiplasmodial, and anti-phospholipase A_2 properties, Compound **1** also demonstrated moderate α-glucosidase inhibitory activity, with an IC_{50} value of 9.21 ± 0.54 μM, significantly more potent than the reference inhibitor acarbose (IC_{50} = 280.62 ± 5.0 μM).

2.4.9 Anti-inflammatory

Anti-inflammatory refers to the property of substances or treatments that reduce inflammation, which is the body's protective response to injury, infection, or harmful stimuli. Redness, swelling, discomfort, and heat are all signs of inflammation. Its goal is to get rid of the cause of tissue injury and start the healing process. Anti-inflammatory drugs stop the molecular pathways and substances that cause inflammation, like prostaglandins and cytokines (Ahuja, 2004; Al-Qahtani, 2024).

Hyrtiosulawesine, **1** was reported to have anti-inflammatory properties. According to Ha *et al.* (2022), compound **1** demonstrated anti-inflammatory activity against NO production with more than 50% when LPS stimulated RAW 264.7 cells

together with IC_{50} 175.2 ± 6.3 µM which is higher than that of the positive control (NG-methyl-l-arginine acetate- IC_{50} 36.33 ± 4.7 µM).

2.5 *In silico* Analysis of Hyrtiosulawesine Derivatives

2.5.1 Molecular Docking

Molecular Docking is a virtual screening technique that uses computer-generated three-dimensional structures of small molecules to place them in a target structure in a variety of positions, conformations, and orientations (Meng *et al.,* 2011). In detail, docking involves the interaction between a small molecule and a macromolecule, known as protein-ligand docking (Figure 2.10), and used in many drug discovery applications. Protein-ligand docking is a novel idea with numerous applications. Because of its importance in structure-based drug design, lead optimization, biochemical pathway evaluation, and De Novo drug design, so that it acts as a vivacious explore domain (Chaudhary & Mishra, 2016). Besides a simple and safe approach, molecular docking is also a low-cost tool for investigating, interpreting, explaining, and identifying molecular properties using three-dimensional structures (Raval & Ganatra, 2022). The binding mode and affinity of the complex formed are estimated using this convenient tool, which aids in the molecular recognition process docking towards the discovery of potential new drug leads (Agu *et al.,* 2023).

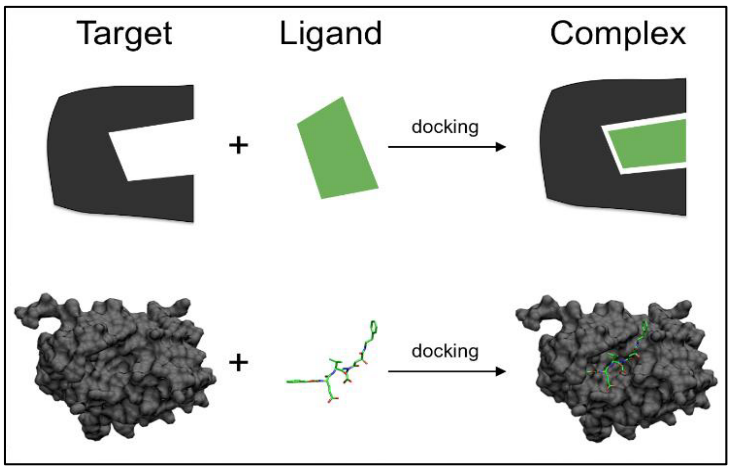

Figure 2.10 Schematic Diagram of Protein-Ligand Interactions (Dnyandev *et al.,* 2021)

Molecular Docking is frequently used to aid in the prediction of the drug candidate binding orientation to the specified groove or pocket of the target protein while investigating the affinity and activity of the small molecule. This can be accomplished using a common user-defined fitness or the docking software scoring functions of AutoDock, AutoDock Vina, and PLANTS (Raval & Ganatra, 2022). This software can help to evaluate and rank the potential binding poses of ligand molecules and protein active sites using a scoring function. Scoring functions are important in virtual screening, where large databases of chemical compounds are computationally screened to identify and help to prioritize the potential lead compounds from a vast chemical database. In addition, scoring function can also take into account of van der Waals forces, hydrogen bonding, electrostatic interactions, and desolvation effects. Even so, scoring function accuracy varies, and different scoring functions may perform better for specific protein-ligand systems or types of interactions. Still, researchers must conduct experimental assays to validate the results of molecular docking studies (Zhao *et al.,* (2025).

Several molecular docking studies were reported to investigate the antimalarial potential of β-carboline derivatives towards *P. falciparum* enzymes. As demonstrated by Jaromin *et al.* (2021), their synthesis compound of 1-substituted tetrahydro-β-carbolines were subjected to docking analysis against multiple *P. falciparum* proteins. This important enzyme includes phosphoethanolamine methyltransferase (*Pf*PMT), lactate dehydrogenase (*Pf*LDH), malate dehydrogenase (*Pf*MDH), and cysteine proteases falcipain-2 and falcipain-3. *Pf*PMT and *Pf*LDH are involved in membrane biosynthesis and energy metabolism, whereas *Pf*MDH, FP2, and FP3 are central to redox regulation and hemoglobin digestion. Inhibition of these active sites leads to disruption of essential biological processes unique to the parasite, with minimal impact on human homologs. From the docking results, it shows strong interactions between the ligand and the active sites of these enzymes (Figure 2.11), corroborating with experimentally antiplasmodial activity.

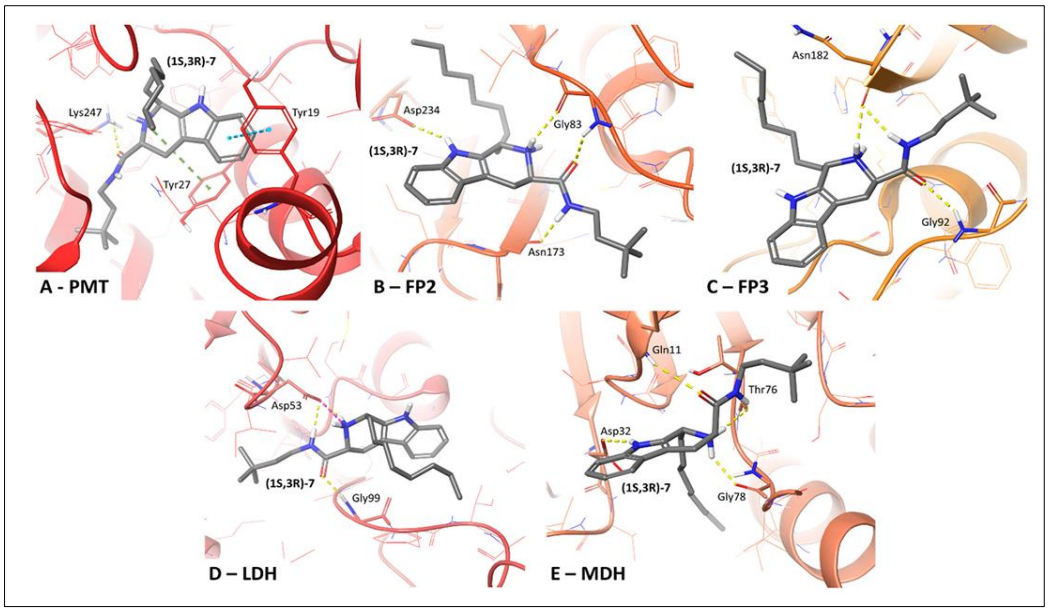

Figure 2.11 Binding Interactions Between 1-Substituted Tetrahydro-β-Carbolines Compound within Their Active Site of (A) Phosphoethanolamine Methyltransferase (PMT); (B) Falcipain-2 (FP2); (C) Falcipain-3 (FP3); (D) Lactate Dehydrogenase (LDH); and (E) Malate Dehydrogenase (MDH) within 4 Å (Jaromin *et al.,* 2021)

Similarly, Eagon *et al.* (2020) investigation on tetrahydro-β-carboline derivatives against *P. falciparum* heat-shock protein 90 (*Pf*Hsp90), revealing significant binding within its ATP-binding site. In addition, docking study by Gorki *et al.* shows good interaction on the binding pocket, rationalizing the biological activity of β-carboline analogues. This study highlights the importance of substitutions at the C-1 position in enhancing interactions with malarial targets. While examples related to hyrtiosulawesine scaffold and indole moiety at C-1 are still limited, these results collectively affirm β-carbolines as potential scaffolds for antimalarial drug development and demonstrate the efficacy of molecular docking in predicting their protein-ligand interactions.

2.5.2 Molecular Dynamics (MD) Simulation

Despite the fact that molecular docking is accurate and effective for screening purposes, there are still limitations. The disadvantages of molecular docking include imprecise binding prediction, scoring functions, and limited solvent representation. Molecular docking also presents a static view of binding while ignoring ligand binding kinetics and hence does not correctly reflect the biological environment. To address

the limitations of molecular docking, molecular dynamics (MD) was introduced. MD simulation was designed to supplement docking studies by providing a more thorough and realistic perspective of molecular interactions and behavior.

In drug development, MD plays a key role in assisting scientists in identifying weak or unstable bonds between drugs and the targets, as well as modifying chemical compounds to increase potency. Techniques such as free energy perturbation (FEP) and MM/PBSA enable researcher to objectively rank therapeutic variants, leading the selection of molecules with higher and more consistent activity. Moreover, MD can also reveal temporary binding pockets or allosteric sites, providing new options for increasing a drug's effectiveness. As a result, MD helps streamline the drug discovery process by focusing on lead compounds, minimizing unnecessary synthesis, and eventually saving time and cost (Case *et al.,* 2005).

While no published study was identified that reports MD simulations specifically on hyrtiosulawesine backbone or β-carbolines bearing an indole docked to *Plasmodium* proteins, several closely related investigations have applied MD to β-carboline scaffolds against malaria targets. A few closely comparable studies have utilized MD to β-carboline scaffolds against malaria targets, but no published study that presents molecular-dynamics simulations specifically on hyrtiosulawesine backbone or β-carbolines containing an indole that docked to *Plasmodium* proteins was found.

Earlier research by Wang *et al.* used molecular dynamics (MD) simulations to examine the stability of aminoalcohol-carbazole combinations within the *Plasmodium falciparum* Hsp90 active site. They tracked the positional deviations of atoms from the initial docked structure during the simulation by tracking Root Mean Square Deviation (RMSD) values. Additionally, the MD simulations were utilized to assess the stability of the ligand-protein complexes and to fine-tune the docking positions of *Pf*Hsp90 inhibitors. The results show from the RMSD profiles (Figure 2.12) of the aminoalcohol-carbazole analogues remain stable over time.

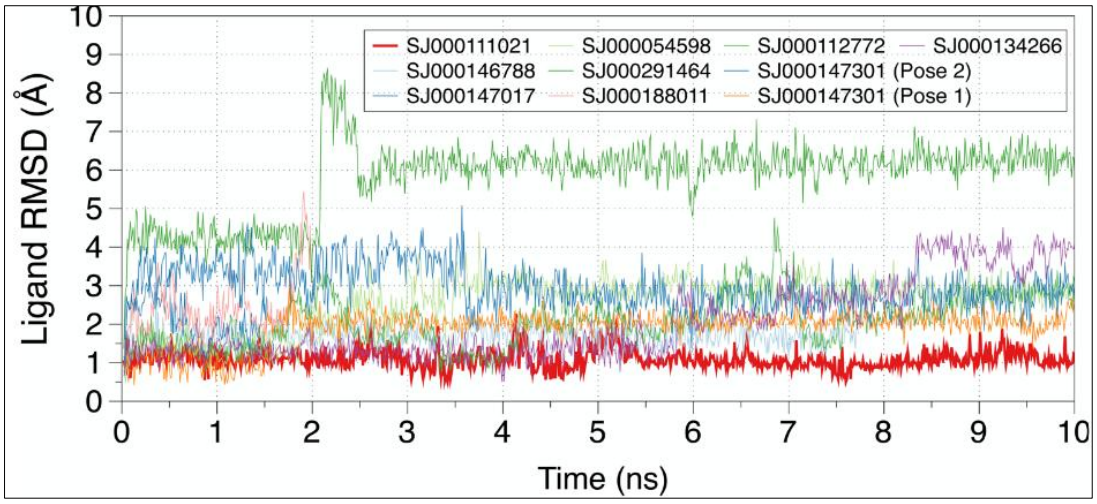

Figure 2.12 Ligand RMSD of 10 Hits Preselected Against *Pf*Hsp90 (Wang *et al.,* 2016)

In particular, Marinović and colleagues performed MD simulations on harmicine or harmine-derived β-carbolines bound to the ATP-binding pocket of *P. falciparum* Hsp90. In his study, the stability of ligand and amino acid residue were computed from binding free energies to rationalizing observed activity (Marinović *et al.,* 2020). From the data, the calculated binding free energies (ΔG_bind) for the harmicine derivatives were negative and better than that of the reference inhibitor (geldanamycin). This indicates that the harmicines form stable and energetically favorable complexes within the *Pf*Hsp90 ATP-binding site. Taken together, the literature supports the use of MD as a validating step for β-carboline hits against *Plasmodium* proteins, even though an exact MD report on 1-indolyl C-1 β-carbolines was not found.

CHAPTER 3
RESEARCH METHODOLOGY

3.1 Research Framework

This chapter outlines the methodology used in this research, encompassing the synthesis of hyrtiosulawesine and its 40 derivatives, antimalarial screening and cytotoxicity evaluation, and supported by computational analysis (Figure 3.1). The overall research framework illustrating the study workflow is presented in the following section.

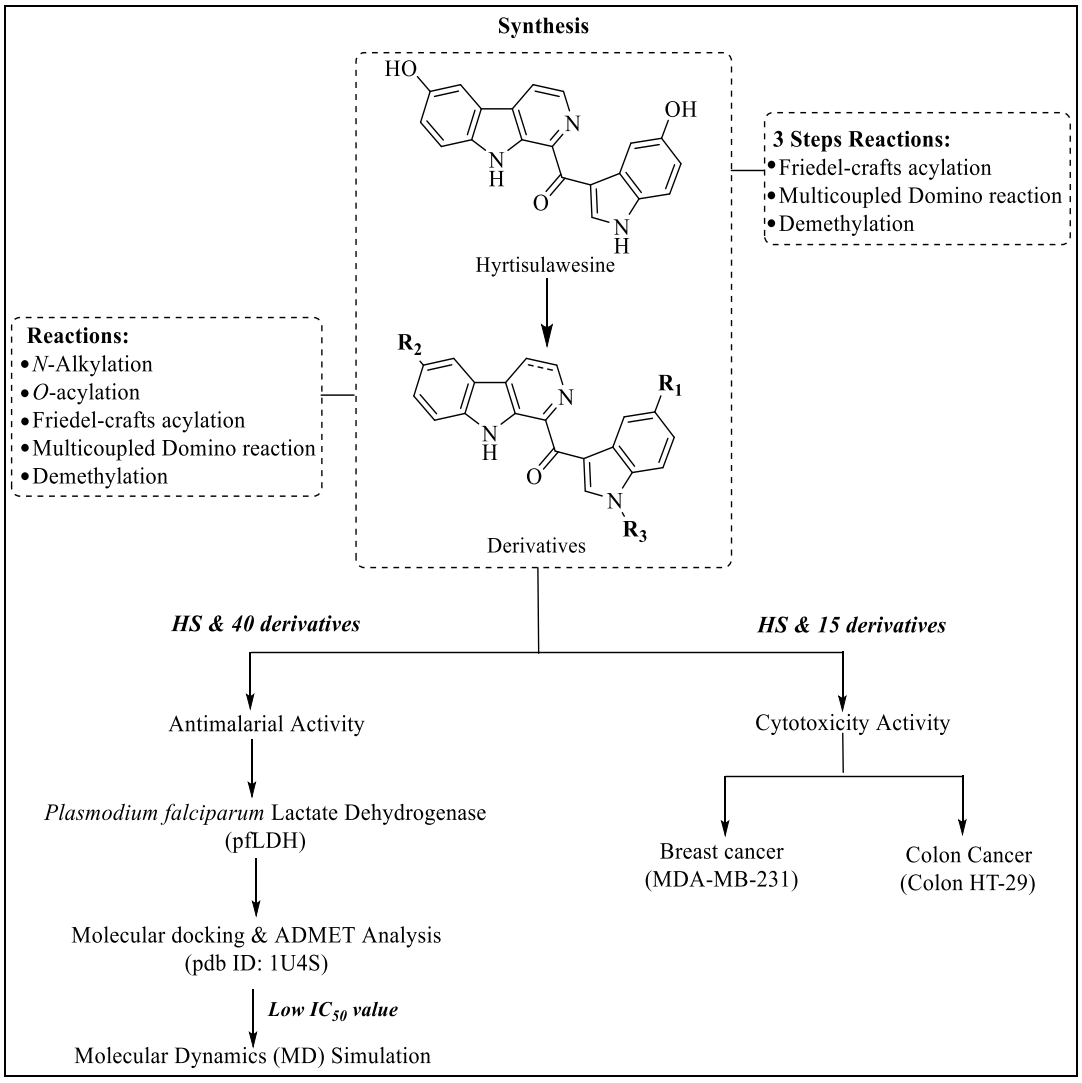

Figure 3.1 Research Framework for The Synthesis, Biological Evaluation, and Computational Analysis of Hyrtiosulawesine and Its Derivatives

3.2 General Experimental Procedure

3.2.1 Melting Points

All the solid compounds were analyzed for their melting points using electrothermal melting points apparatus or an automatic FP62 melting point apparatus from Mettler Toledo. The range values were recorded and uncorrected.

3.2.2 Infrared Spectra (IR)

Attenuated Total Reflectance-Fourier Transformed Infrared (ATR-FTIR) absorption spectra was used to identify the functional group of the isolated compounds. The absorption was recorded in the spectral range of 4000 to 400 cm^{-1} and selected frequencies (V_{max}) were reported. ATR-FTIR was chosen because it can run a broad range of sample types including liquids, solids, powders, semisolids, and pastes.

3.2.3 Chromatography Mass Spectroscopy (GC-MS)

The molecular weight of all the intermediate compounds was analyzed using GCMS Agilent Technologies 7890 A (GC System). The Agilent Technologies used was 5975C inert XLEI/CI MSD with Triple-Axis Detector. The inlet was operated in split mode (10:1 ratio) at 200 °C, with helium carrier gas at a pressure of 8.23 psi. The oven temperature program started at 60 °C, ramped to 120 °C at 3 °C/min, then to 180 °C at 1 °C/min, and finally to 250 °C at 10 °C/min. The total analysis time was 87 min.

3.2.4 Liquid Chromatography Mass Spectroscopy (LC-MS)

The mass data of the final products were obtained using reverse-phase UHPLC system coupled with Orbitrap mass spectrometry under positive ionization mode. The separation is performed using a C18 column under a gradient elution scheme, with formic acid-modified aqueous and organic mobile phases. The gradient program was: 0-30 min, 10-100% B; 30-35 min, 100% B. The injection volume was 5 µL, and UV detection was set at 210, 254, and 280 nm. The electrospray ionization interface allows

for detection under tightly controlled source conditions, optimizing ionization efficiency and sensitivity.

3.2.5 Nuclear Magnetic Resonance (NMR)

All the synthesized compounds were analyzed by proton nuclear magnetic resonance (^{1}H NMR) using JEOL NMR spectrometer instrument operating at 400 MHz. All the compounds were weighed and dissolved in deuterated solvents of $CDCl_3$, CD_3OD and C_2D_6OS depending on their solubility. Carbon spectrum was analyzed using APT nuclear magnetic resonance spectrum with JEOL NMR spectrometer instrument operating at 100 MHz.

3.3 General Procedure for The Synthesis and Characterization of Compounds

3.3.1 *O*-Acylation of 5-Hydroxyindole

3.3.1.1 Reaction of 5-Hydroxyindole, 2, With Acetyl Chloride to Produce 1H-Indol-5-yl-acetate, 57

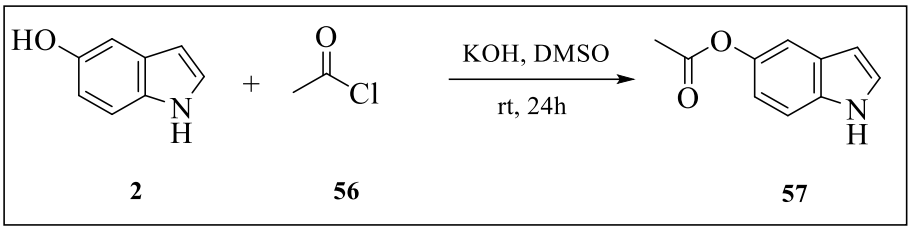

2 **56** **57**

To a stirring solution of 5-hydroxyindole (0.1 g, 0.751 mmol) in DMSO (25 mL) was added KOH (0.06 g, 1.127 mmol). The reaction mixture was stirred at room temperature for 15 min. Acetyl chloride (0.05 mL, 0.751 mmol) was then introduced to the suspension, and the mixture was left to stir for 24 h at room temperature. After the reaction was completed, water was added, and the mixture was extracted with ethyl acetate (3x). The combined organic phase was dried over Na_2SO_4 and concentrated at reduced pressure. The residue was purified by chromatography on a silica gel using hexane: ethyl acetate (1:1), (R_f value = 0.34) as eluent to give the desired product **57** as a brown solid (83% yield), m.p 111-112°C. The analytical data of compound **57**: ^{1}H

NMR (400 MHz, CD_3OD) δ 7.34 (dt, *J*= 0.8, 8.8 Hz, 1H), 7.23 (dd, *J*= 3.2, 10.8 Hz, 2H), 6.80 (dd, *J*= 2.0, 8.8 Hz, 1H), 6.42 (dd, *J*= 0.8, 3.2 Hz, 1H), 2.25 (s, 3H), N-H proton was missing due to deuterium exchange; ^{13}CNMR (100 MHz, CD_3OD): δ 171.7, 144.1, 134.2, 128.2, 125.8, 115.0, 111.8, 111.1, 101.3, 19.9. IR V_{max} (cm^{-1}): 3327 (N-H), 3012 (C-H), 1720 (C=O), 1287 (C-O). The *m/z* (%): 175.22 [M^+] calculated for $C_{10}H_9NO_2$.

3.3.1.2 Reaction of 5-Hydroxyindole, 2, With 2-Chlorobenzoyl Chloride to Produce 1H-Indol-5-yl 2-chlorobenzoate, 59

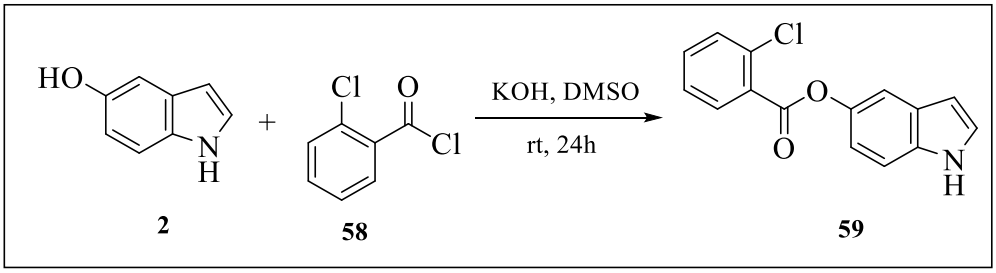

2 **58** **59**

To a stirring solution of 5-hydroxyindole (0.1 g, 0.751 mmol) in DMSO (25 mL) was added KOH (0.06 g, 1.127 mmol). The reaction mixture was stirred at room temperature for 15 min. 2-chlorobenzoyl chloride (0.1 mL, 0.751 mmol) was then introduced to the suspension, and the mixture was left to stir for 24 h at room temperature. After the reaction was completed, water was added, and the mixture was extracted with ethyl acetate (3x). The combined organic phase was dried over Na_2SO_4 and concentrated at reduced pressure. The residue was purified by chromatography on a silica gel using hexane: ethyl acetate (6:4), (R_f value = 0.40) as eluent to give the desired product **59** as a light brown crystal (90% yield), m.p 158-159°C, m.p 111-112°C. The analytical data of compound **59:** ^{1}H NMR (400 MHz, $CDCl_3$) δ 8.35 (brs, 1H), 8.06 (dd, *J*= 2.0, 7.6 Hz, 1H), 7.50 (m, 3H), 7.39 (m, 2H), 7.24 (t, *J*= 2.4 Hz, 1H), 7.06 (dd, *J*= 2.4, 8.8 Hz 1H), 6.56 (m, 1H); ^{13}CNMR (100 MHz, $CDCl_3$): δ 165.3, 144.4, 134.3, 133.9, 133.0, 131.9, 131.3, 130.0, 128.3, 126.8, 125.8, 116.1, 112.8, 111.6, 103.1. IR V_{max} (cm^{-1}): 3411 (N-H), 2989 (C-H), 1711 (C=O), 1251 (C-O). The *m/z* (%): 271.13 [M^+] calculated for $C_{15}H_{10}ClNO_2$.

3.3.1.3 Reaction of 5-Hydroxyindole, 2, With 3-Trifluoromethylbenzoyl Chloride to Produce 1H-Indol-5-yl 3-(trifluoromethyl)benzoate, 61

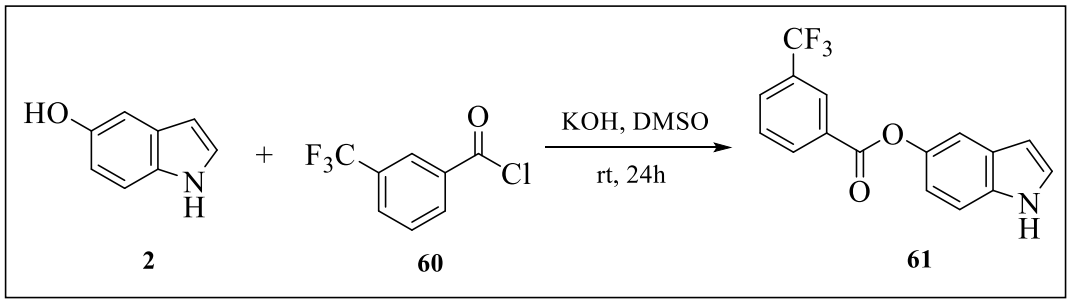

To a stirring solution of 5-hydroxyindole (0.1 g, 0.751 mmol) in DMSO (25 mL) was added KOH (0.06 g, 1.127 mmol). The reaction mixture was stirred at room temperature for 15 min. 3-trifluoromethylbenzoyl chloride (0.11 mL, 0.751 mmol) was then introduced to the suspension, and the mixture was left to stir for 24 h at room temperature. After the reaction was completed, water was added, and the mixture was extracted with ethyl acetate (3x). The combined organic phase was dried over Na_2SO_4 and concentrated at reduced pressure. The residue was purified by chromatography on a silica gel using hexane: ethyl acetate (6:4), (R_f value = 0.40) as eluent to give the desired product **61** as a white solid (87% yield), m.p 140-141°C. The analytical data of compound **61:** ^{1}H NMR (400 MHz, CD_3OD) δ 8.39 (d, *J*= 7.6 Hz, 2H), 7.94 (d, *J*= 8.8, 1H), 7.72 (t, *J*= 7.6 Hz, 1H), 7.37 (m, 2H), 7.27 (d, *J*= 3.2 Hz, 1H), 6.94 (dd, *J*= 8.8, 2.4 Hz, 1H), 6.44 (d, *J*= 3.2 Hz, 1H), N-H proton was missing due to deuterium exchange; ^{13}CNMR (100 MHz, CD_3OD): δ 164.9, 144.0, 134.4, 133.2, 131.1, 129.7, 129.7, 128.3, 126.2, 125.9, 125.3, 122.6, 114.9, 111.9, 111.3, 101.4. IR V_{max} (cm^{-1}): 3419 (N-H), 2767 (C-H), 1319 (C-F), 1713 (C=O), 1300 (C-O). The *m/z* (%): 305.11 [M^+] calculated for $C_{16}H_{10}F_3NO_2$.

3.3.1.4 Reaction of 5-Hydroxyindole, 2, With 4-Fluorobenzoyl Chloride to Produce 1H-Indol-5-yl 4-fluorobenzoate, 63

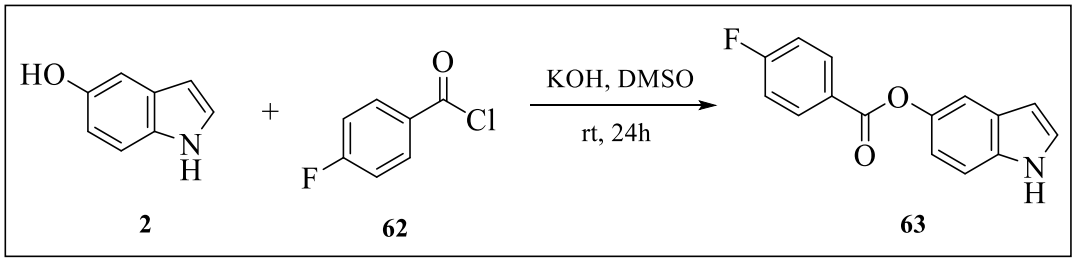

To a stirring solution of 5-hydroxyindole (0.1 g, 0.751 mmol) in DMSO (25 mL) was added KOH (0.06 g, 1.127 mmol). The reaction mixture was stirred at room temperature for 15 min. 4-fluorobenzoyl chloride (0.09 mL, 0.751 mmol) was then introduced to the suspension, and the mixture was left to stir for 24 h at room temperature. After the reaction was completed, water was added, and the mixture was extracted with ethyl acetate (3x). The combined organic phase was dried over Na_2SO_4 and concentrated at reduced pressure. The residue was purified by chromatography on a silica gel using hexane: ethyl acetate (1:1), (R_f value = 0.38) as eluent to give the desired product **63** as a light brown solid (83% yield), m.p 144-145°C. The analytical data of compound **63:** ^{1}H NMR (400 MHz, $CDCl_3$) δ 8.68 (brs, 1H), 8.24 (q, *J*= 8.8 Hz, 1H), 7.35 (m, 2H), 7.17 (m, 3H), 7.06 (t, *J*= 8.8 Hz, 1H), 6.97 (dd, *J*= 2.4, 8.8 Hz, 1H), 6.51 (m, 1H). ^{13}CNMR (100 MHz, $CDCl_3$): δ 167.4, 164.9, 144.5, 133.9, 132.9, 132.8, 128.3, 126.4, 125.9, 116.0, 115.9, 115.7, 112.8, 111.7, 102.8. IR V_{max} (cm^{-1}): 3510 (N-H), 2976 (C-H), 1712 (C=O), 1249 (C-F), 1185 (C-O). The *m/z* (%): 255.20 [M^+] calculated for $C_{15}H_{10}FNO_2$.

3.3.1.5 Reaction of 5-Hydroxyindole, 2, With 3,4,5-Trifluorobenzoyl Chloride to Produce 1H-Indol-5-yl 3,4,5-trifluorobenzoate, 65

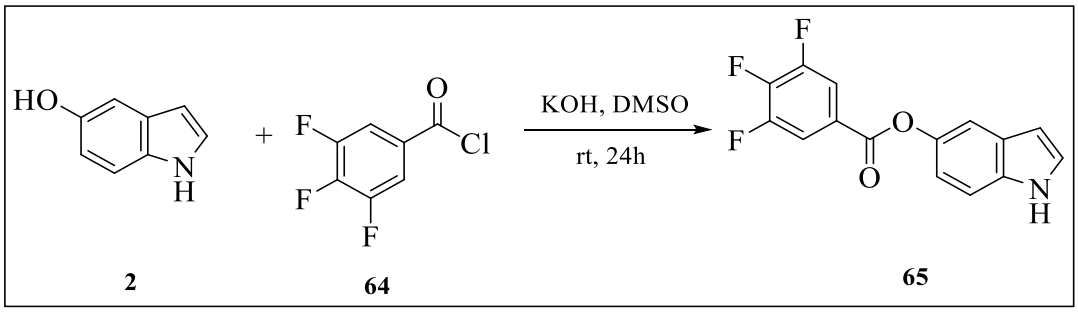

2 **64** **65**

To a stirring solution of 5-hydroxyindole (0.1 g, 0.751 mmol) in DMSO (25 mL) was added KOH (0.06 g, 1.127 mmol). The reaction mixture was stirred at room temperature for 15 min. 3,4,5-trifluorobenzoyl chloride (0.10 mL, 0.751 mmol) was then introduced to the suspension, and the mixture was left to stir for 24 h at room temperature. After the reaction was completed, water was added, and the mixture was extracted with ethyl acetate (3x). The combined organic phase was dried over Na_2SO_4 and concentrated at reduced pressure. The residue was purified by chromatography on a silica gel using hexane: ethyl acetate (7:3), (R_f value = 0.35) as eluent to give the

desired product **65** as a brown solid (59% yield), m.p 138-139°C. The analytical data of compound **65:** ^{1}H NMR (400 MHz, $CDCl_3$) δ 8.51 (brs, 1H), 8.42 (d, *J*=8.0 Hz, 1H), 7.88 (d, *J*= 6.8, 1H), 7.65 (t, *J*= 8.0 Hz, 1H), 7.45 (d, *J*= 2.4 Hz, 1H), 7.20 (m, 1H), 7.00 (dd, *J*= 2.4, 8.8 Hz, 1H), 6.54 (m, 1H); ^{13}CNMR (100 MHz, $CDCl_3$): δ 165.0, 144.3, 134.0, 133.5, 1301, 130.0, 129.3, 128.3, 127.1, 125.9, 125.1, 115.9, 112.7, 111.8, 103.0. IR V_{max} cm^{-1}: 3432 (N-H), 3010 (C-H), 1712 (C=O), 1450 (C-F), 1020 (C-O). The *m/z* (%): 291.10 [M^+] calculated for $C_{15}H_8F_3NO_2$.

3.3.1.6 Reaction of 5-Hydroxyindole, 2, With Cinnamoyl Chloride to Produce 1H-Indol-5-yl cinnamate, 67

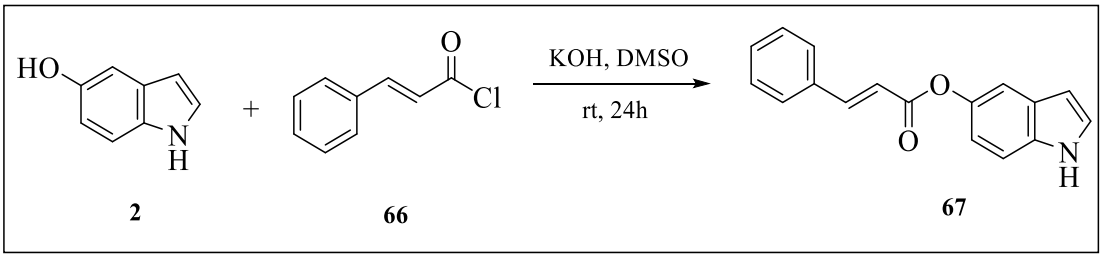

2 **66** **67**

To a stirring solution of 5-hydroxyindole (0.1 g, 0.751 mmol) in DMSO (25 mL) was added KOH (0.06 g, 1.127 mmol). The reaction mixture was stirred at room temperature for 15 min. Cinnamoyl chloride (0.13 g, 0.751 mmol) was then introduced to the suspension, and the mixture was left to stir for 24 h at room temperature. After the reaction was completed, water was added, and the mixture was extracted with ethyl acetate (3x). The combined organic phase was dried over Na_2SO_4 and concentrated at reduced pressure. The residue was purified by chromatography on a silica gel using hexane: ethyl acetate (1:1), (R_f value = 0.40) as eluent to give the desired product **67** as a green solid (80% yield), m.p 82-84°C. The analytical data of compound **67:** ^{1}H NMR (400 MHz, $CDCl_3$) δ 8.24 (brs, 1H), 7.89 (d, *J*=15.0 Hz, 1H), 7.60 (m, 2H), 7.41 (m, 5H), 7.24 (m, 1H), 6.99 (dd, *J*= 2.4, 8.8 Hz, 1H), 6.68 (d, *J*= 16 Hz, 1H), 6.55 (m, 1H); ^{13}CNMR (100 MHz, $CDCl_3$): δ 166.3, 144.6, 137.3, 133.9, 133.5, 130.3, 130.1, 129.3, 128.6, 128.5, 126.4, 125.8, 116.1, 112.8, 111.7, 105.0, 102.8. IR V_{max} cm^{-1}: 3450 (N-H), 2949 (C-H), 1700 (C=O), 1197 (C-O). The *m/z* (%): 263.12 [M^+] calculated for $C_{17}H_{13}NO_2$.

3.3.2 ***N*-alkylation of Indole**

3.3.2.1 Reaction of Indole, 36a, With Iodomethane to Produce 1-Methylindole, 37a

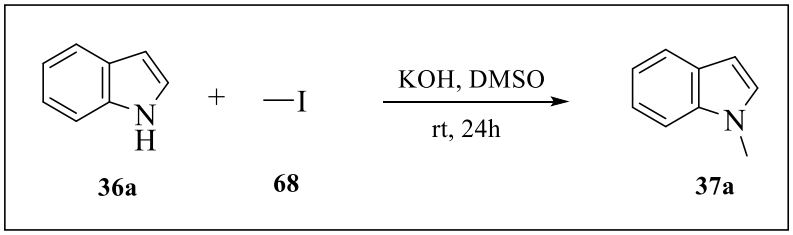

To a stirring solution of indole (0.2 g, 1.702 mmol) in DMSO (25 mL) KOH was added (0.47 g, 3.404 mmol). The reaction mixture was stirred at room temperature for 15 min. Iodomethane (0.11 mL, 1.702 mmol) was then introduced to the suspension, and the mixture was left to stir for 24 h at room temperature. After the reaction was completed, water was added, and the mixture was extracted with ethyl acetate (3x). The combined organic phase was dried over Na_2SO_4 and concentrated at reduced pressure. The residue was purified by chromatography on a silica gel using hexane: ethyl acetate (1:1), (R_f value = 0.4) as eluent to give the desired product **37a** as a white solid (90% yield), m.p 82-83°C. The analytical data of compound **37a:** ^{1}H NMR (400 MHz, C_2D_6SO) δ 7.45 (d, *J*= 7.2 Hz, 1H), 7.17 (d, *J*= 8.0 Hz, 1H), 7.05 (m, 1H), 6.94 (m, 1H), 6.90 (d, *J*= 2.8 Hz, 1H), 6.31 (d, *J*= 2.8 Hz, 1H), 3.63 (s, 3H); ^{13}CNMR (100 MHz, C_2D_6SO): δ 136.6, 128.9, 128.4, 121.3, 120.7, 119.2, 109.2, 100.8, 32.8. IR V_{max} cm^{-1}: 2877 (C-H). The *m/z* (%): 131.27 [M^+] calculated for C_9H_9N.

3.3.2.2 Reaction of Indole, 36a, With Iodoethane to Produce 1-Ethylindole, 37b

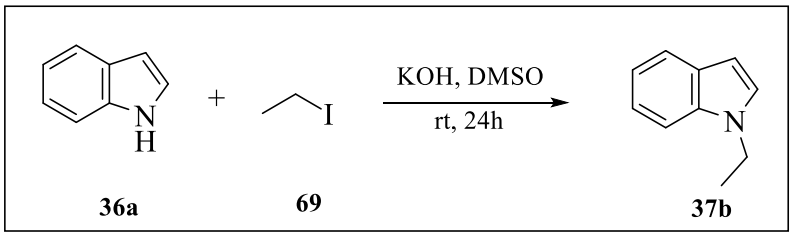

To a stirring solution of indole (0.2 g, 1.702 mmol) in DMSO (25 mL) KOH was added (0.47 g, 3.404 mmol). The reaction mixture was stirred at room temperature for 15 min. Iodoethane (0.14 mL, 1.702 mmol) was then introduced to the suspension,

and the mixture was left to stir for 24 h at room temperature. After the reaction was completed, water was added, and the mixture was extracted with ethyl acetate (3x). The combined organic phase was dried over Na_2SO_4 and concentrated at reduced pressure. The residue was purified by chromatography on a silica gel using hexane: ethyl acetate (6:4), (R_f value = 0.40) as eluent to give the desired product **37b** as a light-yellow liquid (86% yield). The analytical data of compound **37b:** ^{1}H NMR (400 MHz, C_2D_6SO) δ 7.51 (dt, *J*= 2.0, 8.0 Hz, 1H), 7.34 (dd, *J*= 0.8, 8.0 Hz, 1H), 7.16 (d, *J*= 3.2 Hz, 1H), 7.11 (m, 1H), 6.99 (m, 1H), 6.39 (dd, *J*= 0.8, 3.2 Hz, 1H), 4.12 (q, *J*= 7.2 Hz, 2H), 1.34 (t, 7.2 Hz, 3H); ^{13}CNMR (100 MHz, C_2D_6SO): δ 135.8, 128.8, 127.3, 121.1, 120.5, 118.9, 109.3, 100.5, 40.5, 14.8. IR V_{max} cm^{-1}: 2950 (C-H). The *m/z* (%): 145.32 [M^+] calculated for $C_{10}H_{11}N$.

3.3.2.3 Reaction of Indole, 36a, With 1-Iodopropane to Produce 1-Propylindole, 71

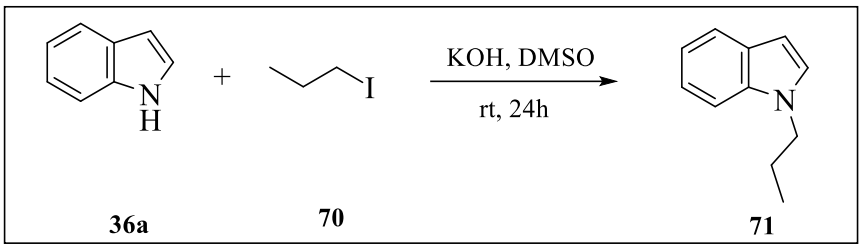

To a stirring solution of indole (0.2 g, 1.702 mmol) in DMSO (25 mL) KOH was added (0.47 g, 3.404 mmol). The reaction mixture was stirred at room temperature for 15 min. Iodopropane (0.17 mL, 1.702 mmol) was then introduced to the suspension, and the mixture was left to stir for 24 h at room temperature. After the reaction was completed, water was added, and the mixture was extracted with ethyl acetate (3x). The combined organic phase was dried over Na_2SO_4 and concentrated at reduced pressure. The residue was purified by chromatography on a silica gel using hexane: ethyl acetate (6:4), (R_f value = 0.40) as eluent to give the desired product **71** as a light-yellow (78% yield). The analytical data of compound **71:** ^{1}H NMR (400 MHz, C_2D_6SO) δ 7.50 (dt, *J*= 1.2, 7.6 Hz, 1H), 7.30 (dd, *J*= 1.2, 8.4 Hz, 1H), 7.11 (d, *J*= 2.8 Hz, 1H), 7.08 (m, 1H), 6.98 (m, 1H), 6.37 (dd, *J*= 1.2, 3.2 Hz, 1H), 4.00 (t, *J*= 8.8 Hz, 2H), 1.74 (m, 2H), 0.80 (t, *J*= 7.6 Hz, 3H); ^{13}CNMR (100 MHz, C_2D_6SO) δ 136.2, 128.8, 128.0, 121.0, 120.5, 118.8, 109.3, 100.3, 47.4, 23.4, 10.6. Anal. IR V_{max} cm^{-1}: 2870 (C-H). The *m/z* (%): 159.15 [M^+] calculated for $C_{11}H_{13}N$.

3.3.2.4 Reaction of Indole, 36a, With N-Butyl Bromide to Produce 1-Butylindole, 73

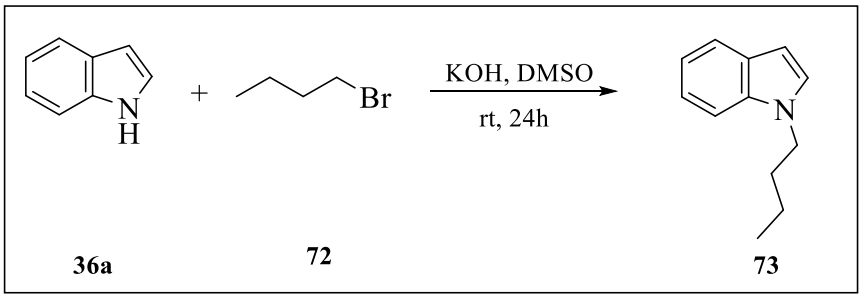

To a stirring solution of indole (0.2 g, 1.702 mmol) in DMSO (25 mL) was added KOH (0.47 g, 3.404 mmol). The reaction mixture was stirred at room temperature for 15 min. n-butyl bromide (0.18 mL, 1.702 mmol) was then introduced to the suspension, and the mixture was left to stir for 24 h at room temperature. After the reaction was completed, water was added, and the mixture was extracted with ethyl acetate (3x). The combined organic phase was dried over Na_2SO_4 and concentrated at reduced pressure. The residue was purified by chromatography on a silica gel using hexane: ethyl acetate (7:3), (R_f value = 0.36) as eluent to give the desired product **73** as a light-yellow liquid (74% yield). The analytical data of compound **73:** ^{1}H NMR (400 MHz, C_2D_6SO) δ 7.49 (dt, *J*= 1.2, 7.6 Hz, 1H), 7.25 (dd, *J*= 0.8, 8.0 Hz, 1H), 7.07 (m, 1H), 7.02 (d, 3.2 Hz, 1H), 6.97 (m, 1H), 6.36 (dd, *J*= 0.8, 3.2 Hz, 1H), 3.95 (t, *J*= 7.2 Hz, 2H), 1.63 (m, 2H), 1.17 (m, 2H), 0.81 (t, *J*= 7.6 Hz, 3H); ^{13}CNMR (100 MHz, C_2D_6SO): δ 136.1, 128.8, 127.7, 120.9, 120.4, 118.7, 109.1, 100.6, 45.5, 32.2, 19.8, 12.9. IR V_{max} cm^{-1}: 2887 (C-H). The *m/z* (%): 173.22 [M^+] calculated for $C_{12}H_{15}N$.

3.3.2.5 Reaction of Indole, 36a, With 1-Iodohexane to Produce 1-Hexylindole, 75

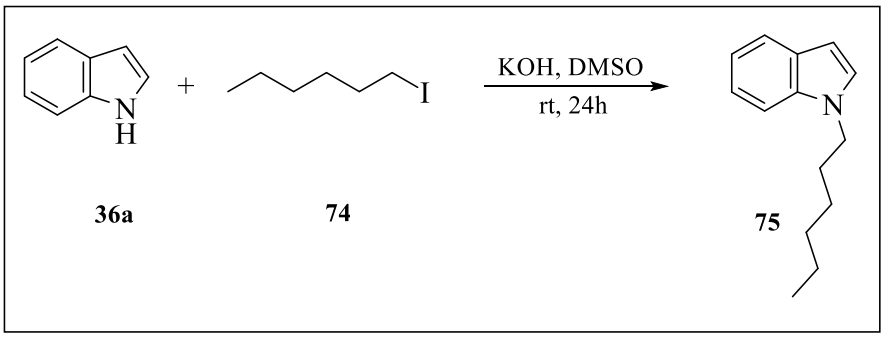

To a stirring solution of indole (0.2 g, 1.702 mmol) in DMSO (25 mL) KOH was added (0.47 g, 3.404 mmol). The reaction mixture was stirred at room temperature for 15 min. 1-Iodohexane (0.25 mL, 1.702 mmol) was then introduced to the suspension, and the mixture was left to stir for 24 h at room temperature. After the reaction was completed, water was added, and the mixture was extracted with ethyl acetate (3x). The combined organic phase was dried over Na_2SO_4 and concentrated at reduced pressure. The residue was purified by chromatography on a silica gel using hexane: ethyl acetate (7:3), (R_f value = 0.40) as eluent to give the desired product **75** as a light-yellow liquid (75% yield). The analytical data of compound **75:** ^{1}H NMR (400 MHz, CD_3OD) δ 7.52 (dt, *J*= 2.0, 7.6 Hz, 1H), 7.35 (dd, *J*= 0.8, 7.2 Hz, 1H), 7.17 (d, *J*= 3.2 Hz, 1H), 7.06 (m, 1H), 6.97 (m, 1H), 6.40 (dd, *J*= 0.8, 2.8 Hz, 1H), 3.50 (t, *J*= 6.4 Hz, 1H), 3.09 (t, *J*= 7.2 Hz, 2H), 1.66 (m, 2H), 1.24 (m, 5H), 0.86 (t, 3.2 Hz, 3H); ^{13}CNMR (100 MHz, CD_3OD): δ 136.3, 128.1, 124.3, 120.9, 120.0, 118.8, 111.0, 101.1, 61.8, 33.4, 32.4, 29.9, 22.3, 13.2. IR V_{max} cm^{-1}: 2989 (C-H). The *m/z* (%): 201.25 [M^+] calculated for $C_{14}H_{19}N$.

3.3.2.6 Reaction of Indole, 36a, With Benzyl Bromide to Produce 1-Benzylindole, 37c

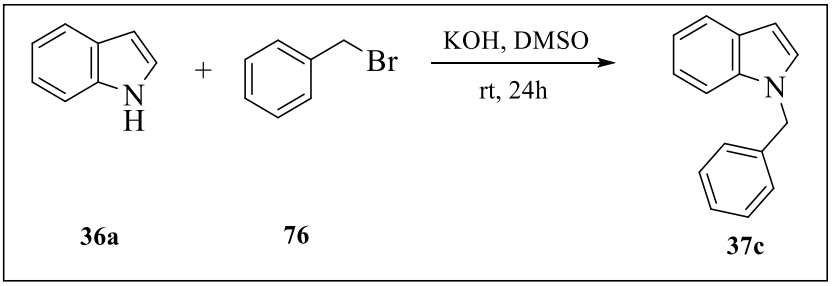

To a stirring solution of indole (0.2 g, 1.702 mmol) in DMSO (25 mL) was added KOH (0.47 g, 3.404 mmol). The reaction mixture was stirred at room temperature for 15 min. Benzyl bromide (0.20 mL, 1.702 mmol) was then introduced to the suspension, and the mixture was left to stir for 24 h at room temperature. After the reaction was completed, water was added, and the mixture was extracted with ethyl acetate (3x). The combined organic phase was dried over Na_2SO_4 and concentrated at reduced pressure. The residue was purified by chromatography on a silica gel using hexane: ethyl acetate (8:2), (R_f value = 0.38) as eluent to give the desired product **37c** as a white solid (84% yield), m.p 60-61°C. The analytical data of compound **37c:** ^{1}H NMR (400 MHz, C_2D_6SO) δ 7.52 (dt, *J*= 2.0, 7.6 Hz, 1H), 7.35 (dd, *J*= 0.8, 7.2 Hz,

1H), 7.25 (m, 3H), 7.13 (m, 2H), 7.09 (d, *J*= 3.2 Hz, 1H), 6.98 (m, 2H), 6.43 (dd, *J*=1.2, 3.2 Hz, 1H), 5.14 (s, 2H); ^{13}CNMR (100 MHz, C_2D_6SO): δ 138.2, 136.3, 129.0, 128.4, 128.2, 128.2, 127.3, 126.7, 125.5, 121.3, 120.6, 119.2, 109.7, 101.1, 49.4. IR V_{max} cm^{-1}: 2789 (C-H). The *m/z* (%): 207.17 [M^+] calculated for $C_{15}H_{13}N$.

3.3.3 Synthesis of 5-Substituted-3-acetylindole

3.3.3.1 Reaction of Indole, 36a, With Acetyl Chloride to Produce 3-Acetylindole, 77

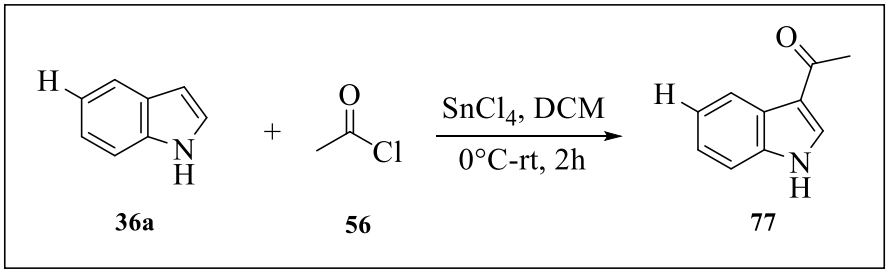

36a **56** **77**

To a stirring solution of indole (0.1 g, 0.854 mmol) in CH_2Cl_2 (20 mL) under argon at 0°C was added $SnCl_4$ (0.12 mL, 1.248mmol) in a single portion *via* syringe. The ice bath was removed, and the mixture allowed to stir at room temperature for 30 min. The acetyl chloride (0.06 mL, 0.854) was introduced in small portions to the suspension, followed by nitromethane (15 mL). The mixture was left to stir for 2 h at room temperature with progress monitored by TLC. The reaction was quenched with ice water and filtered to remove inorganic precipitates, and the organic material was extracted with ethyl acetate (3x). The organic phase was dried over Na_2SO_4 and concentrated at reduced pressure. The residue was purified by chromatography on a silica gel using hexane: ethyl acetate (6:4), (R_f value = 0.35) as eluent to give the desired product **77** as a yellow solid (87% yield) m.p 96-97°C. The analytical data of compound **77**: ^{1}H NMR (400 MHz, C_2D_6SO): δ 8.26 (s, 1H), 8.14 (d, 1H), 7.43 (d, 1H), 7.15 (m, 2H), 2.41 (s, 3H), N-H proton was missing due to deuterium exchange; ^{13}C NMR (100 MHz, C_2D_6SO): δ 193.3, 137.2, 134.9, 125.8, 123.3, 122.2, 121.8, 117.3, 112.6, 27.8. IR V_{max} cm^{-1}: 3410 (N-H), 2923 (C-H), 1669 (C=O). The *m/z* (%): 159.08 [M^+] calculated for $C_{10}H_9NO$.

3.3.3.2 Reaction of 5-Bromoindole, 36c, With Acetyl Chloride to Produce 5-Bromo-3-acetylindole, 78

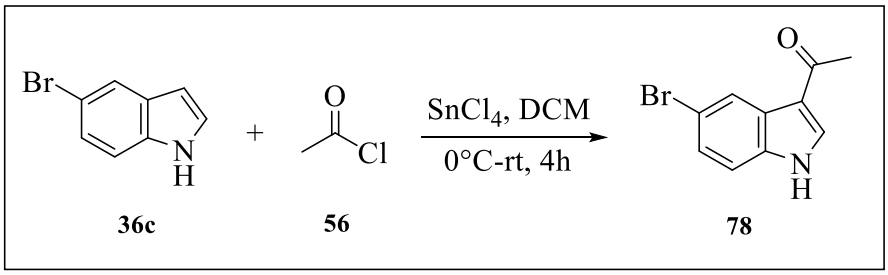

36c **56** **78**

To a stirring solution of 5-bromoindole (0.1 g, 0.510 mmol) in CH_2Cl_2 (20 mL) under argon at 0°C was added $SnCl_4$ (0.07 mL, 0.612 mmol) in a single portion *via* syringe. The ice bath was removed, and the mixture allowed to stir at room temperature for 30 min. The acetyl chloride (0.04 mL, 0.510 mmol) was introduced in small portions to the suspension, followed by nitromethane (15 mL). The mixture was left to stir for 4 h at room temperature with progress monitored by TLC. The reaction was quenched with ice water and filtered to remove inorganic precipitates, and the organic material was extracted with ethyl acetate (3x). The organic phase was dried over Na_2SO_4 and concentrated at reduced pressure. The residue was purified by chromatography on a silica gel using hexane: ethyl acetate (1:1), (R_f value = 0.34) as eluent to give the desired product **78** as a brown solid (60% yield), m.p 145-147°C.The analytical data of compound **78:** ^{1}H NMR (400 MHz, CD_3OD): δ 8.34 (s, 1H), 8.13 (s, 1H), 7.33 (m, 2H), 2.48 (s, 3H), N-H proton was missing due to deuterium exchange; ^{13}C NMR (100 MHz, CD_3OD): δ 195.0, 135.8, 135.2, 127.1, 125.8, 124.0, 116.6, 116.6, 115.2, 113.2, 25.8. IR V_{max} cm^{-1}: 3414 (N-H), 3112 (C-H), 1626 (C=O), 569 (C-Br). The *m/z* (%): 236.09 [M^+] calculated for $C_{10}H_8BrNO$.

3.3.3.3 Reaction of 5-Chloroindole, 79, With Acetyl Chloride to Produce 5-Chloro-3-acetylindole, 80

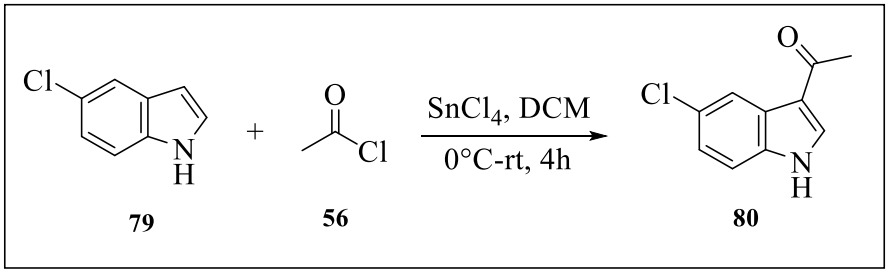

79 **56** **80**

To a stirring solution of 5-chloroindole (0.1 g, 0.660 mmol) in CH_2Cl_2 (20 mL) under argon at 0°C was added $SnCl_4$ (0.09 mL, 0.792 mmol) in a single portion *via*

syringe. The ice bath was removed, and the mixture allowed to stir at room temperature for 30 min. The acetyl chloride (0.05 mL, 0.660 mmol) was introduced in small portions to the suspension, followed by nitromethane (15 mL). The mixture was left to stir for 4 h at room temperature with progress monitored by TLC. The reaction was quenched with ice water and filtered to remove inorganic precipitates, and the organic material was extracted with ethyl acetate (3x). The organic phase was dried over Na_2SO_4 and concentrated at reduced pressure. The residue was purified by chromatography on a silica gel using hexane: ethyl acetate (1:1), (R_f value = 0.34) as eluent to give the desired product **80** as a brown solid (60% yield), m.p 150-152°C. The analytical data of compound **80:** ^{1}H NMR (400 MHz, CD_3OD): δ 8.20 (s, 1H), 8.10 (s, 1H), 7.40 (d, 1H), 7.18 (d, 1H), 2.48 (s, 3H), N-H proton was missing due to deuterium exchange. ^{13}C NMR (100 MHz, CD_3OD): δ 194.9, 135.5, 135.3, 127.7, 126.6, 123.2, 120.9, 116.7, 112.8, 25.8. IR V_{max} cm^{-1}: 3441 (N-H), 2938 (C-H), 1618 (C=O), 748 (C-Cl). The *m/z* (%): 193.04 [M^+] calculated for $C_{10}H_8ClNO$.

3.3.3.4 Reaction of 5-Fluoroindole, 81, With Acetyl Chloride to Produce 5-Fluoro-3-acetylindole, 82

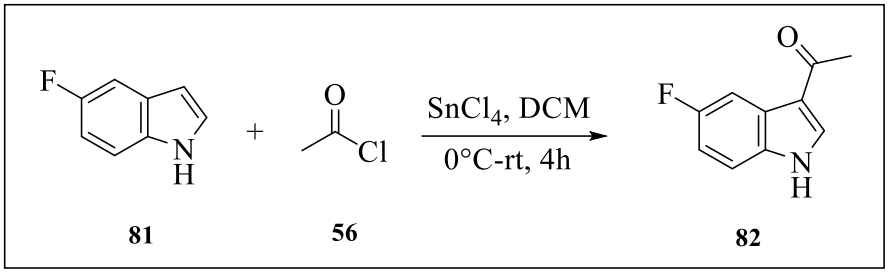

81 **56** **82**

To a stirring solution of 5-chloroindole (0.1 g, 0.740 mmol) in CH_2Cl_2 (20 mL) under argon at 0°C was added $SnCl_4$ (0.10 mL, 0.888 mmol) in a single portion *via* syringe. The ice bath was removed, and the mixture allowed to stir at room temperature for 30 min. The acetyl chloride (0.05 mL, 0.740 mmol) was introduced in small portions to the suspension, followed by nitromethane (15 mL). The mixture was left to stir for 4 h at room temperature with progress monitored by TLC. The reaction was quenched with ice water and filtered to remove inorganic precipitates, and the organic material was extracted with ethyl acetate. The organic phase was dried over Na_2SO_4 and concentrated at reduced pressure. The residue was purified by chromatography on a silica gel using hexane: ethyl acetate (1:1), (R_f value = 0.33) as eluent to give the

desired product **82** as a light brown solid (62% yield), m.p 116-117°C. The analytical data of compound **82**: ^{1}H NMR (400 MHz, CD_3OD): δ 8.16 (s, 1H), 7.84 (d, *J*= 2.4, 9.6 Hz, 1H), 7.34 (q, *J*= 4.8 Hz. 1H), 6.97 (m, 1H), 2.47 (s, 3H), N-H proton was missing due to deuterium exchange; ^{13}C NMR (100 MHz, CD_3OD): δ 195.1, 160.7, 135.7, 133.6, 126.1, 112.6, 112.6, 111.2, 106.6, 25.7. IR V_{max} cm^{-1}: 3451 (N-H), 2921 (C-H), 1620 (C=O), 1189 (C-F). The *m/z* (%): 177.07 [M^+] calculated for $C_{11}H_8FNO$.

3.3.3.5 Reaction of 5-Cyanoindole, 83, With Acetyl Chloride to Produce 5-Cyano-3-acetylindole, 84

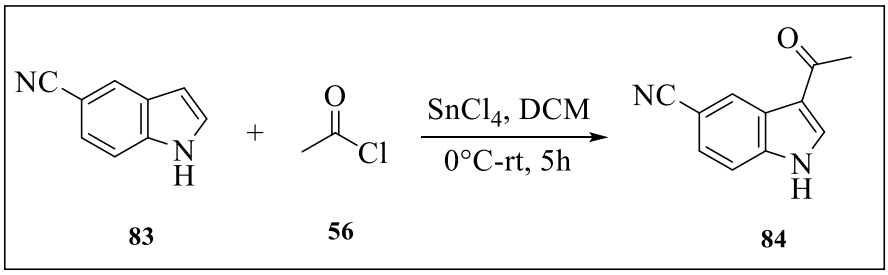

83 **56** **84**

To a stirring solution of 5-cyanoindole (0.1 g, 0.703 mmol) in CH_2Cl_2 (20 mL) under argon at 0°C was added $SnCl_4$ (0.10 mL, 0.844 mmol) in a single portion *via* syringe. The ice bath was removed, and the mixture allowed to stir at room temperature for 30 min. The acetyl chloride (0.05 mL, 0.703 mmol) was introduced in small portions to the suspension, followed by nitromethane (15 mL). The mixture was left to stir for 5 h at room temperature with progress monitored by TLC. The reaction was quenched with ice water and filtered to remove inorganic precipitates, and the organic material was extracted with ethyl acetate (3x). The organic phase was dried over Na_2SO_4 and concentrated at reduced pressure. The residue was purified by chromatography on a silica gel using hexane: ethyl acetate (1:1), (R_f value = 0.30) as eluent to give the desired product **84** as a white solid (72% yield), m.p 181-182°C. The analytical data of compound **84**: ^{1}H NMR (400 MHz, C_2D_6SO): δ 12.38 (brs, 1H), 8.59 (s, 1H), 8.31 (s, 1H), 7.58 (s, 1H), 7.50 (d, 1H), 2.52 (s, 3H). ^{13}C NMR (100 MHz, C_2D_6SO): δ 195.8, 140.8, 137.2, 133.7, 127.1, 126.6, 124.0, 118.4, 116.3, 112.1, 26.0. IR V_{max} cm^{-1}: 3423 (N-H), 2932 (C-H), 2259 (C≡N), 1611 (C=O). The *m/z* (%): 184.07 [M^+] calculated for $C_{11}H_8N_2O$.

3.3.3.6 Reaction of 5-Trifluoromethyl Indole, 85, With Acetyl Chloride to Produce 5-Trifluoromethyl-3-acetylindole, 86

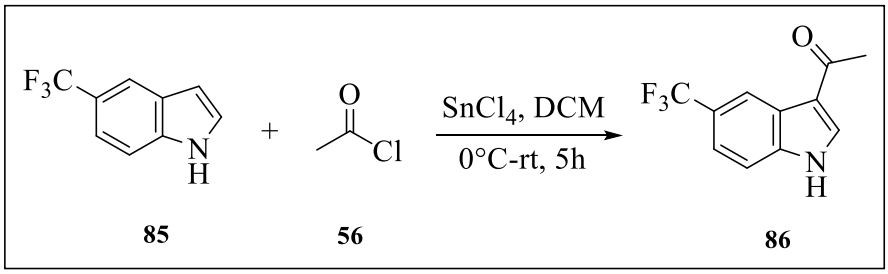

85 **56** **86**

To a stirring solution of 5-trifluoromethyl indole (0.1 g, 0.540 mmol) in CH_2Cl_2 (20 mL) under argon at 0°C was added $SnCl_4$ (0.08 mL, 0.648 mmol) in a single portion *via* syringe. The ice bath was removed, and the mixture allowed to stir at room temperature for 30 min. The acetyl chloride (0.04 mL, 0.540 mmol) was introduced in small portions to the suspension, followed by nitromethane (15 mL). The mixture was left to stir for 5 h at room temperature with progress monitored by TLC. The reaction was quenched with ice water and filtered to remove inorganic precipitates, and the organic material was extracted with ethyl acetate (3x). The organic phase was dried over Na_2SO_4 and concentrated at reduced pressure. The residue was purified by chromatography on a silica gel using hexane: ethyl acetate (1:1), (R_f value = 0.28) as eluent to give the desired product **86** as a green solid (70% yield), m.p 110-112°C. The analytical data of compound **86**: ^{1}H NMR (400 MHz, CD_3OD): δ 8.27 (s, 1H), 8.00 (s, 1H), 7.71 (d, 1H), 7.64 (d, 1H), 2.52 (s, 3H), N-H proton was missing due to deuterium exchange; ^{13}C NMR (400 MHz, CD_3OD): δ 195.3, 139.9, 133.4, 126.4, 124.7, 123.3, 117.5, 116.1, 113.9, 110.8, 25.7. IR $\bar{V}_{max}$ cm^{-1}: 3460 (N-H), 2945 (C-H), 1623 (C=O), 1428 (C=C) 1323 (C-F). The *m/z* (%): 227.07 [M^+] calculated for $C_{11}H_8F_3NO$.

3.3.3.7 Reaction of 5-Nitroindole, 87, With Acetyl Chloride to Produce 5-Nitro-3-acetylindole, 88

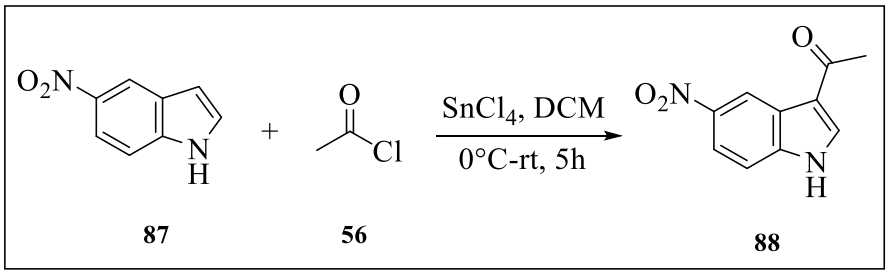

87 **56** **88**

To a stirring solution of 5-nitroindole (0.1 g, 0.617 mmol) in CH_2Cl_2 (20 mL) under argon at 0°C was added $SnCl_4$ (0.09 mL, 0.740 mmol) in a single portion via syringe. The ice bath was removed, and the mixture allowed to stir at room temperature for 30 min. The acetyl chloride (0.04 mL, 0.617 mmol) was introduced in small portions to the suspension, followed by nitromethane (15 mL). The mixture was left to stir for 5 h at room temperature with progress monitored by TLC. The reaction was quenched with ice water and filtered to remove inorganic precipitates, and the organic material was extracted with ethyl acetate (3x). The organic phase was dried over Na_2SO_4 and concentrated at reduced pressure. The residue was purified by chromatography on a silica gel using hexane: ethyl acetate (1:1), (R_f value = 0.30) as eluent to give the desired product **88** as a yellow solid (69% yield), m.p 184-185°C. The analytical data of compound **88:** ^{1}H NMR (400 MHz, C_2D_6SO): δ11.30 (brs, 1H), 8.98 (d, 1H), 8.52 (d, 1H), 8.07 (d, 1H), 7.62 (dd, *J*= 2.4, 9.2 Hz, 1H), 2.46 (s, 3H). ^{13}C NMR (100 MHz, C_2D_6SO): δ 193.5, 143.2, 140.3, 138.2, 130.6, 125.2, 118.3, 118.1, 113.3, 27.8. IR V_{max} cm^{-1}: 3436 (N-H), 2962 (C-H), 1631 (C=O), 1433 (C=C). The *m/z* (%): 204.06 [M^+] calculated for $C_{10}H_8N_2O_3$.

3.3.3.8 Reaction of 5-Methoxyindole, 36d, With Acetyl Chloride to Produce 5-Methoxy-3-acetylindole, 89

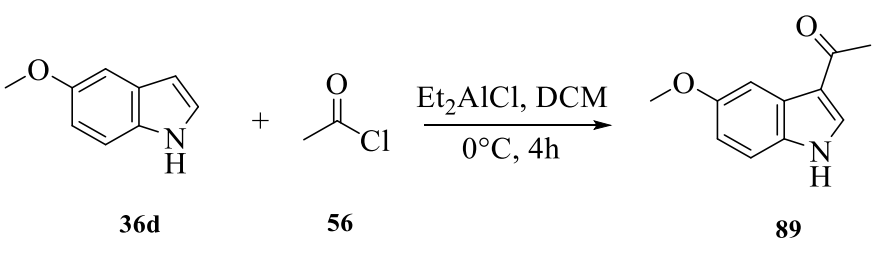

36d **56** **89**

To a stirring solution of 5-methoxyindole (0.1 g, 0.679 mmol) in CH_2Cl_2 (20 mL) under argon at 0°C was added 0.9 mol/L Et_2AlCl in hexane (0.75 mL) in a single

portion via syringe. The mixture was allowed to stir for 30 min. The acetyl chloride (0.05 mL, 0.679 mmol) in DCM was introduced in small portions to the suspension. The mixture was left to stir for 4 h maintained at 0°C with progress monitored by TLC. The reaction was quenched with pH 7 aqueous buffer to quench the reaction and filtered to obtain the product. The residue was purified by chromatography on a silica gel using hexane: ethyl acetate (6:4), (R_f value = 0.30) as eluent to give the desired product **89** as a brown solid (77% yield), m.p 129-130°C. The analytical data of compound **89**: ^{1}H NMR (400 MHz, CD_3OD): δ 8.22 (s, 1H), 7.67 (s, 1H), 7.34 (d, 1H), 6.84 (d, 1H), 3.77 (s, 3H), 2.42 (s, 3H), N-H proton was missing due to deuterium exchange. ^{13}C NMR (100 MHz, CD_3OD): δ 194.0, 153.1, 131.3, 129.9, 127.2, 116.5, 112.2, 111.1, 103.8, 60.1, 26.5. IR V_{max} cm^{-1}: 3371 (N-H), 2998 (C-H), 1677 (C=O), 1421 (C=C), 1207 (C-O). The *m/z* (%): 189.09 [M^+] calculated for $C_{11}H_{11}NO_2$.

3.3.3.9 Reaction of 5-Acetylindole, 57, With Acetyl Chloride to Produce 5-Acetyl-3-acetylindole, 90

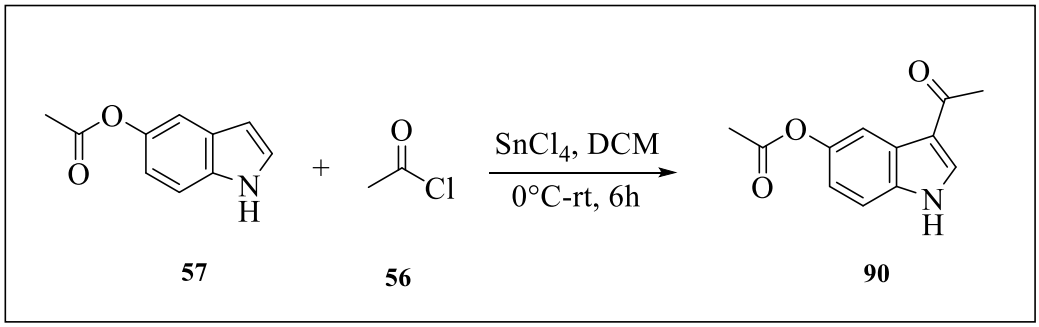

57 **56** **90**

To a stirring solution of 5-acetylindole (0.1 g, 0.571 mmol) in CH_2Cl_2 (20 mL) under argon at 0°C was added $SnCl_4$ (0.03 mL, 0.343 mmol) in a single portion via syringe. The ice bath was removed, and the mixture allowed to stir at room temperature for 30 min. The acetyl chloride (0.04 mL, 0.571 mmol) was introduced in small portions to the suspension, followed by nitromethane (15 mL). The mixture was left to stir for 6 h at room temperature with progress monitored by TLC. The reaction was quenched with ice water and filtered to remove inorganic precipitates, and the organic material was extracted with ethyl acetate (3x). The organic phase was dried over Na_2SO_4 and concentrated at reduced pressure. The residue was purified by chromatography on a silica gel using hexane: ethyl acetate (1:1), (R_f value = 0.30) as eluent to give the desired product **90** as a dark brown semi-solid (50% yield), m.p 198-

199 °C. The analytical data of compound **90:** ^{1}H NMR (400 MHz, C_2D_6SO): δ 11.81 (s, 1H), 8.23 (s, 1H), 7.68 (s, 1H), 7.36 (d, *J*= 8.8 Hz, 1H), 6.84 (dd, *J*= 2.8, 8.8 Hz, 1H), 2.49 (s, 3H), 2.78 (s, 3H); ^{13}C NMR (100 MHz, C_2D_6SO): δ 195.2, 174.8, 156.3, 134.4, 132.0, 126.3, 117.0, 113.1, 112.2, 102.6, 30.5, 25.7. IR ν_{max} cm^{-1}: 3371 (N-H), 3099 (C-H), 1726 (C=O), 1655 (C=O), 1439 (C=C), 1315 (C-O). The *m/z* (%): 217.10 [M^+] calculated for $C_{12}H_{11}NO_3$.

3.3.3.10 Reaction of 1H-Indol-5-yl 2-chlorobenzoate, 59, With Acetyl Chloride to Produce 3-Acetyl-1H-Indol-5-yl 2-chlorobenzoate, 91

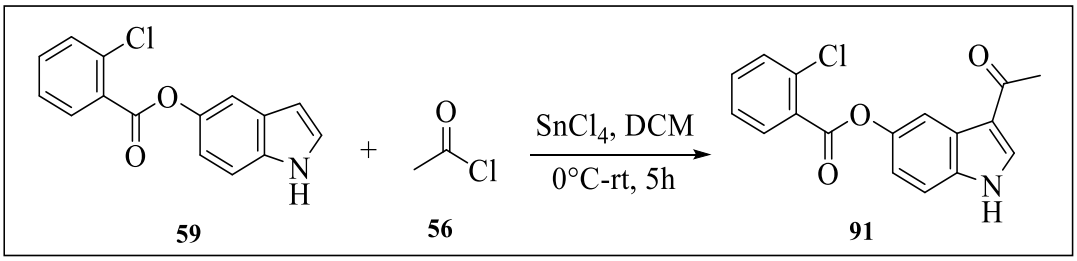

To a stirring solution of 1H-indol-5-yl 2-chlorobenzoate (0.1 g, 0.368 mmol) in CH_2Cl_2 (20 mL) under argon at 0°C was added $SnCl_4$ (0.05 mL, 0.442 mmol) in a single portion via syringe. The ice bath was removed, and the mixture allowed to stir at room temperature for 30 min. The acetyl chloride (0.03 mL, 0.368 mmol) was introduced in small portions to the suspension, followed by nitromethane (15 mL). The mixture was left to stir for 5 h at room temperature with progress monitored by TLC. The reaction was quenched with ice water and filtered to remove inorganic precipitates, and the organic material was extracted with ethyl acetate (3x). The organic phase was dried over Na_2SO_4 and concentrated at reduced pressure. The residue was purified by chromatography on a silica gel using hexane: ethyl acetate (1:1), (R_f value = 0.34) as eluent to give the desired product **91** as a white solid (78% yield) m.p 183-184°C. The analytical data of compound **91:** ^{1}H NMR (400 MHz, CD_3OD): δ 8.16 (s, 1H), 8.05 (dd, *J*= 0.4, 2.4 Hz, 1H), 8.01 (m, 1H), 7.53 (m, 1H), 7.44 (m, 3H), 7.08 (dd, *J*= 2.4, 8.88 Hz, 1H) 2.47 (s, 3H). ^{13}C NMR (100 MHz, CD_3OD): δ 195.0, 165.1, 146.4, 135.4, 135.0, 133.3, 133.1, 131.3, 130.9, 129.8, 126.9, 125.9, 117.3, 117.1, 113.9, 112.2, 25.8. IR ν_{max} cm^{-1}: 3411 (N-H), 2948 (C-H), 1727 (C=O), 1603 (C=O), 1425 (C=C), 1221 (C-O). The *m/z* (%): 313.28 [M^+] calculated for $C_{17}H_{12}NO_3$.

3.3.3.11 Reaction of 1H-Indol-5-yl 3-(trifluoromethyl)benzoate, 61, With Acetyl Chloride to Produce 3-Acetyl-1H-indol-5-yl 3-(trifluoromethyl)benzoate, 92

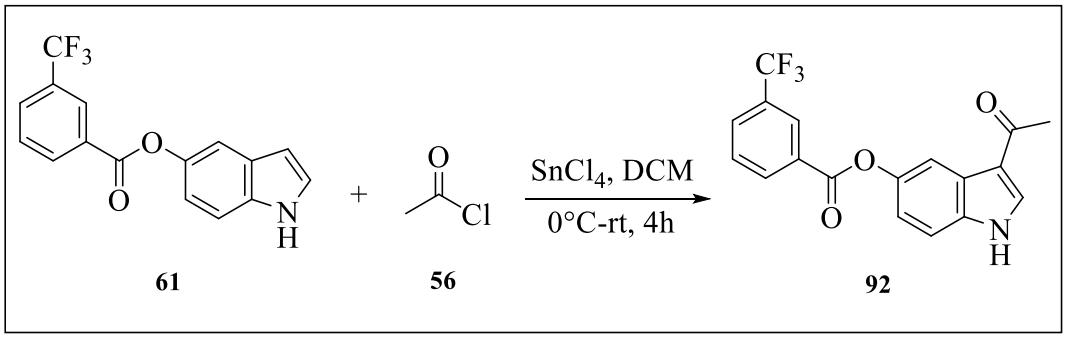

To a stirring solution of 1H-indol-5-yl 3-(trifluoromethyl) benzoate (0.1 g, 0.328 mmol) in CH_2Cl_2 (20 mL) under argon at 0°C was added $SnCl_4$ (0.05 mL, 0.393 mmol) in a single portion via syringe. The ice bath was removed, and the mixture allowed to stir at room temperature for 30 min. The acetyl chloride (0.02 mL, 0.328 mmol) was introduced in small portions to the suspension, followed by nitromethane (15 mL). The mixture was left to stir for 4 h at room temperature with progress monitored by TLC. The reaction was quenched with ice water and filtered to remove inorganic precipitates, and the organic material was extracted with ethyl acetate (3x). The organic phase was dried over Na_2SO_4 and concentrated at reduced pressure. The residue was purified by chromatography on a silica gel using hexane: ethyl acetate (1:1), (R_f value = 0.35) as eluent to give the desired product **92** as a brown solid (76% yield), m.p 189-191°C. The analytical data of compound **92:** ^{1}H NMR (400 MHz, CD_3OD): δ 8.41 (d, 2H), 8.17 (s, 1H), 8.04 (s, 1H), 7.96 (d, 1H), 7.75 (t, 1H), 7.47 (d, 1H), 7.10 (d, 1H) 2.48 (s, 3H), N-H proton was missing due to deuterium exchange. ^{13}C NMR (100 MHz, CD_3OD): δ 195.0, 164.6, 146.5, 135.5, 135.1, 133.3, 130.8, 129.8, 129.7, 126.2, 126.0, 125.2, 122.5, 117.3, 117.2, 113.9, 112.2, 25.8. IR V_{max} cm^{-1}: 3412 (N-H), 2918 (C-H), 1730 (C=O), 1653 (C=O), 1438 (C=C), 1438 (C=C), 1331 (C-O), 1223 (C-F). The *m/z* (%): 347.59 [M^+] calculated for $C_{18}H_{12}F_3NO_2$.

3.3.3.12 Reaction of 1H-indol-5-yl 4-fluorobenzoate, 63, with acetyl chloride to produce 3-acetyl-1H-indol-5-yl 4-fluorobenzoate,93

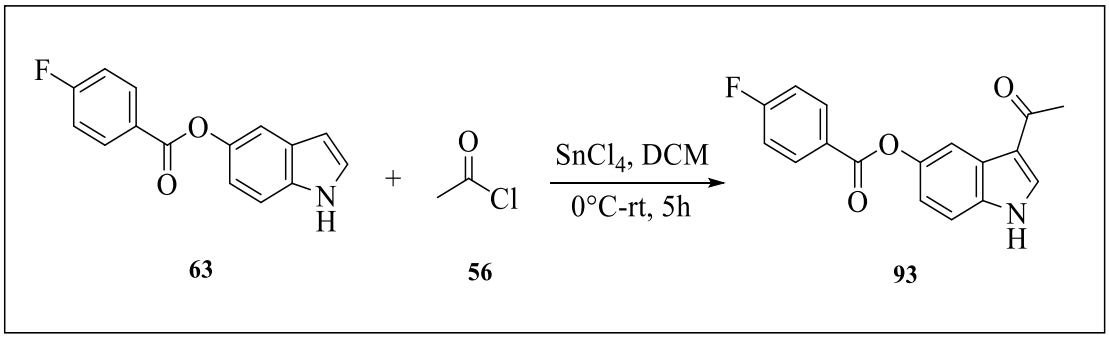

To a stirring solution of 1H-indol-5-yl 4-fluorobenzoate (0.1 g, 0.392 mmol) in CH_2Cl_2 (20 mL) under argon at 0°C was added $SnCl_4$ (0.05 mL, 0.470 mmol) in a single portion via syringe. The ice bath was removed, and the mixture allowed to stir at room temperature for 30 min. The acetyl chloride (0.03 mL, 0.392 mmol) was introduced in small portions to the suspension, followed by nitromethane (15 mL). The mixture was left to stir for 5 h at room temperature with progress monitored by TLC. The reaction was quenched with ice water and filtered to remove inorganic precipitates, and the organic material was extracted with ethyl acetate (3x). The organic phase was dried over Na_2SO_4 and concentrated at reduced pressure. The residue was purified by chromatography on a silica gel using hexane: ethyl acetate (4:6), (R_f value = 0.30) as eluent to give the desired product **93** as a cream solid (70% yield), m.p 179-180°C. The analytical data of compound **93**: ^{1}H NMR (400 MHz, CD_3OD): δ 8.19 (m, 1H), 8.03 (m, 1H), 7.37 (m, 1H), 7.23 (m, 2H), 7.13 (m, 3H), 2.44 (s, 3H), N-H proton was missing due to deuterium exchange; ^{13}CNMR (100 MHz, CD_3OD): δ 195.0, 160.7, 148.4, 136.7, 135.6, 133.6, 126.2, 126.1, 121.6, 117.1, 112.6, 112.5, 111.2, 110.9, 106.5, 106.3, 25.7. IR V_{max} cm^{-1}: 3477 (N-H), 2948 (C-H), 1727 (C=O), 1603 (C=O), 1436 (C=C), 1255 (C-O), 1227 (C-F). The *m/z* (%): 297.21 [M^+] calculated for $C_{17}H_{12}FNO_3$.

3.3.3.13 Reaction of 1H-Indol-5-yl 3,4,5-trifluorobenzoate, 65, With Acetyl Chloride to Produce 3-Acetyl-1H-indol-5-yl 3,4,5-trifluorobenzoate, 94

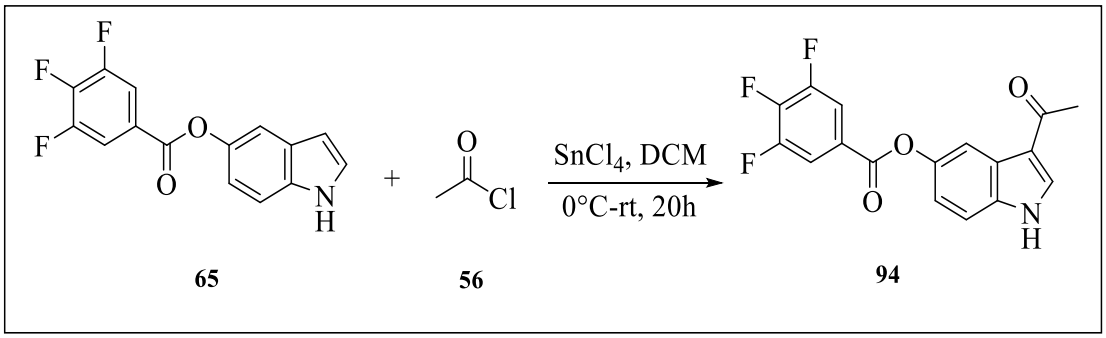

To a stirring solution of 1H-indol-5-yl 3,4,5-trifluorobenzoate (0.1 g, 0.343 mmol) in CH_2Cl_2 (20 mL) under argon at 0°C was added $SnCl_4$ (0.05 mL, 0.412 mmol) in a single portion via syringe. The ice bath was removed, and the mixture allowed to stir at room temperature for 30 min. The acetyl chloride (0.02 mL, 0.392 mmol) was introduced in small portions to the suspension, followed by nitromethane (15 mL). The mixture was left to stir for 20 h at room temperature with progress monitored by TLC. The reaction was quenched with ice water and filtered to remove inorganic precipitates, and the organic material was extracted with ethyl acetate (3x). The organic phase was dried over Na_2SO_4 and concentrated at reduced pressure. The residue was purified by chromatography on a silica gel using hexane: ethyl acetate (4:6), (R_f value = 0.30) as eluent to give the desired product **94** as a brown solid (59% yield), m.p 197-199°C. The analytical data of compound **94:** ^{1}H NMR (400 MHz, C_2D_6SO): δ 12.11 (s, 1H), 8.40 (d, *J*= 1.6 Hz, 1H), 8.08 (t, *J*= 8.0 Hz, 1H), 8.01 (s, 2H), 7.53 (d, *J*= 8.0 Hz, 1H), 7.13 (m, 1H), 2.45 (s, 3H); ^{13}CNMR (100 MHz, C_2D_6SO): δ 193.3, 163.3, 152.1, 149.7, 146.1, 144.4, 141.8, 136.3, 135.1, 126.0, 117.5, 117.4, 115.6, 115.5, 114.1, 113.3, 27.7 IR ν_{max} cm^{-1}: 3503 (N-H), 2990 (C-H), 1788 (C=O), 1687 (C=O), 1456 (C=C), 1299 (C-O), 1225 (C-F). The *m/z* (%): 333.11 [M^+] calculated for $C_{17}H_{10}F_3NO_3$.

3.3.3.14 Reaction of 1-Methyl-1H-indole, 37a, With Acetyl Chloride to Produce 1-Methyl-3-acetylindole, 95

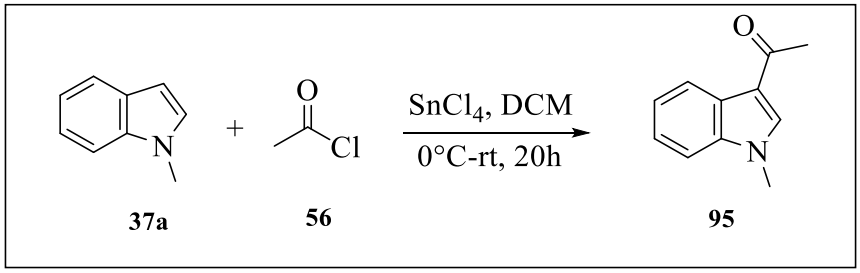

To a stirring solution of 1-methyl-1H-indole (0.1 g, 0.762 mmol) in CH_2Cl_2 (20 mL) under argon at 0°C was added $SnCl_4$ (0.11 mL, 0.915 mmol) in a single portion via syringe. The ice bath was removed, and the mixture allowed to stir at room temperature for 30 min. The acetyl chloride (0.05 mL, 0.762 mmol) was introduced in small portions to suspension, followed by nitromethane (15 mL). The mixture was left to stir for 20 h at room temperature with progress monitored by TLC. The reaction was quenched with ice water and filtered to remove inorganic precipitates, and the organic material was extracted with ethyl acetate (3x). The organic phase was dried over Na_2SO_4 and concentrated at reduced pressure. The residue was purified by chromatography on a silica gel using hexane: ethyl acetate (3:7), (R_f value = 0.35) as eluent to give the desired product **95** as a brown solid (80% yield), m.p 90-92°C. The analytical data of compound **95**: ^{1}H NMR (400 MHz, CD_3OD): δ 8.16 (m, 1H), 7.93 (s, 1H), 7.32 (m, 1H), 7.20 (m, 2H), 3.72 (s, 3H), 2.39 (s, 3H); ^{13}C NMR (100 MHz, CD_3OD): δ 194.6, 138.0, 137.8, 126.1, 123.0, 122.2, 121.7, 115.9, 109.8, 32.3, 25.9. IR V_{max} cm^{-1}: 2998 (C-H), 1676 (C=O), 1511 (C=C). The *m/z* (%): 173.22 [M^+] calculated for $C_{11}H_{11}NO$.

3.3.3.15 Reaction of 1-Ethyl-1H-indole, 37b, With Acetyl Chloride to Produce 1-Ethyl-3-acetylindole, 96

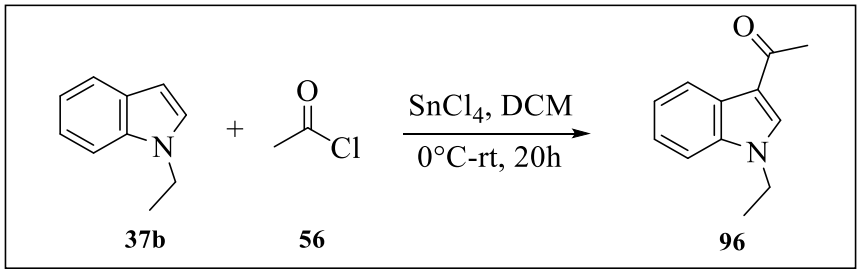

To a stirring solution of 1-ethyl-1H-indole (0.1 g, 0.689 mmol) in CH_2Cl_2 (20 mL) under argon at 0°C was added $SnCl_4$ (0.10 mL, 0.826 mmol) in a single portion via syringe. The ice bath was removed, and the mixture allowed to stir at room temperature for 30 min. The acetyl chloride (0.05 mL, 0.689 mmol) was introduced in small portions to suspension, followed by nitromethane (15 mL). The mixture was left to stir for 20 h at room temperature with progress monitored by TLC. The reaction was quenched with ice water and filtered to remove inorganic precipitates, and the organic material was extracted with ethyl acetate (3x). The organic phase was dried over Na_2SO_4 and concentrated at reduced pressure. The residue was purified by

chromatography on a silica gel using hexane: ethyl acetate (3:7), (R_f value = 0.36) as eluent to give the desired product **96** as a white solid (79% yield) m.p 94-95°C. The analytical data of compound **96:** ^{1}H NMR (400 MHz, C_2D_6SO): δ 8.27 (dd, *J*= 2.8, 7.2 Hz, 1H), 8.08 (s, 1H), 7.41 (dd, *J*= 1.6, 6.8 Hz, 1H), 7.24 (m, 2H), 4.18 (q, *J*= 14.8 Hz, 2H), 2.46 (s, 3H), 1.42 (t, *J*= 7.2 Hz, 3H); ^{13}CNMR (100 MHz, C_2D_6SO): δ 176.6, 135.8, 128.8, 127.3, 121.1, 120.5, 118.9, 109.3, 100.5, 40.5, 39.1, 14.8. IR V_{max} cm^{-1}: 2988 (C-H), 1735 (C=O), 1455 (C=C). The *m/z* (%): 187.42 [M^+] calculated for $C_{12}H_{13}NO$.

3.3.3.16 Reaction of 1-Propyl-1H-indole, 71, With Acetyl Chloride to Produce 1-Propyl-3-acetylindole, 97

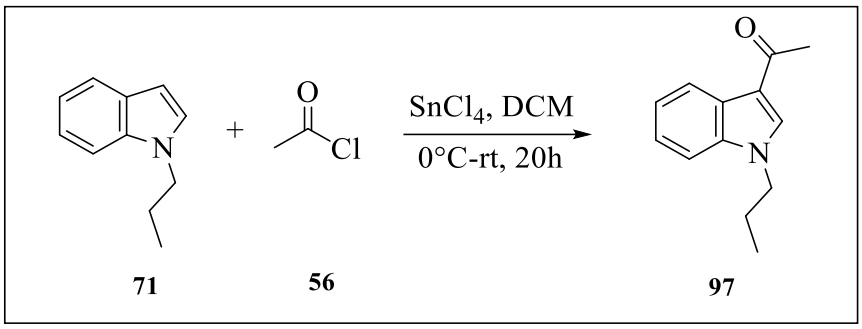

71 **56** **97**

To a stirring solution of 1-propyl-1H-indole (0.1 g, 0.628 mmol) in CH_2Cl_2 (20 mL) under argon at 0°C was added $SnCl_4$ (0.9 mL, 0.754 mmol) in a single portion via syringe. The ice bath was removed, and the mixture allowed to stir at room temperature for 30 min. The acetyl chloride (0.04 mL, 0.628 mmol) was introduced in small portions to suspension, followed by nitromethane (15 mL). The mixture was left to stir for 20 h at room temperature with progress monitored by TLC. The reaction was quenched with ice water and filtered to remove inorganic precipitates, and the organic material was extracted with ethyl acetate (3x). The organic phase was dried over Na_2SO_4 and concentrated at reduced pressure. The residue was purified by chromatography on a silica gel using hexane: ethyl acetate (3:7), (R_f value = 0.35) as eluent to give the desired product **97** as a white solid (78% yield), m.p 92-93°C. The analytical data of compound **97:** ^{1}H NMR (400 MHz, C_2D_6SO): δ 8.24 (m, 1H), 7.99 (s, 1H), 7.33 (dd, *J*= 1.6, 6.0 Hz, 1H), 7.19 (m, 2H), 4.02 (t, *J*= 7.2 Hz, 2H), 2.42 (s, 3H), 1.76 (m, 2H), 0.83 (t, *J*= 7.6 Hz, 3H); ^{13}CNMR (100 MHz, C_2D_6SO): δ 194.5, 137.1, 126.3, 123.0, 122.2, 121.9, 116.0, 110.1, 48.1, 38.7, 26.0, 22.9, 10.3. IR V_{max}

cm^{-1}: 2877 (C-H), 1715 (C=O), 5011 (C=C). The *m/z* (%): 201.44 [M^+] calculated for $C_{13}H_{15}NO$.

3.3.3.17 Reaction of 1-Butyl-1H-indole, 73, With Acetyl Chloride to Produce 1-Butyl-3-acetylindole, 98

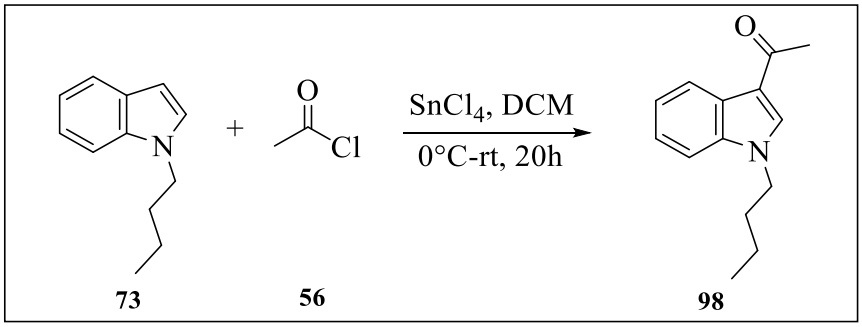

To a stirring solution of 1-butyl-1H-indole (0.1 g, 0.577 mmol) in CH_2Cl_2 (20 mL) under argon at 0°C was added $SnCl_4$ (0.8 mL, 0.693 mmol) in a single portion via syringe. The ice bath was removed, and the mixture allowed to stir at room temperature for 30 min. The acetyl chloride (0.04 mL, 0.577 mmol) was introduced in small portions to suspension, followed by nitromethane (15 mL). The mixture was left to stir for 20 h at room temperature with progress monitored by TLC. The reaction was quenched with ice water and filtered to remove inorganic precipitates, and the organic material was extracted with ethyl acetate (3x). The organic phase was dried over Na_2SO_4 and concentrated at reduced pressure. The residue was purified by chromatography on a silica gel using hexane: ethyl acetate (4:6), (R_f value = 0.30) as eluent to give the desired product **98** as a white solid (76% yield) m.p 101-102°C. The analytical data of compound **98**: ^{1}H NMR (400 MHz, CD_3OD): δ 8.26 (m, 1H), 8.01 (s, 1H), 7.43 (m, 1H), 7.19 (m, 2H), 4.00 (t, *J*= 7.2 Hz, 2H), 2.60 (s, 3H), 1.74 (m, 2H), 1.33 (m, 2H), 0.89 (t, *J* = 7.6 Hz, 3H); ^{13}CNMR (100 MHz, CD_3OD): δ 197.2, 136.8, 127.0, 123.4, 122.8, 121.7, 118.4, 111.5, 49.2, 39.2, 30.3, 22.4, 14.0, 26.7. IR V_{max} cm^{-1}: 2992 (C-H), 1720 (C=O), 1506 (C=C). The *m/z* (%): 215.24 [M^+] calculated for $C_{14}H_{17}NO$.

3.3.3.18 Reaction of 1-Hexyl-1H-indole, 75, With Acetyl Chloride to Produce 1-Hexyl-3-acetylindole, 99

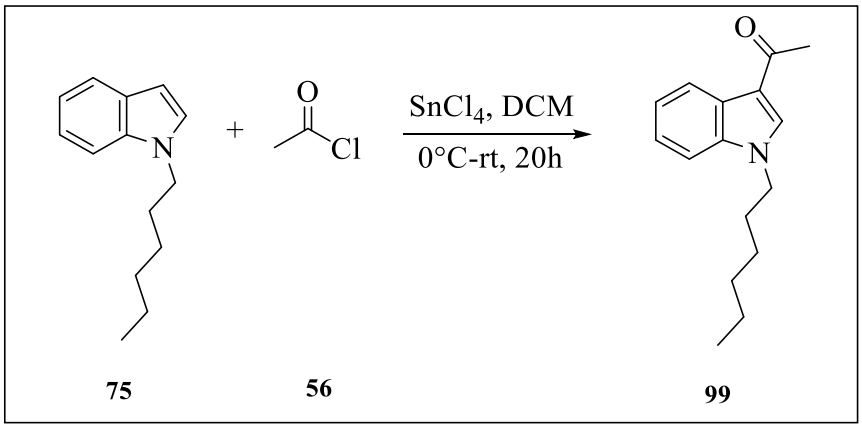

To a stirring solution of 1-hexyl-1H-indole (0.1 g, 0.497 mmol) in CH_2Cl_2 (20 mL) under argon at 0°C was added $SnCl_4$ (0.07 mL, 0.596 mmol) in a single portion via syringe. The ice bath was removed, and the mixture allowed to stir at room temperature for 30 min. The acetyl chloride (0.04 mL, 0.497 mmol) was introduced in small portions to suspension, followed by nitromethane (15 mL). The mixture was left to stir for 20 h at room temperature with progress monitored by TLC. The reaction was quenched with ice water and filtered to remove inorganic precipitates, and the organic material was extracted with ethyl acetate (3x). The organic phase was dried over Na_2SO_4 and concentrated at reduced pressure. The residue was purified by chromatography on a silica gel using hexane: ethyl acetate (4:6), (R_f value = 0.29) as eluent to give the desired product **99** as a white solid (77% yield), m.p 126-127°C. The analytical data of compound **99**: ^{1}H NMR (400 MHz, CD_3OD): δ 8.20 (m, 1H), 8.12 (s, 1H), 7.41 (m, 1H), 7.19 (m, 2H), 4.18 (t, *J*= 7.2 Hz, 2H), 2.47 (s, 3H), 1.82 (m, 2H), 1.27 (m, 6H), 0.84 (t, *J*= 6.8 Hz, 3H); ^{13}CNMR (100 MHz, CD_3OD): δ 194.7, 137.1, 126.3, 123.0, 122.1, 121.9, 117.2, 116.1, 110.0, 46.6, 31.2, 29.6, 26.2, 25.9, 22.2, 13.0. IR V_{max} cm^{-1}: 3102 (N-H), 1702 (C=O), 1447 (C=C). The *m/z* (%): 243.54 [M^+] calculated for $C_{16}H_{21}NO$.

3.3.3.19 Reaction of 1-Benzyl-1H-indole, 37c, With Acetyl Chloride to Produce 1-Benzyl-3-acetylindole, 100

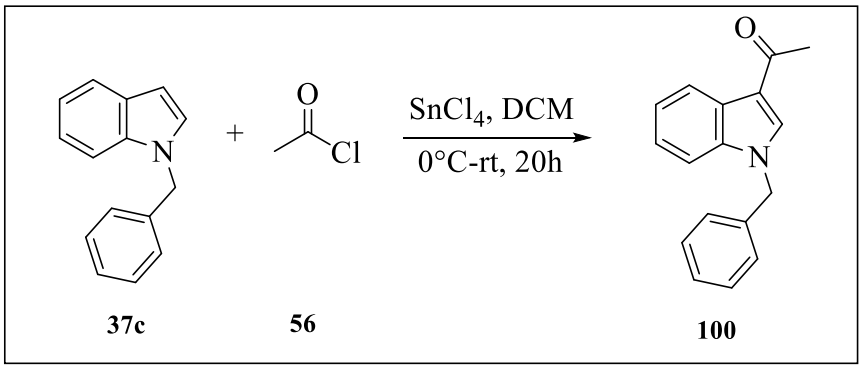

37c **56** **100**

To a stirring solution of 1-benzyl-1H-indole (0.1 g, 0.482 mmol) in CH_2Cl_2 (20 mL) under argon at 0°C was added $SnCl_4$ (0.07 mL, 0.579 mmol) in a single portion via syringe. The ice bath was removed, and the mixture allowed to stir at room temperature for 30 min. The acetyl chloride (0.03 mL, 0.482 mmol) was introduced in small portions to suspension, followed by nitromethane (15 mL). The mixture was left to stir for 20 h at room temperature with progress monitored by TLC. The reaction was quenched with ice water and filtered to remove inorganic precipitates, and the organic material was extracted with ethyl acetate. The organic phase was dried over Na_2SO_4 and concentrated at reduced pressure. The residue was purified by chromatography on a silica gel using hexane: ethyl acetate (1:1), (R_f value = 0.34) as eluent to give the desired product **100** as a white solid (75% yield) m.p 110-111°C. The analytical data of compound **100:** ^{1}H NMR (400 MHz, CD_3OD): δ 8.26 (m, 1H), 8.14 (s, 1H), 7.31 (m, 2H), 7.26 (m, 2H), 7.19 (m, 2H), 7.15 (m, 2H), 5.35 (s, 2H), 2.47 (s, 3H); ^{13}CNMR (125 MHz, CD_3OD): δ 194.8, 137.3, 137.2, 136.6, 128.6, 128.1, 127.7, 127.5, 126.8, 126.4, 123.2, 122.4, 122.0, 116.6, 110.5, 50.2, 26.1. IR V_{max} cm^{-1}: 2955 (C-H), 1699 (C=O), 1499 (C=C). The *m/z* (%): 249.23 [M^+] calculated for $C_{17}H_{15}NO$.

3.3.4 Multicoupled Domino Reaction

3.3.4.1 Reaction of 3-Acetylindole, 77, With Tryptamine to Produce (1H-Indol-3-yl)(9H-pyrido[3,4-b]indol-1-yl)methanone, 18, and (4,9-Dihydro-3H-pyrido[3,4-b]indol-1-yl)(1H-indol-3-yl)methanone, 101

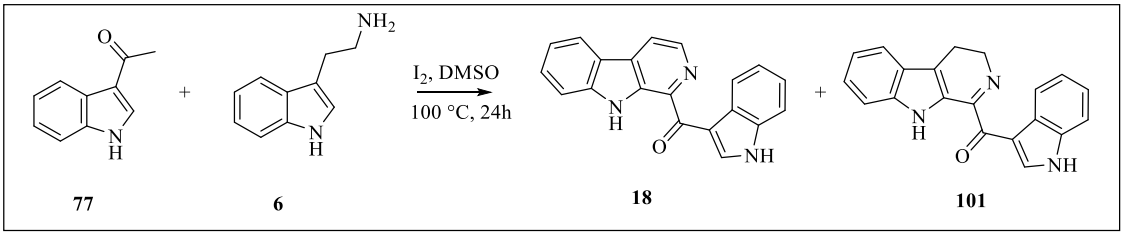

A stirred solution of 3-acetylindole (0.1 g, 0.628 mmol) in DMSO (20 mL) was treated with iodine (0.13 g, 0.503 mmol). The resulting mixture was heated at 100 °C for 2 hours, with reaction progress monitored by TLC until complete consumption of the starting material. Subsequently, tryptamine (0.1 g, 0.628 mmol) was added, and the reaction mixture was stirred at room temperature for 24 hours. After completion, the mixture was cooled to room temperature, diluted with water, and extracted with ethyl acetate (3x). The combined organic layers were washed, dried over Na_2SO_4, filtered, and concentrated under reduced pressure. The residue was purified by chromatography on a silica gel using hexane: ethyl acetate (8:2), (R_f value = 0.40) as eluent to give the desired product **18** as a yellow solid (30% yield) m.p 160-161°C. The analytical data of compound **18** ^{1}H NMR (400 MHz, C_2D_6SO) δ 12.12 (brs, 1H), 12.02 (s, 1H), 9.26 (d, *J* = 3.2 Hz, 1H), 8.56 (d, *J* = 4.8 Hz, 2H), 8.41 (d, *J* = 5.2 Hz, 1H), 8.31 (d, *J* = 7.6 Hz, 1H), 7.83 (d, *J* = 7.6 Hz, 1H), 7.60 (m, 2H), 7.29 (m, 3H); ^{13}CNMR (100 MHz, C_2D_6SO): δ 187.0, 141.2, 138.1, 137.5, 136.6, 135.6, 134.6, 130.4, 128.3, 126.8, 122.5, 121.7, 121.3, 121.3, 119.7, 119.5, 117.6, 113.8, 112.6, 111.9. IR V_{max} cm^{-1}: 3410 (N-H), 2923 (C-H), 1595 (C=O), 1421 (C=C). HR-ESI-Orbitrap-MS *m/z:* 312.1131 $[M+H]^+$ (calculated 311.1059for $C_{20}H_{13}N_3O$).

The side product of **101** observed as a yellow solid (12 % yield), m.p: 150-151°C. The analytical data of compound **101** ^{1}H NMR (400 MHz, C_2D_6OS): δ 9.73 (brs, 1H), 9.63 (s, 1H), 8.50 (d, *J* = 3.2 Hz, 1H), 8.47 (d, *J* = 6.4 Hz, 1H), 8.35 (m, 2H),7.59 (d, *J*= 8.0 Hz, 1H), 7.29 (m, 3H), 7.13 (m, 1H), 4.10 (q, *J*= 10.0 Hz, 2H), 2.97 (q, *J*= 8.0 Hz, 2H); ^{13}CNMR (100 MHz, C_2D_6OS): δ 194.2, 157.5, 136.5, 136.3, 132.2, 130.0, 126.7, 125.5, 124.9, 123.7, 123.3, 122.8, 122.3, 120.2, 118.4, 114.4, 112.5, 111.7, 48.4, 19.2. IR V_{max} cm^{-1}: 3457 (N-H), 2921 (C-H), 1685 (C=O), 1441 (C=C). HR-ESI-Orbitrap-MS *m/z:* 314.1289 $[M+H]^+$ (calculated 313.1215 for $C_{20}H_{15}N_3O$).

3.3.4.2 Reaction of 5-Chloro-3-acetylindole, 80, With Tryptamine to Produce (5-Chloro-1H-indol-3-yl)(9H-pyrido[3,4-b]indol-1-yl)methanone, 102, and (5-Chloro-1H-indol-3-yl)(4,9-dihydro-3H-pyrido[3,4-b]indol-1-yl)methanone, 103

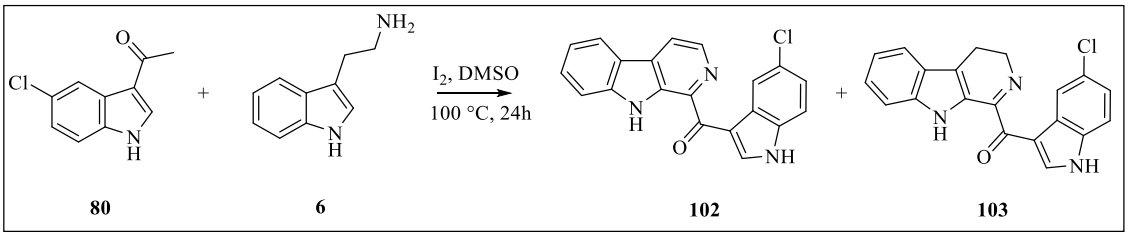

A stirred solution of 5-chloro-3-acetylindole (0.1 g, 0.516 mmol) in DMSO (20 mL) was treated with iodine (0.10 g, 0.413 mmol). The resulting mixture was heated at 100 °C for 2 hours, with reaction progress monitored by TLC until complete consumption of the starting material. Subsequently, tryptamine (0.08 g, 0.516 mmol) was added, and the reaction mixture was stirred at room temperature for 24 hours. After completion, the mixture was cooled to room temperature, diluted with water, and extracted with ethyl acetate (3x). The combined organic layers were washed, dried over Na_2SO_4, filtered, and concentrated under reduced pressure. The residue was purified by chromatography on a silica gel using hexane: ethyl acetate (7:3), (R_f value = 0.40) as eluent to give the desired product **102** as a yellow solid (42% yield) m.p 260-261 °C. The analytical data of compound **102** ^{1}H NMR (400 MHz, $CDCl_3$): δ 10.98 (brs, 1H), 10.91 (s, 1H), 9.00 (s, 1H), 8.51 (m, 2H), 8.16 (dd, *J*= 5.2, 14.8 Hz, 2H), 7.61 (d, *J*= 3.2 Hz, 2H), 7.32 (m, 2H), 7.21 (dd, *J*= 1.6, 8.0 Hz, 1H).^{13}CNMR (100 MHz, $CDCl_3$): δ 192.4, 141.3, 138.4, 138.3, 136.5, 133.0, 130.0, 128.7, 124.1, 123.8, 122.1, 121.9, 121.0, 119.6, 118.0, 115.2, 113.8, 112.9, 112.7, 112.3. IR ν_{max} cm^{-1}: 3411 (N-H), 2896 (C-H), 1601 (C=O), 1427 (C=C). HR-ESI-Orbitrap-MS *m/z* 346.0744 $[M+H]^+$ (calculated 345.0744 for $C_{20}H_{12}ClN_3O$).

The side product of **103** observed as a yellow solid (10 % yield), m.p: 256-257 °C. The analytical data of compound **103** ^{1}H NMR (400 MHz, C_2D_6OS): δ 11.96 (brs, 1H), 11.13 (brs, 1H), 9.72 (s, 1H), 8.52 (dd, *J*= 0.4, 2 Hz, 1H), 8.37 (d, *J*= 5.2 Hz, 1H), 8.27 (m, 2H), 7.56 (m, 2H), 7.24 (m, 1H), 4.00 (m, 2H), 2.89 (m, 2H); ^{13}CNMR (100 MHz, C_2D_6OS): δ 187.7, 142.1, 138.7, 137.6, 135.6, 131.4, 129.3, 129.1, 127.1, 122.3, 121.4, 120.6, 120.5, 118.8, 114.7, 114.3, 113.5, 110.9, 37.1, 29.7. IR ν_{max} cm^{-1}: 3402

(N-H), 2931 (C-H), 1623 (C=O), 1484 (C=C). HR-ESI-Orbitrap-MS *m/z:* 348.0710 $[M+H]^+$ (calculated 47.0825 for $C_{20}H_{14}ClN_3O$).

3.3.4.3 Reaction of 5-Bromo-3-acetylindole, 78, With Tryptamine to Produce (5-bromo-1H-indol-3-yl)(9H-pyrido[3,4-b]indol-1-yl)methanone, 20a, and (5-Bromo-1H-indol-3-yl)(4,9-dihydro-3H-pyrido[3,4-b]indol-1-yl)methanone, 104

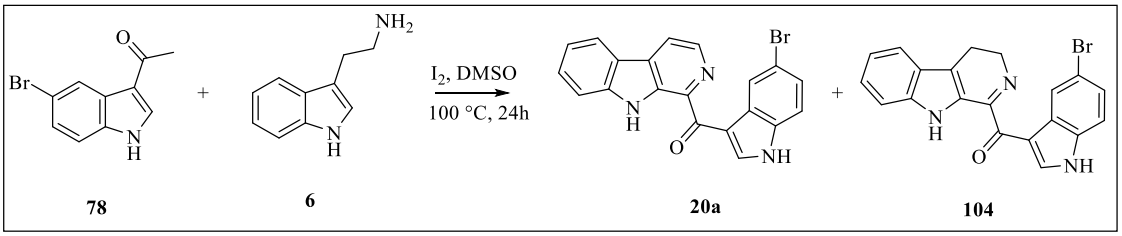

A stirred solution of 5-bromo-3-acetylindole (0.1 g, 0.420 mmol) in DMSO (20 mL) was treated with iodine (0.09 g, 0.336 mmol). The resulting mixture was heated at 100 °C for 2 hours, with reaction progress monitored by TLC until complete consumption of the starting material. Subsequently, tryptamine (0.07 g, 0.420 mmol) was added, and the reaction mixture was stirred at room temperature for 24 hours. After completion, the mixture was cooled to room temperature, diluted with water, and extracted with ethyl acetate (3x). The combined organic layers were washed, dried over Na_2SO_4, filtered, and concentrated under reduced pressure. The residue was purified by chromatography on a silica gel using hexane: ethyl acetate (7:3), (R_f value = 0.40) as eluent to give the desired product **20a** as a yellow solid (46% yield), m.p 181-182°C. The analytical data of compound **20a** ^{1}H NMR (400 MHz, C_2D_6OS): δ 12.23 (s, 1H), 11.98 (s, 1H), 9.28 (s, 1H), 8.70 (d, 2.8, 1H), 8.53 (d, *J*= 4.8 Hz, 1H) , 8.38 (d, *J*= 5.6 Hz, 1H), 8.27 (d, *J*= 8 Hz, 1H), 7.95 (m, 1H), 7.56 (m, 1H), 7.51 (d, *J*= 9.2 Hz, 1H), 7.38 (dd, 2.0, 8.4 Hz, 1H), 7.26 (m, 1H).^{13}CNMR (100 MHz, C_2D_6OS): δ 181.9, 142.2, 137.6, 135.6, 135.2, 131.4, 130.0, 129.6, 128.8, 125.9, 124.5, 122.3, 120.6, 120.5, 118.8, 118.3, 115.4, 114.9, 114.9, 113.5. IR ν_{max} cm^{-1}: 3415 (N-H), 2920 (C-H), 1600 (C=O), 1427 (C=C), 688 (C-Br). HR-ESI-Orbitrap-MS *m/z:* 390.0238 $[M+H]^+$ (calculated 389.0164 for $C_{20}H_{12}BrN_3O$).

The side product of **104** observed as a yellow solid (16% yield), m.p: 163-165°C. The analytical data of compound **104** ^{1}H NMR (400 MHz, CD_3OD) δ 12.59 (s, 1H), 13.74 (s, 1H), 9.90 (s, 1H), 9.93 (d,*J*= 2.0 Hz, 1H), 8.94 (m, 3H) , 8.81 (dd, *J*=

2.0, 8.4 Hz, 1H), 8.59 (t, *J*= 5.6 Hz, 1H), 8.44 (t, *J*= 9.2 Hz, 1H), 5.44 (t, *J*= 8.8 Hz, 2H), 4.32 (t, *J*= 9.6 Hz, 2H).^{13}CNMR (125 MHz, CD_3OD): δ 193.4, 157.7, 139.7, 137.7, 136.1, 135.9, 128.7, 127.5, 126.6, 126.2, 124.8, 124.6, 124.1, 120.0, 116.7, 115.6, 115.0, 113.5, 48.8, 19.0. IR V_{max} cm^{-1}: 3548 (N-H), 2936 (C-H), 1627 (C=O), 1434 (C=C), 679 (C-Br). HR-ESI-Orbitrap-MS *m/z:* 392.0213 $[M+H]^+$ (calculated 391.0320 for $C_{20}H_{14}BrN_3O$).

3.3.4.4 Reaction of 5-Fluoro-3-acetylindole, 82, with Tryptamine to Produce (5-Fluoro-1H-indol-3-yl)(9H-pyrido[3,4-b]indol-1-yl)methanone, 105, and (5-Fluoro-1H-indol-3-yl)(4,9-dihydro-3H-pyrido[3,4-b]indol-1-yl)methanone, 106

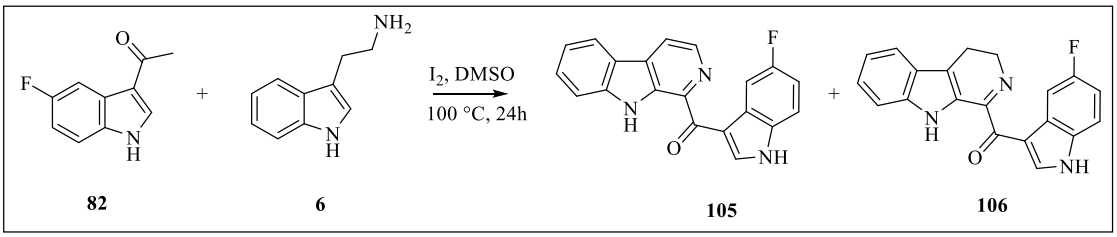

82 **6** **105** **106**

A stirred solution of 5-fluoro-3-acetylindole (0.1 g, 0.564 mmol) in DMSO (20 mL) was treated with iodine (0.11 g, 0.452 mmol). The resulting mixture was heated at 100 °C for 2 hours, with reaction progress monitored by TLC until complete consumption of the starting material. Subsequently, tryptamine (0.09 g, 0.564 mmol) was added, and the reaction mixture was stirred at room temperature for 24 hours. After completion, the mixture was cooled to room temperature, diluted with water, and extracted with ethyl acetate (3x). The combined organic layers were washed, dried over Na_2SO_4, filtered, and concentrated under reduced pressure. The residue was purified by chromatography on a silica gel using hexane: ethyl acetate (8:2), (R_f value = 0.38) as eluent to give the desired product **105** as a yellow solid (27% yield) m.p 248-250°C. The analytical data of compound **105** ^{1}H NMR (400 MHz, C_2D_6OS): δ 12.19 (brs, 1H), 11.97 (s, 1H), 9.292 (d, *J*=3.2, 1H), 8.538 (d, *J*= 4.8 Hz, 1H), 8.382 (d, *J*= 0.4 Hz, 1H), 8.276 (m, 1H), 8.196 (dd, *J*= 2.8 Hz, 1H), 7.804 (dt, *J*= 0.8, 8.0 Hz, 1H), 7.555 (m, 2H), 7.262 (m, 1H). 7.105 (m, 1H). ^{13}CNMR (100 MHz, C_2D_6OS): δ 187.0, 160.5, 158.2, 142.2, 139.8, 138.6, 137.6, 135.6, 133.1, 131.4, 129.3, 122.3, 120.6, 120.4, 118.7, 114.8, 114.0, 113.6, 111.5, 107.2. IR V_{max} cm^{-1}: 3402 (N-H), 2916 (C-H), 1632

(C=O), 1478 (C=C), 1165 (C-F). HR-ESI-Orbitrap-MS *m/z:* 330.1042 $[M+H]^+$ (calculated 329.0964 for $C_{20}H_{12}FN_3O$).

The side product of **106** observed as a yellow solid (15% yield), m.p: 237-238°C. The analytical data of compound **106** ^{1}H NMR (400 MHz, CD_3OD): δ 8.34 (s, 1H), 8.07 (dd, *J*= 2.8, 9.6 Hz, 1H), 7.55 (d, *J*= 9.2 Hz, 1H) , 7.42 (m, 2H), 7.20 (t, *J*= 8.0 Hz, 1H), 7.02 (m, 2H), 4.01 (t, *J*= 7.2 Hz, 2H), 2.97 (t, *J*= 11.2 Hz, 2H), N-H proton was missing due to deuterium exchange.^{13}CNMR (100 MHz, CD_3OD): δ 187.8, 161.0, 158.7, 138.9, 137.9, 133.5, 127.3, 126.2, 124.7, 119.6, 119.4, 117.8, 114.1, 112.8, 112.3, 111.5, 111.3, 106.9, 41.1, 39.0. IR V_{max} cm^{-1}: 3545 (N-H), 2838 (C-H), 1675 (C=O), 1501 (C=C), 1199 (C-F). HR-ESI-Orbitrap-MS *m/z:* 332.1077 $[M+H]^+$ (calculated 331.1121 for $C_{20}H_{14}FN_3O$).

3.3.4.5 Reaction of 5-Trifluoromethyl-3-acetylindole, 86, With Tryptamine to Produce (5-Ftriluoromethyl-1H-indol-3-yl)(9H-pyrido[3,4-b]indol-1-yl)methanone, 107, and (5-Trifluoromethyl-1H-indol-3-yl)(4,9-dihydro-3H-pyrido[3,4-b]indol-1-yl)methanone, 108

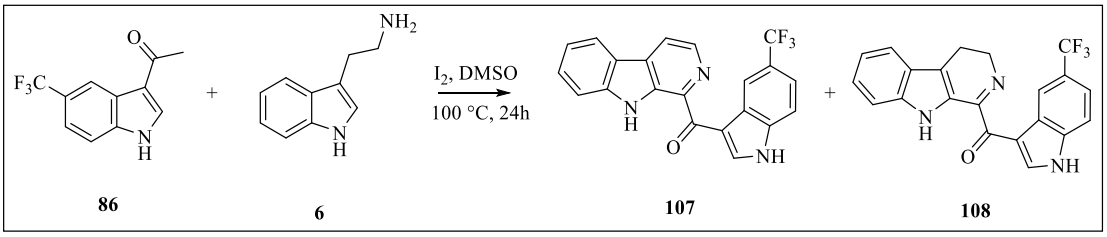

86 **6** **107** **108**

A stirred solution of 5-trifluoromethyl-3-acetylindole (0.1 g, 0.440 mmol) in DMSO (20 mL) was treated with iodine (0.09 g, 0.352 mmol). The resulting mixture was heated at 100 °C for 2 hours, with reaction progress monitored by TLC until complete consumption of the starting material. Subsequently, tryptamine (0.09 g, 0.440 mmol) was added, and the reaction mixture was stirred at room temperature for 24 hours. After completion, the mixture was cooled to room temperature, diluted with water, and extracted with ethyl acetate (3x). The combined organic layers were washed, dried over Na_2SO_4, filtered, and concentrated under reduced pressure. The residue was purified by chromatography on a silica gel using hexane: ethyl acetate (8:2), (R_f value = 0.37) as eluent to give the desired product **107** as a yellow solid (47% yield) m.p 192-193°C. The analytical data of compound **107** ^{1}H NMR (400 MHz, C_2D_6SO) δ 12.46

(brs, 1H), 12.04 (s, 1H), 9.43 (s, 1H), 8.90 (d, *J*= 1.2 Hz, 1H), 8.56 (d, *J*=5.2 Hz, 1H), 8.40 (d, *J*=4.8 Hz, 1H), 8.28 (d, *J*=7.6 Hz, 1H), 7.80 (d, *J*=8.4 Hz, 1H), 7.74 (m, 1H), 7.56 (m, 2H), 7.27 (t, *J*=7.2 Hz, 1H). ^{13}CNMR (100 MHz, C_2D_6SO) δ 180.1, 167.09, 145.24, 142.24, 140.16, 138.32, 137.69, 131.50, 129.36, 129.09, 127.29, 122.31, 121.91, 120.70, 120.54, 119.32, 118.96, 117.50, 114.61, 113.85, 113.59. IR ν_{max} cm^{-1}: 3552 (N-H), 2921 (C-H), 1623 (C=O), 1429 (C=C), 1319 (C-F). HR-ESI-Orbitrap-MS *m/z:* 380.1076 $[M+H]^+$ (calculated 379.0932 for $C_{21}H_{12}F_3N_3O$).

The side product of **108** observed as a yellow solid (11% yield), m.p: 176-177°C. The analytical data of compound **108** ^{1}H NMR (400 MHz, CD_3OD) δ 8.51 (s, 1H), 8.28 (s, 1H), 7.64 (t, *J*= 8.8 Hz, 2H) , 7.47 (m, 1H), 7.42 (m, 1H), 7.26 (m, 1H), 7.09 (t, *J*= 6.8 Hz, 1H), 4.08 (t, *J*= 8.0 Hz, 2H), 3.11 (t, *J*= 8.0, 9.6 Hz, 2H), N-H proton was missing due to deuterium exchange. ^{13}CNMR (100 MHz, CD_3OD): δ 180.1, 163.3, 153.9, 150.8, 145.1, 142.1, 135.8, 130.6, 127.4, 126.9, 120.2, 119.7, 119.1, 116.8, 115.7, 112.6, 112.5, 112.3, 112.2, 39.6, 18.7. IR ν_{max} cm^{-1}: 3574 (N-H), 2938 (C-H), 1682 (C=O), 1438 (C=C), 1319 (C-F). HR-ESI-Orbitrap-MS *m/z:* 382.0112 $[M+H]^+$ (calculated 381.1089 for $C_{21}H_{14}F_3N_3O$).

3.3.4.6 Reaction of 5-Nitro-3-acetylindole, 88, With Tryptamine to Produce (5-Ftriluoromethyl-1H-indol-3-yl)(9H-pyrido[3,4-b]indol-1-yl)methanone, 20b, and (5-Nitro-1H-indol-3-yl)(4,9-dihydro-3H-pyrido[3,4-b]indol-1-yl)methanone, 109

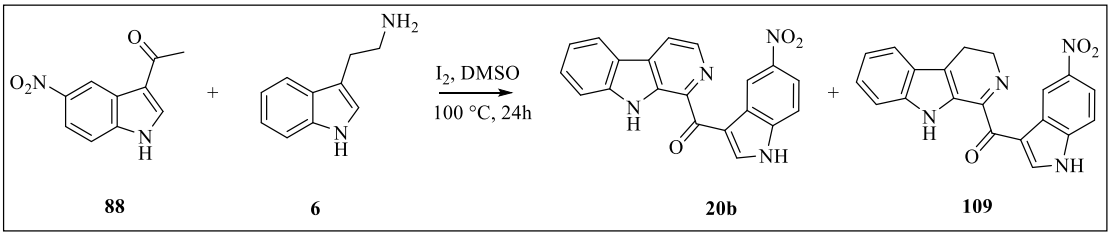

A stirred solution of 5-nitro-3-acetylindole (0.1 g, 0.490 mmol) in DMSO (20 mL) was treated with iodine (0.10 g, 0.392 mmol). The resulting mixture was heated at 100 °C for 2 hours, with reaction progress monitored by TLC until complete consumption of the starting material. Subsequently, tryptamine (0.08 g, 0.490 mmol) was added, and the reaction mixture was stirred at room temperature for 24 hours. After completion, the mixture was cooled to room temperature, diluted with water, and extracted with ethyl acetate (3x). The combined organic layers were washed, dried over

Na_2SO_4, filtered, and concentrated under reduced pressure. The residue was purified by chromatography on a silica gel using hexane: ethyl acetate (8:2), (R_f value = 0.43) as eluent to give the desired product **20b** as a yellow solid (53% yield) m.p 202-203°C. The analytical data of compound **20b** ^{1}H NMR (400 MHz, C_2D_6SO): δ 12.09 (s, 1H), 11.70 (s, 1H), 9.491 (m, 2H), 8.556 (d, *J*= 4.8 Hz, 1H), 8.407 (d, *J*= 5.2 Hz, 1H) , 8.274 (d, *J*= 7.6 Hz, 1H), 8.139 (dd, *J*=2.4, 9.2 Hz, 1H), 7.812 (d, *J*= 8.4 Hz, 1H), 7.733 (d, *J*= 9.2 Hz, 1H), 7.562 (m, 1H), 7.285 (m, 1H).^{13}CNMR (100 MHz, C_2D_6SO): δ 187.0, 149.2, 143.4, 142.3, 139.7, 137.7, 135.7, 131.6, 129.4, 127.8, 127.6, 122.7, 122.5, 122.3, 120.6, 120.5, 119.2, 119.0, 116.0, 113.6. IR V_{max} cm^{-1}: 3310 (N-H), 2852 (C-H), 1603 (C=O), 1426 (C=C), 1317 (NO_2). HR-ESI-Orbitrap-MS *m/z:* 357.0984 $[M+H]^+$ (calculated 356.0909 for $C_{20}H_{12}N_4O_3$).

The side product of **109** observed as a yellow solid (4% yield), m.p: 195-196°C. The analytical data of compound **109** ^{1}H NMR (400 MHz, C_2D_6SO) δ 12.11 (s, 1H), 11.25 (s, 1H), 9.22 (d, *J*= 2.0 Hz, 1H), 8.79 (s, 1H), 8.13 (dd, *J*= 2.4, 8.8 Hz, 1H) , 7.71 (d, *J*=9.6 Hz, 1H), 7.56 (dt, *J*= 0.8, 9.2 Hz, 1H), 7.48 (dt, *J*=0.8, 8.4 Hz, 1H), 7.17 (m, 1H), 7.01 (m, 1H), 4.04 (q, *J*= 1.2, 8.8 Hz, 2H), 2.92 (q, *J*= 2.4, 7.6 Hz, 2H).^{13}CNMR (125 MHz, C_2D_6SO): δ 187.8, 157.5, 143.6, 142.0, 140.2, 137.8, 126.5, 124.7, 124.7, 120.1, 120.0, 119.1, 118.3, 117.1, 116.1, 114.9, 113.8, 113.6, 48.9, 19.0. IR V_{max} cm^{-1}: 3421 (N-H), 2923 (C-H), 1650 (C=O), 1452 (C=C), 1375 (NO_2). HR-ESI-Orbitrap-MS *m/z* 359.1140 $[M+H]^+$ (calculated 358.1066 for $C_{20}H_{14}N_4O_3$).

3.3.4.7 Reaction of 3-Acetyl-1H-indole-5-carbonitrile, 84, With Tryptamine to Produce 3-(9H-Pyrido[3,4-b]indole-1-carbonyl)-1H-indole-5-carbonitrile, 110, and 3-(4,9-Dihydro-3H-pyrido[3,4-b]indole-1-carbonyl)-1H-indole-5-carbonitrile, 111

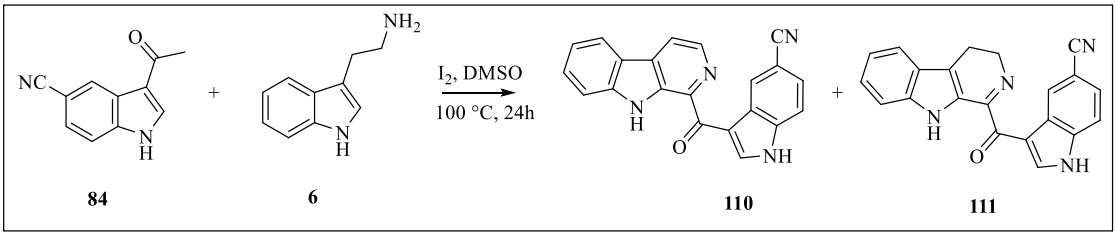

A stirred solution of 3-acetyl-1H-indole-5-carbonitrile (0.1 g, 0.543 mmol) in DMSO (20 mL) was treated with iodine (0.11 g, 0.434 mmol). The resulting mixture was heated at 100 °C for 2 hours, with reaction progress monitored by TLC until

complete consumption of the starting material. Subsequently, tryptamine (0.09 g, 0.490 mmol) was added, and the reaction mixture was stirred at room temperature for 24 hours. After completion, the mixture was cooled to room temperature, diluted with water, and extracted with ethyl acetate (3x). The combined organic layers were washed, dried over Na_2SO_4, filtered, and concentrated under reduced pressure. The residue was purified by chromatography on a silica gel using hexane: ethyl acetate (7:3), (R_f value = 0.40) as eluent to give the desired product **110** as a solid orange (50% yield), m.p 200-203°C. The analytical data of compound **110** ^{1}H NMR (400 MHz, CD_3OD): δ 13.49 (s, 1H), 10.89 (s, 1H), 10.37 (d, *J*= 2.0 Hz, 1H), 10.04 (d, *J*= 4.8 Hz, 1H) , 9.90 (d, *J*= 5.2, 1H), 9.77 (d, *J*= 6.8 Hz, 1H), 9.31 (d, *J*= 9.2, 1H), 9.22 (d, *J*= 8.4 Hz, 1H), 9.11 (dd, *J*= 1.6, 8.4 Hz, 2H), 9.06 (t, *J*= 6.0 Hz, 1H), 8.76 (t, *J*= 8.0 Hz, 1H).^{13}CNMR (100 MHz, CD_3OD): δ 197.4, 151.7, 149.8, 147.9, 147.6, 147.2, 145.1, 141.0, 138.9, 137.0, 136.7, 135.8, 131.8, 130.3, 130.0, 130.0, 128.5, 124.3, 123.9, 123.0, 114.2. IR V_{max} cm^{-1}: 3414 (N-H), 2917 (C-H), 2226 (C ≡ N), 1602 (C=O), 1424 (C=C). HR-ESI-Orbitrap-MS *m/z:* 337.1086 $[M+H]^+$ (calculated 336.1011 for $C_{21}H_{12}N_4O$).

The side product of **111** observed as a semi-solid orange (9 % yield). The analytical data of compound **111** ^{1}H NMR (400 MHz, C_2D_6SO) δ 9.93 (brs, 1H), 9.79 (s, 1H), 8.82 (t, *J*= 1.6 Hz, 1H), 8.63 (s, 1H), 7.57 (d, *J*= 4.0 Hz, 1H) , 7.47 (m, 2H), 7.42 (d, *J*= 11.2 Hz, 1H), 7.27 (m, 1H), 7.11 (m, 1H), 4.08 (t, *J*= 6.8 Hz, 2H), 2.97 (t, *J*= 7.2 Hz, 2H).^{13}CNMR (100 MHz, C_2D_6SO): δ 197.3, 157.1, 148.9, 137.0, 129.9, 127.0, 126.5, 125.1, 122.0, 120.4, 120.2, 112.4, 48.8, 26.4 IR V_{max} cm^{-1}: 3367 (N-H), 2899 (C-H), 2303 (C ≡ N), 1686 (C=O), 1462 (C=C). HR-ESI-Orbitrap-MS *m/z:* 339.1237 $[M+H]^+$ (calculated 338.1237 for $C_{21}H_{14}N_4O$).

3.3.4.8 Reaction of 5-Methoxy-3-acetylindole, 89, With Tryptamine to Produce (5-Methoxy-1H-indol-3-yl)(9H-pyrido[3,4-b]indol-1-yl)methanone, 20c, and (5-Methoxy-1H-indol-3-yl)(4,9-dihydro-3H-pyrido[3,4-b]indol-1-yl)methanone, 112

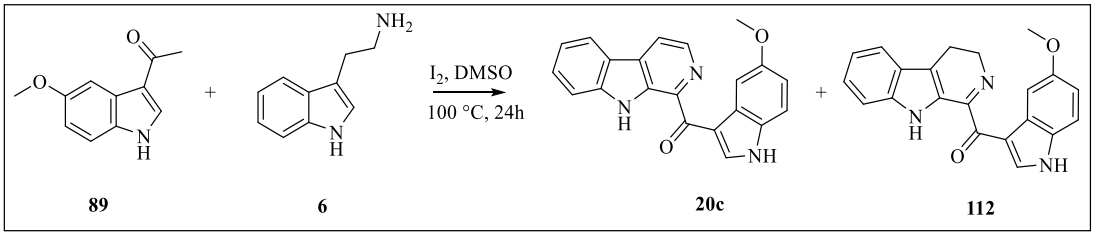

89 6 20c 112

A stirred solution of 5-methoxy-3-acetylindole (0.1 g, 0.529 mmol) in DMSO (20 mL) was treated with iodine (0.11 g, 0.423 mmol). The resulting mixture was heated at 100 °C for 2 hours, with reaction progress monitored by TLC until complete consumption of the starting material. Subsequently, tryptamine (0.08 g, 0.529 mmol) was added, and the reaction mixture was stirred at room temperature for 24 hours. After completion, the mixture was cooled to room temperature, diluted with water, and extracted with ethyl acetate (3x). The combined organic layers were washed, dried over Na_2SO_4, filtered, and concentrated under reduced pressure. The residue was purified by chromatography on a silica gel using hexane: ethyl acetate (7:3), (R_f value = 0.38) as eluent to give the desired product **20c** as a yellow solid (28% yield), m.p 190-192°C. The analytical data of compound **20c** ^{1}H NMR (400 MHz, C_2D_6SO) δ 11.98 (s, 1H), 11.19 (s, 1H), 9.19 (s, 1H), 8.52 (d, *J*= 4.8 Hz, 1H), 8.36 (d, *J*= 5.2 Hz, 1H) , 8.26 (d, *J*= 7.6 Hz, 1H), 8.07 (d, *J*= 2.8 Hz, 1H), 7.81 (d, *J*= 7.6 Hz, 1H), 7.54 (t, *J*= 7.6 Hz, 1H), 7.42 (d, *J*= 8.8 Hz, 1H), 7.25 (d, *J*= 2.8 Hz, 1H), 6.86 (dd, *J*= 2.8, 9.2 Hz, 1H), 3.81 (s, 3H).^{13}CNMR (100 MHz, C_2D_6SO): δ 187.8, 156.2, 153.9, 142.2, 142.1, 138.8, 135.6, 132.5, 131.4, 131.3, 128.9, 128.6, 122.9, 121.0, 120.6, 119.9, 116.3, 114.7, 114.5, 112.6, 111.4, 51.3. IR V_{max} cm^{-1}: 3423 (N-H), 1579 (C=O), 1487 (C=C), 1206 (C-O). HR-ESI-Orbitrap-MS *m/z:* 342.1241 $[M+H]^+$ (calculated 341.1164 for $C_{21}H_{15}N_3O_2$).

The side product of **112** observed as a yellow solid (15 % yield), m.p: 183-184°C. The analytical data of compound **112** ^{1}H NMR (400 MHz, C_2D_6SO) δ 12.08 (brs, 1H), 11.23 (s, 1H), 8.42 (d, *J*= 3.2 Hz, 1H), 7.85 (d, *J*= 2.8 Hz, 1H), 7.56 (d, *J*= 8.0 Hz, 1H) , 7.28 (m, 2H), 7.17 (t, *J*= 7.2 Hz, 1H), 7.01 (t, *J*= 7.2 Hz, 1H), 6.87 (dd, *J*= 2 Hz, 1H), 3.99 (t, *J*= 7.6 Hz, 2H), 2.92 (t, *J*= 9.6 Hz, 2H), 3.78 (s, 3H).^{13}CNMR (100 MHz, C_2D_6SO) δ 186.9, 158.2, 156.4, 149.1, 139.0, 138.0, 133.0, 131.8, 130.7, 127.7, 127.5, 126.5, 125.0, 124.8, 122.5, 120.3, 113.9, 113.7, 103.7, 50.2, 48.3, 25.9. IR V_{max} cm^{-1}: 3428 (N-H), 2924 (C-H), 1610 (C=O), 1488 (C=C), 1207 (C-O). HR-ESI-Orbitrap-MS *m/z* 344.1034 $[M+H]^+$ (calculated 343.1321 for $C_{21}H_{17}N_3O_2$).

3.3.4.9 Reaction of 5-Methoxy-3-acetylindole, 89, With 5-Methoxytryptamine to Produce (5-Methoxy-1H-indol-3-yl)(6-methoxy-9H-pyrido[3,4b]indol1yl)methanone 53

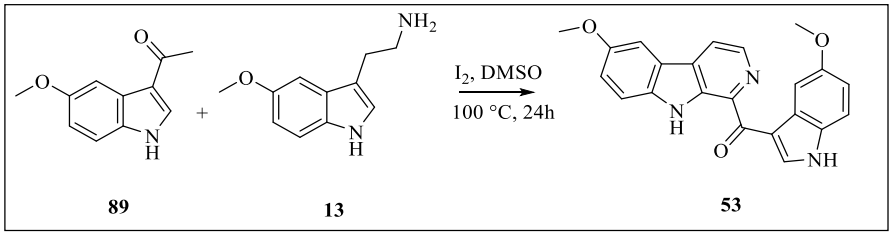

A stirred solution of 5-methoxy-3-acetylindole (0.1 g, 0.529 mmol) in DMSO (20 mL) was treated with iodine (0.11 g, 0.423 mmol). The resulting mixture was heated at 100 °C for 2 hours, with reaction progress monitored by TLC until complete consumption of the starting material. Subsequently, tryptamine (0.10 g, 0.529 mmol) was added, and the reaction mixture was stirred at room temperature for 24 hours. After completion, the mixture was cooled to room temperature, diluted with water, and extracted with ethyl acetate (3x). The combined organic layers were washed, dried over Na_2SO_4, filtered, and concentrated under reduced pressure. The residue was purified by chromatography on a silica gel using hexane: ethyl acetate (7:3), (R_f value = 0.40) as eluent to give the desired product **53** as a yellow solid (47% yield) m.p 206-207°C.

The analytical data of compound **53** ^{1}H NMR (600 MHz, CD_3OD): δ 8.90 (s, 1H), 8.43 (d, *J* = 6 Hz, 1H), 8.16 (d, *J* = 6.6 Hz, 1H), 8.03 (d, *J* = 3.0 Hz, 1H), 7.58 (d, *J* = 3.0 Hz, 1H), 7.56 (d, *J*= 10.8 Hz, 1H), 7.33 (d, *J*= 10.2 Hz, 1H), 7.15 (dd, *J*= 3.0 Hz, 1H), 6.83 (dd, *J*= 3.0 Hz, 1H), 3.95 (s, 3H), 3.93 (s, 3H), N-H proton was missing due to deuterium exchange; ^{13}CNMR (150 MHz, CD_3OD): δ 189.92, 154.45, 152.66, 140.38, 139.12, 137.54, 137.38, 137.36, 132.49, 132.38, 129.87, 122.64, 119.86, 118.44, 117.2, 116.09, 113.88, 113.27, 108.06, 106.83, 54.9, 54.6. IR V_{max} cm^{-1}: 3749 (N-H), 2922 (C-H), 1729 (C=O), 1487 (C=C), 1207 (C-O). HR-ESI-Orbitrap-MS *m/z* 372.1342 $[M+H]^+$ (calculated 371.2701 for $C_{22}H_{17}N_3O_3$).

3.3.4.10 Reaction of 3-Acetyl-1H-indol-5-yl acetate, 90, With Tryptamine to Produce 3-(9H-Pyrido[3,4-b]indole-1-carbonyl)-1H-indol-5-yl acetate, 113, and 3-(4,9-Dihydro-3H-pyrido[3,4-b]indole-1-carbonyl)-1H-indol-5-yl acetate, 114

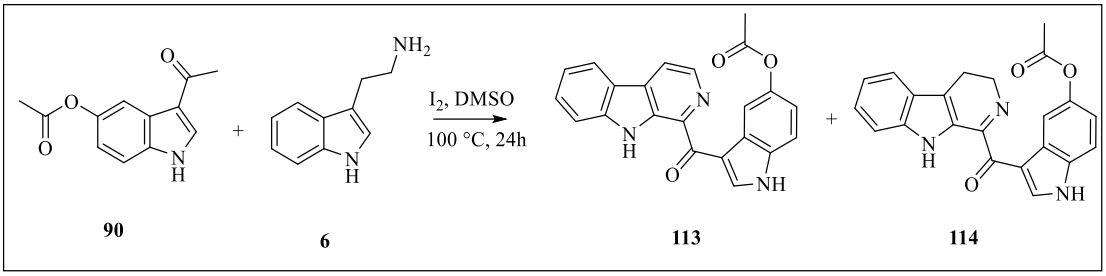

90 **6** **113** **114**

A stirred solution of 3-acetyl-1H-indol-5-yl acetate (0.1 g, 0.460 mmol) in DMSO (20 mL) was treated with iodine (0.09 g, 0.368 mmol). The resulting mixture was heated at 100 °C for 2 hours, with reaction progress monitored by TLC until complete consumption of the starting material. Subsequently, tryptamine (0.07 g, 0.460 mmol) was added, and the reaction mixture was stirred at room temperature for 24 hours. After completion, the mixture was cooled to room temperature, diluted with water, and extracted with ethyl acetate (3x). The combined organic layers were washed, dried over Na_2SO_4, filtered, and concentrated under reduced pressure. The residue was purified by chromatography on a silica gel using hexane: ethyl acetate (8:2), (R_f value = 0.44) as eluent to give the desired product **113** as a yellow solid (27% yield) m.p 161-162°C. The analytical data of compound **113** ^{1}H NMR (400 MHz, C_2D_6SO) δ 12.25 (s,1H), 11.98 (s, 1H), 9.32 (d, *J*= 3.2 Hz, 1H), 8.55 (d, *J*= 5.2 Hz, 1H), 8.39 (m, 2H) , 8.28 (m, 1H), 8.07 (dd, *J*= 2.0, 7.6 Hz, 1H), 7.78 (m, 1H), 7.66 (m, 1H), 7.26 (m, 1H), 7.20 (dd, *J*= 2.4, 6.0 Hz, 1H), 2.04 (s, 3H). ^{13}CNMR (100 MHz, C_2D_6SO): δ 176.5, 165.1, 156.5, 146.4, 142.2, 138.7, 137.6, 135.6, 134.5, 134.3, 131.9, 131.4, 129.3, 128.2, 128.0, 122.3, 120.6, 118.7, 117.5, 114.9, 114.6, 29.4. IR V_{max} cm^{-1}: 3419 (N-H), 2856 (C-H), 1717 (C=O), 1670 (C=O), 1488 (C=C), 1136 (C-O). HR-ESI-Orbitrap-MS *m/z:* 370.1022 $[M+H]^+$ (calculated 369.1113 for $C_{22}H_{15}N_3O_3$).

The side product of **114** observed as a yellow solid (17% yield), m.p: 150-151°C. The analytical data of compound **114** ^{1}H NMR (400 MHz, C_2D_6SO) δ 12.31 (s, 1H), 11.18 (s, 1H), 8.58 (d, *J*= 3.2 Hz, 1H), 8.21 (d, *J*= 2.4 Hz, 1H), 8.07 (d, *J*= 6.8 Hz, 1H) , 7.98 (q, *J*= 2.4, 7.6 Hz, 1H), 7.54 (m, 1H), 7.46 (d, *J*= 8.0 Hz, 1H), 7.18 (m, 1H), 7.01 (m, 1H), 4.02 (q, *J*= 2.4, 10 Hz, 2H), 2.91 (q, *J*=2.4, 9.6 Hz, 2H), 2.59 (s, 3H).^{13}CNMR (100 MHz, C_2D_6SO) δ 187.1, 169.8, 157.9, 146.6, 137.8, 135.0, 134.3, 132.0, 131.5, 128.2, 127.3, 126.7, 124.8, 124.6, 120.0, 116.9, 114.4, 113.8, 113.6, 48.8, 27.7, 19.1. IR V_{max} cm^{-1}: 3427 (N-H), 2928 (C-H), 1753 (C=O), 1689 (C=O), 1503 (C=C), 1167 (C-O). HR-ESI-Orbitrap-MS *m/z* 372.0027 $[M+H]^+$ (calculated 371.1270 for $C_{22}H_{17}N_3O_3$).

3.3.4.11 Reaction of 3-Acetyl-1H-indol-5-yl 2-chlorobenzoate, 91, With Tryptamine to Produce 3-(9H-Pyrido[3,4-b]indole-1-carbonyl)-1H-indol-5-yl 2-chlorobenzoate, 115, and 3-(4,9-Dihydro-3H-pyrido[3,4-b]indole-1-carbonyl)-1H-indol-5-yl-2-chlorobenzoate, 116

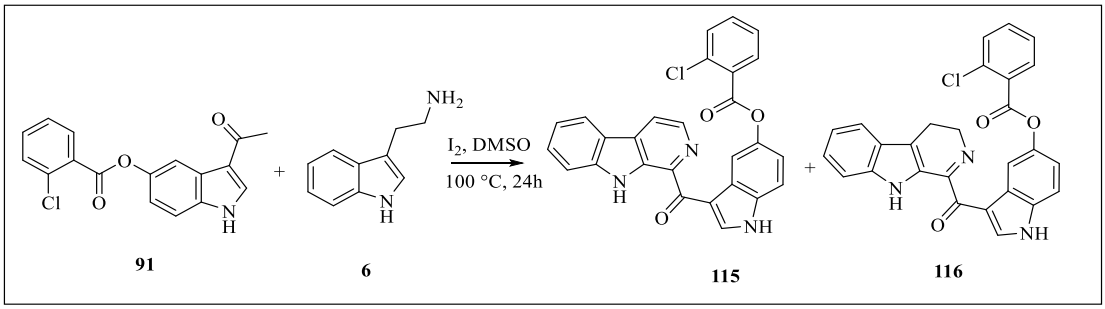

A stirred solution of 3-acetyl-1H-indol-5-yl 2-chlorobenzoate (0.1 g, 0.319 mmol) in DMSO (20 mL) was treated with iodine (0.06 g, 0.255 mmol). The resulting mixture was heated at 100 °C for 2 hours, with reaction progress monitored by TLC until complete consumption of the starting material. Subsequently, tryptamine (0.05 g, 0.319 mmol) was added, and the reaction mixture was stirred at room temperature for 24 hours. After completion, the mixture was cooled to room temperature, diluted with water, and extracted with ethyl acetate (3x). The combined organic layers were washed, dried over Na_2SO_4, filtered, and concentrated under reduced pressure. The residue was purified by chromatography on a silica gel using hexane: ethyl acetate (8:2), (R_f value = 0.41) as eluent to give the desired product **115** as a yellow solid (30% yield) m.p 207-208°C. The analytical data of compound **115** ^{1}H NMR (600 MHz, CD_3OD) δ 9.11 (s, 1H), 8.44 (d, *J*= 5.4 Hz, 1H), 8.40 (d, *J*= 1.8 Hz, 1H) , 8.18 (d, *J*= 5.4 Hz, 1H), 8.14 (d, *J*= 7.8 Hz, 1H), 8.00 (d, *J*= 8.4 Hz, 1H), 7.62 (d, *J*= 8.4 Hz, 1H), 7.00 (m, 5H), 7.20 (t, *J*= 7.2 Hz, 1H), 7.08 (dd, *J*= 2.4, 9.0 Hz, 1H), N-H proton was missing due to deuterium exchange.^{13}CNMR (100 MHz, CD_3OD): δ 185.6, 171.9, 165.8, 142.6, 136.8, 134.3, 133.3, 133.0, 131.6, 131.2, 130.8, 129.8, 128.6, 128.1, 126.9, 124.5, 121.4, 121.1, 120.8, 119.9, 118.0, 117.4, 117.3, 116.9, 116.6, 114.4, 112.0. IR ν_{max} cm^{-1}: 3411 (N-H), 2150 (C-H), 1710 (C=O), 1588 (C=O), 1428 (C=C), 1166 (C-O). HR-ESI-Orbitrap-MS *m/z:* 466.0965 $[M+H]^+$ (calculated 465.0880 for $C_{27}H_{16}ClN_3O_3$).

The side product of **116** observed as a yellow solid (12 % yield), m.p: 193-194°C. The analytical data of compound **116** ^{1}H NMR (400 MHz, $CDCl_3$): δ 9.85 (s, 1H), 9.57 (s, 1H), 8.59 (d, *J*= 2.8 Hz, 1H), 8.28 (d, *J*= 2.8 Hz, 1H), 8.05 (dd, *J*= 2.0,

8.0 Hz, 1H) , 7.53 (m, 3H), 7.39 (m, 3H), 7.31 (t, *J*= 6.8 Hz, 1H), 7.13 (m, 2H), 4.14 (t, *J*= 8.4 Hz, 2H), 3.02 (t, *J*= 9.2 Hz, 2H). ^{13}CNMR (100 MHz, $CDCl_3$): δ 187.3, 167.4, 157.0, 146.9, 138.0, 137.0, 133.8, 133.2, 132.1, 131.4, 130.7, 129.6, 127.6, 127.3, 126.9, 125.0, 124.8, 120.2, 119.9, 119.2, 118.1, 117.8, 115.1, 115.7, 112.2, 49.0, 29.8. IR V_{max} cm^{-1}: 3421 (N-H), 2181 (C-H), 1728 (C=O), 1678 (C=O), 1477 (C=C), 1296 (C-O). HR-ESI-Orbitrap-MS *m/z:* 468.0927 $[M+H]^+$ (calculated 467.1037 for $C_{27}H_{18}ClN_3O_3$).

3.3.4.12 Reaction of 3-Acetyl-1H-indol-5-yl 3-(trifluoromethyl)benzoate, 92, With Tryptamine to Produce 3-(9H-Pyrido[3,4-b]indole-1-carbonyl)-1H-indol-5-yl 3-(trifluoromethyl)benzoate, 117, and 3-(4,9-Dihydro-3H-pyrido[3,4-b]indole-1-carbonyl)-1H-indol-5-yl 3-(trifluoromethyl)benzoate, 118

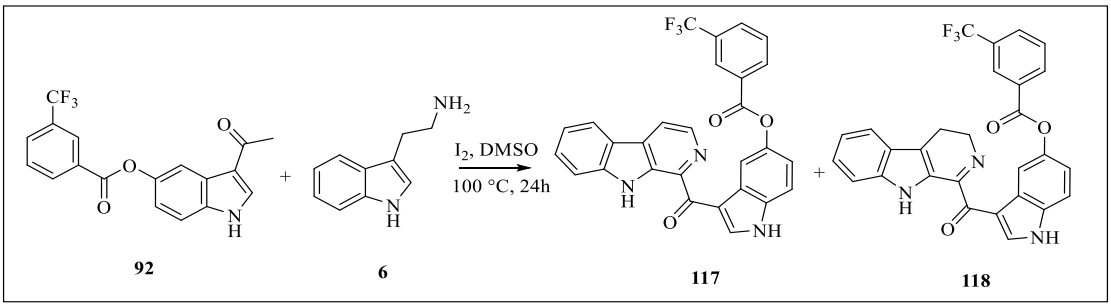

A stirred solution of 3-acetyl-1H-indol-5-yl 3-(trifluoromethyl)benzoate (0.1 g, 0.319 mmol) in DMSO (20 mL) was treated with iodine (0.06 g, 0.255 mmol). The resulting mixture was heated at 100 °C for 2 hours, with reaction progress monitored by TLC until complete consumption of the starting material. Subsequently, tryptamine (0.05 g, 0.319 mmol) was added, and the reaction mixture was stirred at room temperature for 24 hours. After completion, the mixture was cooled to room temperature, diluted with water, and extracted with ethyl acetate (3x). The combined organic layers were washed, dried over Na_2SO_4, filtered, and concentrated under reduced pressure. The residue was purified by chromatography on a silica gel using hexane: ethyl acetate (8:2), (R_f value = 0.40) as eluent to give the desired product **117** as a yellow solid (30% yield) m.p 191-192°C. The analytical data of compound **117** ^{1}H NMR (400 MHz, CD_3OD) δ 9.21 (s, 1H), 8.54 (d, *J*= 4.0 Hz, 1H), 8.52 (brs, 1H), 8.50 (m, 1H), 8.29 (d, *J*= 4.0 Hz, 1H) , 8.24 (d, *J*= 6.4 Hz, 1H), 8.06 (d, *J*= 6.0 Hz, 1H), 7.85 (t, *J*= 6.0 Hz, 1H), 7.71 (d, *J*= 6.4 Hz, 1H), 7.59 (m, 1H), 7.45 (m, 2H), 7.34 (t,

J= 5.2 Hz, 1H), 7.28 (m, 2H), 7.20 (dd, *J*= 2.0, 7.2 Hz, 1H). ^{13}CNMR (100 MHz, CD_3OD): δ 188.3, 170.3, 164.6, 146.5, 141.7, 138.5, 135.7, 134.3, 133.2, 131.4, 130.9, 129.7, 129.6, 128.6, 128.0, 126.7, 122.8, 121.2, 120.5, 119.9, 119.1, 117.9, 117.4, 116.9, 115.2, 114.4, 112.0, 111.9. IR V_{max} cm^{-1}: 3420 (N-H), 2852 (C-H), 1703 (C=O), 1633 (C=O), 1467 (C=C), 1301 (C-F), 1234 (C-O). HR-ESI-Orbitrap-MS *m/z:* 500.1206 $[M+H]^+$ (calculated 499.1144 for $C_{28}H_{16}F_3N_3O_3$).

The side product of **118** observed as a yellow solid (16 % yield), m.p: 183-184°C. The analytical data of compound **118** ^{1}H NMR (400 MHz, CD_3OD): δ 8.22 (s, 1H), 8.05 (d, *J*= 5.6 Hz, 1H), 7.87 (d, *J*= 1.6 Hz, 1H) , 7.84 (t, *J*= 5.2 Hz, 1H), 7.61 (m, 3H), 7.25 (t, *J*= 5.6 Hz, 1H), 7.22 (dd, *J*= 1.6, 5.6 Hz, 1H), 7.10 (t, *J*= 4.8 Hz, 2H), 6.84 (dd, *J*= 1.6, 5.6 Hz, 1H), 4.07 (m, 2H), 3.05 (m, 2H), N-H proton was missing due to deuterium exchange. ^{13}CNMR (100 MHz, CD_3OD): δ 187.1, 168.3, 159.2, 153.5, 149.2, 137.9, 137.9, 131.5, 130.8, 129.6, 129.4, 127.5, 126.8, 126.7, 126.3, 124.7, 124.5, 121.8, 121.7, 119.6, 119.3, 117.7, 113.8, 112.9, 112.2, 111.1, 31.7, 22.3. IR V_{max} cm^{-1}: 3452 (N-H), 2923 (C-H), 1736 (C=O), 1614 (C=O), 1487 (C=C), 1335 (C-F), 1255 (C-O). HR-ESI-Orbitrap-MS *m/z* 502.1372 $[M+H]^+$ (calculated 501.1300 for $C_{28}H_{18}F_3N_3O_3$).

3.3.4.13 Reaction of 3-Acetyl-1H-indol-5-yl 4-fluorobenzoate, 93, With Tryptamine to Produce 3-(9H-Pyrido[3,4-b]indole-1-carbonyl)-1H-indol-5-yl 4-fluorobenzoate, 119, and 3-(4,9-Dihydro-3H-pyrido[3,4-b]indole-1-carbonyl)-1H-indol-5-yl-4-fluoro benzoate, 120

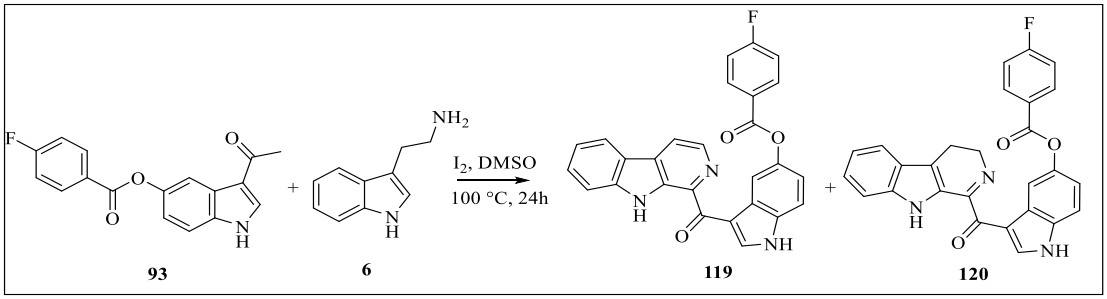

A stirred solution of 3-acetyl-1H-indol-5-yl 4-fluorobenzoate (0.1 g, 0.336 mmol) in DMSO (20 mL) was treated with iodine (0.07 g, 0.269 mmol). The resulting mixture was heated at 100 °C for 2 hours, with reaction progress monitored by TLC until complete consumption of the starting material. Subsequently, tryptamine (0.05 g,

0.336 mmol) was added, and the reaction mixture was stirred at room temperature for 24 hours. After completion, the mixture was cooled to room temperature, diluted with water, and extracted with ethyl acetate (3x). The combined organic layers were washed, dried over Na_2SO_4, filtered, and concentrated under reduced pressure. The residue was purified by chromatography on a silica gel using hexane: ethyl acetate (9:1), (R_f value = 0.38) as eluent to give the desired product **119** as a yellow solid (18% yield) m.p 189-190°C. The analytical data of compound **119** ^{1}H NMR (400 MHz, CD_3OD): δ 9.16 (s, 1H), 8.50 (d, *J*= 4.8 Hz, 1H), 8.42 (d, *J*= 3.2 Hz, 1H) , 8.28 (m, 2H), 8.24 (d, *J*= 4.4 Hz, 1H), 8.20 (d, *J*= 8.0 Hz, 1H), 7.67 (d, *J*= 10.8 Hz, 1H), 7.55 (m, 2H), 7.28 (m, 3H), 7.11 (dd, *J*= 2.4, 8.8 Hz, 1H), N-H proton was missing due to deuterium exchange. ^{13}CNMR (100 MHz, CD_3OD): δ 208.81, 177.1, 170.4, 162.4, 156.6, 147.6, 146.6, 138.6, 138.1, 136.84, 134.3, 132.6, 132.5, 131.4, 128.7, 128.0, 121.2, 120.5, 119.9, 117.4, 116.1, 115.6, 115.4, 114.5, 112.0, 112.0, 110.5. IR V_{max} cm^{-1}: 3421 (N-H), 2872 (C-H), 1755 (C=O), 1659 (C=O),1483 (C=C), 1210 (C-F), 1189 (C-O). HR-ESI-Orbitrap-MS *m/z:* 450.2746 $[M+H]^+$ (calculated 449.1176 for $C_{27}H_{16}FN_3O_3$).

The side product of **120** observed as a yellow solid (13% yield), m.p: 171-172°C. The analytical data of compound **120** ^{1}H NMR (400 MHz, CD_3OD): δ 9.20 (s, 1H), 8.422 (m, 2H), 8.29 (d, *J*= 3.6 Hz, 1H), 8.21 (d, *J*= 7.8 Hz, 1H), 7.81 (d, *J*= 10.2 Hz, 1H), 7.55 (m, 2H), 7.30 (m, 3H), 7.12 (dd, *J*= 2.0, 8.4 Hz, 1H), 4.10 (m, 2H), 3.10 (m, 2H), N-H proton was missing due to deuterium exchange. ^{13}CNMR (100 MHz, CD_3OD): δ 200.1, 178.0, 169.1, 162.9, 157.3, 148.0, 139.5, 138.4, 136.9, 135.1, 133.3, 132.9, 131.8, 129.6, 128.4, 121.5, 121.3, 117.9, 117.3, 115.8, 115.3, 112.7, 112.5, 111.5, 32.3, 23.2. IR V_{max} cm^{-1}: 3421 (N-H), 2989 (C-H), 1762 (C=O), 1620 (C=O), 1501 (C=C), 1288 (C-F), 1209 (C-O). HR-ESI-Orbitrap-MS *m/z* 452.2766 $[M+H]^+$ (calculated 451.1332 for $C_{27}H_{18}FN_3O_3$).

3.3.4.14 Reaction of 3-Acetyl-1H-indol-5-yl 3,4,5-trifluorobenzoate, 94, With Trypt amine to Produce 3-(9H-Pyrido[3,4-b]indole-1-carbonyl)-1H-indol-5-yl 3,4,5-trifluorobenzoate, 121, and 3-(4,9-Dihydro-3H-pyrido[3,4-b]indole-1-carbonyl)-1H-indol-5-yl 3,4,5-trifluorobenzoate, 122

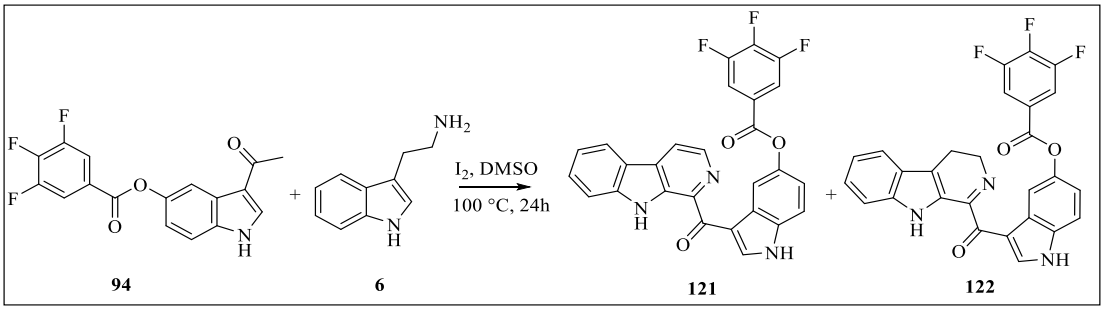

A stirred solution of 3-acetyl-1H-indol-5-yl 3,4,5-trifluorobenzoate (0.1 g, 0.336 mmol) in DMSO (20 mL) was treated with iodine (0.07 g, 0.269 mmol). The resulting mixture was heated at 100 °C for 2 hours, with reaction progress monitored by TLC until complete consumption of the starting material. Subsequently, tryptamine (0.05 g, 0.336 mmol) was added, and the reaction mixture was stirred at room temperature for 24 hours. After completion, the mixture was cooled to room temperature, diluted with water, and extracted with ethyl acetate (3x). The combined organic layers were washed, dried over Na_2SO_4, filtered, and concentrated under reduced pressure. The residue was purified by chromatography on a silica gel using hexane: ethyl acetate (9:1), (R_f value = 0.37) as eluent to give the desired product **121** as a yellow solid (16% yield) m.p 225-227°C. The analytical data of compound **121** ^{1}H NMR (400 MHz, CD_3OD): δ 8.48 (s, 1H), 8.43 (d, *J*= 3.6 Hz, 1H), 8.39 (d, *J*= 3.2 Hz, 1H), 8.16 (d, *J*= 3.6 Hz, 1H), 7.78 (d, *J*= 1.6 Hz, 1H) , 7.60 (m, 2H), 7.39 (d, *J*= 6.0 Hz, 1H), 7.11 (m, 3H), 6.83 (dd, *J*= 2.0, 6.2 Hz, 1H), N-H proton was missing due to deuterium exchange. ^{13}CNMR (100 MHz, CD_3OD): δ 181.2, 167.7, 155.5, 154.3, 154.2, 147.8, 143.9, 143.7, 140.2, 139.7, 138.9, 135.6, 127.8, 126.0, 121.0, 120.8, 120.7,118.5, 118.1, 117.7, 115.3, 115.1, 113.4, 113.0, 112.9, 110.8, 108.0. IR V_{max} cm^{-1}: 3366 (N-H), 2644 (C-H), 1717 (C=O), 1683 (C=O), 1487 (C=C), 1349 (C-F), 1105 (C-F). HR-ESI-Orbitrap-MS *m/z:* 486.1086 $[M+H]^+$ (calculated 485.0987 for $C_{27}H_{14}F_3N_3O_3$).

The side product of **122** observed as a yellow solid (19% yield), m.p: 211-212°C. The analytical data of compound **122** ^{1}H NMR (400 MHz, CD_3OD): δ 8.093 (s, 1H), 7.894 (t, *J*= 4.4 Hz, 1H), 7.736 (d, *J*= 1.6 Hz, 1H) , 7.494 (m, 2H), 7.335 (d, *J*= 5.2 Hz, 1H), 7.224 (d, *J*= 6.0 Hz, 1H), 7.163 (m, 1H), 6.998 (m, 1H), 6.734 (dd, *J*= 1.6, 5.6 Hz, 1H), 3.961 (m, 2H), 2.985 (m, 2H), N-H proton was missing due to deuterium exchange. ^{13}CNMR (100 MHz, CD_3OD): δ 184.8, 168.2, 155.3, 155.2, 155.1, 148.2, 143.9, 140.9, 140.3, 139.4, 136.4, 128.8, 126.1, 121.4, 121.2, 121.1, 118.9, 118.7,

115.9, 115.6, 113.9, 113.8, 112.8, 111.1, 107.8, 34.2, 25.6. IR V_{max} cm^{-1}: 3378 (N-H), 2654 (C-H), 1718 (C=O), 1655 (C=O), 1510 (C=C), 1224 (C-F), 1100 (C-O). HR-ESI-Orbitrap-MS *m/z:* 488.1116 $[M+H]^+$ (calculated 487.1144 for $C_{27}H_{16}F_3N_3O_3$).

3.3.4.15 Reaction of 1-(1-Methyl-1H-indol-3-yl)ethan-1-one, 95, With Tryptamine to Produce (1-Methyl-1H-indol-3-yl)(9H-pyrido[3,4-b]indol-1-yl)methanone, 123, and (4,9-Dihydro-3H-pyrido[3,4-b]indol-1-yl)(1-methyl-1H-indol-3-yl)methanone, 124

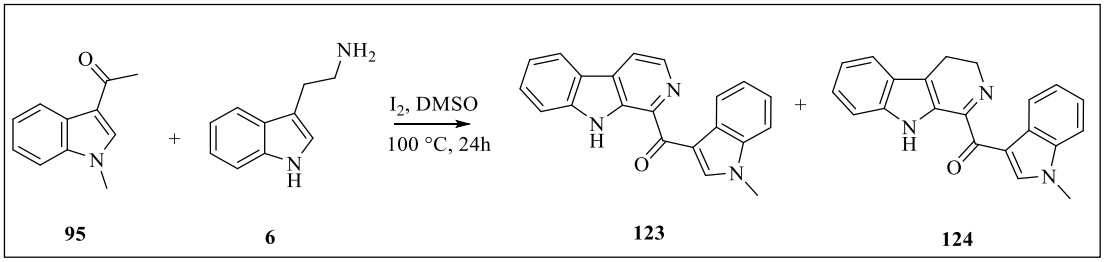

95 **6** **123** **124**

A stirred solution of 1-(1-methyl-1H-indol-3-yl)ethan-1-one (0.1 g, 0.577 mmol) in DMSO (20 mL) was treated with iodine (0.12 g, 0.462 mmol). The resulting mixture was heated at 100 °C for 2 hours, with reaction progress monitored by TLC until complete consumption of the starting material. Subsequently, tryptamine (0.09 g, 0.577 mmol) was added, and the reaction mixture was stirred at room temperature for 24 hours. After completion, the mixture was cooled to room temperature, diluted with water, and extracted with ethyl acetate (3x). The combined organic layers were washed, dried over Na_2SO_4, filtered, and concentrated under reduced pressure. The residue was purified by chromatography on a silica gel using hexane: ethyl acetate (8:2), (R_f value = 0.39) as eluent to give the desired product **123** as a yellow solid (31% yield) m.p 111-112°C. The analytical data of compound **123** ^{1}H NMR (400 MHz, CD_3OD): δ 8.97 (s, 1H), 8.58 (m, 1H), 8.50 (d, *J*= 4.8 Hz, 1H) , 8.25 (d, *J*= 4.8 Hz,1H), 8.22 (dd, *J*= 2.0, 9.2 Hz, 1H), 7.69 (dd, *J*= 2.0, 8.4 Hz, 1H), 7.57 (m, 1H), 7.51 (m, 1H), 7.30 (m, 3H), 3.99 (s, 3H), N-H proton was missing due to deuterium exchange. ^{13}CNMR (100 MHz, CD_3OD): δ 172.1, 142.4, 137.7, 136.8, 134.4, 129.8, 128.8, 128.3, 125.9, 124.1, 123.1, 122.3, 122.2, 121.3, 120.0, 118.4, 117.3, 114.8, 112.0, 109.8, 34.0. IR V_{max} cm^{-1}: 3127 (N-H), 2850 (C-H), 1615 (C=O), 1456 (C=C). HR-ESI-Orbitrap-MS *m/z:* 326.1593 $[M+H]^+$ (calculated 325.1215 for $C_{21}H_{15}N_3O$).

The side product of **124** observed as a yellow solid (20 % yield), m.p: 99-100°C. The analytical data of compound **124** ^{1}H NMR (400 MHz, CD_3OD): δ 8.428 (m, 1H),

8.294 (s, 1H), 7.736 (dt, *J*= 0.8, 8.4 Hz, 1H), 7.51 (m, 1H), 7.421 (dt, *J*= 0.8, 8.4 Hz, 1H), 7.336 (m, 2H), 7.229 (m, 1H), 7.075 (m, 1H), 4.054 (t, *J*= 8.4 Hz, 2H), 3.896 (s, 3H), 3.057 (t, *J*= 6.8 Hz, 2H), N-H proton was missing due to deuterium exchange. ^{13}CNMR (100 MHz, CD_3OD): δ 181.1, 141.4, 128.3, 127.0, 124.9, 123.6, 122.8, 122.0, 121.6, 119.8, 119.5, 118.3, 112.3, 110.8, 110.1, 108.6, 107.2, 103.6, 89.6, 32.5, 18.7. IR V_{max} cm^{-1}: 3208 (N-H), 2961 (C-H), 1711 (C=O), 1477 (C=C). HR-ESI-Orbitrap-MS *m/z:* 328.0478 $[M+H]^+$ (calculated 327.1372 for $C_{21}H_{17}N_3O$).

3.3.4.16 Reaction of 1-(1-Ethyl-1H-indol-3-yl)ethan-1-one, 96, With Tryptamine to Produce (1-Ethyl-1H-indol-3-yl)(9H-pyrido[3,4-b]indol-1-yl)methanone, 125, and (4,9-Dihydro-3H-pyrido[3,4-b]indol-1-yl)(1-ethyl-1H-indol-3-yl)methanone, 126

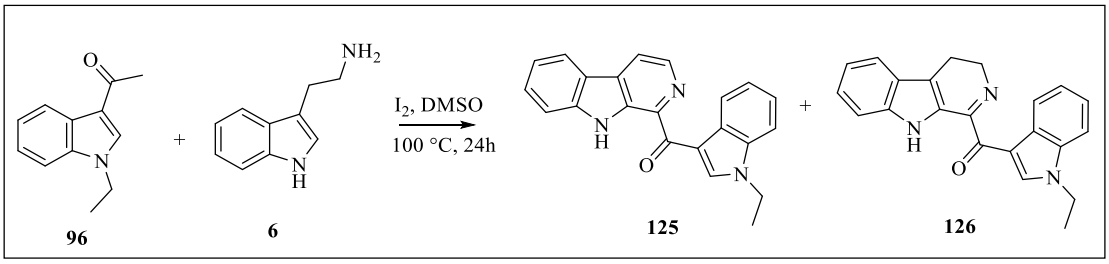

96 6 125 126

A stirred solution of 1-(1-ethyl-1H-indol-3-yl)ethan-1-one (0.1 g, 0.534 mmol) in DMSO (20 mL) was treated with iodine (0.11 g, 0.427 mmol). The resulting mixture was heated at 100 °C for 2 hours, with reaction progress monitored by TLC until complete consumption of the starting material. Subsequently, tryptamine (0.09 g, 0.534 mmol) was added, and the reaction mixture was stirred at room temperature for 24 hours. After completion, the mixture was cooled to room temperature, diluted with water, and extracted with ethyl acetate (3x). The combined organic layers were washed, dried over Na_2SO_4, filtered, and concentrated under reduced pressure. The residue was purified by chromatography on a silica gel using hexane: ethyl acetate (8:2), (R_f value = 0.40) as eluent to give the desired product **125** as a yellow solid (34% yield) m.p 129-130°C. The analytical data of compound **125** ^{1}H NMR (400 MHz, CD_3OD): δ 8.51 (s, 1H), 8.44 (d, *J*= 3.6 Hz, 1H), 8.43 (d, *J*= 3.2 Hz, 1H), 7.63 (m, 4H), 7.41 (m, 1H), 7.30 (m, 2H), 7.01 (m, 1H), 4.19 (q, *J*= 7.0, 12 Hz, 2H), 1.24 (t, *J*= 7.2 Hz, 3H), N-H proton was missing due to deuterium exchange. ^{13}CNMR (100 MHz, CD_3OD): δ 179.7, 154.1, 140.0, 138.9, 137.0, 136.3, 126.6, 125.8, 124.2, 124.0, 123.1, 122.0, 121.3, 120.0, 118.8, 118.4, 116.5, 112.6, 112.3, 109.4, 40.2, 13.5. IR V_{max} cm^{-1}: 3221 (N-H), 2660

(C-H), 1657 (C=O), 1412 (C=C). HR-ESI-Orbitrap-MS *m/z:* 340.1447 $[M+H]^+$ (calculated 339.1372 for $C_{22}H_{17}N_3O$).

The side product of **126** is observed as a yellow solid (19 % yield), m.p: 116-117°C. The analytical data of compound **126** ^{1}H NMR (400 MHz, CD_3OD): δ 8.43 (m, 1H), 8.32 (s, 1H), 7.58 (dt, *J*= 1.2, 8.0 Hz, 1H) , 7.53 (m, 1H), 7.41 (dt, *J*=1.2, 8.0 Hz, 1H), 7.31 (m, 2H), 7.21 (m, 1H), 7.06 (m, 1H), 4.29 (q, *J*= 7.2, 14 Hz, 2H), 4.04 (t, *J*= 6.8 Hz, 2H), 3.01 (t, *J*= 10.4 Hz, 2H), 1.47 (t, *J*= 7.2 Hz, 3H), N-H proton was missing due to deuterium exchange. ^{13}CNMR (100 MHz, CD_3OD): δ 186.8, 159.1, 139.9, 138.0, 136.9, 127.3, 126.3, 124.7, 124.6, 123.5, 122.7, 122.2, 119.7, 119.4, 117.8, 113.1, 112.3, 110.2, 41.7, 29.4, 18.7, 14.2. IR V_{max} cm^{-1}: 3198 (N-H), 2675 (C-H), 1692 (C=O), 1499 (C=C). HR-ESI-Orbitrap-MS *m/z:* 342.1603 $[M+H]^+$ (calculated 341.1528 for $C_{22}H_{19}N_3O$).

3.3.4.17 Reaction of 1-(1-Propyl-1H-indol-3-yl)ethan-1-one, 97, With Tryptamine to Produce (1-Propyl-1H-indol-3-yl)(9H-pyrido[3,4-b]indol-1-yl)methanone, 127, and (4,9-Dihydro-3H-pyrido[3,4-b]indol-1-yl)(1-propyl-1H-indol-3-yl)methanone, 128

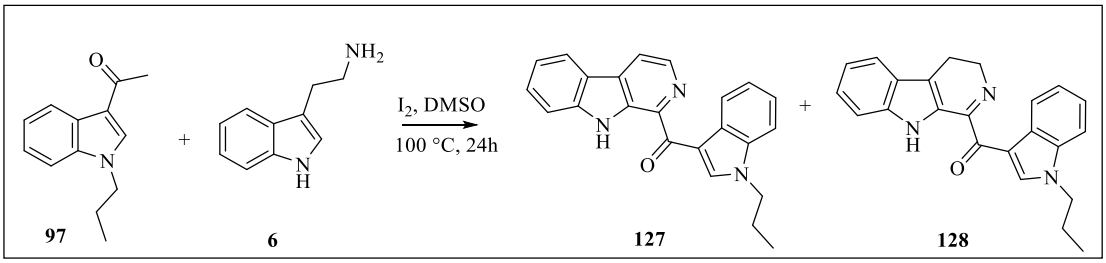

A stirred solution of 1-(1-propyl-1H-indol-3-yl)ethan-1-one (0.1 g, 0.497 mmol) in DMSO (20 mL) was treated with iodine (0.11 g, 0.397 mmol). The resulting mixture was heated at 100 °C for 2 hours, with reaction progress monitored by TLC until complete consumption of the starting material. Subsequently, tryptamine (0.08 g, 0.497 mmol) was added, and the reaction mixture was stirred at room temperature for 24 hours. After completion, the mixture was cooled to room temperature, diluted with water, and extracted with ethyl acetate (3x). The combined organic layers were washed, dried over Na_2SO_4, filtered, and concentrated under reduced pressure. The residue was purified by chromatography on a silica gel using hexane: ethyl acetate (8:2), (R_f value = 0.40) as eluent to give the desired product **127** as a yellow solid (35% yield) m.p 143-144°C. The analytical data of compound **127** ^{1}H NMR (400 MHz, CD_3OD): δ 8.21 (dd,

J= 2.4, 8.0 Hz, 1H), 8.15 (s, 1H), 7.46 (dd, *J*= 1.2, 8.0 Hz, 1H) , 7.40 (m, 3H), 7.30 (m, 2H), 7.23 (m, 2H), 7.19 (m, 1H), 4.20 (q, *J*= 2.8, 10 Hz, 2H), 1.87 (q, *J*= 2.0, 11.0 Hz, 2H), 7.11 (t, *J*= 5.6 Hz, 3H), N-H proton was missing due to deuterium exchange. ^{13}CNMR (100 MHz, CD_3OD): δ 194.7, 153.6, 142.3, 137.2, 132.3, 129.7, 126.7, 126.3, 124.6, 123.5, 123.0, 122.1, 121.9, 119.6, 117.9, 116.0, 112.3, 110.1, 108.7, 104.7, 26.0, 23.0, 10.1. IR V_{max} cm^{-1}: 3433 (N-H), 2951 (C-H), 1722 (C=O), 1471 (C=C). HR-ESI-Orbitrap-MS *m/z* 354.1605 $[M+H]^+$ (calculated 353.1528 for $C_{23}H_{19}N_3O$).

The side product of **128** observed as a yellow solid (14 % yield), m.p: 166-167°C. The analytical data of compound **128** ^{1}H NMR (400 MHz, CD_3OD): δ 8.30 (m, 1H), 8.31 (s, 1H), 7.57 (d, *J*= 8.0 Hz, 1H) , 7.51 (m, 1H), 7.28 (m, 3H), 7.19 (m, 1H), 7.05 (t, *J*= 7.2 Hz, 1H), 4.21 (t, *J*= 4.0 Hz, 2H), 4.03 (t, *J*= 8.4 Hz, 2H), 3.01 (t, *J*= 9.6 Hz, 2H), 1.89 (q, *J*= 4.0, 7.2 Hz, 2H), 0.92 (t, *J*= 4.8 Hz, 3H), N-H proton was missing due to deuterium exchange. ^{13}CNMR (100 MHz, CD_3OD): δ 175.6, 155.5, 138.0, 137.2, 129.6, 127.3, 126.7, 124.7, 124.5, 123.4, 122.7, 122.2, 119.4, 119.2, 117.8, 113.0, 112.3, 110.4, 31.7, 26.0, 23.0, 18.7, 12.6. IR V_{max} cm^{-1}: 3411 (N-H), 2923 (C-H), 1603 (C=O), 1455 (C=C). HR-ESI-Orbitrap-MS *m/z* 356.1662 $[M+H]^+$ (calculated 355.1685 for $C_{23}H_{21}N_3O$).

3.3.4.18 Reaction of 1-(1-Butyl-1H-indol-3-yl)ethan-1-one, 98, With Tryptamine to Produce (1-Butyl-1H-indol-3-yl)(9H-pyrido[3,4-b]indol-1-yl)methanone, 129, and (4,9-Dihydro-3H-pyrido[3,4-b]indol-1-yl)(1-butyl-1H-indol-3-yl)methanone, 130

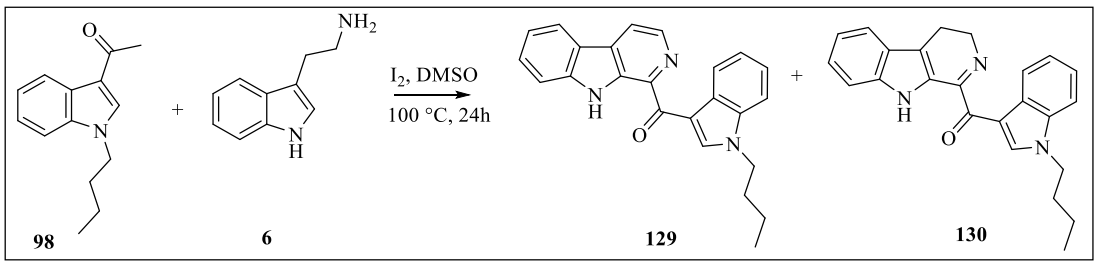

A stirred solution of 1-(1-butyl-1H-indol-3-yl)ethan-1-one (0.1 g, 0.497 mmol) in DMSO (20 mL) was treated with iodine (0.09 g, 0.464 mmol). The resulting mixture was heated at 100 °C for 2 hours, with reaction progress monitored by TLC until complete consumption of the starting material. Subsequently, tryptamine (0.07 g, 0.497 mmol) was added, and the reaction mixture was stirred at room temperature for 24 hours. After completion, the mixture was cooled to room temperature, diluted with

water, and extracted with ethyl acetate (3x). The combined organic layers were washed, dried over Na_2SO_4, filtered, and concentrated under reduced pressure. The residue was purified by chromatography on a silica gel using hexane: ethyl acetate (9:1), (R_f value = 0.36) as eluent to give the desired product **129** as a yellow solid (33% yield) m.p 150-151°C. The analytical data of compound **129** ^{1}H NMR (400 MHz, C_2D_6SO): δ 11.94 (s, 1H), 9.20 (s, 1H), 8.54 (m, 2H), 8.30 (dd, *J*= 4.4, 10 Hz, 2H) , 7.69 (m, 2H), 7.27 (m, 4H), 4.30 (t, *J*= 10 Hz, 2H), 2.46 (t, *J*= 2.8 Hz, 2H), 1.75 (m, 2H), 1.27 (t, *J*= 6.4 Hz, 3H). ^{13}CNMR (100 MHz, C_2D_6SO): δ 188.0, 142.6, 141.4, 139.4, 138.0, 136.9, 136.1, 131.8, 131.2, 129.7, 128.9, 124.0, 123.4, 123.0, 122.7, 121.1, 120.9, 119.0, 114.3, 111.9, 47.1, 32.7, 20.5, 15.0. IR V_{max} cm^{-1}: 3113 (N-H), 2855 (C-H), 1673 (C=O), 1487 (C=C). HR-ESI-Orbitrap-MS *m/z:* 368.1761 $[M+H]^+$ (calculated 367.1685 for $C_{24}H_{21}N_3O$).

The side product of **130** observed as a yellow solid (14 % yield), m.p: 162-164°C. The analytical data of compound **130** ^{1}H NMR (400 MHz, C_2D_6SO): δ 11.13 (s, 1H), 8.52 (s, 1H), 8.35 (m, 1H), 8.12 (q, *J*= 8.0, 14.8 Hz, 1H), 7.63 (m, 1H) , 7.56 (m, 1H), 7.47 (d, *J*= 8.4 Hz, 1H), 7.29 (m, 1H), 7.17 (m, 1H), 7.02 (t, *J*= 6.8 Hz, 1H), 4.26 (q, *J*= 6.8, 14.4 Hz, 2H), 4.01 (t, *J*= 8.4 Hz, 2H), 2.93 (q, *J*= 8.0, 9.6 Hz, 2H), 1.73 (m, 2H), 1.23 (m, 2H), 0.84 (t, 4.4 Hz, 3H). ^{13}CNMR (100 MHz, C_2D_6SO): δ 184.0, 141.4, 141.2, 137.9, 137.3, 137.0, 127.4, 125.9, 124.8, 123.8, 123.5, 123.2, 122.7, 122.2, 113.7, 114.0, 113.6, 111.7, 46.7, 46.5, 32.2, 31.9, 20.0, 14.0. IR V_{max} cm^{-1}: 3194 (N-H), 2924 (C-H), 1600 (C=O), 1463 (C=C). HR-ESI-Orbitrap-MS *m/z:* 370.1761 $[M+H]^+$ (calculated 369.1841 for $C_{24}H_{23}N_3O$).

3.3.4.19 Reaction of 1-(1-Hexyl-1H-indol-3-yl)ethan-1-one, 99, With Tryptamine to Produce (1-Hexyl-1H-indol-3-yl)(9H-pyrido[3,4-b]indol-1-yl)methanone, 131, and (4,9-dihydro-3H-pyrido[3,4-b]indol-1-yl)(1-hexyl-1H-indol-3-yl)methanone, 132

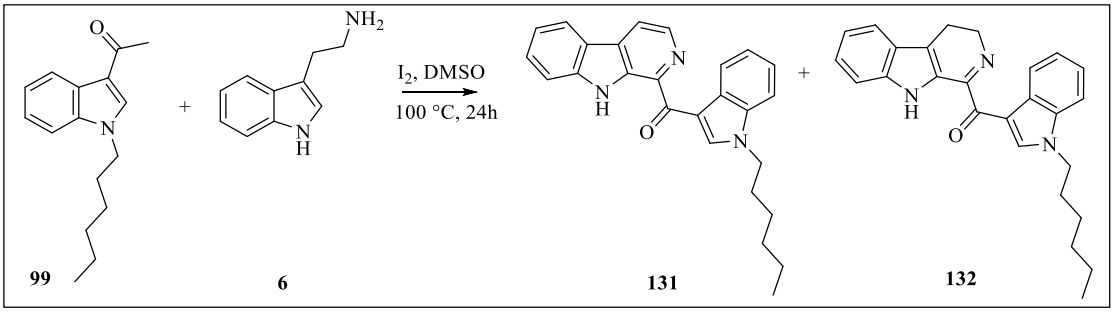

99 **6** **131** **132**

A stirred solution of 1-(1-hexyl-1H-indol-3-yl)-ethan-1-one (0.1 g, 0.411 mmol) in DMSO (20 mL) was treated with iodine (0.08 g, 0.329 mmol). The resulting mixture was heated at 100 °C for 2 hours, with reaction progress monitored by TLC until complete consumption of the starting material. Subsequently, tryptamine (0.07 g, 0.411 mmol) was added, and the reaction mixture was stirred at room temperature for 24 hours. After completion, the mixture was cooled to room temperature, diluted with water, and extracted with ethyl acetate (EtOAc). The combined organic layers were washed, dried over Na_2SO_4, filtered, and concentrated under reduced pressure. The residue was purified by chromatography on a silica gel using hexane: ethyl acetate (9:1), (R_f value = 0.34) as eluent to give the desired product **131** as a yellow solid (30% yield) m.p 175-176°C. The analytical data of compound **131** ^{1}H NMR (400 MHz, (C_2D_6SO): δ 11.96 (s, 1H), 9.23 (s, 1H), 8.53 (d, *J*= 5.2 Hz, 1H), 8.48 (s, 1H), 8.37 (d, *J*= 4.8 Hz, 1H), 8.27 (d, *J*= 7.2 Hz, 1H), 7.79 (d, *J*= 8.4 Hz, 1H), 7.63 (m, 1H), 7.55 (t, *J*= 7.6 Hz, 1H), 7.44 (m, 1H), 7.29 (m, 2H), 4.33 (t, *J*= 7.2 Hz, 2H), 1.80 (m, 1H), 1.19 (m, 6H), 0.80 (t, *J*= 4.0 Hz, 3H) . ^{13}CNMR (100 MHz, C_2D_6SO): δ 187.4, 144.6, 142.1, 140.9, 137.5, 136.5, 136.4, 131.3, 130.7, 129.6, 129.2, 128.4, 123.5, 122.7, 122.2, 120.6, 120.4, 118.5, 113.5, 111.4, 46.8, 31.3, 30.1, 26.3, 22.5, 14.4. IR V_{max} cm^{-1}: 3620 (N-H), 2855 (C-H), 1609 (C=O), 1462 (C=C). HR-ESI-Orbitrap-MS *m/z:* 396.2054 $[M+H]^+$ (calculated 395.1998 for $C_{26}H_{25}N_3O$).

The side product of **132** observed as a yellow solid (10 % yield), m.p: 181-182°C. The analytical data of compound **132** ^{1}H NMR (400 MHz, CD_3OD): δ 8.42 (m, 1H), 8.30 (s, 1H), 7.58 (d, *J*= 8.4 Hz, 1H) , 7.51 (m, 1H), 7.40 (d, *J*= 8.4 Hz, 1H), 7.30 (m, 1H), 7.20 (t, *J*= 8.0 Hz, 1H), 7.05 (t, *J*= 8.0 Hz, 2H), 4.24 (t, *J*= 6.4 Hz, 2H), 4.03 (t, *J*= 8.4 Hz, 2H), 3.01 (t, *J*= 9.2 Hz, 2H), 1.85 (t, *J*= 6.8 Hz, 2H), 1.28 (m, 6H), 0.83 (t, *J*= 6.8 Hz, 3H), N-H proton was missing due to deuterium exchange. ^{13}CNMR (100 MHz, CD_3OD): δ 186.7, 158.0, 141.3, 137.7, 136.9, 127.4, 126.8, 124.8, 124.5, 123.7, 123.1, 122.2, 120.0, 120.0, 116.8, 113.6, 112.7, 111.6, 48.8, 46.8, 31.2, 30.0, 26.2, 22.5, 19.1, 14.3. IR V_{max} cm^{-1}: 3744 (N-H), 2922 (C-H), 1623 (C=O,) 1487 (C=C). HR-ESI-Orbitrap-MS *m/z:* 398.2231 $[M+H]^+$ (calculated 397.2154 for $C_{26}H_{27}N_3O$).

3.3.4.20 Reaction of 1-(1-Benzyl-1H-indol-3-yl)ethan-1-one, 100, With Tryptamine to Produce (1-Benzyl-1H-indol-3-yl)(9H-pyrido[3,4-b]indol-1-yl)methanone, 133, and(4,9-Dihydro-3H-pyrido[3,4-b]indol-1-yl)(1-benzyl-1H-indol-3yl)methanone,134

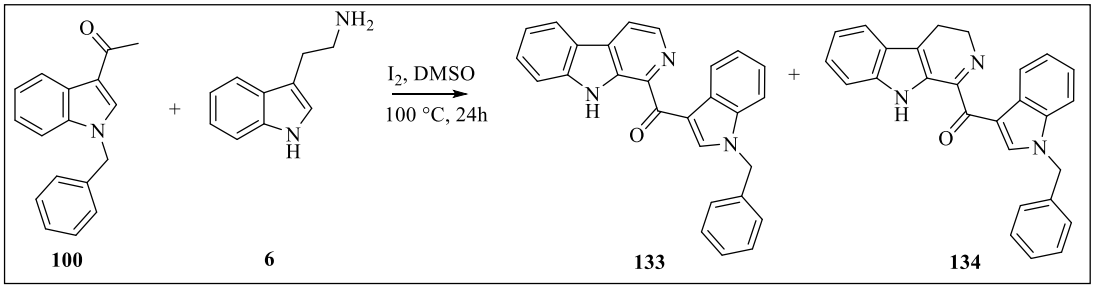

A stirred solution of 1-(1-benzyl-1H-indol-3-yl)-ethan-1-one (0.1 g, 0.411 mmol) in DMSO (20 mL) was treated with iodine (0.08 g, 0.329 mmol). The resulting mixture was heated at 100 °C for 2 hours, with reaction progress monitored by TLC until complete consumption of the starting material. Subsequently, tryptamine (0.07 g, 0.411 mmol) was added, and the reaction mixture was stirred at room temperature for 24 hours. After completion, the mixture was cooled to room temperature, diluted with water, and extracted with ethyl acetate (3x). The combined organic layers were washed, dried over Na_2SO_4, filtered, and concentrated under reduced pressure. The residue was purified by chromatography on a silica gel using hexane: ethyl acetate (8:2), (R_f value = 0.40) as eluent to give the desired product **133** as a yellow solid (32% yield) m.p 157-158°C. The analytical data of compound **133** ^{1}H NMR (400 MHz, C_2D_6SO) δ 11.90 (s, 1H), 9.42 (s, 1H), 8.56 (dd, *J*= 3.2, 6.8 Hz, 1H), 8.52 (d, *J*= 5.2 Hz, 1H) , 8.37 (d, *J*= 5.2 Hz, 1H), 8.27 (d, *J*= 7.6 Hz, 1H), 7.80 (d, *J*= 8.0 Hz, 1H), 7.55 (m, 2H), 7.43 (m, 2H), 7.27 (m, 6H), 5.63 (s, 2H). ^{13}CNMR (100 MHz, C_2D_6SO): δ 187.6, 142.2, 141.3, 138.8, 137.7, 137.5, 136.5, 135.6, 131.3, 130.7, 129.3, 129.3, 128.5, 128.2, 127.6, 127.6, 123.7, 123.0, 122.6, 122.5, 122.3, 120.6, 120.4, 118.6, 114.2, 113.6, 111.8, 50.3. IR V_{max} cm^{-1}: 3141 (N-H), 2923 (C-H), 1603 (C=O), 1487 (C=C). HR-ESI-Orbitrap-MS *m/z:* 402.1604 $[M+H]^+$ (calculated 401.1528 for $C_{27}H_{19}N_3O$).

The side product of **134** is observed as a yellow solid (20% yield), m.p: 144-146°C. The analytical data of compound **134** ^{1}H NMR (400 MHz, CD_3OD) δ 9.00 (s, 1H), 8.73 (dd, *J*= 3.2, 6.8 Hz, 1H), 8.31 (d, *J*= 7.0 Hz, 1H), 7.99 (d, *J*= 8.4 Hz, 1H), 7.58 (m, 2H), 7.62 (m, 2H), 7.30 (m, 6H), 5.66 (s, 2H), 4.06 (t, *J*= 6.8 Hz, 2H), 3.10 (t, *J*= 9.8 Hz, 2H), N-H proton was missing due to deuterium exchange. ^{13}CNMR (100 MHz, CD_3OD): δ 199.8, 141.3, 139.9, 138.2, 138.0, 137.9, 136.0, 132.1, 131.3, 129.9, 129.9, 129.0, 128.2, 127.0, 123.9, 123.8, 123.7, 122.8, 122.0, 121.8, 120.9, 115.1, 114.0, 112.1, 50.4, 46.3, 19.2. IR V_{max} cm^{-1}: 3411 (N-H), 2988 (C-H), 1733 (C=O),

1463 (C=C). HR-ESI-Orbitrap-MS *m/z:* 404.1672 $[M+H]^+$ (calculated 403.1685 for $C_{27}H_{21}N_3O$).

3.3.4.21 Reaction of 3-Acetylindole, 77, With 5-Benzyloxytryptamine to Produce (6-Benzyl-9H-pyrido[3,4-b]indol-1-yl)(1H-indol-3-yl)methanone, 136

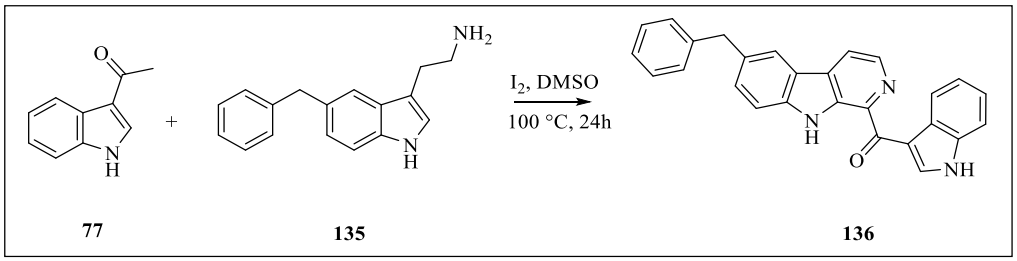

77 **135** **136**

A stirred solution of 3-acetylindole (0.1 g, 0.628 mmol) in DMSO (20 mL) was treated with iodine (0.13 g, 0.503 mmol). The resulting mixture was heated at 100 °C for 2 hours, with reaction progress monitored by TLC until complete consumption of the starting material. Subsequently, tryptamine (0.16 g, 0.628 mmol) was added, and the reaction mixture was stirred at room temperature for 24 hours. After completion, the mixture was cooled to room temperature, diluted with water, and extracted with ethyl acetate (3x). The combined organic layers were washed, dried over Na_2SO_4, filtered, and concentrated under reduced pressure. The residue was purified by chromatography on a silica gel using hexane: ethyl acetate (9:1), (R_f value = 0.37) as eluent to give the desired product **136** as a yellow solid (60% yield) m.p 147-148°C.

The analytical data of compound **136** ^{1}H NMR (400 MHz, $CDCl_3$): δ 10.82 (s, 1H), 10.62 (s,1H), 9.40 (d, *J*= 3.2 Hz, 1H), 8.68 (d, *J*= 6.0 Hz, 1H), 8.51 (d, *J*= 4.8 Hz, 1H) , 8.06 (d, *J*= 4.2 Hz, 1H), 7.67 (d, *J*= 2.8 Hz, 1H), 7.39 (m, 10 H), 5.18 (s, 2H), N-H proton was missing due to deuterium exchange. ^{13}CNMR (100 MHz, $CDCl_3$): δ 189.0, 160.0, 153.6, 137.3, 137.1, 136.9, 136.2, 135.6, 131.4, 128.7, 128.7, 128.1, 127.7, 127.6, 127.6, 127.5, 123.7, 122.9, 122.8, 121.3, 119.6, 117.9, 115.9, 112.8, 111.4, 105.5, 71.2. IR V_{max} cm^{-1}: 3409 (N-H), 2918 (C-H), 1549 (C=O), 1487 (C=C). HR-ESI-Orbitrap-MS *m/z:* 402.1672 $[M+H]^+$ (calculated 401.1512 for $C_{27}H_{19}N_3O$).

3.3.5 Demethylation of (5-methoxy-1H-indol-3-yl)(6-methoxy-9H-pyrido[3,4-b]indol-1-yl)methanone, 53, to Produce Hyrtiosulawesine, 1.

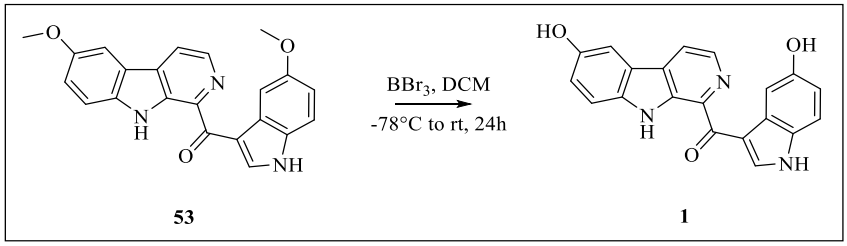

53 1

Product **53** (0.05 g, 0.13 mmol) was dissolved in CH_2Cl_2 and a 1.0 mol/L of aqueous borontribromide (BBr_3) was added dropwise at -78°C. The reaction was kept at ambient temperature for 24 hours. After the reaction is completed, carefully quench the mixture with water at low temperature and then extracted with CH_2Cl_2. After the solvent was removed, the products of hyrtiosulwaesine was obtained and characterized using spectroscopic and spectrometry. The residue was purified by chromatography on a silica gel using hexane: ethyl acetate (9:1), (R_f value = 0.30) as eluent to give the desired product **1** as a yellow solid (80% yield) m.p 240-241°C. The analytical data of compound **1** ^{1}H NMR (600 MHz, CD_3OD): δ 8.90 (s, 1H), 8.44 (d, *J*= 6.0 Hz, 1H), 8.16 (d, *J*= 6.6 Hz, 1H), 8.03 (d, *J*= 3.0 Hz, 1H), 7.58 (d, *J*= 3.0 Hz, 1H), 7.55 (d, *J*= 10.8 Hz, 1H), 7.33 (d, *J*= 10.2 Hz, 1H), 7.15 (dd, *J*= 3.0, 10.2 Hz, 1H), 6.83 (dd, *J*= 3.0, 10.2 Hz, 1H). ^{13}CNMR (126 MHz, CD_3OD) δ 189.9, 154.4, 152.6, 140.3, 139.1, 137.5, 137.4, 137.4, 137.3, 132.4, 132.3, 129.8, 122.6, 119.9, 118.4, 116.1, 113.9, 113.3, 108.1, 106.8. IR V_{max} cm^{-1}: 3470 (N-H), 3228 (O-H), 2916 (C-H), 1556 (C=O), 1483 (C=C), 1233 (C-O). HR-ESI-Orbitrap-MS *m/z:* 344.1031 $[M+H]^+$ (calculated 343.0957 for $C_{20}H_{13}N_3O_3$).

3.4 *In vitro* Antimalarial Assay

3.4.1 Reagents and Biological Materials

Antimalarial assays were assessed using *Plasmodium* lactate dehydrogenase (pLDH) assays. All 40 compounds were included in our screening study. Stock solutions of the compounds (Sigma-Aldrich, St. Louis, MO, USA) were prepared in 5% dimethyl sulfoxide (DMSO) and stored at room temperature until needed. A negative control without enzyme in 2% DMSO was used as a background to test if there was any solvent interference, and a positive control with oxamate was utilized to compare the inhibition to other probable inhibitors. All were properly prepared for each test.

A recombinant *Pf*LDH enzyme was purchased from Sino Biological Inc. (Catalog No. 40303-N08E, Beijing, China). The enzyme was provided in a lyophilized form and reconstituted as per the manufacturer's instructions prior to use. The LDH assay kit was purchased from from Bita Lifescience Sdn. Bhd. (Malaysia) and the kit contain necessary reagents including NADH standard, LDH assay buffer, LDH positive control and LDH substrate mixture. All reagent preparation was carried out according to the manufacturer's instructions.

3.4.2 Inhibition of *Pf*LDH Activity by The Selected Compounds

All compounds were initially screened at a single concentration of 1 μM against *Pf*LDH. Test compounds were incubated in triplicate in a 96-well plate. DMSO and oxamate served as negative and positive controls. After 1 hour room temperature (27°C) incubation with reagents and inhibitors, enzyme was added. Absorbance at 450 nm was measured every minute for 30 minutes at 37 °C. Inhibition was assessed by comparing enzyme activity with and without compounds, and percent inhibition was calculated. Most compounds showed minimal activity (less than 30% inhibition) and were not pursued further. Only compounds exhibiting measurable inhibition (compounds **53**, **113**, and **114**, respectively) were selected for IC_{50} determination with 10 serial dilutions (ranging from 2-20 μM) to accurately assess their inhibitory potency. Parasite viability was calculated relative to the untreated control, and dose-response curves were generated in GraphPad Prism. IC_{50} values were obtained from the fitted sigmoidal curves (Mphahlele *et al.,* 2017).

3.5 Cytotoxicity Assay

3.5.1 Cell Culture

The triple-negative MDA-MB-231 breast cancer and HT-29 colon cancer cell lines were purchased from American Type and Culture Collection (ATCC, Manassas, VA, USA). Both MDA-MB-231 breast cancer cells and HT-29 colon cancer cells were grown in DMEM supplemented with 10% foetal bovine serum and 1% penicillin-streptomycin (complete growth culture media). All cells were cultured at 37 °C in an

atmosphere of 5% carbon dioxide (CO_2). Once confluence, the cells were digested with 0.1% trypsin.

3.5.2 Determination of cell Growth Inhibition

MDA-MB-231 and HT-29 cells were seeded in 96-well plates with 5000 cells per well in 100 µL of complete growth culture media. The cells were incubated at 37 °C (5% CO_2 and 95% air) for 24 hours to allow cell attachment. Compounds (Hyrtiosulawesine and 15 derivatives) were dissolved and screened at single concentration of 100 uM. The cells were then treated with compounds for 48 hours. Negative control cells treated with 0.4% DMSO alone were also included. Compounds with more than 50% cell growth inhibition at 100 µM were selected for full dose-response studies to determine IC_{50} values using 6 serial dilutions (ranging from 5 to 80 µM). At the end of the experiment, MTT (20 µL, 5 mg mL-1 in PBS) was added into each well and the plate was incubated for 3 hours. Excess MTT was then aspirated and the formazan crystals formed were dissolved using 150 µL of DMSO. The absorbance, which was proportional to cell viability, was measured at 570 nm and a reference wavelength of 630 nm by using a microplate reader (BioTek Epoch 2, Leiden, Netherlands). Cell viability was calculated using the following equation:

$$Percentage\ of\ cell\ viability\ (\%) = \frac{OD570 - 630\ treatment}{OD570 - 630\ control}\ x\ 100\%$$

Percentage of cell viability (%)=(OD570-630 treatment)/(OD570-630 control) x 100%

3.6 *In silico* Study

3.6.1 Molecular Docking

Molecular docking stands as a robust method enabling the prediction of how small molecules bind and orient themselves within specific protein active sites, thereby illuminating their potential as therapeutic agents.

3.6.1.1 Structural Protein Preparation

In this study, the crystal structure of *Pf*LDH has been utilized as a drug target. The crystal structure in protein data bank (PDB) file format (PDB ID: 1U4S) was retrieved from the RCSB web site at a resolution of 2.0 Å. Initially, the water molecules and co crystallized ligands were removed from its crystal structure to make good protein-ligand interaction since the protein is complexed with heteroatom, water molecule, and unwanted ligand. Polar hydrogen atoms and Kollman charges were subsequently added using ADT 1.5.6. The optimized protein structure was then saved in PDBQT format for subsequent molecular docking investigations.

3.6.1.2 Ligand Preparation

Prior to molecular docking analysis, the ligand, hyrtiosulawesine and its derivatives were primarily designed and illustrated using ChemDraw Pro 16.0. Their 3D structures were generated with Chem3D 16.0, and energy minimization (MM2 force field) was performed using the same software. The optimized ligands were individually saved in PDB format and then used in AutoDockTools (ADT) 1.5.6 (Morris *et al.,* 2009). The Gasteiger charges were calculated, and the files were saved in PDBQT format.

3.6.1.3 Defining Grid Box for Docking

A grid box was created using AutoGrid in ADT 1.5.6 to encompass all amino acid residues within the active site of interest, including the area occupied by the co-crystallized ligand (naphthalene-2,6-disulfonic acid). The dimensions of the grid cavity were 25 Å × 25 Å × 25 Å, centered at coordinates 23.587 × 17.939 × 5.185 along the x, y and z-axes, respectively. A grid spacing of 0.375 Å was set to ensure sufficient coverage and resolution for accurate docking calculations.

3.6.1.4 Molecular Docking Using Auto Dock Vina

Molecular docking analysis was conducted using AutoDock Vina 1.5.6, employing a genetic algorithm for its search method and semi-empirical approaches to

compute free energy as its scoring function. Prior to docking, input configuration files were prepared, including protein and ligand structures in PDBQT format, along with defined grid coordinates. The molecular docking process commenced with a meticulous validation between the protein (PDB ID: 1U4S) and its native ligand. The naphthalene-2,6-disulfonic acid was successfully redocked with an RMSD value of 0.694 and the docked pose matched the native ligand's position in the crystal structure, underscoring the accuracy of this approach (Botón-Fernández *et al*., 2016).

The docking parameters were set with 10 modes, an energy range of 4 and exhaustiveness set to 100. The process was executed *via* command mode and results were assessed based on the binding affinity values (kcal/mol). Additionally, Discovery Studio and PyMOL were utilized for 2D and 3D visualization to analyze chemical interactions, including the hydrogen bonds, hydrophobic interactions and bond distances.



Figure 3.2 Crystal Structure of *Plasmodium falciparum* Lactate Dehydrogenase (PDB 1U4S)

3.6.2 Molecular Dynamic Simulation

MD simulation was run with Desmond. The systems were configured in Maestro using the "System Builder" feature. To build a hydration model, the energy of the ligand-protein combination with target protein was minimized using an upgraded Optimized Potentials for Liquid Simulations (OPLS3e) molecular mechanics force field. The force field was then placed in a cubic box with a buffer distance of 10 Å. Water molecules were put between the ligand-receptor combination using a simple point charge (SPC) water model. The simulation parameters were set at a time step of

2.0 fs, a van der Waals cut-off of 9 Å, an initial temperature of 300 K, and a pressure of 1.01 bar. During the equilibration stage, positional restraints were applied using of 0.1 kcal/mol/Å² of a harmonic force constant to stabilize the structure. To evaluate the electrostatic force of the Desmond system, near-term and far-term were divided by a boundary at 9 Å. Finally, MD simulations were performed under the NPT ensemble for 200 ns. The result was recorded for every 50 ps with a total of 2000 frames.

3.6.3 ADMET Analysis

Physiochemical evaluation plays a pivotal role in assessing the potential drug-likeness of compounds, predicting crucial parameters such as absorption, distribution, metabolism and excretion (ADME) (Parihar *et al.,* 2022). Drug likeness scores for all analogues were determined using the SwissADME server, inputting SMILES notations generated during ligand preparation. According to Lipinski's Rule of Five (Ro5), drug-like compounds must adhere to specific parameters: molecular weight (g/mol), number of hydrogen bond donors (HBD), number of hydrogen bond acceptors (HBA), topological polar surface area (TPSA), x log P calculation (Log P), with allowance for no more than one violation. ADMET analysis also gave information about human intestinal absorption (HIA), aqueous solubility (AS), blood-brain barrier (BBB), cytochrome P450 2D6 (CYP2D6), plasma protein binding (PPB), hepatotoxicity (HT), atom-based logP (Alog P98), and polar surface area (PSA) descriptors.

CHAPTER 4
RESULTS AND DISCUSSIONS

4.1 General Overview

Hyrtiosulawesine, is one of natural marine alkaloid and reported to have various pharmacological properties particularly on antimalarial and anticancer activity. The previous synthesis of hyrtiosulawesine involved multi-step procedures that generated low overall yield. This emphasizes the need for a more streamlined and effective synthetic strategy. In this study, a short three step synthetic route was developed encompassing Friedel-Crafts acylation, multicoupled-domino reaction, and demethylation to synthesize hyrtiosulawesine, achieving an overall yield of 28%. Utilizing this method, a series of 40 derivatives bearing different substituents were successfully synthesized in low to moderate yields.

All compounds were subsequently screened for antimalarial assays, and three derivatives (**53**, **113** and **114**) demonstrated the highest inhibition against parasite development. This data was further supported by *in silico* molecular docking analysis which revealed the binding affinities and molecular interactions of all compounds against *Pf*LDH protein (PDB ID: 1U4S). Then, these three top compounds were subjected to MD simulation to assess their stability and flexibility in the complex form. Furthermore, ADMET predictions were carried out for these three compounds to evaluate their pharmacokinetic profiles. In addition to antimalarial testing, the anticancer activity of hyrtiosulawesine and some derivatives were examined using MTT cytotoxicity assays against breast (MDA-MB-231) and colon (HT-29) cancer cell lines. Several of these derivatives exhibited significant activity. All the strategies employed, and the data obtained were discussed in this chapter.

4.2 Total Synthesis of Hyrtiosulawesine

4.2.1 Formation of 5-Hydroxy-3-acetylindole *via* Friedel-Crafts Acylation

As previously reported, the synthesis of hyrtiosulawesine remains quite challenging. Several methods were attempted and are detailed in this section. According to Scheme 1.1, the proposed synthetic route involves three steps which are Friedel-Crafts acylation, Kornblum oxidation, and Pictet-Spengler condensation. Scheme 4.1 shows the first step to obtain hyrtiosulawesine through Friedel-Crafts acylation of 5-hydroxyindole.

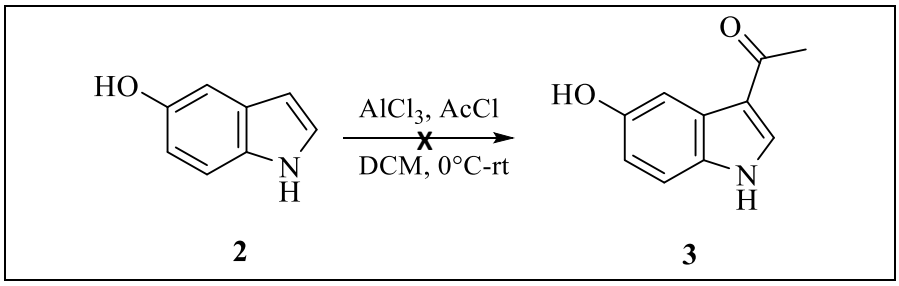

Scheme 4.1 Friedel-Crafts Acylation of 5-hydroxyindole to give 5-hydroxy-3-acetylindole

In this reaction, a limitation was encountered due to the starting material of 5-hydroxyindole. The presence of hydroxyl group substituent limits the solubility of the compound in dichloromethane (DCM). Although polar aprotic solvents such as dimethyl sulfoxide (DMSO) and tetrahydrofuran (THF) can efficiently dissolve the 5-hydroxyindole, they present significant operational drawbacks. These solvents are highly hygroscopic and difficult to maintain under inert and anhydrous conditions. The residual moisture trapped within these solvents tends to interact and deactivate the Lewis acid used and finally affect the reaction efficiency. Therefore, DCM is widely used for Friedel-Crafts acylation because it can dissolve most organic compounds, immiscibility with water, chemical inertness, and low boiling point properties (Heravi *et al.,* 2018).

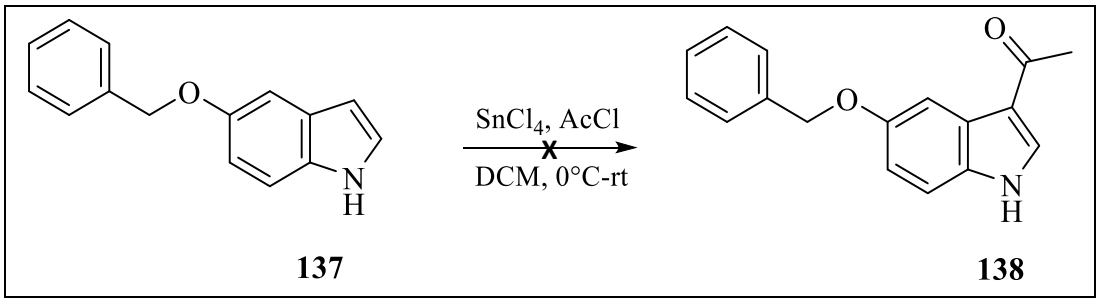

Scheme 4.2 Friedel-Crafts Acylation of 5-benzyloxyindole to give 5-benzyloxy-3-acetylindole

Consequently, an additional step was introduced wherein the 5-hydroxyindole was protected using benzyl bromide prior to the Friedel-Crafts acylation. Multiple attempts were made to obtain the product, as the initial trial resulted in product decomposition. After several adjustments, the product (**137**) was successfully isolated and was subjected to Friedel-Crafts acylation. However, no product was formed and yielded many spots on TLC, indicating low product selectivity and yield (Scheme 4.2). Besides, the reaction with $SnCl_4$ leads to cleavage of the product and regeneration of 5-hydroxyindole. This is due to the benzyl group which is an electron-donating substituent through an inductive effect. Thus, increase the electron density on the indole ring and can make it more reactive towards $SnCl_4$. The Lewis acid can also coordinate with the electron-rich oxygen or nitrogen, which facilitate the cleavage of the bond between the indole and the benzyl group. This results in the unsuccessful reaction due to removal of the benzyl group and regeneration of the parent 5-hydroxyindole.

4.2.2 Formation of 5-Methoxy-3-acetylindole *via* Friedel-Crafts Acylation

Given the high cost of 5-hydroxyindole and serotonin, an amine for Pictet-Spengler condensation reaction, a change in starting materials was implemented. Serotonin is difficult to control during reactions. This is because its hydroxy group can usually create multiple reactive sites (Orr *et al.,* 2022). Moreover, handling hydroxy substituents usually involves additional protecting and deprotecting steps. Therefore, 5-methoxyindole (**36d**) was chosen as starting material for the initial steps (Scheme 4.3). However, complications persisted since indole is inherently electron-rich, and the presence of methoxy substituent can increase reactivity of the ring towards Lewis acids. Therefore, this necessitated careful selection of the Lewis acid to achieve the desired regioselectivity.

Initially, 5-methoxyindole (**36d**) undergoes Friedel-Crafts acylation in the presence of Lewis acids and acetyl chloride under inert conditions. Given that indole is an electron-rich compound, common Lewis acids are generally not suitable, especially when an electron-donating group like methoxy is present as a substituent. To control the reactivity at the C-3 position of 5-methoxyindole, an additional step was applied. The nitrogen atom was protected first with a *tert*-butoxycarbonyl (Boc) group prior to the Friedel-Crafts acylation. Since Boc is acid-sensitive, the use of $SnCl_4$ is not suitable as it results in Boc cleavage and recovery of the starting material. Given that most

protecting groups are acid-labile and Friedel-Crafts acylation require Lewis acids, hence this approaches not practically suitable.

The 5-methoxyindole reaction was performed using different Lewis's acids, including $AlCl_3$, $TiCl_4$, and $SnCl_4$ and produced varying outcomes. Initial attempts using $AlCl_3$ as the Lewis acid resulted in no product formation. This outcome is likely due to decomposition and oligomerization of the product (Okauchi *et al.,* 2003). Subsequent attempt using $TiCl_4$ and $SnCl_4$ successfully afforded the desired product, but in low yields of approximately 10%. In both instances, the TLC showed few spots complicating their isolation and NMR spectra indicated the existence of unidentified side products like messy, overlapping, and inadequately resolved peaks. Table 4.1 illustrates the percentage yield differed significantly depending on the Lewis acid employed.

Table 4.1
Optimization of The Friedel-Crafts Acylation of 5-Methoxyindole (**36d**)

Entry	Lewis acids	Temperature	Time	Yield (%)
1	$SnCl_4$	0°C to rt	6h	10
2	$TiCl_4$	0°C to rt	5h	9
3	$AlCl_3$	0°C to rt	5h	-
4	Et_2AlCl	0°C	4h	77

$AlCl_3$ is a more reactive Lewis acid than both $SnCl_4$ and $TiCl_4$. This is due to its higher electrophilicity and stronger coordination ability with electron-rich compound. In contrast, tin and titanium have larger atomic sizes and more diffused electron clouds compared to aluminum. Therefore, the atom is less efficient to accept electron pairs and less coordination interaction. The relative order of Lewis acidity ($AlCl_3$ > $TiCl_4$ > $SnCl_4$) is supported by computational and experimental studies in several reaction contexts like Diels-Alder and hydroxyalkylation reactions (Pratihar, 2016). To mitigate both possibility of oligomerization and poor yield, diethyl aluminum chloride (Et_2AlCl) was used as an alternative to $AlCl_3$ and $SnCl_4$ in reactions involving indoles substituted with strong electron donating groups.

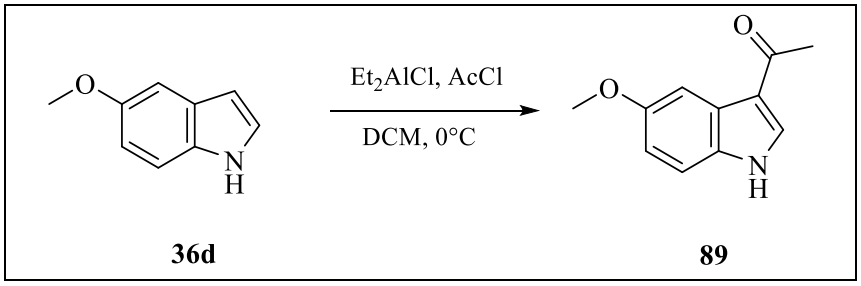

Scheme 4.3 Friedel-Crafts Acylation of 5-methoxyindole to give 5-methoxy-3-acetylindole

The findings show that using Et_2AlCl increased the percentage yields of 5-methoxy-3-acetylindole from 10% to 77%. This could be due to the aluminum atom having ethyl groups on it, which makes Et_2AlCl less Lewis acidic than common aluminum chloride. The inductive electron-donating effect of the ethyl groups increases the electron density on the aluminum atom, reducing its electrophilicity compared to $AlCl_3$ and $SnCl_4$ and lead to less side reactions. This result shows that Et_2AlCl works best for Friedel-Crafts acylation of indoles with strong electron-donating groups. The proposed mechanism is depicted in Scheme 4.4.

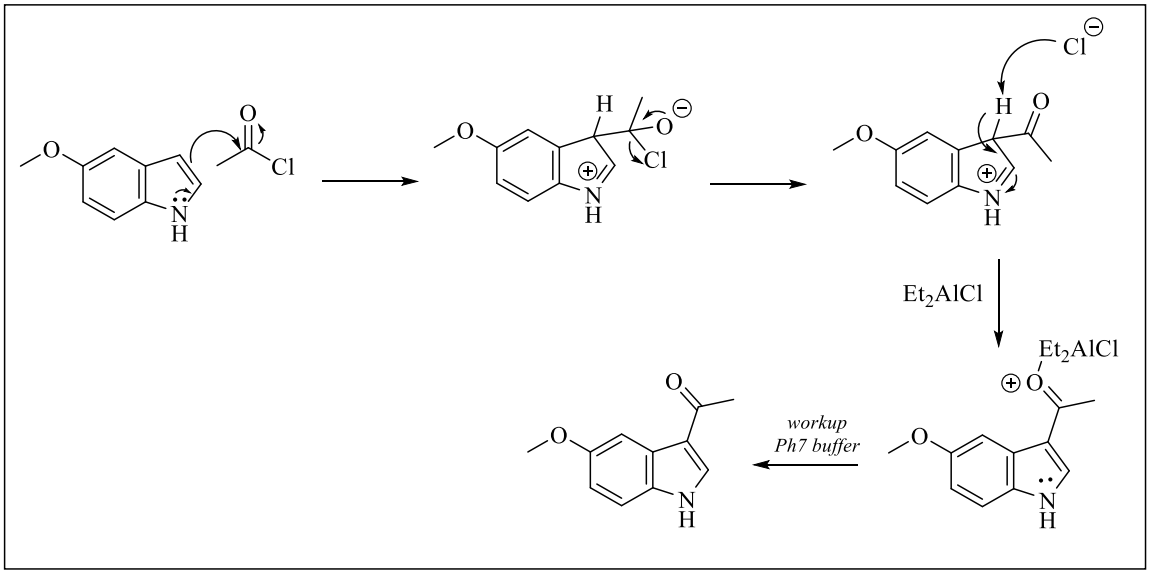

Scheme 4.4 Plausible Mechanism of 3-Acylindole Derivatives

The products of Friedel-Crafts were obtained and underwent Kornblum oxidation to produce the glyoxal intermediate. The product is only 10%, which is insufficient for the subsequent Pictet-Spengler reaction (Scheme 4.5). This occurs because of the highly polar and unstable glyoxal intermediate (**139**), which caused strong retention and subsequent decomposition on the silica gel column during

purification (Fabheber & Seinfeld, 2015). As a result of low intermediate yield, the synthetic route was revised to improve the overall yields and secure sufficient material for biological assays. The new synthetic pathway was proposed and outlined in Scheme 4.6.

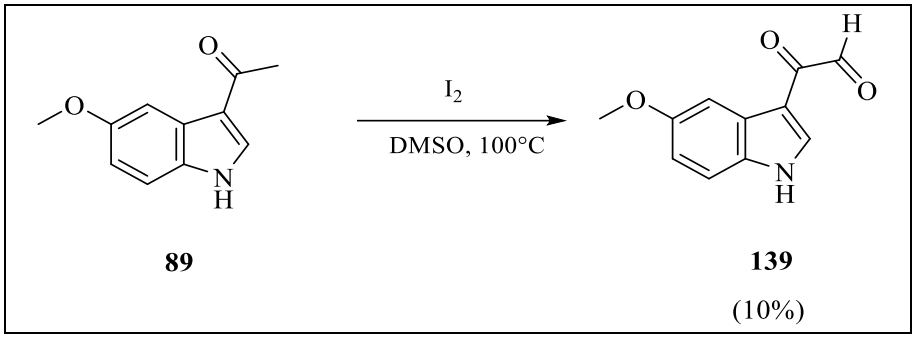

Scheme 4.5 Kornblum Oxidation of 5-methoxy-3-acetylindole

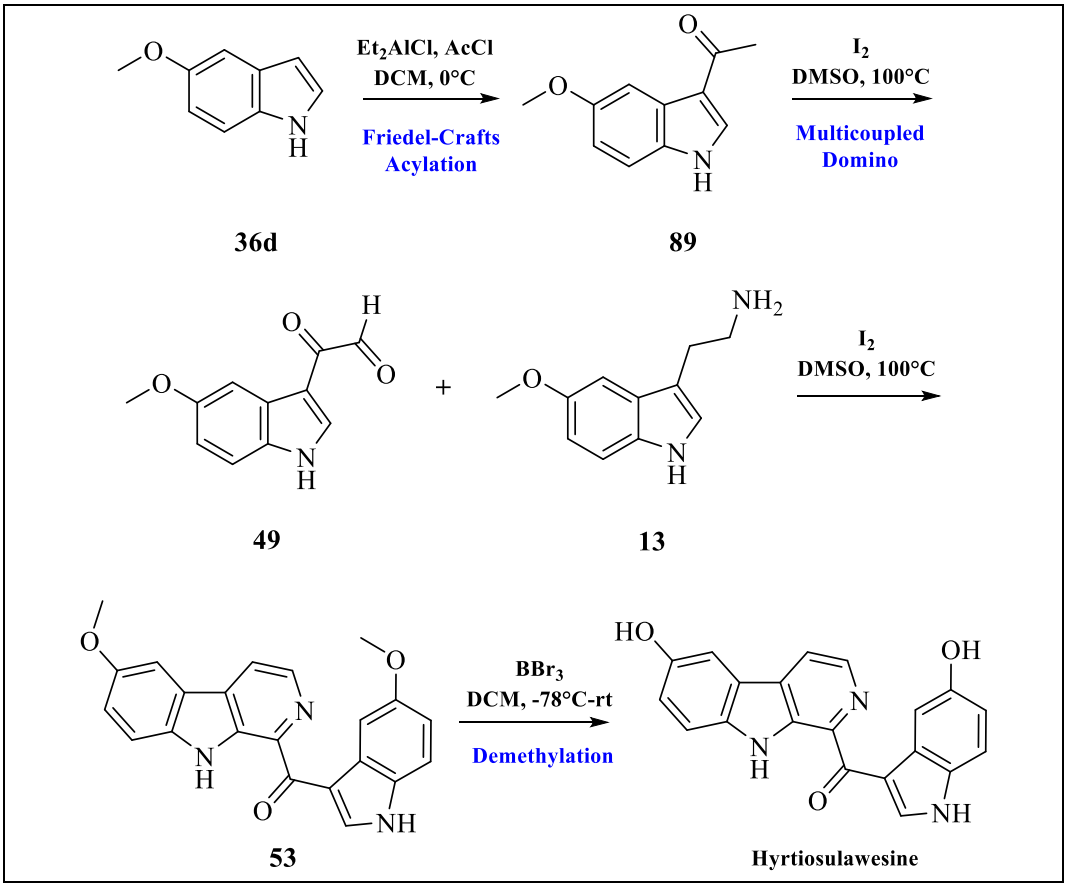

Scheme 4.6 Synthesis Route of Hyrtiosulawesine

To improve the synthetic method, a three-step reaction process was developed to minimize the use of strong chemicals and prevent additional protection and deprotection steps. The develop method maintains the first steps of Friedel-Crafts

acylation, followed multicoupled domino and demethylation process. Each process explains in the following subtopics.

4.2.3 Formation of (5-Methoxy-1H-indol-3-yl)(6-methoxy-9H-pyrido[3,4b]indol 1-yl)methanone, 53 *via* Multicouple Domino Reaction

Multicoupled domino reactions are specifically designed for cyclization processes. This approach was selected because the initially proposed route relied on Kornblum oxidation of the Friedel-Crafts product. However, due to low yields and instability of the intermediate, the isolation of intermediate was avoided to prevent product loss. Therefore, using the same reaction conditions without isolation, additional tryptamine can be directly added to afford the final product (Scheme 4.7).

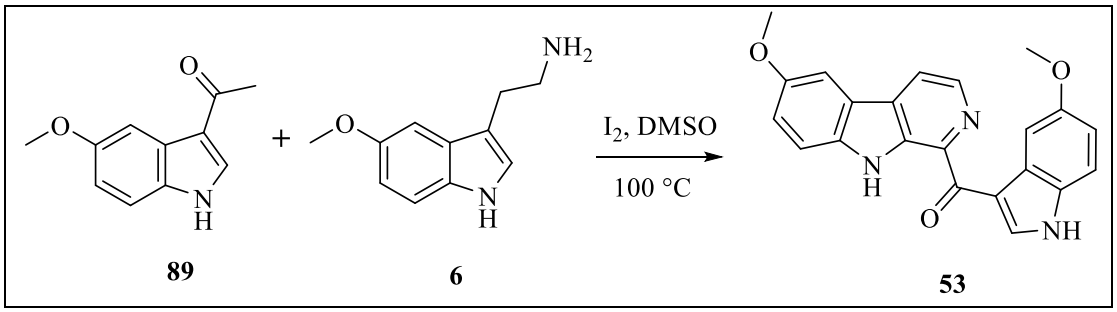

Scheme 4.7 Multicouple Domino of 5-methoxyindole with 5-methoxytryptamine to give intermediate **53**

The subsequent step involves a one-step multicoupled domino reaction in which iodine acts as a catalyst. In this reaction, iodine used to facilitate the generation of reactive intermediates, iodomethyl group, which can initiate or propagate the domino sequence for subsequent reactions (Tietze, 1996). Observations demonstrated that the reaction time depends heavily on different equivalents of iodine (Table 4.2). The use of polar aprotic solvent, DMSO in this reaction, is an oxidizing agent which enables reactive intermediate formation for subsequent steps. Besides, DMSO will act as a nucleophile to perform an SN_2 reaction against the iodomethyl intermediate (-CH_2I) by

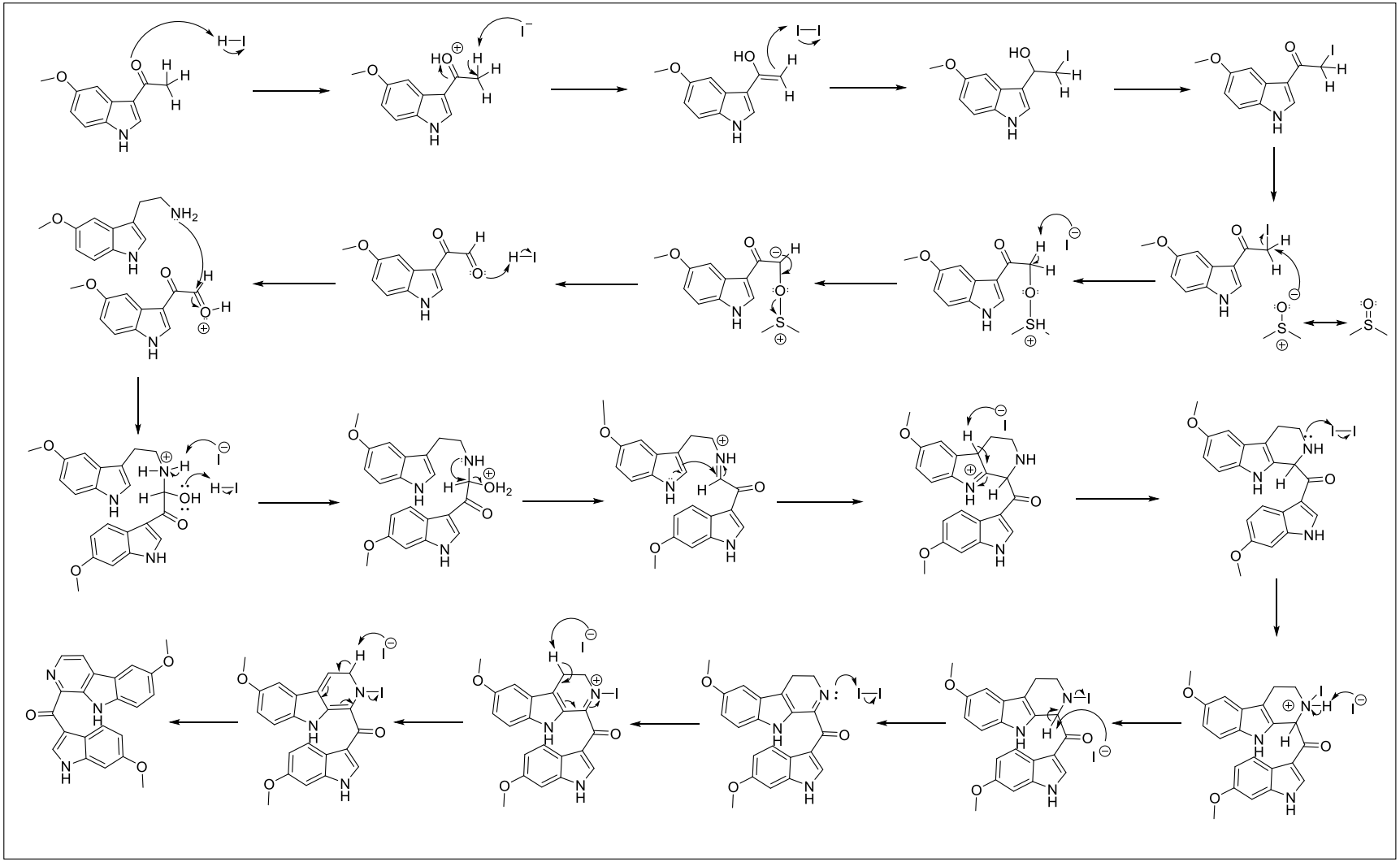

Scheme 4.8 Proposed Mechanism of Domino Reaction to Afford **53**

attacking the carbon attached to iodine, since iodine is a good leaving group as shown in Scheme 4.8 (Reichardt & Welton, 2011).

As depicted in Scheme 4.8, the reaction is driven by a combination of iodine or hydroiodic acid (HI) and DMSO which cooperatively act as an oxidative system to transform the starting material of 3-acetyl-5-methoxyindole into a highly reactive indole-3-glyoxal intermediate. Specifically, the iodine source acts as an electrophile to iodinate the α-carbon of the acetyl group, while DMSO serves as an oxygen-nucleophile to displace the resulting iodide and to yield the bis-carbonyl species and volatile dimethyl sulfide (Me_2S). This glyoxal intermediate was ready to be attacked by an amine, form an iminium ion and ready for ring closure. Beyond this initial oxidation, the iodine or iodide species continue to act as crucial oxidative reagents in the final stages of the domino sequence, where they mediate sequential oxidation iodination and HI eliminations to drive the aromatization to afford the conjugated polycyclic product **53**.

While the one-pot approach successfully overcomes the challenges with the intermediate instability and isolation losses, it inherently results in a lower overall product yield (Ramachary & Jain, 2011). This is because the instability and highly reactive intermediates potentially lead to side products and reduce the overall yield of the target product (Tietze, 1996). In addition, during purification process it is found challenging as domino reactions could form complex mixtures of products and byproducts. This eventually causes decreases the final yield as detailed in Table 4.2. Hence, several variations in this reaction were conducted to optimize the yield.

Table 4.2
Optimization of the Domino Reaction of 5-methoxy-3-acetylindole (**89**)

Entry	Solvent	Iodine (eq)	Time	Yield (%)
1	DMSO	0.5	24h	3
2	DMSO	0.8	12h	47
3	DMSO	1.2	8h	12

From the results, the optimization of equivalent of iodine is essential to maximize the yield of the target product while minimizing side reactions. As shown, both excess and insufficient iodine can adversely affect domino reactions. Insufficient iodine may hinder the reaction's progression, slow reaction rate and lead to extended reaction times which eventually increase the possibility of side reactions. In

comparison, when excessive iodine was applied, the reaction time was faster yet the yield very low. This possibly caused by over-oxidation of the substrate or intermediate and results in unwanted byproducts and side reactions. Additionally, the formation of iodinated byproducts or the degradation of sensitive intermediates (Zhdankin, 2013). Therefore, the optimal equivalent of iodine in this reaction was 0.8 equivalent.

4.2.4 Formation of Hyrtiosulawesine *via* Demethylation

The final step in the synthesis of hyrtiosulawesine involves the demethylation process where the methoxy group is converted to a hydroxyl group (Scheme 4.9). This process follows the previously established method, utilizing excess tribromoborane (BBr_3) under inert conditions, while anhydrous dichloromethane as the solvent. The reaction mixture was quenched with methanol, which serves as the proton source to cleave the boron-oxygen intermediate and generate the final product of hyrtiosulawesine (**1**).

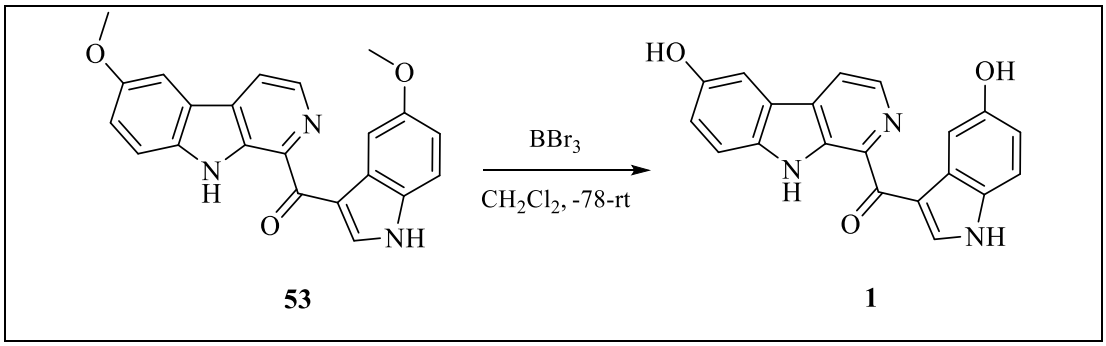

53 **1**

Scheme 4.9 Demethylation of intermediate **53** to afford hyrtiosulawesine

The reaction effectively replaces the methoxy group with a hydroxyl group, which is essential for obtaining the desired compound. However, the reaction does not result in complete consumption of the starting material and yielding 80% of the product (Table 4.3). Despite this, the method yields enough product for further purification and isolation. The targeted product was then characterized through FTIR, ^{1}H-NMR, ^{13}C-NMR, and HRMS, and a percent yield of hyrtiosulawesine improved to 28.2% in comparison to prior study 16%. The NMR data align with those reported in previous investigation (Table 4.4). Both ^{1}H- and APT-NMR spectra are shown in Figure 4.1 and Figure 4.2 and the mechanism depicted in Scheme 4.10.

Table 4.3
Optimization of Demethylation Reaction to Afford **1**

Entry	Solvent	BBr_3 (eq)	Time	Yield (%)
1	DCM	2.0	24h	-
2	DCM	20.0	24h	Trace amount
3	DCM	324	24h	80

Table 4.4
Comparison of ^{1}H and ^{13}C NMR Data of Hyrtiosulawesine With Reported Study

Position	δ ^{1}H (ppm) (J Hz) *	δ ^{13}C * (ppm)	δ ^{1}H (ppm) (J Hz)	δ ^{13}C (ppm)
1		140.6		140.4
2		-		-
3	8.41 (1H, d, 4.8)	137.6	8.438 (1H, d, 6.0)	137.4
4	8.14 (1H, d, 4.8)	118.8	8.167 (1H, d, 6.6)	118.4
4a		132.8		132.5
4b		122.9		122.6
5	7.56 (1H, d, 2.4)	107.1	7.586 (1H, d, 3.0)	106.8
6		152.9		152.7
7	7.13 (1H, dd, 2.4, 4.5)	120.1	7.153 (1H, dd, 3.0, 10.2)	119.9
8	7.53 (1H, d, 8.5)	114.2	7.558 (1H, d, 10.8)	113.9
8a		137.8		137.5
8b		137.7		137.4
1’		-		-
2’	8.88 (1H, s)	139.4	8.900 (1H, s)	139.1
3’		116.4		116.1
3’a		130.2		129.9
4’	8.01 (1H, d, 2.4)	108.3	8.034 (1H, d, 3.0)	108.1
5’		154.7		154.4
6’	6.81 (1H, dd, 2.4, 8.5)	114.1	6.830 (1H, dd, 3.0, 10.2)	113.8
7’	7.31 (1H, d, 8.5)	113.6	7.335 (1H, d, 10.2)	113.3
7’a		132.6		132.4
8’		190.2		189.9

*Salmoun *et al.,* 2002; 600 MHz, CD_3OD

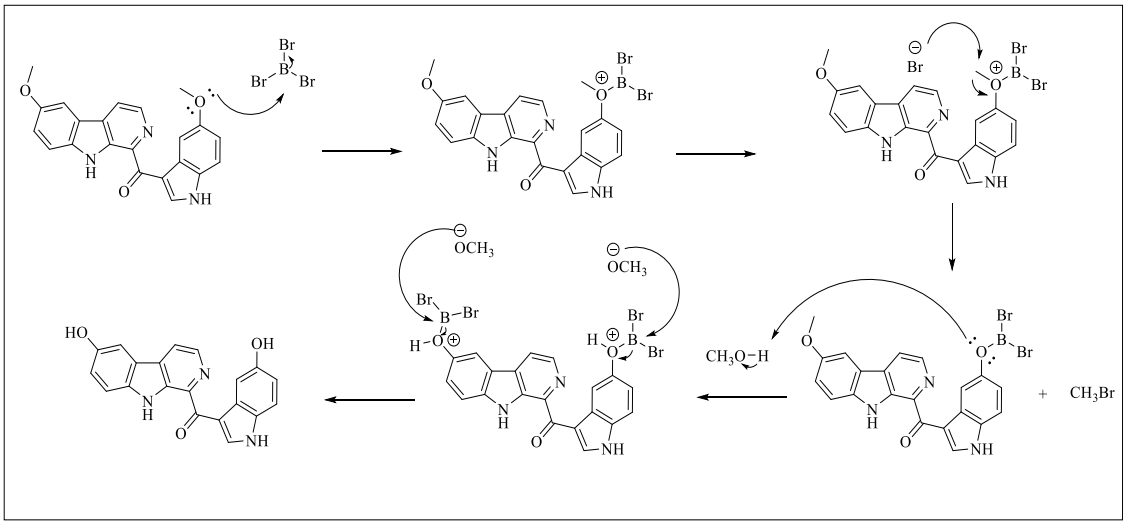

Scheme 4.10 Proposed Mechanism of Demethylation Reaction to Afford **1**

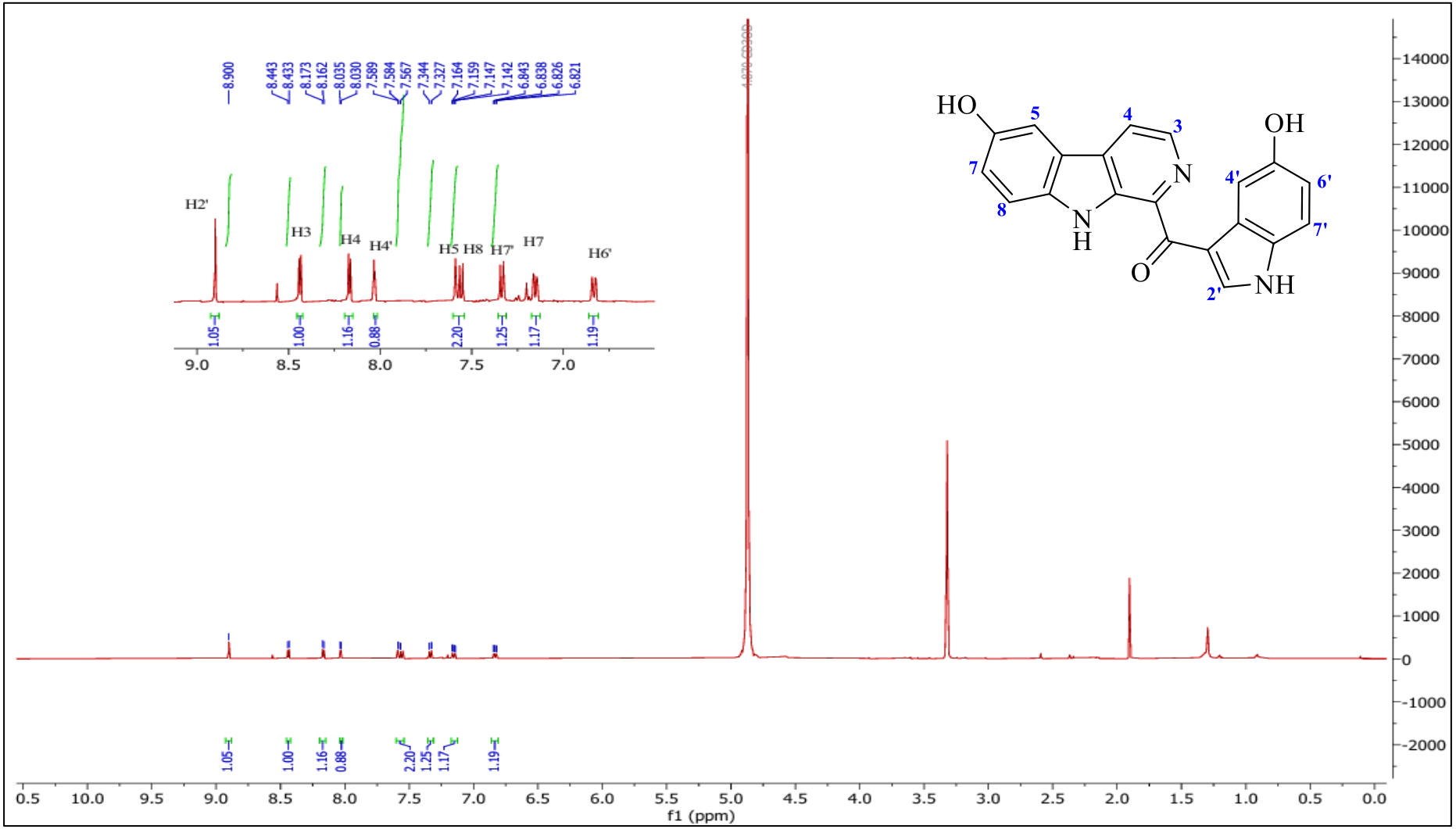

Figure 4.1 ^{1}H NMR Spectrum of Hyrtiosulawesine

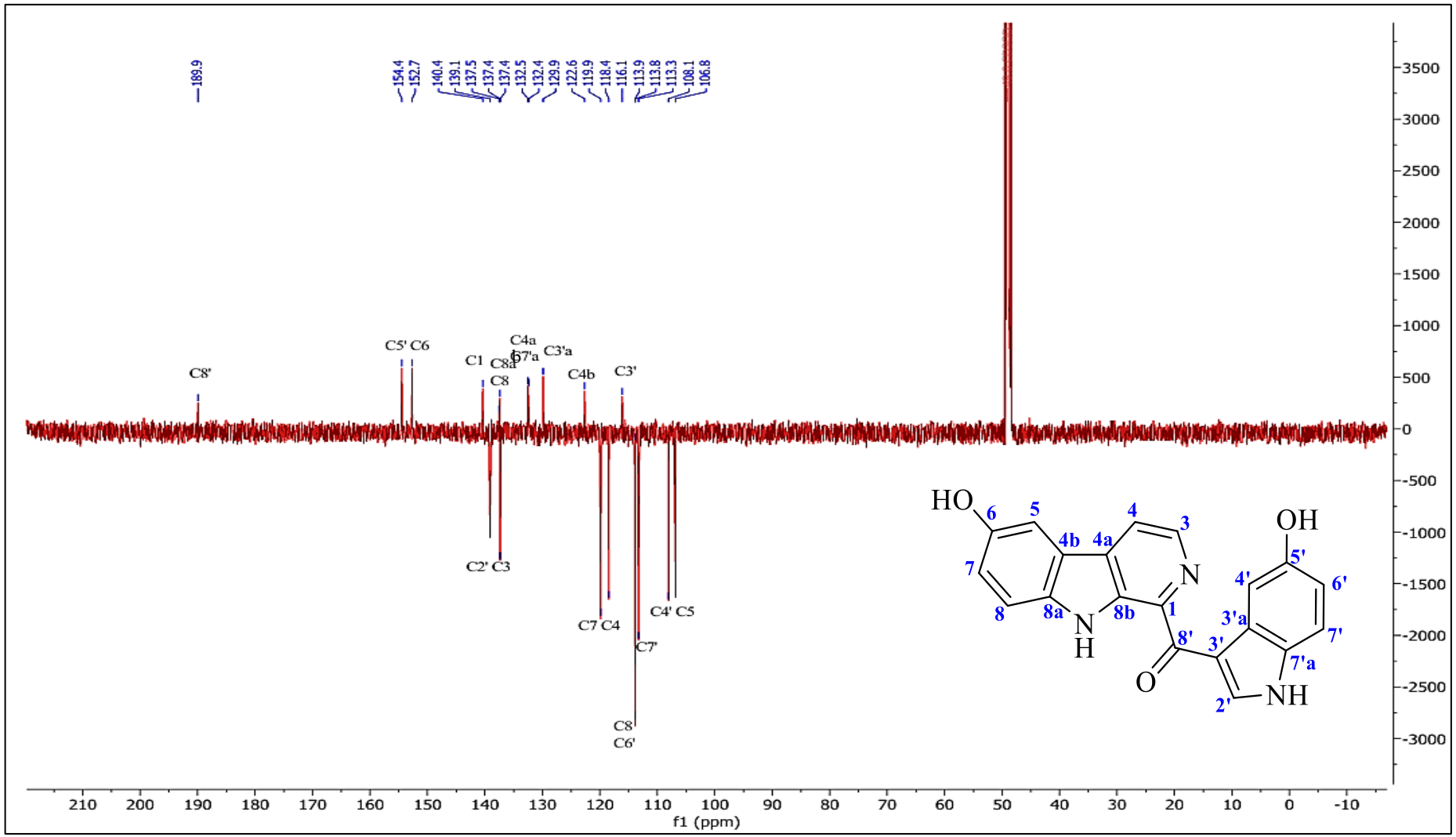

Figure 4.2 APT-NMR Spectrum of Hyrtiosulawesine

4.3 Synthesis of Hyrtiosulawesine's Derivatives

The total synthesis of hyrtiosulawesine was successfully achieved by optimizing various reaction conditions, such as the use of selective Lewis acids, iodine catalysts, and reaction times adjusted to maximize both the yield and purity of the compound. Following this success, its derivatives were further explored to observe how substituents group affected bioactivity. Using the same synthetic approach, acylation and alkylation reactions with different acylating and alkylating reagents at the C-5 and N-position of indole were investigated (Scheme 4.11).

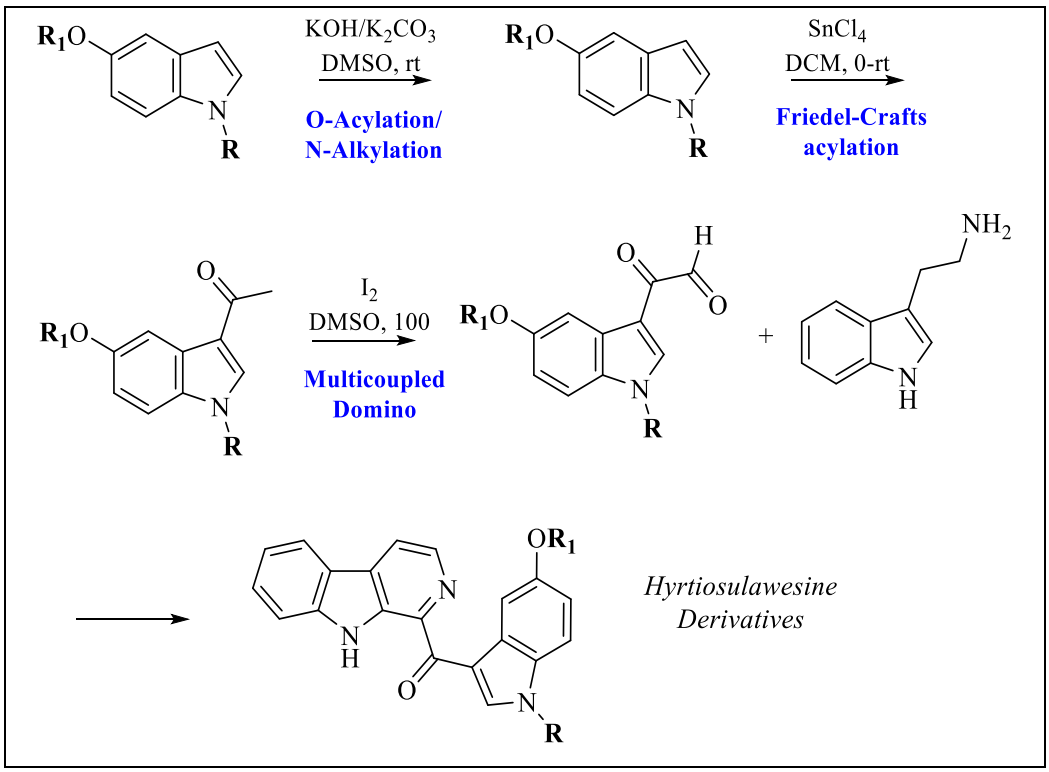

Scheme 4.11 Synthesis Route of Hyrtiosulawesine's Derivatives

4.3.1 *O*-Acylation of Indole at C-5 Position

Alteration at the C-5 position of the indole ring has been shown to significantly influence the biological activity of indole-based compounds (Yu *et al.,* 2012). Acyl chloride derivatives are known to exhibit consistent bioactivity. This prompted the investigation to substitute different chlorides on the hydroxyl group of indoles. As shown in Scheme 4.12, *O*-acyl derivatives were successfully achieved via the reaction

of 5-hydroxyindole (**2**) with various acyl chlorides. The product yield varies according to substituents presences (Table 4.5)

Following the results, the reaction rates and percentage yields were heavily influenced by the electronic and steric profiles of the substituents attached to the acyl chlorides. Within the substituted benzoyl chloride series, the presence of electron-withdrawing groups (EWGs) enhanced the electrophilicity of the carbonyl carbon via the inductive effect. This can be observed through compound **61**, (3-trifluoromethyl) benzoyl chloride, which produces 87% yield of the target product with 6 hours reaction time. However, compound **65** (3,4,5-trifluorobenzoyl chloride) bearing three fluorine atoms that were expected to highly activate the carbonyl yet gave the lowest yield (59%) with prolonged reaction time. This might be due to the electron-donating resonance effect dominating its electron-withdrawing inductive effect of the *para*-fluorine atom which increases the electron density at the carbonyl carbon, thus partially deactivates it towards nucleophilic attack.

Furthermore, the aliphatic and unsaturated acyl chloride sterically unhindered acetyl chloride (**57**) produces the corresponding product with 83% yield. In contrast, cinnamoyl chloride (**67**) displayed good reactivity by completing the reaction in the shortest duration of just 5 hours with an 80% yield. This significant reactivity of compound **67** is attributed to the presence of the conjugated π system, which stabilizes the transition state during the nucleophilic attack, thereby accelerating the overall reaction rate.

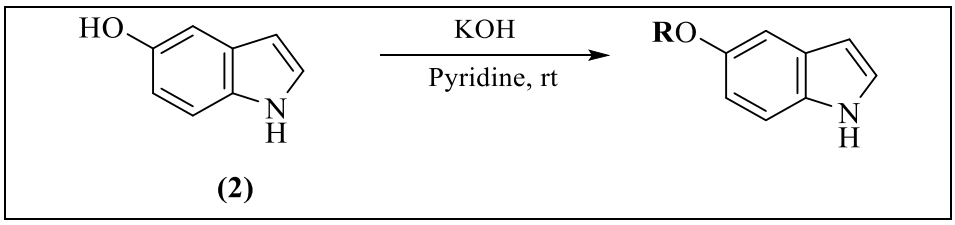

(2)

Scheme 4.12 *O*-Acylation of 5-Hydroxyindole

Table 4.5
O-Acylation of 5-Hydroxyindole (**2**)

Compound	R	KOH (eq)	Temperature	Time	Yields (%)
57		2	RT	12h	83
59	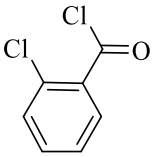	2	RT	10h	90
61	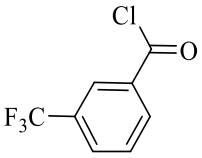	2	RT	6h	87
63	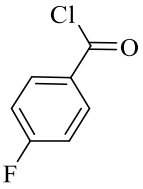	2	RT	15h	73
65	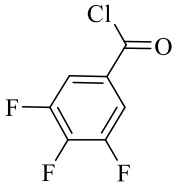	2	RT	14h	59
67	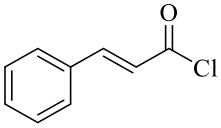	2	RT	5h	80

As depicted in Scheme 4.13, this reaction was facilitated by the presence of two equivalents of potassium hydroxide (KOH) which act as a base in a pyridine medium at room temperature. A 5-hydroxyindole was first deprotonated by KOH to produce nucleophilic phenoxide intermediate. This negatively charged oxygen using its high-energy HOMO to attack the electrophilic LUMO (antibonding orbital) of the 2-chlorobenzoyl chloride's carbonyl carbon, pushing the carbonyl pi electrons onto the oxygen to create a transient tetrahedral intermediate. attack on the electrophilic carbonyl carbon of the chlorobenzoyl chloride, pushing the carbonyl pi electrons onto the oxygen to create a tetrahedral intermediate. The intermediate quickly collapses, expelling the chloride ion as an excellent leaving group, deprotonate the positively charged hydrogen, and yield the stable ester product, along with an HCl byproduct.

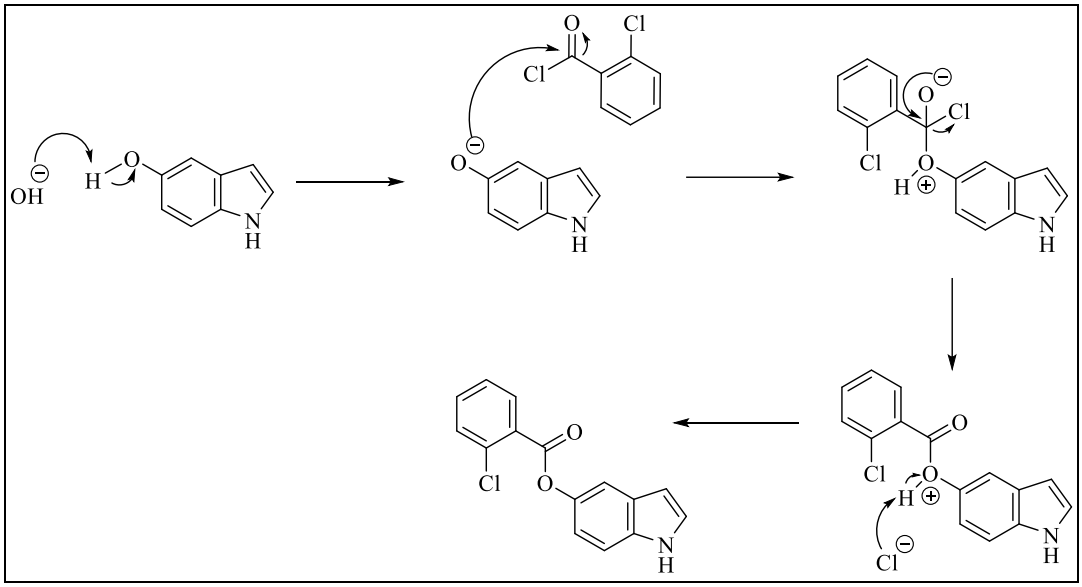

Scheme 4.13 Proposed Mechanism of 5-Hydroxyindole With Acyl Chloride

4.3.2 *N*-Alkylation of Indole

Following *O*-acylation of 5-hydroxyindole, different alkylating agents were utilized to substitute various alkyl groups at the nitrogen (NH) position of the indole ring (Scheme 4.14). N-substituted indoles often display altered pharmacokinetics and bioactivity profiles, making this position a key site for tuning drug-like properties (Chadha & Silakari, 2018). This modification consists of placing different alkylating groups at NH atom to measure their effects on the biological activity of the final compounds. Prior to Friedel-Crafts acylation, the starting material indole (**36a**) were introduced with different alkyl group to expand structural diversity at the nitrogen atom for subsequent screening of *Pf*LDH enzymatic inhibition. Table 4.6 summarizes the experimental outcomes which demonstrated significant yields of the alkyl substituted product.

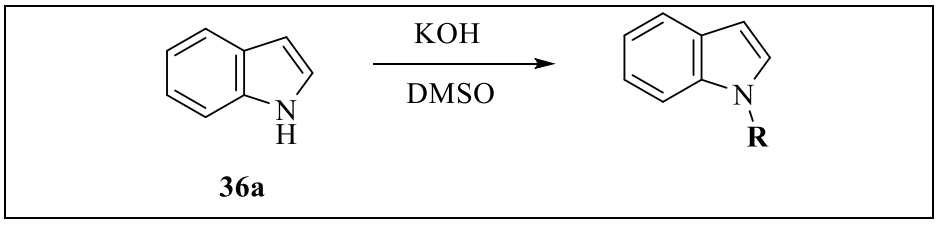

Scheme 4.14 *N*-Alkylation of indole

Table 4.6
N-alkylation of Indole (**36a**)

Compound	R	KOH (eq)	Temperature	Time	Yields (%)
37a		1.5	RT	8h	90
37b		1.5	RT	8h	86
71		1.5	RT	8h	78
73		1.5	RT	8h	74
75		1.5	RT	10h	75
37c		1.5	RT	5h	84

The selection of alkylating agent together with the alkyl chain characteristics determined the reaction results. This is because the yield percentages differed according to the length and structure of the substituted chains. According to Table 4.6, the reaction yields improved when using shorter alkyl groups (**37a**) or those with less steric hindrance but decreased when using longer or bulkier alkyl groups and reduced alkylating agent reactivity. The resulting yield maintained a substantial value despite this. The varying yields demonstrate the difference of alkylating agent and optimizing reaction conditions can lead to different outcomes.

Moreover, the selection of the base is critical in directing the alkylation site on the indole ring. To selectively obtain *N*-alkylation, the choice of the base is crucial. If the strong base is applied, it often results in C-3 alkylation due to the tight coordination of the metal cation (Na+) to the nitrogen atom, which shifts the nucleophilic attack to the C-3 position (Heaney & Ley, 1973). While a mild base like K_2CO_3 was implemented, it cannot generate a reactive intermediate and lead to no product formation. This difference in regioselectivity resulting from base strength can be clearly observed by the analysis of the ^{1}H-NMR spectrum shown in Figure 4.3. When a moderate base like KOH is used, alkylation occurs selectively at the N-H position of the indole. The successful formation of the *N*-alkylation product was confirmed by the presence of H-3 proton signals in the ^{1}H NMR spectrum. Conversely, under strongly basic conditions, the C-3 alkylation becomes the dominant pathway, suppressing the desired *N*-alkylation product.

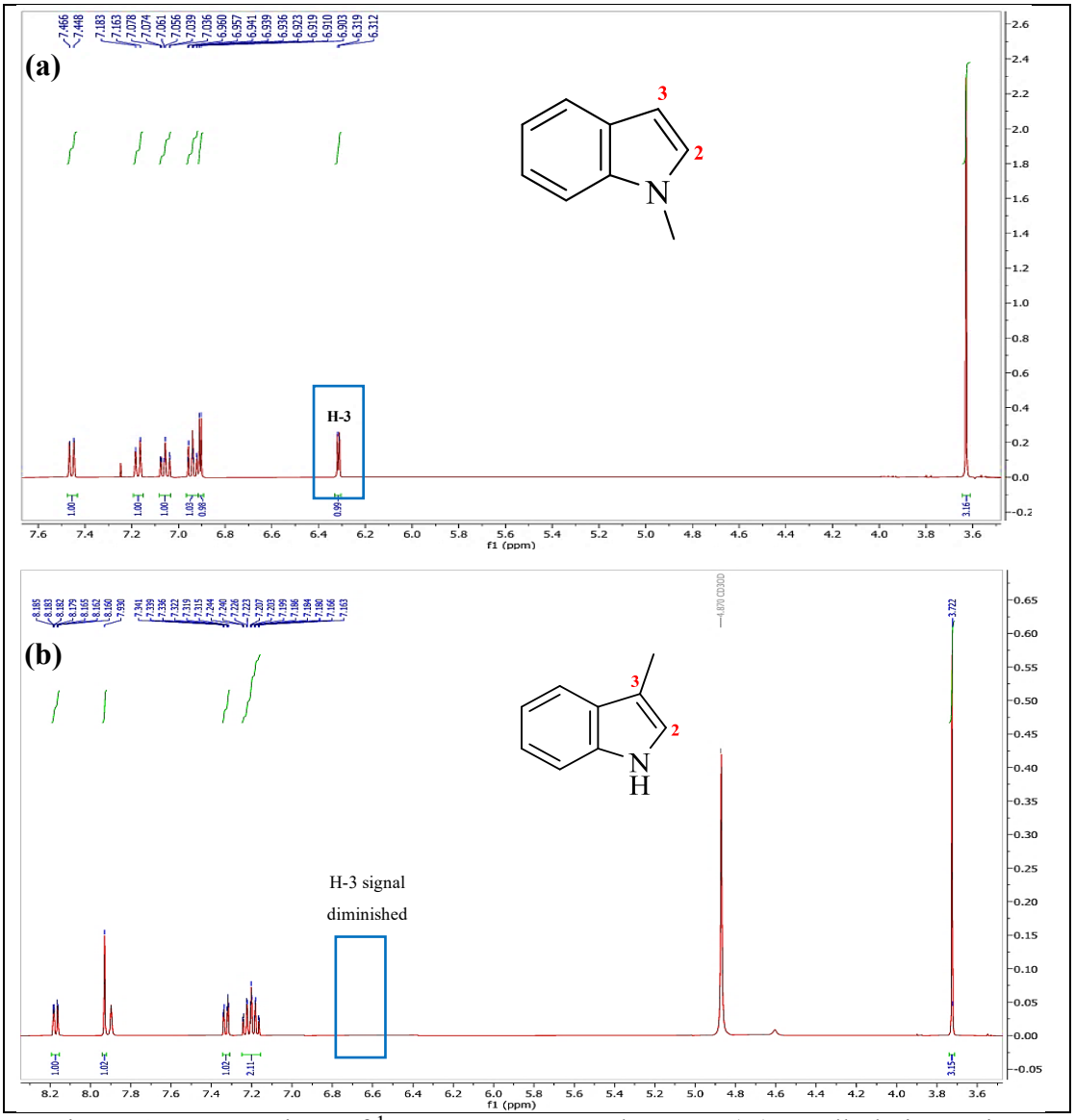

Figure 4.3 Comparison of ^{1}H NMR Spectrum between (A) *N*-Alkylation Using Potassium Hydroxide Base and (B) *N*-Alkylation Using Sodium Hydride Base

4.3.3 Friedel-Crafts Acylation of *N*- and 5-Substituted Indole

The Friedel-Crafts acylation reaction was executed after the acylating and alkylating agents were successfully introduced. The essential step enabled further modification of the indole structure. This study shows how systematic evaluation of their effects on the reaction and compound's properties. Table 4.7 presents the summary of research findings.

According to the table below, the expected products were successfully synthesized, yielding moderate to high yields. The efficiency of the Friedel-Crafts acylation is based on the electronic effects of the substituents at R_1 position and the

steric hindrance introduced at the R_2 position. When the R_1 and R_2 positions are unsubstituted (Compound **77**), the yield is excellent due to unhindered ring nucleophilicity. However, introducing halogens groups at R_1 (Compounds **78**, **80**, and **82**) decreases the yield and double the reaction time. This occurs due to strong inductive electron-withdrawing effect of halogens, effectively reducing the nucleophilicity at the C-3 position. Interestingly, compounds **84**, **86**, and **88** with stronger electron-withdrawing groups obtain higher yield. While these deactivated rings possess lower nucleophilicity and are expected to decrease percent yield yet produce high percent yield. This is due to slower reaction rates which can prevent over-acylation or decomposition side pathways and finally produce high yield.

Compound **94** with the 3,4,5-trifluorobenzoyl substituent was found to significantly reduce the electron density at the nucleophilic C-3 site via extended resonance effects, thereby suppressing the reaction rate. Conversely, *N*-alkyl modifications enhance ring nucleophilicity through inductive donation but introduce severe steric clashes adjacent to the C-3 center and necessitate prolonged reaction times to achieve high yields. Furthermore, Cinnamoyl substituents have often been reported in the literature to display promising biological activity, which initially encouraged to use this group in this study. However, the synthetic attempts proved unsuccessful. When using $SnCl_4$ and Et_2AlCl as Lewis acid promoters, no target product was obtained. In the case of Et_2AlCl, the starting material was largely not fully consumed even after 10 hours. These results suggest that the insufficient to activate the starting material and cinnamoyl is sensitive to acids environment, therefore, this substitution was not pursued further.

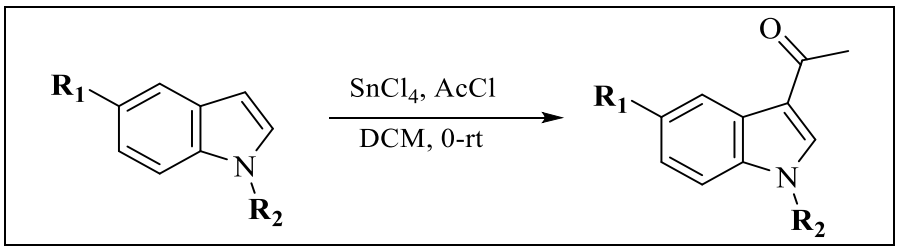

Scheme 4.15 Friedel-Crafts Acylation of Substituted Indole

Table 4.7
Friedel-Crafts Acylation of substituted Indole

Compound	R_1	R_2	Time	Yields (%)
77	H	H	2h	87
78	Br	H	4h	60
80	Cl	H	4h	60
82	F	H	4h	62
84	CN	H	5h	72
86	CF_3	H	5h	70
88	NO_2	H	5h	69
90	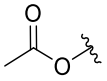	H	6h	50
91	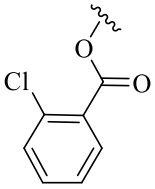	H	5h	78
92	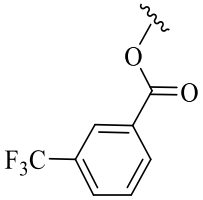	H	4h	76
93	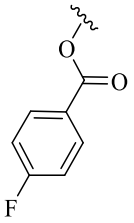	H	5h	70
94	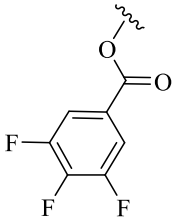	H	20h	59
140	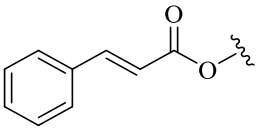	H	12h	0
95	H		18h	80
96	H		20h	79
97	H	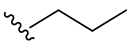	20h	78
98	H	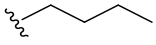	20h	76
99	H	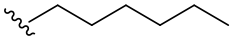	20h	77
100	H	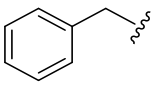	20h	75

4.3.4 Formation of Hyrtiosulawesine Derivatives *via* Multicouple Domino Reaction

The β-carbolines have been reported to be synthesized efficiently through one-pot and domino methods. This strategy was applied to accelerate the reaction. The one-pot multicoupled cyclization reduces the number of steps, thereby minimizing yield loss and perhaps improving efficiency. Proceeding with the final stages, the product obtained from the successful Friedel-Crafts acylation reaction was subjected to this reaction. Utilizing the previously optimized methodologies, resulting in the desired compounds as well as several partially derived side products as detailed in Table 4.8.

The data demonstrated that different substituents attached on the molecule alter the effectiveness of the domino reaction to convert substituted 3-acetylindoles into fully aromatized β-carboline derivatives (a) and partially aromatized dihydro-β-carboline derivatives (b). The target products heavily dictated by the electronic and steric properties of the substituents. When the modifications were done at the R_1 position, a clear correlation observed between the electron-withdrawing capabilities of the substituent and the isolated yield of the fully aromatized products. Strong EWG's compounds enhance the electrophilicity of the 2-oxoaldehyde intermediate which generated via Kornblum oxidation. Consequently, strong deactivated groups like compounds **20b** (-NO_2, 53%), **110** (-CN, 50%), and **111** (-CF_3, 47%) show the highest yields of the fully aromatized species in comparison to EDG methoxy derivative, compound **20c** (-OCH_3, 28%).

For halogen group, the result shows a steady increase in yield from fluorine (27%) to chlorine (42%) and bromine (46%), which highlights a balance between inductive effects and atom polarizability. However, when bulky aromatic ester chains were introduced at R_1, the yields drop, ranging between 15% and 30%. Although the introduction of a benzoyl chloride substituent should enhance the electrophilicity of the glyoxal moiety via electronic deactivation, a lower reaction yield was observed. This is attributed by steric hindrance imposed by the bulky benzoyl group which hindered the nucleophilic approach of tryptamine while can promotes side reactions with traces of water. In comparison, the smaller nitro substituent (**20b**) gives a better yield. Like benzoyl chloride, it deactivates the ring and makes the glyoxal ready for tryptamine attack. However, because it is smaller, it effectively minimizes steric hindrance while maintaining the required electron-withdrawing effect.

In terms of the functionalization at the indole nitrogen (R_2) when the unsubstituted -NH reacted (**18**), it requires a prolonged reaction time of 24 hours to achieve a 30% yield. Whilst the *N*-alkylation efficiently accelerates the reaction time for 14 hours across a homologous series. This demonstrated from the methyl group in compound **123** (31% yield) up to the extended pentyl chain in compound **131** (30% yield), is attributed to the inductive electron-donating effect of the aliphatic chain. This electron donation improves the cyclization rate and suppresses intermolecular proton-transfer side reactions by capping its acidic proton (-NH). Thus, while benzoyl chloride experiences both steric hindrance and unwanted side reactions, the nitro group succeeds due to its minimal steric hindrance and the EDG has moderate cyclization rate and preventing side reactions. Finally, adding a benzyl group at R_3 position speeds up the reaction to 12 hours and gives the highest yield (60%) of the final product. This might be due to electronic conjugation and activation provided by the benzyl group can lower the activation energy for oxidative dehydrogenation. To summarize, hyrtiosulawesine's derivative was successfully synthesize with yields ranged between 4% and 60% regardless of its complex structure. The production of these compounds is enough to conduct thorough biological and computational investigations.

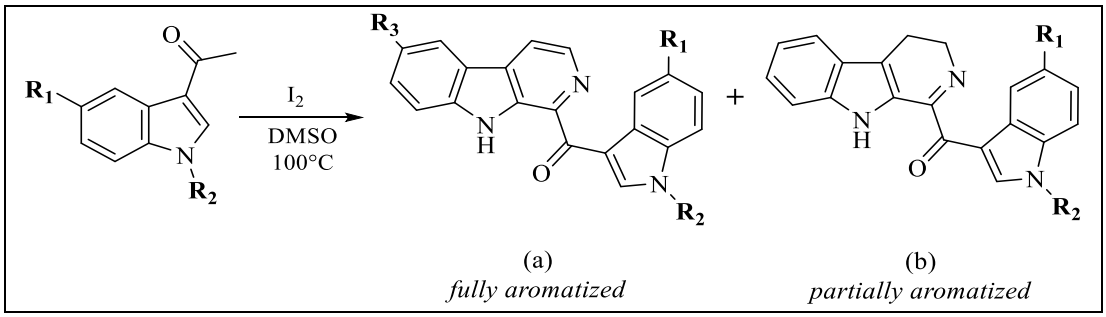

Scheme 4.16 Multicouple Domino of substituted-3-acetylindole to obtain Hyrtiosulawesine Derivatives

Table 4.8
Domino Reactions of Hyrtiosulawesine Derivatives

R_1	R_2	R_3	Time	Compound Yields (%)	
				(a)	(b)
H	H	H	24h	**18**: 30	**101**: 12
Cl	H	H	24h	**102**: 42	**103**: 10
Br	H	H	24h	**20a**: 46	**104**: 16
F	H	H	24h	**105**: 27	**106**: 15
CF_3	H	H	24h	**107**: 47	**108**: 11
NO_2	H	H	24h	**20b**: 53	**109**: 4
CN	H	H	24h	**110**: 50	**111**: 9
OCH3	H	H	24h	**20c**: 28	**112**: 15

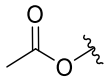	H	H	24h	**113**: 27	**114**: 22
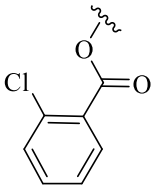	H	H	24h	**115**: 30	**116**: 12
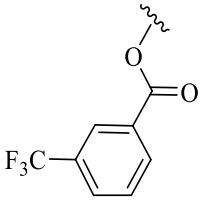	H	H	24h	**117**: 30	**118**: 16
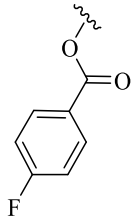	H	H	24h	**119**: 20	**120**: 10
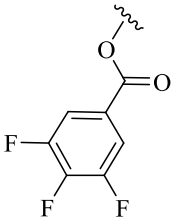	H	H	24h	**121**: 15	**122**: 10
H		H	14h	**123**: 31	**124**: 20
H		H	14h	**125**: 34	**126**: 19
H	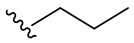	H	14h	**127**: 35	**128**: 14
H	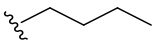	H	14h	**129**: 33	**130**: 14
H	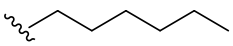	H	14h	**131**: 30	**132**: 10
H	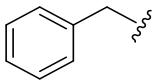	H	14h	**133**: 32	**134**: 20
H	H	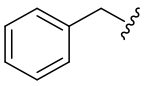	12h	**136**: 60	-

4.4 Biological Activities of Hyrtiosulawesine and Its Derivatives

4.4.1 Antimalarial Activity

In a previous investigation, Liew *et al.* (2014) has reported significant antimalarial activity of hyrtiosulawesine with a potency of 1.0 μM against the chloroquine-resistant strain (FcB1) of *Plasmodium falciparum*. Building upon these findings, subsequent investigations were carried out through an *in vitro* antimalarial

enzymatic assay, which focused on lactate dehydrogenase (LDH) as the target enzyme. This enzyme was chosen due to its crucial role in the ATP production of cells, and its presence across all *Plasmodium* species. Inhibition of LDH disrupts the parasite's energy metabolism, thereby offering a promising mechanism for antimalarial activity (Figure 4.4).

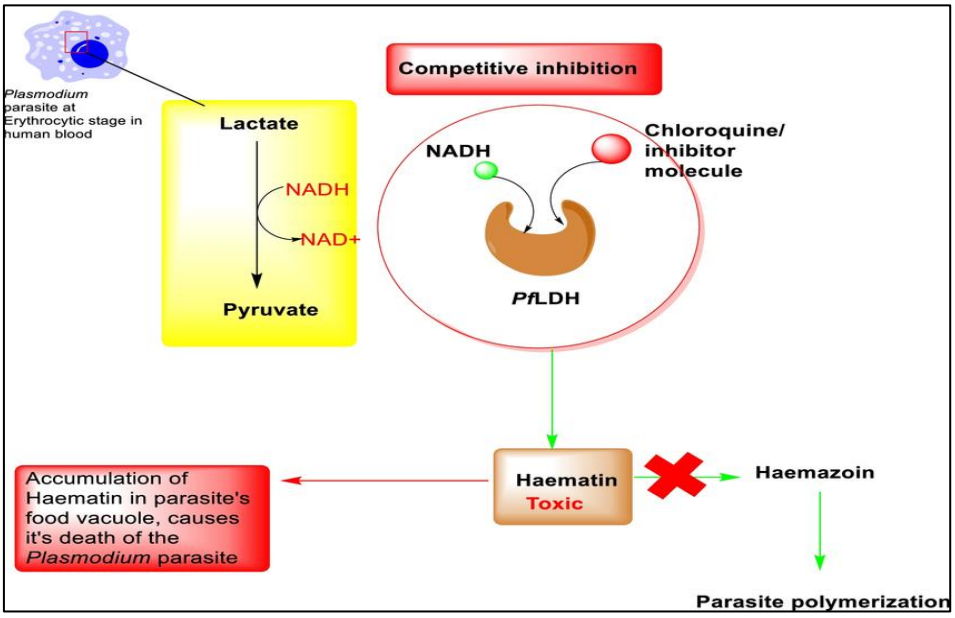

Figure 4.4 Schematic Illustration of Competitive Inhibition of *Pf*ldh. An Inhibitor (E.G., Chloroquine) Competes with NADH at the Active Site of *Pf*ldh, Impairing NADH-Dependent Conversion of Lactate to Pyruvate. This Inhibition Interrupts ATP Production, Leading to The Accumulation of Toxic Haematin. Inhibited Polymerization into Haemozoin Ultimately Causes Parasite Death. (Dey *et al.,* 2022)

In this study, the screening was performed at 1 µM instead of the usual conventional 100 µM. This decision is due to practical limitations, including the large number of compounds to be tested, the stability of the enzyme, and the requirement to perform triplicates and subsequent IC_{50} assays. Although higher screening concentrations are commonly used to increase the probability of detecting weak inhibitors, single-point screening at 1 µM is still acceptable and has been reported in previous studies (Zheng & Polli, 2010; Inglese *et al.,* 2006). Despite the lower concentration, several compounds showed more than 30% inhibition, allowing the identification of the three most promising candidates for further evaluation. All the derivatives of hyrtiosulawesine were screened for their ability to inhibit this enzyme, and the results are summarized accordingly in Table 4.9.

Table 4.9
Percentage Inhibition (%) of *Pf*LDH by Hyrtiosulawesine Derivatives Screened at 1 μM Concentration.

Compound	Structure	Percent Inhibition (%)
114	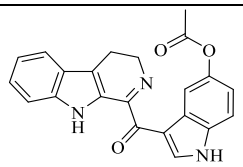	39.1
113	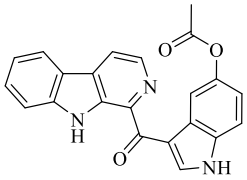	30.6
53	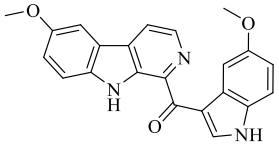	33.1
119	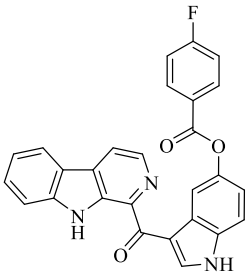	25.3
117	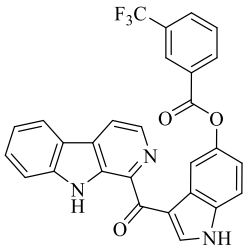	22.4
115	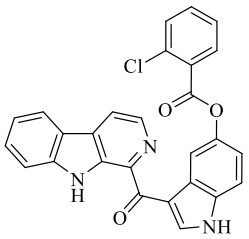	19.1
125	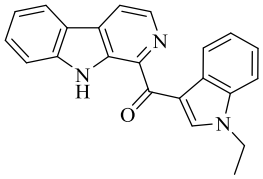	18.2

131	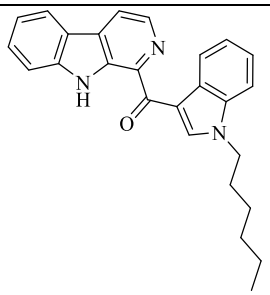	17.3
112	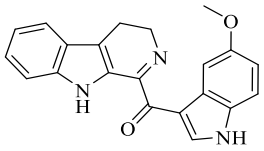	15.4
128	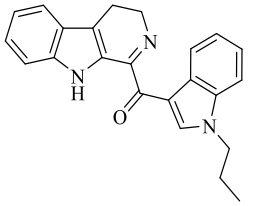	15.3
101	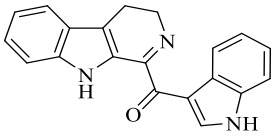	14.5
120	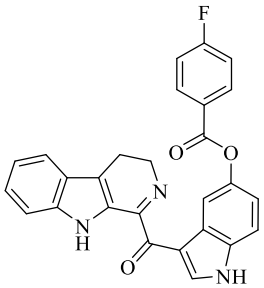	14.1
121	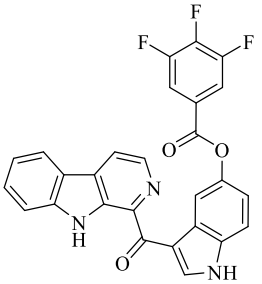	13.9
127	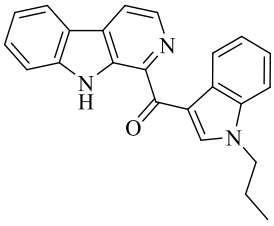	13.6
108	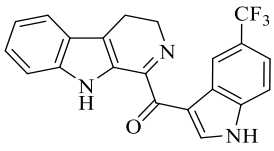	11.6

109	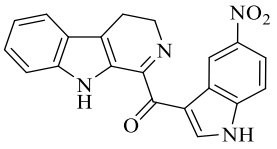	12.1
18	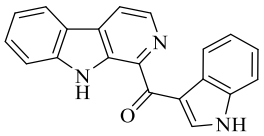	11.2
126	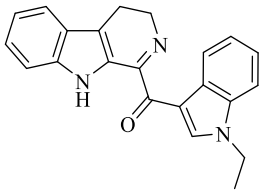	11.0
20c	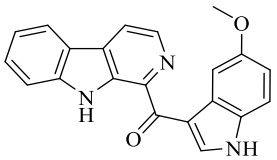	10.8
102	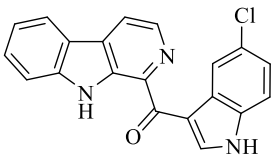	9.1
103	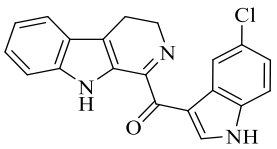	7.6
107	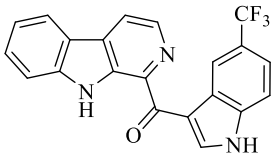	2.4
130	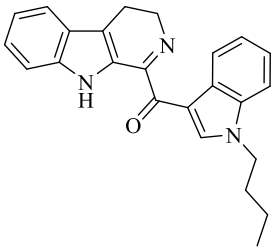	2.4
110	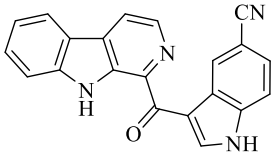	0.7
124	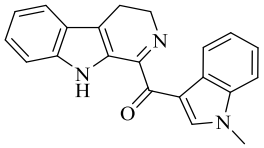	NI

20a	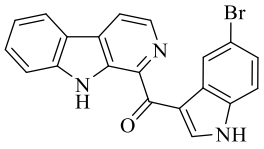	NI
104	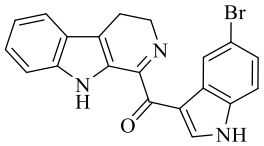	NI
106	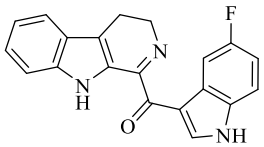	NI
105	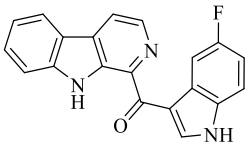	NI
111	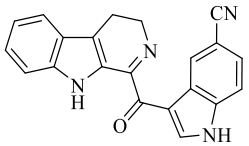	NI
133	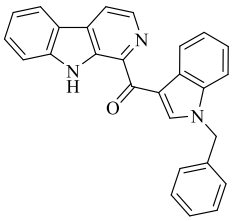	NI
134	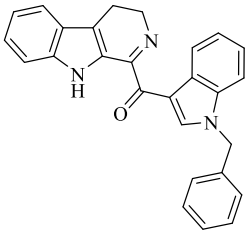	NI
122	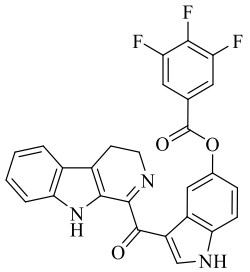	NI
1	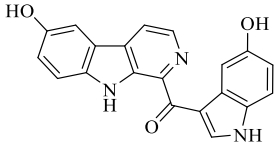	NI
136	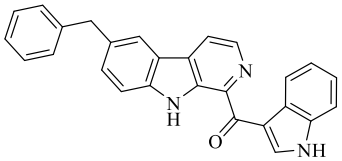	NI

20b	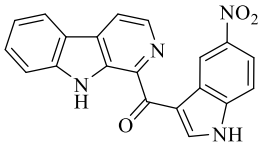	NI
116	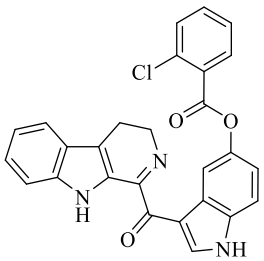	NI
118	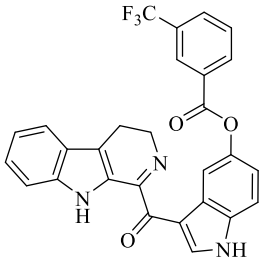	NI
123	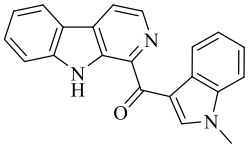	NI
129	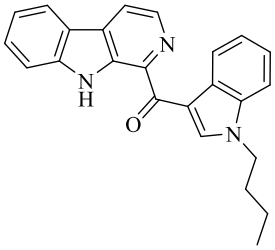	NI
132	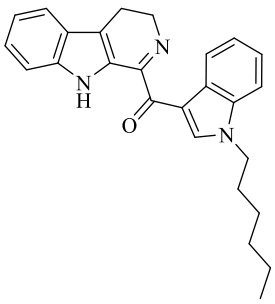	NI

*NI= No Inhibition

All selected derivatives of hyrtiosulawesine were screened and exhibited minimal to no inhibition at a concentration of 1 μM. Among these, approximately 23 compounds demonstrated inhibition in comparison to the negative control (no inhibitors). To date, eight compounds showed better inhibition than the positive control, oxamate, which was used in this study. Although oxamate exhibits modest potency and is not a commercially available antimalarial drug, it was utilized in this study as an established reference inhibitor due to its well-characterized competitive inhibition

mechanism against *Pf*LDH, and its analogues have been reported to possess potent antimalarial activity. Oxamate was chosen as the positive control since it similar structure to pyruvate, confusing the enzyme into considering it either pyruvate or an inhibitor.

As shown in Figure 4.5, three compounds, **53**, **113** and **114,** were further advanced from the top group for IC_{50} determination, each showing about 30% inhibition at 1 µM concentration tested. To ensure reliability, these results were re-evaluated to confirm similarity in percentage inhibition prior to IC_{50} determination and the data obtained were found to be highly reproducible. These compounds were selected for their greater inhibitory potential and thus promising for further optimization. The IC_{50} determination assay results are presented in Table 4.10.

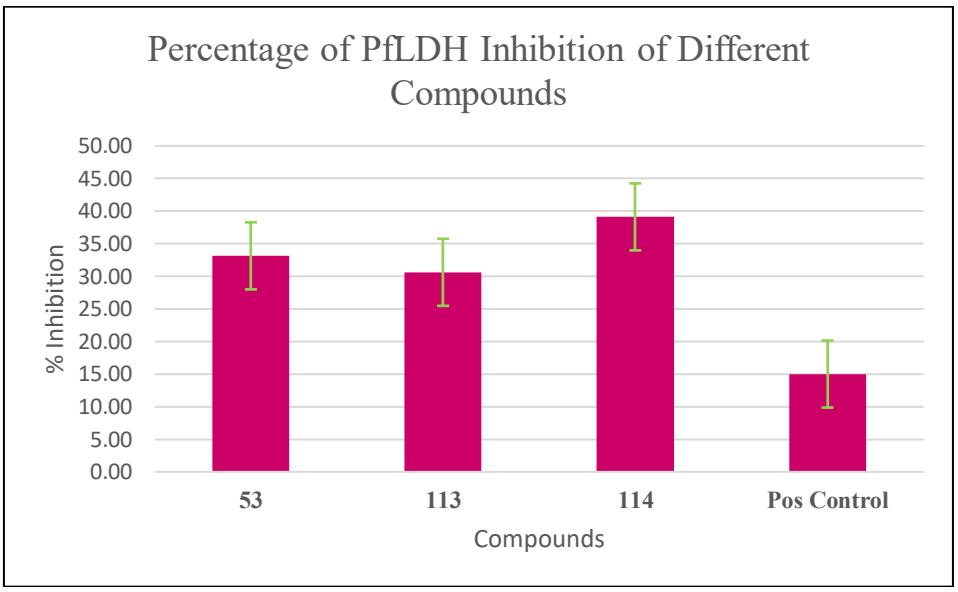

Figure 4.5 Percentage of *Pf*LDH Inhibition of Different Compounds. Compound **114** Shows the Highest Inhibition at 39.1% of *Pf*LDH

Table 4.10
Antimalarial Activity Against *Pf*LDH of Selected Hyrtiosulawesine's Derivatives

Compound	IC_{50} Value (μM) ± SEM
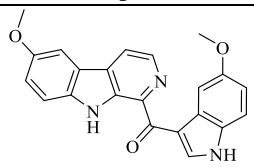 **53**	5.44 ± 0.48 μM
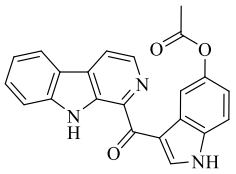 **113**	13.32 ± 2.30 μM
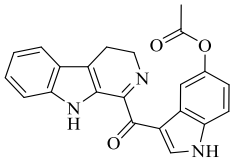 **114**	8.40 ± 0.42 μM
Oxamate (positive control)	6.60 ± 0.78

Interestingly, compound **53** stands out as the most effective inhibitor among our parent compounds with an IC_{50} value of 5.44 ± 0.48 μM (Table 4.10). The insertion of a methoxy group at the C-5 position of an alkaloid backbone often enhances the biological potency or efficacy of the compound. This is supported by structure-activity relationship (SAR) studies in various alkaloid classes, which indicate that a methoxy substituent at C-5 of indole can improve cytotoxicity or inhibitory activity compared to other functional groups (Preciado *et al.,* 2023). It can also be observed in Table 4.9, when two methoxy groups presence it shows better inhibition compared to one methoxy group like compound **20c** with 10% inhibition.

Derivatives **114** and **113** showed lower inhibition through their IC_{50} values of 8.4 ± 0.42 μM and 13.32 ± 2.30 μM. The antimalarial effectiveness of the compounds reduces when structural alterations are applied through **113,** a fully aromatized β-carboline and **114** the partial β-carboline. The acyl substituents at the C-5 position of indole in both compounds contribute to their moderate biological activity. The different activities observed demonstrate that the chemical structure controls biological properties of these compounds while emphasizing the requirement for structural optimization work.

To better understand these trends, a structure-activity relationship (SAR) summary was compiled (Table 4.11), correlating substitution patterns with *Pf*LDH inhibitory potency while incorporating findings from docking and molecular dynamics analysis. The data demonstrates that the C-5 methoxy group acts as the main factor for potency while partial β-carboline aromaticity enhances binding. Although the IC_{50} values remain in the low micromolar range, these results are promising for early-stage enzyme-targeted inhibitors. Importantly, the identification of **53** as both synthetically accessible and biologically active establishes a practical lead scaffold. The current enzyme-based findings serve as a rational foundation for future parasite culture assays, which are being conducted to confirm cellular efficacy.

Table 4.11
Summary of Structure-Activity Relationships (SAR) For Hyrtiosulawesine Derivatives Against *Pf*LDH

Modification site	**Compound**	**Structural change**	**IC_{50} (μM) and activity trend**
Indole C-5 and β-Carboline C-6	**53**	Methoxy at C-5 and C-6' of β-carboline	5.44 ± 0.48 (moderate to potent activity)
Indole C-5	Halogenated analogues	Bulky EWG	Inactive
β-Carboline core	**114** vs **113**	Partially vs fully aromatization	8.40 ± 0.42 (**114**) 13.32 ± 2.30 (**113**) (partially aromatized better activity)
N-alkylation	Short alkyl chains Long and bulky alkyl	Nitrogen of indole	Inactive Inactive
Acyl substituents at indole C-5	Various	Electron-withdrawing acyl	weak to inactive

*****IC_{50} < 0.06 μM: **highly potent**; IC_{50} 0.06 - 5 μM: **active;** IC_{50} 5 – 10 μM: **weakly active;** IC_{50} > 10 μM: **inactive** (Onguéné *et al.,* 2014)

4.4.2 Cytotoxicity Activity

Though initially created and evaluated for antimalarial activity, these compounds have structural features that point to possible anticancer effects. Given the β-carboline-indole scaffold in hyrtiosulawesine derivatives, which are well-documented for enhanced cytotoxicity against breast and colon cancer cell lines (Soni *et al.,* 2021; Soni *et al.,* 2023). Chosen for their epithelial morphology and differentiation potential, HT-29 cells were chosen as the colon cancer model whereas

triple negative breast cancer model MDA-MB-231 was chosen for its aggressive growth and resistance to receptor targeted drugs. All 16 compounds were evaluated using MTT cytotoxicity assay and the data were tabulated in Table 4.12.

Table 4.12
Cytotoxic IC_{50} (μM) of Tested Compounds in Breast and Colon Cancer Cells

Compound	Structure	Inhibition Concentration, IC_{50} (μM) ± SD	
		MDA-MB-231	HT-29
110	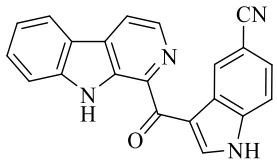	26 ± 4.00	>80
106	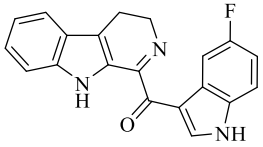	39 ± 4.00	35 ± 4.00
118	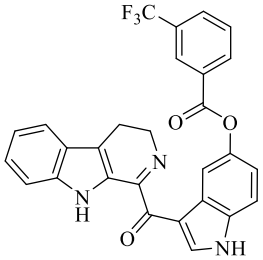	39 ± 3.00	42 ± 5.00
136	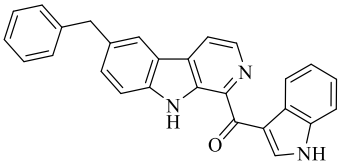	41 ± 7.00	>80
120	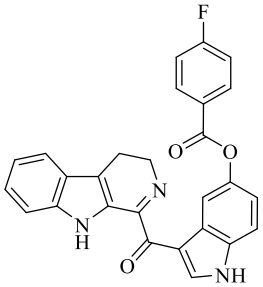	51.5 ± 3.00	>80
108	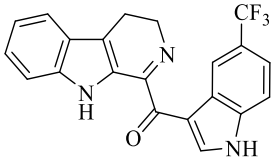	>80	57 ± 9.00
20a	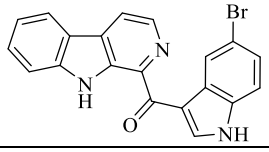	>80	>80

105	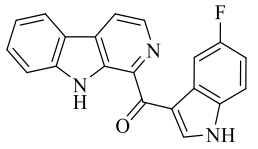	>80	>80
107	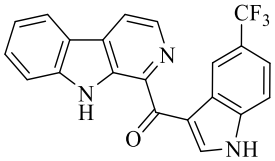	>80	>80
102	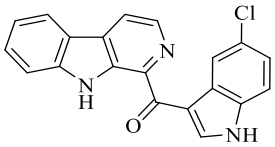	>80	>80
20c	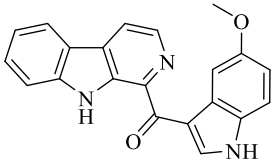	>80	>80
18	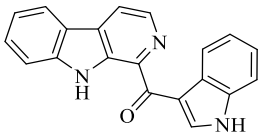	>80	>80
104	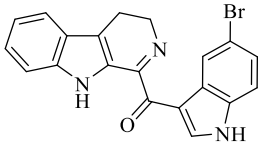	>80	>80
101	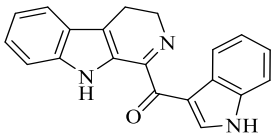	>80	>80
1	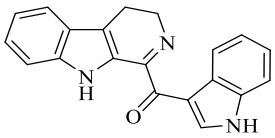	>80	>80
116	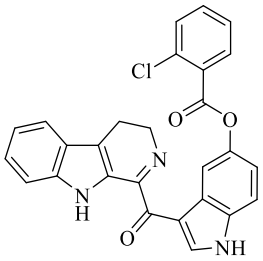	>80	>80
117	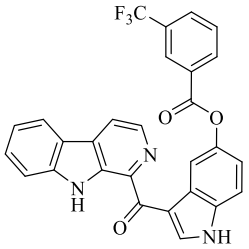	>80	>80
Doxorubicin*		7.78 ± 3.45	7.78 ± 3.45

*Peeva *et al.,* 2024

Based on the table above, most compounds are inactive since the IC_{50} value is more than 80 μM. However, some show moderate activity against both MDA-MB-231 (breast cancer) and HT-29 (colon cancer). Compound **110** (26 μM), bearing cyano substituents inhibits MDA-MB-231 better than parent compound, hyrtiosulawesine. The following compounds tested, **136** (41 μM), **106** (39 μM), **118** (39 μM), and **120** (51.5 μM) reveal moderate activity. This observation shows that specific substituents enhance activity in breast cancer cells. Derivatives containing fluoro or CF_3 substituents on partial aromatized scaffolds or benzyloxy addition to β-carboline demonstrate significant potency. In contrast, fully aromatized β-carboline and halogenated compounds generally inactive (>80 μM), indicating that partial aromatization and selective electron-withdrawing groups may favor binding or cell permeability in MDA-MB-231 cells.

The activity of HT-29 is poor, with only **106** (35 μM), **118** (42 μM) and **108** (57 μM) demonstrate it moderately activity compared to MDA-MB-231. This suggests that colon cancer cells are less susceptible to these scaffolds. Similar to MDA-MB-231, partial aromatization in combination with Fluro and CF_3 substituents may increase activity against HT-29. These Fluorine and CF_3 groups enhanced cytotoxicity against both MDA-MB-231 and HT-29 cells, as evidenced by previous investigation (Chang *et al.,* 2016; Zhang *et al.,* 2020; Ullah *et al.,* 2022). Other compounds, notably acyl chloride derivatives, have little impact (>80 μM), indicating that SAR trends differ across breast and colon cancer cells.

These results suggest that SAR trends diverge across different cancer types, with breast cancer cells showing higher sensitivity than colon cancer cells. The observed differences further emphasize the importance of fine-tuning structural features such as degree of aromatization and substituent type to optimize activity. While the current IC_{50} values remain modest compared to literature reported doxorubicin values (IC_{50} = 7.78 ± 3.45 μM; Peeva *et al.,* 2024), the findings provide a promising basis for lead optimization and scaffold refinement.

4.5 *In silico* Analysis

4.5.1 Molecular Docking

Molecular docking was performed to rationalize the SAR findings and to compare the binding profiles of the most active derivatives with the reference inhibitor oxamate. The molecular docking process commenced with a meticulous validation between the protein (PDB ID: 1U4S) and its native ligand. Figure 4.6 shows that naphthalene-2,6-disulfonic acid was successfully redocked with an RMSD value of 0.694. All subsequent docking investigations strictly followed this methodology, and their binding affinities, ranging from the most potent to the least, were thoroughly documented in Table 4.13.

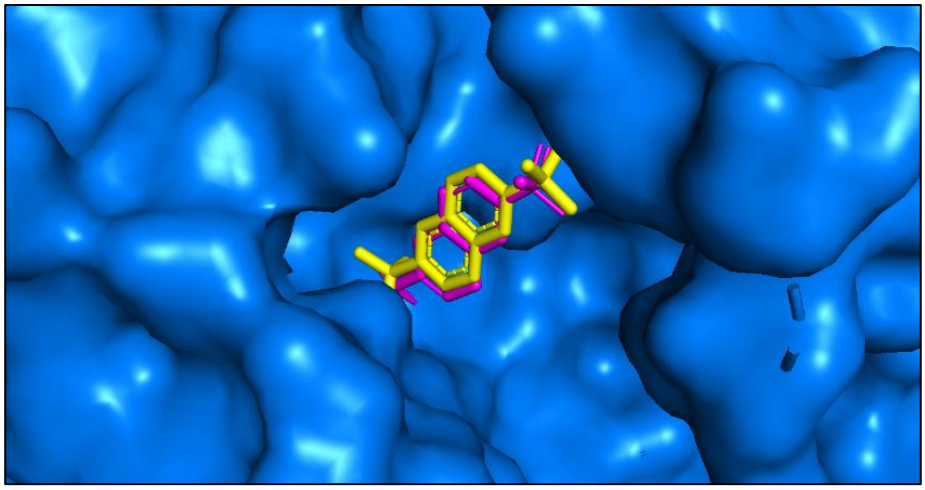

Figure 4.6 Superposition of Naphthalene-2,6-Disulfonic Acid (Pink) as Bound and Redocked Native Ligand (Yellow) with RMSD Value of 0.694

Table 4.13
Molecular Docking Results of Hyrtiosulawesine and Its Derivatives

Compounds	Binding Affinities (kcal/mol)	Amino acid residue having interaction within 4Å distance
116	-9.0	Asn140, Arg171, Ala236, Asn197, Val233, Gly196
118	-8.6	Ala236, Val233, Asn197, Gly196
117	-8.4	Asn140, Arg171, Ala236, Asn197, Val233, Gly196
119	-8.1	Asn140, Arg171, Ala236
120	-8.1	Asn140, Arg171, Ala236, Asn197
121	-8.0	Asn140, Arg171, Ala236
122	-8.0	Asn140, Arg171, Ala236, Asn197
133	-8.0	Asn140, His195
134	-8.0	Asn140, Gly196, His195
115	-7.7	Asn140, Arg171, Ala236
108	-7.6	Asn140, Asn197, Ala236
114	-7.6	Asn140, Arg171, Ala236
136	-7.5	Arg171, Ala236, Asn197
20a	-7.4	Ala236, Arg171
112	-7.4	Ala236, Arg171

107	-7.4	Ala236, Asn140
111	-7.4	Asn197, Ala236
123	-7.4	Asn140, Ala236, His195, Val233
124	-7.4	Asn140, Ala236, Val233
110	-7.4	Ala236, Arg171
126	-7.4	Asn140, Ala236, His195
106	-7.3	Asn140, Ala 236, Val 233
20b	-7.3	Asn140, Ala236
109	-7.3	Asn140, Ala236, Asn197
104	-7.3	Asn197, Ala236, Asn140
103	-7.3	Asn197, Ala236, Asn140
101	-7.3	Asn140, Val233, Ala236
113	-7.3	Asn140, Arg171, Ala236
1	-7.2	Arg109, Gly196, Arg171, Ala236
20c	-7.2	Asn140, Ala236, Arg171
102	-7.2	Ala236, Arg171,
105	-7.2	Asn140, Ala236, Arg171
128	-7.2	Asn140, Ala236, His195, Gly196
125	-7.1	Asn140, Ala236
53	-7.0	Arg171, Ala236, Arg109, Asn140
129	-7.0	Asn140, Ala236, His195
130	-7.0	Asn140, Ala236, His195, Gly196
127	-7.0	Asn140, His195
131	-6.7	Asn140, His195
132	-6.7	Asn140, Ala236, His195, Gly196
Naphthalene-2,6-disulfonic acid	-5.2	Arg 171, Asn 140
Oxamate	-3.4	Gly196, Val233, Arg171, Ala236

Table 4.13 presents ranking of binding affinities for all hyrtiosulawesine and its derivatives, meticulously ordered from the highest to the lowest binding energy, along with the amino acid residues involved in the binding interactions within a 4Å distance. The molecular docking studies have shown that nearly all analogues exhibit moderate binding to the *Pf*LDH, with binding energies ranging from -6.7 kcal/mol to -9.0 kcal/mol. In contrast, the native ligand (-5.2 kcal/mol) and oxamate displayed more modest binding values (-3.4 kcal/mol). Among these, the hyrtiosulawesine derivatives of **116** exhibited the strongest binding interactions with the protein.

Although docking gives useful information about potential binding interactions, binding affinity values might not give an accurate prediction of biological activity. This can be observed in this study when there was mismatch between docking scores and assay data. As demonstrated by compound **116,** the highest docking score (-9.0 kcal/mol) with a few hydrogen bonding interactions show no inhibition in antimalarial activity. In comparison, compounds **53**, **113**, and **114** with moderate docking scores (-7.0 kcal/mol) showed good *Pf*LDH inhibition.

This inconsistency highlights limitations of static molecular docking, particularly its inability to consider for aqueous environments. Even though compound **116** formed numerous hydrogen bonds in vacuum docking poses, these interactions likely favor water-mediated hydrogen bonding under enzyme assay conditions. Thus, it results in ligand displacement from the active site and subsequently loss of inhibitory activity. This is supported by previous investigation showing protein flexibility, solubility, and assay conditions can all contribute to such disparities (Antunes *et al.,* 2025).

The 3D visualization of the protein-ligand complex of all the three best compounds based on assay were depicted in Figure 4.7(a). Derivative **114** demonstrated slightly higher binding affinities (table 4.13) compared to compounds **53** and **112** and formed several interactions. This compound exerts favourable binding interactions via hydrogen bonding with crucial amino acid residues like Asn140, while being stabilized by other residues (Asn197) through carbon hydrogen bonding interactions (Figure 4.7(d)). The ligand-enzyme was further stabilized through contacts of π-σ interactions with the binding site amino acids of Ala236. This interaction enhanced overall binding and was also seen in compounds **53** (Figure 4.8(b)) and **113** (Figure 4.8(c)). In addition, compound **53** (Figure 4.7(b)) formed an additional π-alkyl interaction between the methoxy alkyl group on the β-carboline ring and the catalytic residue Arg109. This further stabilizes the ligand-protein complex where such interaction is absent in compounds **113** and **114**.

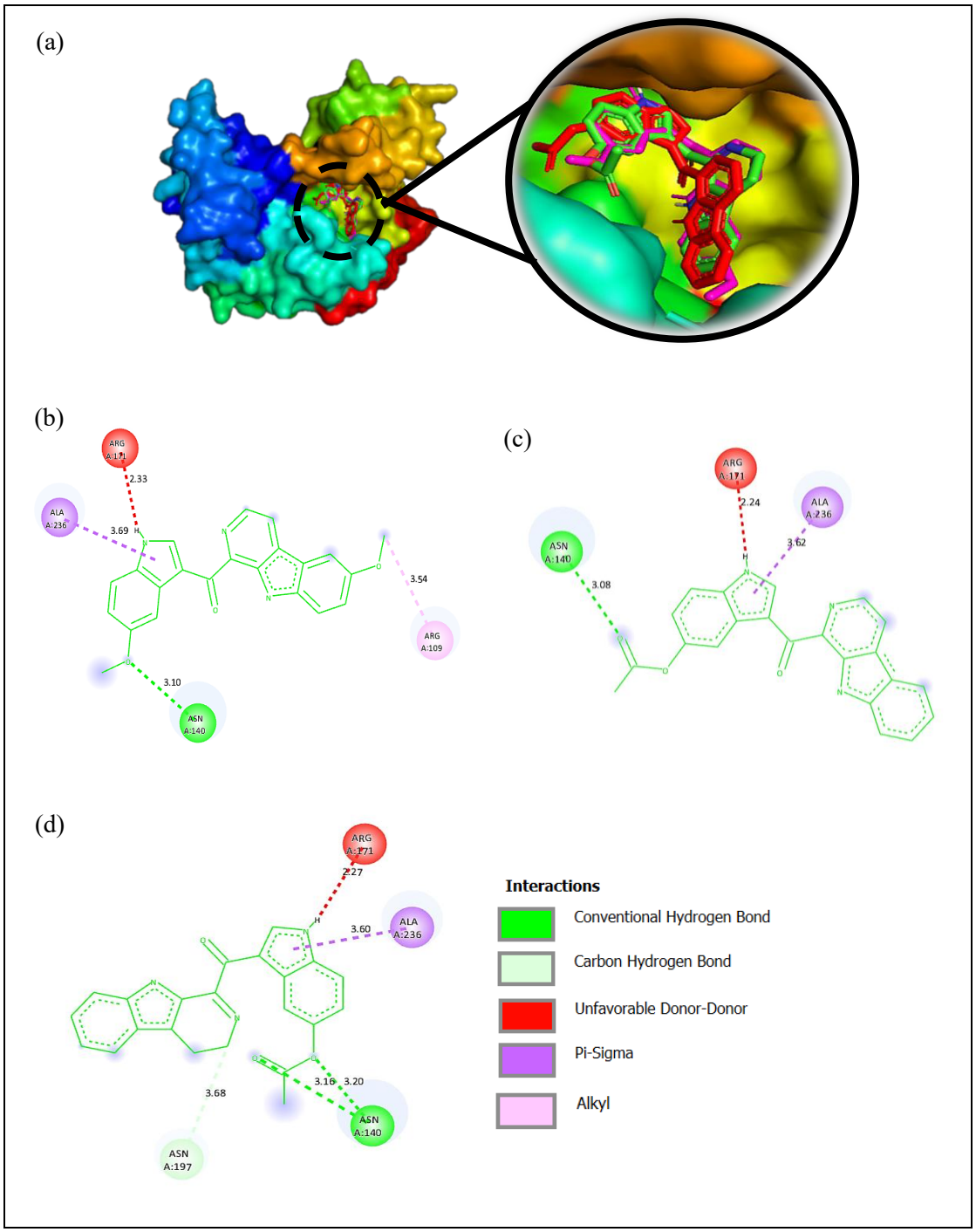

Figure 4.7 (a) 3D Representation Showing the Docking Poses of Ligands **53** (Magenta), **113** (Red) and **114** (Green) Docked at Protein Active Site and 2D Interactions of (b) Compound **53**, (c) Compound **113** and (d) Compound **114**

Remarkably, it shows that oxamate exhibits the lowest binding affinity among all the tested compounds. This might be due to its small structure that lets it enter the active site deeply and creates fewer contacts with amino acids than the larger inhibitors which form broader contacts with more residues. Overall, the docking analysis from

three active compound supports the experimental assay. The C-5 methoxy substitution demonstrates strong hydrogen bonding with Asn140 and hydrophobic interactions with catalytic residue of Arg109, explaining potency of compound **53**. The weaker interactions of oxamate demonstrate the advantage of employing larger, more functionalized scaffolds such as hyrtiosulawesine derivatives to achieve greater levels of inhibition. These findings together not only corroborate SAR but also specify residue-level interactions to be used in designing future analogues.

4.5.2 Molecular Dynamic Simulation

To further characterize ligand-protein interactions, 200 ns MD simulations were performed for compounds **53**, **113**, and **114**. Molecular dynamics (MD) simulations were conducted to investigate the behavior of the best compound activity against *Pf*LDH. The analysis focused on the stability of the selected compounds and their interactions within the active site. The trajectory analyses included RMSD, radius of gyration (Rg), solvent accessible surface area (SASA), and molecular surface area (MolSA). The first parameter evaluated was the Root Mean Square Deviation (RMSD). As shown in Figure 4.8, the stable conformation observed indicated by the RMSD values the protein in complex of compound **53**. The value of the protein is in range between 0.48 Å and 0.54 Å which is far below the 2 Å threshold typically considered stable throughout the simulation. Ligand RMSD for compound **53** exhibited stable binding, with an RMSD of only 0.03 Å maintained for the first 60 ns, before converging and stable at 0.21 Å.

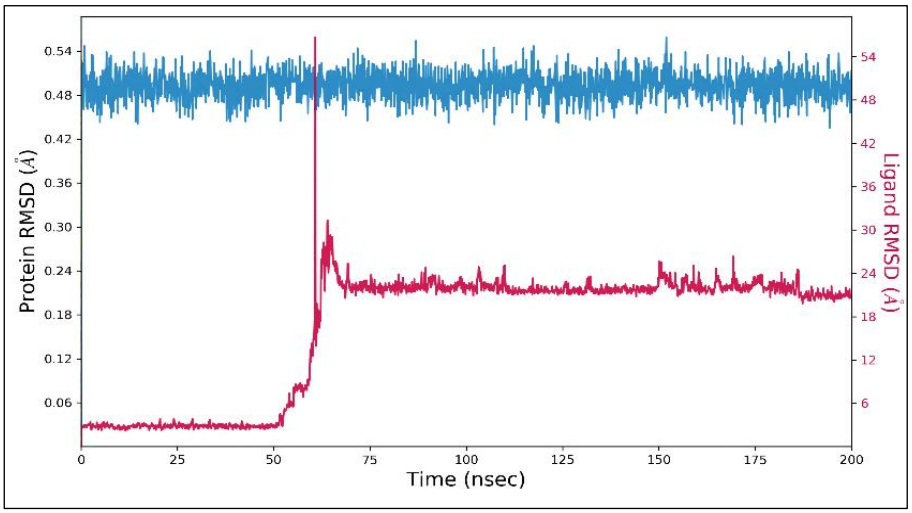

Figure 4.8 Protein (blue)-Ligand (red) RMSD of Derivative **53**

An interesting observation was made for compound **53**. In the simulations the sudden increase in RMSD value at 60 ns was observed demonstrates instability of the compound (Figure 4.8). This suggests the original pose was somewhat unstable at this point, leaving the binding pocket, and make a new interaction with a secondary binding site. This was supported with protein-ligand contact (Figure 4.9a) where the ligand first bound to the primary active site, with several catalytic residues of ARG-109, ASN-140, ASP-168, HIS-195, and ASN-197, over the first 60 ns of simulation time. This initial binding phase could explain the moderate inhibitory effect in the activity assay. However, after 60 ns of simulation time, the ligand began to migrate to a secondary binding region and observed to have frequent contact with GLU-321, LYS-323, ALA-327 and HIS-330 (Figure 4.9a) through a few hydrogens bonding, hydrophobics and water bridge contact (Figure 4.9b).

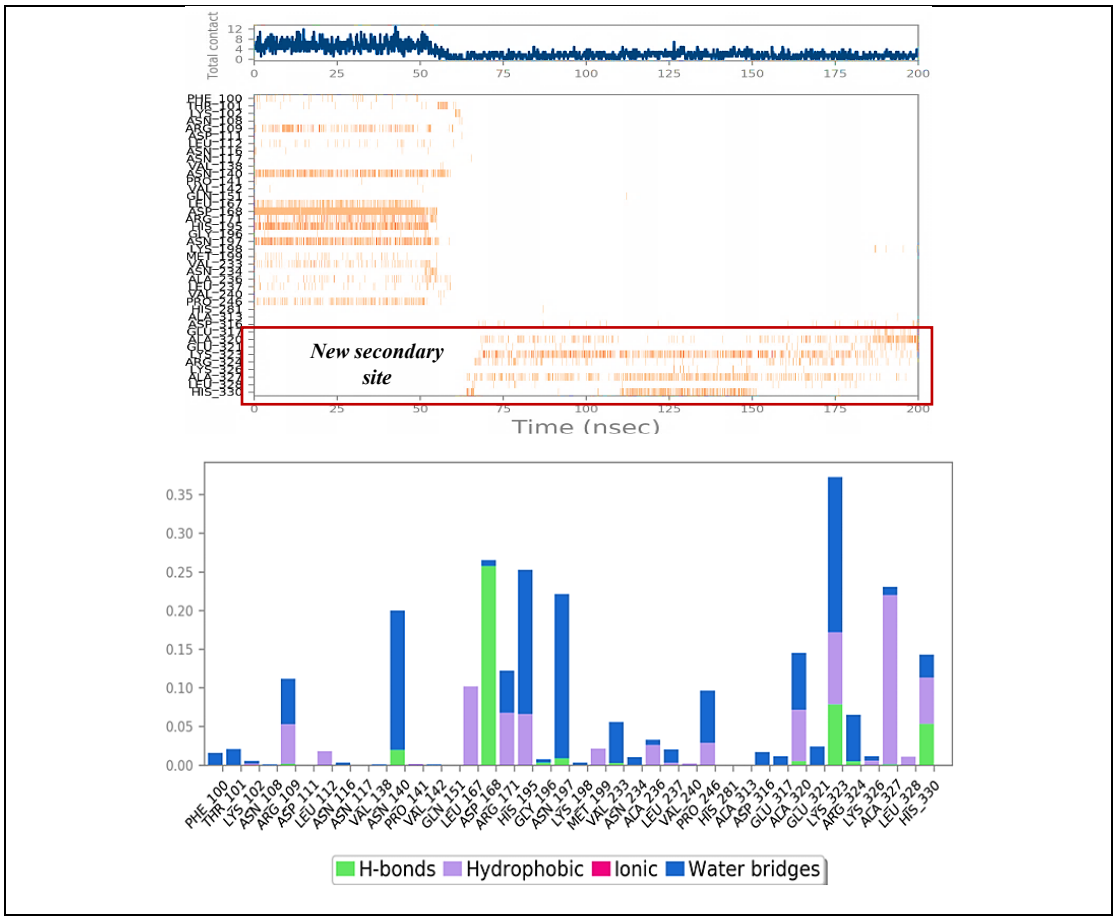

Figure 4.9 (a) Protein-Ligand Contacts Illustrating Ligand Movement and (B) Detailed Protein Interactions with the Ligand of Compound **53**

The stability was supported by the radius of gyration (Rg) parameter. As depicted in Figure 4.10a, compound **53** exhibited low Rg value between 4.00 to 4.25

Å, indicating its structural compactness and limited conformational flexibility during the first 60 ns. The compactness of the structure is primarily driven by the central carbon that connects to the fused aromatic ring system. These structural elements restrict torsional flexibility, as observed by the narrow torsion angle (pink and green) distributions observed in the corresponding bar plots (Figure 4.10b). Methoxy substituents (blue and orange), on the other hand, experience less steric constraints causing them to be more dynamically flexible. Its flexibility allowed them to adapt to local environments within the binding pocket without compromising the overall structural rigidity.

Before the ligand movement, the Molecular Surface Area (MolSA) parameter demonstrates minimal fluctuation between 330 to 340 Å indicates its stability (Figure 4.10a). This might be due to the compound maintaining consistent interaction and tightly bound within the binding pocket rather than being exposed to the surrounding environment which suggests its minimal flexibility. However, the increased MolSA and Solvent Accessible Surface area (SASA) values were noted after that (50 to 65 ns). This indicates that the ligand is now more accessible to the solvent, correlating with the sudden increase in RMSD value.

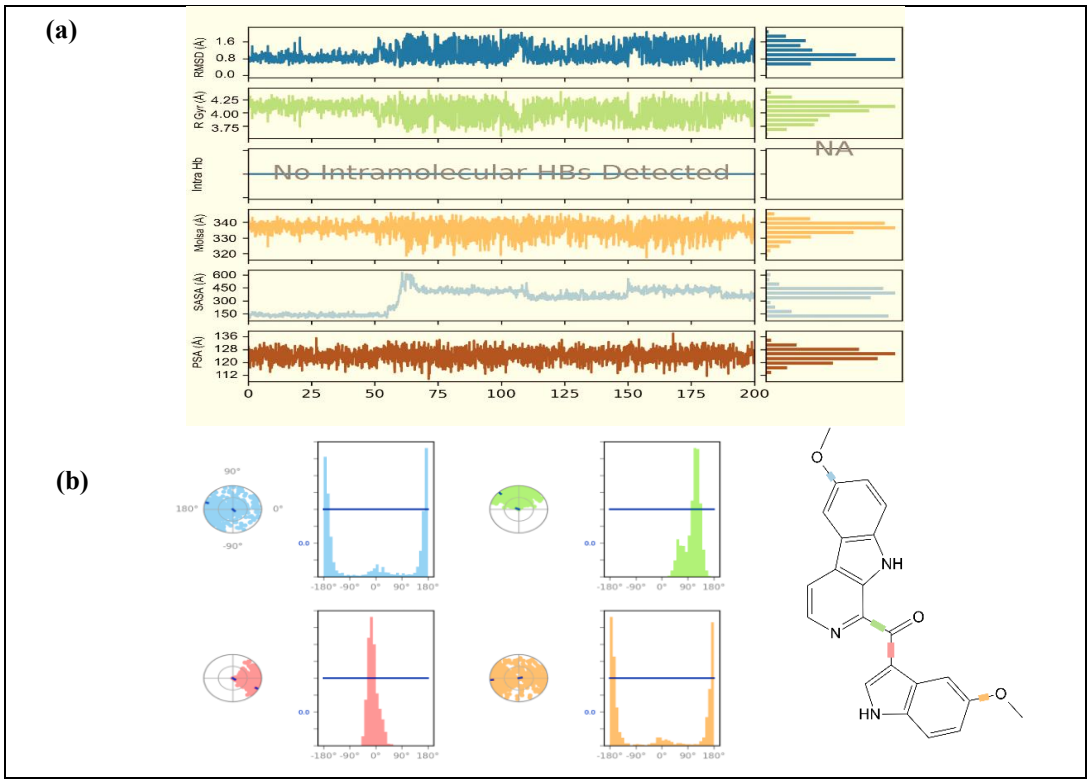

Figure 4.10 (a) Ligand Interaction with RMSD, Rg, Moisa, SASA and PSA, (b) Ligand Torsion Profile of Compound **53**

Notably, the secondary binding region has spatially distinct boundaries in comparison to the canonical active site and is to our knowledge, has not been reported in the literature for *Pf*LDH. The functional role of this binding region is undetermined, but perhaps the ability of the ligand to form interactions in this alternate pocket indicates that it generally wants to remain on the protein surface, and thus the inhibitory activity is somewhat retained through overall binding stability. Additional studies should follow to establish whether this newly observed site may perform a regulatory or structural role. The snapshots of the ligand movement were illustrated in Figure 4.11.

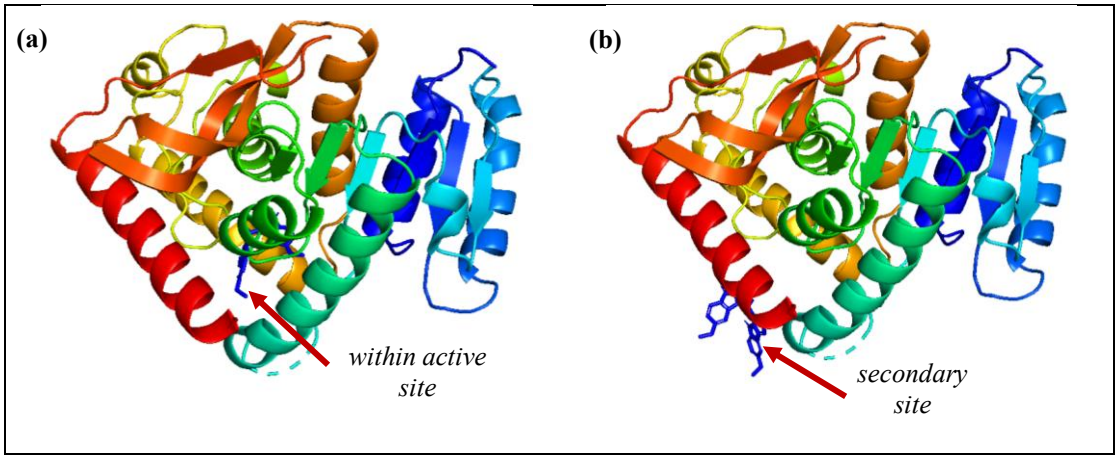

Figure 4.11 Snapshots of Compound **53** Ligand Movement and Protein-Ligand Interactions: (a) Ligand Position within the Active Site During the First 60 ns and (b) Ligand Position After 60 ns

Following compounds **113** and **114**, both parameters were evaluated. As observed, ligand **113** keeps increasing in RMSD value indicating unstable position in the pocket binding site (Figure 4.12a). In comparison, the RMSD value of both protein and ligand **114** remained well below 2 Å throughout simulation. The ligand RMSD for compound **114** demonstrated stable binding by maintaining an RMSD of 0.16 Å during the first 20 ns, followed by fluctuations between 20-40 ns, before converging and stabilizing at 0.40 Å.

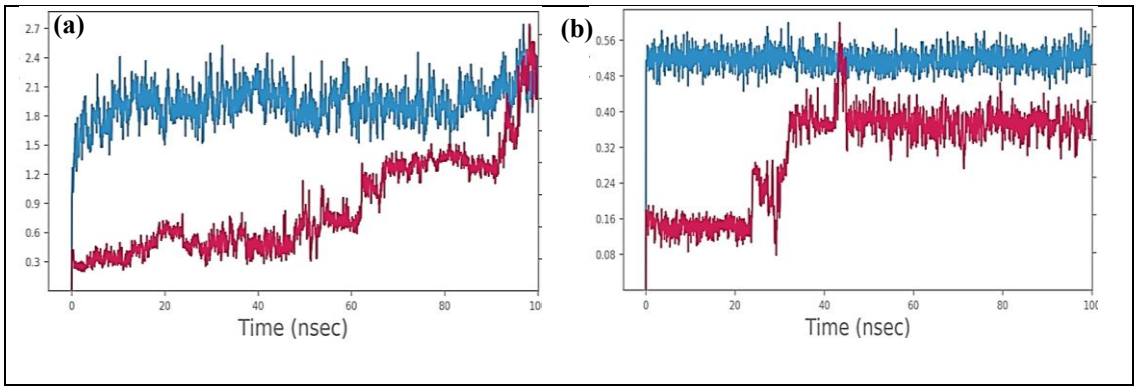

Figure 4.12 Protein (blue)-Ligand (red) RMSD of (a) Compound **113** and (b) Compound **114**

Compound **113** experience moderate stability. The RMSD profile showed (Figure 4.13a) that the ligand generally maintained a consistent orientation within the binding pocket. However, a slight increase in fluctuations was observed at 20 ns, with more substantial fluctuations appearing in the final 40 ns of the simulation, indicating local conformational adjustments. The Rg value remained relatively stable at first (4.0-4.4 Å) suggesting that the ligand retained a compact structure, before fluctuating the rest of simulation. In consistent with fluctuations in SASA values reveals periodic changes in solvent exposure, reflecting ligand reorientation inside the pocket. The torsional angle distribution further highlighted where certain bonds (blue, green, and orange) were locked into defined orientations (Figure 4.13b).

The contact analysis of **113** demonstrated that the ligand maintained its interactions with essential catalytic residues of *Pf*LDH (Arg 109, His195, Arg171) to maintain proper orientation inside the binding pocket (Figure 4.13c). At the same time, the ligand also formed transient contacts with several surrounding residues, indicating a degree of conformational flexibility. This demonstrates that the compound maintains active site residue interactions while showing flexibility within the binding pocket.

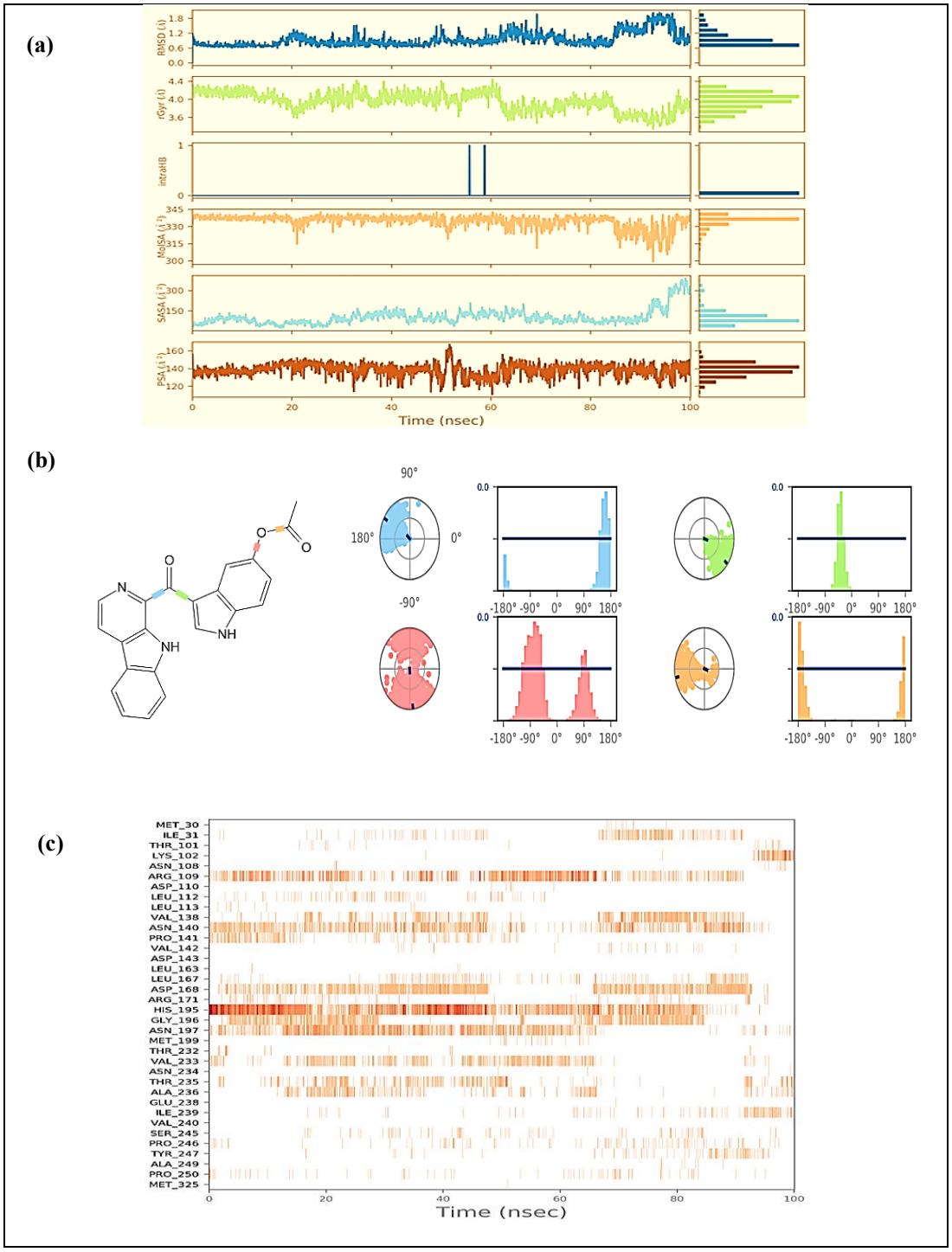

Figure 4.13 (a) Ligand Interaction with RMSD, Rg, Moisa, SASA and PSA, (b) Ligand Torsion Profile and (c) Protein-Ligand Contacts of Compound **113**

The stability of compound **114** was further supported with the Rg parameter. As shown in Figure 4.14a, the Rg values ranged between 4.25-4.50 Å during the first 20 ns, indicating structural compactness and limited conformational flexibility. Similar to **53**, the ligand compactness is primarily caused by the central carbon connecting the fused aromatic ring system and the additional of the carbonyl group of the acyl

substituents (Figure 4.14b). These structural elements restrict torsional flexibility, as evidenced by the small torsion angle distributions (blue, green, and orange) observed in the corresponding bar plots. In contrast, the C-O bond connecting the indole ring and acetyl substituents (pink) has less steric hindrance, making it comparatively more flexible in its dynamics.

The flexibility of the compound within the active site was evaluated through SASA analysis. The results indicated the molecule was less accessible to the solvent (~100 Å²) during the initial 20 ns, suggesting its strong binding within the active site. However, a sharp increase was observed between 20-40 ns, suggesting greater solvent exposure and a transient reorientation of the ligand. This was followed by stabilization for the remainder of the simulation, in agreement with the MolSA and RMSD fluctuations shown in Figure 4.14b. These findings are consistent with the experimental assay results, which reported an IC_{50} value of 8.4 ± 0.42 µM, further supporting the moderate binding affinity of **114**.

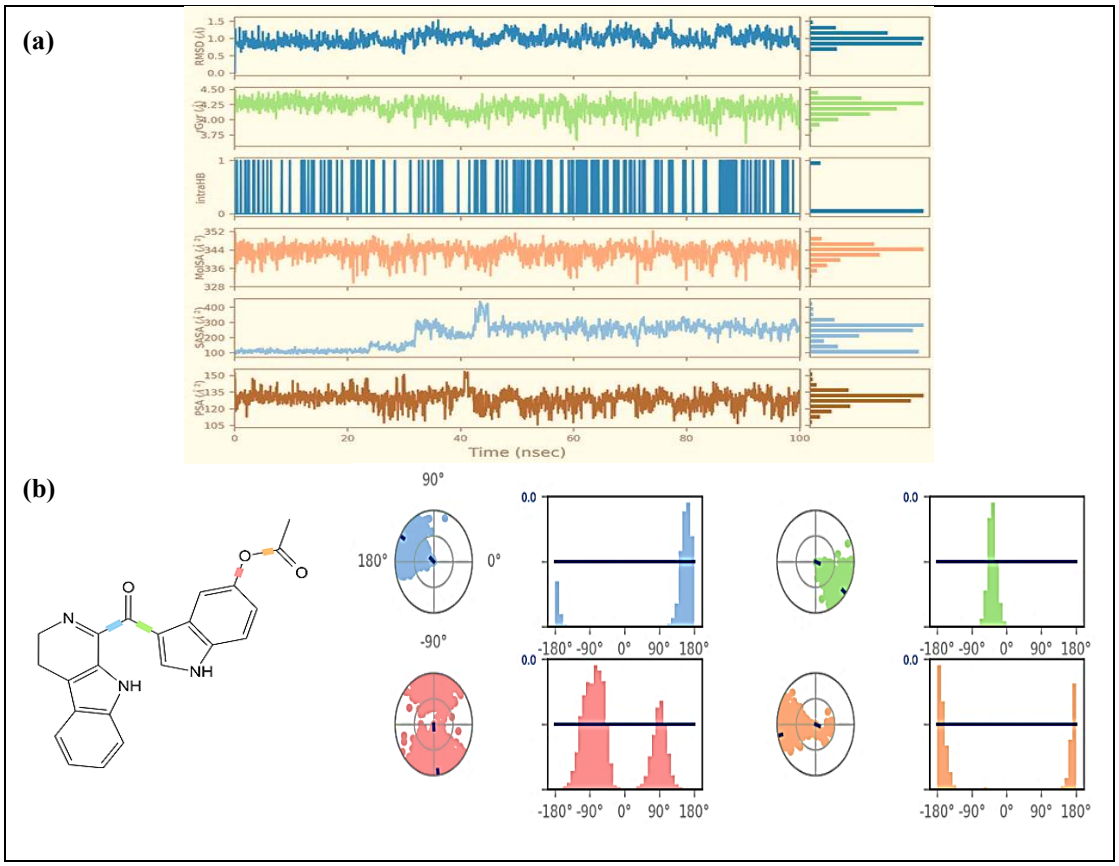

Figure 4.14 (a) Ligand Interaction with RMSD, Rg, MoISA, SASA and PSA, (b) Ligand Torsion Profile of Compound **114**

All these analyses were well-described and closely matched experimental inhibitory data. Ligand **53** from the first simulation was the most potent (IC_{50}= 5 μM) potentially due to the secondary binding pockets after pose displacement. Although compound **53** has the lowest docking score among those tested, results from enzymatic assays suggest it may have better solubility, stability, or accessibility under experimental conditions. On the other hand, the ability of this compound interacts with yet another residue, ARG-109 in docking study, which was not observed in the binding profiles of compounds **113** and **114,** might explain the better inhibition of this compound. Therefore, these considerations demonstrate the assay is one of the main tools to assess the real biological effect, supported with molecular docking for binding affinity and stability by molecular dynamic simulation analysis.

4.5.3 ADMET Analysis

The pharmacokinetics behaviour of the drug candidates can be predicted through *in silico* ADMET (Absorption, Distribution, Metabolism, Excretion and Toxicity) profile. This method is crucial to modern drug discovery and development, as it enables rapid evaluation of the interaction of potential drugs in the body, at the early stage of process which obviates the need of performing costly and time-consuming in *in vitro* and *in vivo* studies (Anklam *et al.,* 2022; Gan *et al.,* 2022). The commonly used tool in this analysis is SwissADME, pkCSM and ProTox 3.0 which can determine whether the chemical substance qualifies drug-likeness criteria or not (Daina *et al.,* 2017).

The Lipinski rule of five (Ro5) guidelines can be helpful in assessing whether a compound has the needed properties to be considered a viable orally active drug in humans. The parameters of the Ro5 rule include molecular weight (g/mol), the number of hydrogen bond donors (HBD), the number of hydrogen bond acceptors (HBA), topological polar surface area (TPSA) and the computation of x log P (Log P), under the condition that there should be no more than one violation. Under the Ro5, the compounds must have molecular weight below 500 Daltons, those above this limit have the potential of missing the ability to go through the cell membranes due to the limited absorption and distribution of the compounds in the body (Nisha *et al.,* 2016). The LogP, logarithm of the partition coefficient between water and n-octanol, is also a quantitation of hydrophobicity of the compound. A value of LogP of more than 5

represents superfluous hydrophobicity, which may lead to absorption, and solubility issues (Darlami *et al.,* 2024). In addition, it should have less than 5 hydrogen bond donors (HBD) because excessive hydrogen bonding may inhibit penetration of cell membranes (Darlami *et al.,* 2024). On the other hand, HBA counts should be lower than 10, as this aspect also reduces the membrane permeability (Darlami *et al.,* 2024).

Table 4.14 indicates that all three active compounds have all passed the stringent requirements of the Lipinski Rule of 5 (Ro5), thereby passing the test of their potential administration by route oral. According to the Ro5, the typical orally drug candidates should obey all the following: less than 5 hydrogen bond donors (HBD), less than 10 hydrogen bond acceptors (HBA), molecular weight less than 500 Daltons, and cLogP of less than five.

Table 4.14
Assessment of Drug-Likeness Based on Lipinski's Rules of Compounds **53, 113** and **114**

Compound	MW (<500 g/mol)	LogP <5	TPSA <140Å^2	HBA <10	HBD <5	Lipinski Rule
53	371.39	2.37	80.00	4	2	Yes; 0 violation
113	369.37	2.51	87.84	4	2	Yes; 0 violation
114	371.39	2.34	87.31	4	2	Yes; 0 violation

The ADMET analysis was done and demonstrated in Table 4.15. All compounds exhibit acceptable physicochemical properties with moderate lipophilicity that favours membrane permeability. Although the predicted solubility is low due to its aromatic heterocycle structure, these compounds still have sufficient dissolved fraction available to enable intestinal absorption, demonstrated by positive Caco-2 permeability and human intestinal absorption (HIA+). This permeability limitation profile highlights that the molecule may be addressed through formulation or optimization strategies. In addition, a BBB+ profile is advantageous because it allows the drug to enter the brain to reduce inflammation and protect brain cells, directly minimizing severe symptoms like seizures and brain swelling caused by cerebral malaria. Besides, this molecule has low likelihood of inducing immune-mediated allergic reactions upon exposure as it shows non-sensitizing to skin prediction.

Even so, some liabilities associated with toxicity were found. These compounds were predicted to have hepatoxicity properties (HHT+), which suggests that they may be intrinsically toxic to hepatocytes. This could result from hepatic accumulation

caused by the compound's lipophilicity and metabolic stress during liver biotransformation. Such toxicity could compromise the integrity of host hepatocytes if it is not sufficiently controlled by dose optimization because the liver is both a major metabolic organ and a crucial location in the *Plasmodium* life cycle. Additionally, these compounds may cause frameshift mutations (AMES+) or base-pair substitutions in DNA. Long-term or frequent dosing may be less appropriate due to this mutagenic liability. In patients with malaria who frequently receive combination therapies, inhibition of several cytochrome P450 enzymes, especially CYP3A4 and CYP2C9, may also disrupt normal drug metabolism and raise the risk of drug-drug interactions.

Table 4.15
ADMET Profiling Enlisting Absorption, Distribution, Metabolism and Toxicity Related Drug-likeness Parameters of Selected Compound **53**, **113** And **114**

Models	53	113	114
A. Physiochemical Property			
Solubility (Log S)	-5.02 (Moderately soluble)	-4.89 (Moderately soluble)	-4.36 (Moderately soluble)
Distribution Coefficient P (Log P)	3.45	3.49	3.22
B. Absorption			
Caco2 permeability (Lop Papp)	Caco2+	Caco2+	Caco2+
P-glycoprotein inhibitor	Inhibitor	Inhibitor	Inhibitor
P-glycoprotein substrate	Substrate	Substrate	Substrate
Human Intestinal Absorption (HIA)	HIA+	HIA+	HIA+
C. Distribution			
Plasma Protein Binding (PPB)	PPB-	PPB-	PPB+
Blood Brain Barrier Permeability (BBB)	BBB+	BBB+	BBB-
D. Metabolism			
CYP1A2 inhibitor	Inhibitor	Inhibitor	Inhibitor
CYP2C19 inhibitor	Inhibitor	Inhibitor	Inhibitor
CYP2C9 inhibitor	Inhibitor	Inhibitor	Inhibitor
CYP2D6 inhibitor	Inhibitor	Non-inhibitor	Non-inhibitor
CYP3A4 inhibitor	Inhibitor	Inhibitor	Inhibitor
E. Toxicity			
heRG Blockers	Non-blockers	Non-blockers	Non-blockers
Human hepatoxicity (H-HT)	HHT+	HHT+	HHT+
AMES mutagenicity	AMES+	AMES+	AMES+
Skin Sensitization, (r) LLNA	Non-sensitizer	Non-sensitizer	Non-sensitizer
Drug Induced Liver Injury (DILI)	DILI-	DILI-	DILI+

To summarize, compound **53** achieves the ideal balance between absorption, potency, and manageable safety risks. Compound **113** and **114** exhibits the least amount of enzyme inhibition and provides no distinct benefit in terms of pharmacokinetic or

safety parameters. Overall, the compound exhibits several advantageous characteristics that support its development as an antimalarial lead. However, additional structural optimization is necessary to reduce concerns regarding genetic and hepatic safety.

CHAPTER 5
CONCLUSION AND RECOMMENDATION

5.1 Synthesis, Bioactivity and Computational Studies of Hyrtiosulawesine and its Derivatives

Hyrtiosulawesine, which consists of a core skeleton of β-carboline and indole, has been reported to be a challenging target for synthesis. Previous studies have shown that this compound possesses diverse biological activities, particularly antimalarial activity. Due to the presence of its β-carboline and indole moieties, hyrtiosulawesine has also been evaluated for potential anticancer activity. In this study, four objectives were established. The first objective is to develop a short synthetic route toward hyrtiosulawesine. The second is to synthesize hyrtiosulawesine derivatives using the successful method. The third objective is to evaluate the antimalarial and anticancer activities of the synthesized compounds against enzyme targets (*Pf*LDH) and cancer cell lines (MDA-MB-231 and HT-19). The fourth objective is to perform molecular docking, molecular dynamics, and ADMET analyses of the active compounds against *Pf*LDH.

5.1.1 Total Synthesis of Hyrtiosulawesine and Its Derivatives

This study successfully developed a concise and streamlined three-step synthetic route for hyrtiosulawesine and its derivatives, comprising Friedel-Crafts acylation, a multicoupled domino approach, and demethylation. The first step involved the Friedel-Crafts acylation of commercially available 5-methoxyindole using a selective Lewis acid, Et_2AlCl, in anhydrous DCM to afford 5-methoxy-3-acetylindole (compound **89**) in a good yield of 77%. The subsequent step involved the formation of a glyoxal intermediate, followed by the addition of 5-methoxytryptamine via a multicoupled domino reaction and produce the hyrtiosulawesine intermediate (compound **53**) with a yield of 47%. Finally, demethylation was carried out using BBr_3 under an inert atmosphere in anhydrous DCM, affording hyrtiosulawesine as the final

product. The overall yield of hyrtiosulawesine improved to 28.2% in comparison to prior study 16%.

This approach improved upon previous lengthy and low yields methods and enabled the accommodation of a series of derivatives with different substituents. Prior to Friedel-Crafts acylation, *N*-alkylation and *O*-acylation take place. The moderate to high yields of derivatives varied depending on the electronic and sterics of the substituents attached to the ring. Especially compound bearing Fluoro substituents consistently provide low yield, due to increases steric hindrance around reactive sites. The care and control over reagent selection are crucial to obtain the product. All the derivatives are shown in the following scheme.

5.1.2 Biological Activities and *in silico* Studies

The hyrtiosulawesine and derivatives were evaluated for antimalarial activity *via* enzymatic assays against *Pf*LDH. Three compounds exhibited better inhibition than positive control, with compound **53** showing the most potent activity with IC_{50} value of 5.44 ± 0.48 μM. This might be due to methoxy group at the C-5 position of an alkaloid backbone supporting with previous investigation. Derivatives **113** and **114** showed moderate inhibition with IC_{50} values of 13.32 ± 2.30 μM and 8.4 ± 0.42 μM. The antimalarial effectiveness of the compounds reduces in fully aromatized β-carboline and better with partial β-carboline.

In cytotoxicity activity, compound **10** with cyano group attached to indole shows better inhibition against MDA-MB-231 with IC_5=26 μM. Following compounds tested, **136** (41 μM), **106** (39 μM), **118** (39 μM), and **120** (51.5 μM) demonstrate moderate activity. The activity on HT-29 is poor, suggesting colon cancer cells are less susceptible to these scaffolds. Cytotoxicity assays indicated that hyrtiosulawesine scaffolds displayed anticancer activity, against the MDA-MB-231 breast cancer cell line compared to the HT-29 colon cancer model.

The assay data reveal supported by molecular docking that compound **53** interacted with an additional catalytic residue, ARG-109, which was not observed in the binding profiles of compounds **113** and **114,** might explains its good inhibition. Compound **53** achieves the ideal balance between absorption, potency, and manageable safety risks in ADMET prediction. MD simulations of compound **53** further

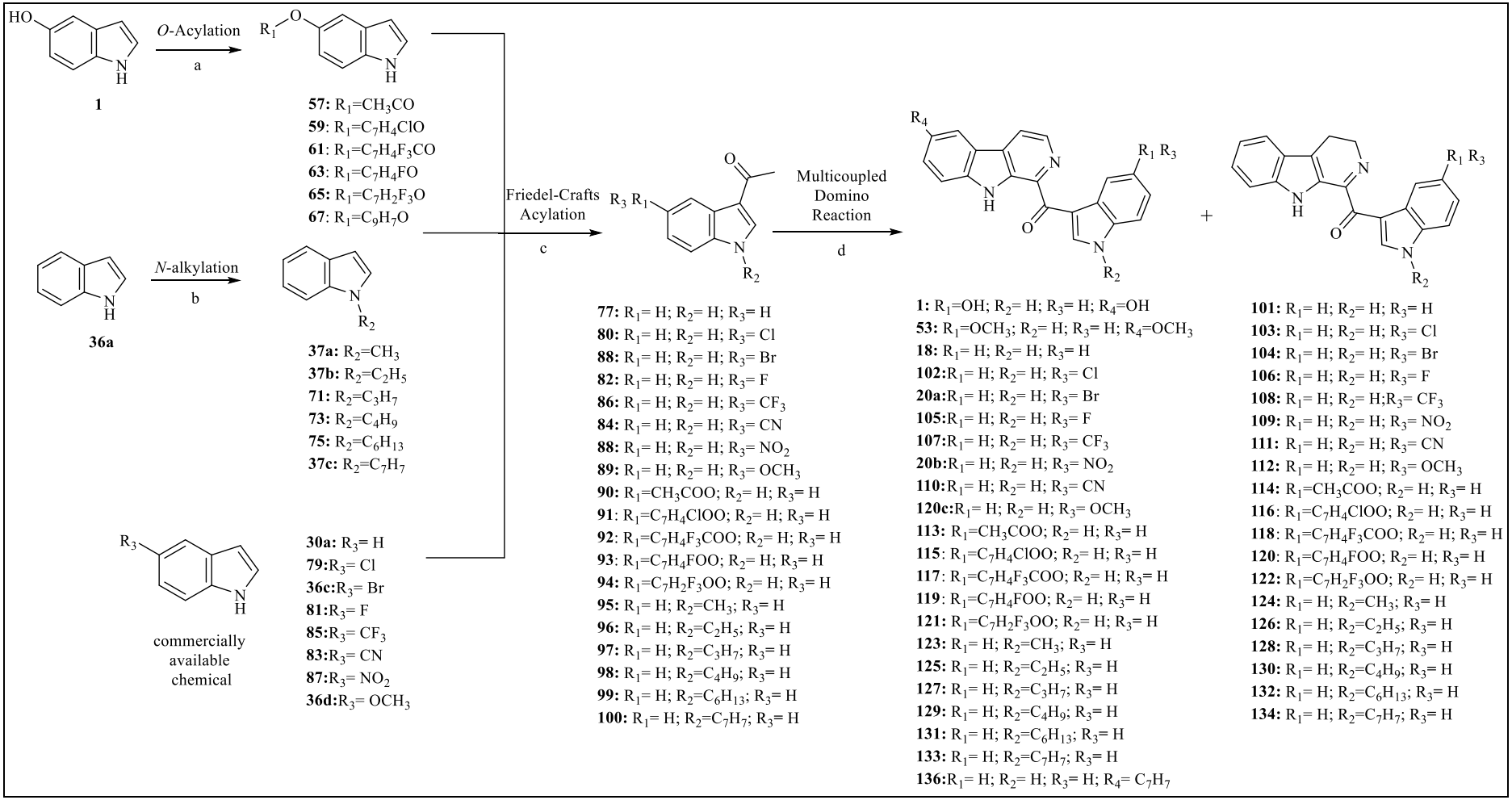

Scheme 5.1 Synthesis of Hyrtiosulawesine and its Derivatives

Method: (a) KOH, Pyridine, r.t, 5-16 h (b) KOH, DMSO, r.t, 5-10 h (c) $Et_2AlCl/SnCl_4$, DCM, 0°C-r.t, 2-20 h. (d) I_2, DMSO, 100°C, 12-24 h

corroborated these findings, since ligand stable during the first 60 ns. Interestingly, after 60 ns, the ligand migrated to a secondary binding region, a phenomenon not previously reported for *Pf*LDH, representing a novel finding of this study.

5.2 Recommendation for Future Study

Some recommendations should be made for future studies. This includes the optimization of the synthetic strategy to improve the overall yields of compounds. The adjusting reaction conditions or exploring alternative catalytic systems can be attempted. For antimalarial assay, it is also recommended that future studies should be done on the *Plasmodium falciparum* cell to examine the real workings of the compound. It is also recommended to check the toxicity of the compounds prior to *in vivo* study with appropriate animal models. Thirdly, it will be very informative to have more sophisticated approaches, such as free energy binding calculations and extended molecular dynamics simulations. This could provide deeper insights into ligand stability and interaction dynamics within the active site. It will also be very useful to fully assess the secondary binding site either it can bind in an allosteric site that could be explored to inhibit enzymes and cells. Future work should focus on structural optimization to maintain *Pf*LDH potency while improving solubility, reducing protein binding, and minimizing hepatotoxicity and mutagenicity. This can be done by adding polar substitutions on structures, metabolically stable modifications, and avoiding known toxic motifs can lead to safer, more effective drug candidates.

REFERENCES

Abdjul, D. B., Yamazaki, H., Ukai, K., & Namikoshi, M. (2015). Two new indole derivatives from a marine sponge Ircinia sp. collected at Iriomote Island. *Journal of natural medicines*, 69, 416-420.

Adan, A., Kiraz, Y., & Baran, Y. (2016). Cell proliferation and cytotoxicity assays. *Current Pharmaceutical Biotechnology*, 17(14), 1213-1221.

Agu, P. C., Afiukwa, C. A., Orji, O. U., Ezeh, E. M., Ofoke, I. H., Ogbu, C. O., & Aja, P. M. (2023). Molecular docking as a tool for the discovery of molecular targets of nutraceuticals in diseases management. *Scientific Reports*, *13*(1), 13398.

Ahuja, V. (2004). Natural products as anti-inflammatory agents: An overview. *Current Medicinal Chemistry*, 11(9), 1105–1120.

Alanzi, A. R., Smith, J. D., Lee, M., Garcia, P., Chen, Y., Patel, R., Nguyen, H., Kumar, S., Wright, A., Johnson, L., Lopez, M., Kim, S., Thompson, J., Wilson, C., Martinez, D., Clark, R., Davis, E., Hernandez, F., Lewis, K., & Martin, T. (2024). A comprehensive drug discovery study using commercial databases, molecular docking, virtual screening, and molecular dynamics simulations to identify potential EGFR inhibitors. *PLoS ONE*, 19(12), e0260012.

Ailioaie, L. M., Ailioaie, C., & Litscher, G. (2023). Photobiomodulation in Alzheimer's Disease-A Complementary Method to State-of-the-Art Pharmaceutical Formulations and Nanomedicine?. *Pharmaceutics*, 15(3), 916.

Anklam, E., Bahl, M. I., Ball, R., Beger, R. D., Cohen, J., Fitzpatrick, S., … & Slikker Jr., W. (2022). Emerging technologies and their impact on regulatory science. *Experimental Biology and Medicine*, 247(1), 1–75.

Al-Qahtani, A. A. (2024). Pro-inflammatory and anti-inflammatory interleukins in infectious diseases: A comprehensive review. *International Journal of Molecular Sciences*, 25(2), 345.

Asmat, U., Abad, K., & Ismail, K. (2016). Diabetes mellitus and oxidative stress-A concise review. *Saudi pharmaceutical journal*, 24(5), 547-553.

Aszrin, F. N., Adam, S. H., Mutalib, M. A., Tang, H. C., & Tang, S. G. H. (2024). An overview of *Centella asiatica* and its therapeutic potential. *Life Sciences and Medicine Bulletin*, 45, 1–12.

Bhagat, S., Martinez, T. L., Chen, W., Perez, A., Johnson, M., Davis, R. L., Wilson, K., Garcia, E., Lee, C., Singh, R., Kumar, S., Patel, N., Thomas, J., White, D., Scott,

L., Adams, F., Turner, S., Martin, J., & Clark, H. (2025). AI-driven drug discovery: Enhancing predictive accuracy of drug efficacy and toxicity profiles. *ACS Omega*, 10(6), 4567–4579.

Bhambhani, S., García-Oliveira, P., Prieto, M. A., & others. (2021). Diversity in chemical structures and biological properties of plant alkaloids: Major categories and subclassification. *Molecules*, 26(9), Article 2629.

Botón-Fernández, M., Martín-Vide, C., Santander-Jiménez, S., & Vega-Rodríguez, M. A. (2016). A new multi-objective approach for molecular docking based on RMSD and binding energy. In E. López-Camacho, M. J. García-Godoy, J. García-Nieto, A. J. Nebro, & J. F. Aldana-Montes (Eds.), *Algorithms for computational biology* (Vol. 9702, pp. 65–77). Springer.

Cao, R., Peng, W., Wang, Z., & Xu, A. (2007). β-Carboline alkaloids: Biochemical and pharmacological functions. *Current Medicinal Chemistry*, 14(4), 479–500.

Case, D. A., Betz, R. M., Cerutti, D. S., Cheatham, T. E., Darden, T. A., Duke, R. E., ... & Kollman, P. A. (2005). *AMBER 9*. University of California, San Francisco.

Chadha, N., & Silakari, O. (2018). Indoles as multitarget directed ligands in medicinal chemistry. In *Key heterocycle cores for designing multitargeting molecules* (pp. 285–321).

Chaudhary, K. K., & Mishra, N. (2016). A review on molecular docking: novel tool for drug discovery. *Databases*, *3*(4), 1029.

Chhikara, B. S., & Parang, K. (2023). Global cancer statistics 2022: The trends projection analysis. *Chemical Biology Letters*, *10*(1), 451.

Chiocchio, I., Mandrone, M., Tomasi, P., Marincich, L., & Poli, F. (2021). Plant secondary metabolites: An opportunity for circular economy. *Molecules*, 26(2), 495.

Clemensen, A. K., Provenza, F. D., Hendrickson, J. R., & Grusak, M. A. (2020). Ecological implications of plant secondary metabolites-phytochemical diversity can enhance agricultural sustainability. *Frontiers in Sustainable Food Systems*, 4, 547826.

Cragg, G. M., & Pezzuto, J. M. (2016). Natural products as a vital source for the discovery of cancer chemotherapeutic and chemopreventive agents. *Medical Principles and Practice*, 25(Suppl. 2), 41–59.

Daina, A., Michielin, O., & Zoete, V. (2017). SwissADME: A free web tool to evaluate pharmacokinetics, drug-likeness and medicinal chemistry friendliness of small molecules. *Scientific Reports*, 7, Article 42717.

Darlami, J., Ghose, A., & Crippen, G. (2024). The role of physicochemical and topological parameters in drug design. *Frontiers in Drug Discovery and Safety*, 2, Article 1424402.

David J. N., & Gordon M. C. (2012). Natural Products as Sources of New Drugs over the 30 Years from 1981 to 2010. *Journal of Natural Products*, 75(3), 1–54.

Dennis, E. A., Cao, J., Hsu, Y. H., Magrioti, V., & Kokotos, G. (2011). Phospholipase A2 enzymes: physical structure, biological function, disease implication, chemical inhibition, and therapeutic intervention. *Chemical reviews*, 111(10), 6130-6185.

Dey, S., Kumar, B. K., Johri, S., Faheem, & Murugesan, S. (2022). Design and study of novel chromone and thiochromone derivatives as PfLDH inhibitors—computational approach. *Structural Chemistry*, *33*(6), 2063-2082.

Dnyandev, K. M., Babasaheb, G. V., Chandrashekhar, K. V., Chandrakant, M. A., & Vasant, O. K. (2021). A Review on Molecular Docking. *International Research Journal of Pure and Applied Chemistry*, 60–68.

Dzobo, K. (2022). The role of natural products as sources of therapeutic agents for innovative drug discovery. In Comprehensive Pharmacology (pp. 408–422). Elsevier.

Eala, M. A. B., Robredo, J. P. G., Dee, E. C., Lin, V., & Lagmay, A. M. F. A. (2022). Climate crisis and cancer: Perspectives from the hardest hit. *The Lancet Oncology*, 23(3), 92.

Eagon, S., Hammill, J. T., Bach, J., Everson, N., Sisley, T. A., Walls, M. J., & Guy, R. K. (2020). Antimalarial activity of tetrahydro-β-carbolines targeting the ATP binding pocket of the Plasmodium falciparum heat shock 90 protein. *Bioorganic & medicinal chemistry letters*, *30*(21), 127502.

Escala, N., Pineda, L. M., Ng, M. G., Coronado, L. M., Spadafora, C., & del Olmo, E. (2023). Antiplasmodial activity, structure–activity relationship and studies on the action of novel benzimidazole derivatives. *Scientific Reports*, *13*(1).

Faßheber, N., & Seinfeld, J. H. (2015). Glyoxal oxidation mechanism: Implications for the reactions in atmospheric and combustion processes. *ACS Publications*.

Gan, J., Bolon, B., Vleet, T. V., & Wood, C. (2022). In W. M. Haschek, C. G. Rousseaux, & M. A. Wallig (Eds.), Haschek and Rousseaux's Handbook of Toxicologic Pathology (pp. 925–966).

Gharu, C. P. (2022). Defense mechanism of natural antioxidants against free radicals. *Central Asian Journal of Medical and Natural Science*, *3*(5), 163-170.

Gohil, K. J., Patel, J. A., & Gajjar, A. K. (2010). Pharmacological review on Centella asiatica: a potential herbal cure-all. *Indian journal of pharmaceutical sciences*, *72*(5), 546.

Gorki, V. S., Wibowo, M. M., Gunawan, C. A., & Patil, S. A. (2020). β-Carboline derivatives tackling malaria: Synthesis, structure–activity relationships, and biological evaluation. *ACS Omega*, 5(27), 16700–16712.

Ha, N. T. T., Quan, P. M., Van Tuyen, N., Tra, N. T., Anh, L. T. T., & Son, N. T. (2022). Chemical Constituents of Alocasia odora Rhizomes and Their Biological Activities: Experimental and Molecular Docking Approaches. *Revista Brasileira de Farmacognosia*, *32*(5), 819-826.

Harris, J. B., & Scott-Davey, T. (2013). Secreted phospholipases A_2 of snake venoms: Effects on the peripheral neuromuscular system with comments on the role of phospholipases A_2 in disorders of the CNS and their uses in industry. *Toxins, 5*(12), 2533–2571.

Heaney, H., & Ley, S. V. (1973). N-alkylation of indole and pyrroles in dimethyl sulphoxide. *Journal of the Chemical Society, Perkin Transactions 1*, 499-500.

Heravi, M. M., Zadsirjan, V., Saedi, P., & Momeni, T. (2018). Applications of Friedel–Crafts reactions in total synthesis of natural products. *RSC Advances*, 8(68), 40061–40063.

Hong, Y., Boiti, A., Vallone, D., & Foulkes, N. S. (2024). Reactive oxygen species signaling and oxidative stress: Transcriptional regulation and evolution. Antioxidants, 13(3), Article 312

Inglese, J., Auld, D. S., Jadhav, A., Johnson, R. L., Simeonov, A., Yasgar, A., Zheng, W., & Austin, C. P. (2006, August 1). Quantitative high-throughput screening: A titration-based approach that efficiently identifies biological activities in large chemical libraries. Proceedings of the National Academy of Sciences of the United States of America, 103(31), 11473–11478.

Jaromin, A., Gryzło, B., Jamrozik, M., Parapini, S., Basilico, N., Cegła, M., & Zagórska, A. (2021). Synthesis, molecular docking and antiplasmodial activities

of new tetrahydro-B-carbolines. *International Journal of Molecular Sciences*, 22(24), 13569.

Kashtoh H, Baek KH. 2022. Recent updates on phytoconstituent alpha-glucosidase inhibitors: an approach towards the treatment of type two diabetes. Plants. 11(20):2722.

Kovvuri, J., Nagaraju, B., Nayak, V. L., Akunuri, R., Rao, M. N., Ajitha, A., & Kamal, A. (2018). Design, synthesis and biological evaluation of new β-carboline-bisindole compounds as DNA binding, photocleavage agents and topoisomerase I inhibitors. *European journal of medicinal chemistry*, 143, 1563-1577.

Kushwaha, P., Kumar, V., & Saha, B. (2023). Current development of β-carboline derived potential antimalarial scaffolds. *European Journal of Medicinal Chemistry*, 252, 115247.

Lazarevic-Pasti, T., Leskovac, A., Momic, T., Petrovic, S., & Vasic, V. (2017). Modulators of acetylcholinesterase activity: From Alzheimer's disease to anti-cancer drugs. *Current medicinal chemistry*, *24*(30), 3283-3309.

Li, J. J. (2009). Bischler–Napieralski reaction. In Name Reactions (pp. 376–385). Springer.

Liew, L. P. P., Fleming, J. M., Longeon, A., Mouray, E., Florent, I., Bourguet-Kondracki, M.-L., & Copp, B. R. (2014). Synthesis of 1-indolyl substituted β-carboline natural products and discovery of antimalarial and cytotoxic activities. *Tetrahedron*, *70*(33), 4910–4920.

Lim, A. W. Y., Tan, J. J., Wong, M. K., Lee, S. H., & Chan, T. F. (2024). Galantamine for dementia due to Alzheimer's disease and mild cognitive impairment. *Cochrane Database of Systematic Reviews*, (11), CD001747.

Lin, B., Zhang, J., Deng, X., Ye, Q., & Zheng, J. (2022). Effects and mechanisms of natural alkaloids for prevention of diseases. *Frontiers in Pharmacology, 13*, Article 952673.

Love, B. E. (1996). Synthesis of β-carbolines. A review. *Organic preparations and procedures international*, *28*(1), 1-64.

Malta, L. G., Tessaro, E. P., Eberlin, M., Pastore, G. M., & Liu, R. H. (2013). Assessment of antioxidant and antiproliferative activities and the identification of phenolic compounds of exotic Brazilian fruits. *Food Research International*, 53(1), 417-425.

Manna, P., & Jain, S. K. (2015). Obesity, oxidative stress, adipose tissue dysfunction, and the associated health risks: causes and therapeutic strategies. *Metabolic syndrome and related disorders*, 13(10), 423-444.

Manzari-Tavakoli, A., Babajani, A., Tavakoli, M. M., Safaeinejad, F., & Jafari, A. (2024). Integrating natural compounds and nanoparticle-based drug delivery systems: A novel strategy for enhanced efficacy and selectivity in cancer therapy. *Cancer Medicine*, 13(5), e7010.

Marinović, M., Bajić, M., Zorc, B., Bertoša, B., Mlinarić-Majerski, K., Landeka Dragičević, T., & Jaromin, A. (2020). Novel harmicines with improved potency against *Plasmodium falciparum*. *Bioorganic Chemistry*, 102, 104062.

Matthews, H. K., Bertoli, C., & de Bruin, R. A. M. (2022). Cell cycle control in cancer. *Nature Reviews Molecular Cell Biology*, 23(1), 74–88.

Meng, X. Y., Zhang, H. X., Mezei, M., & Cui, M. (2011). Molecular docking: a powerful approach for structure-based drug discovery. *Current computer-aided drug design*, *7*(2), 146-157.

Mihaylova, D., Desseva, I., Popova, A., Dincheva, I., Vrancheva, R., Lante, A., & Krastanov, A. (2021). GC-MS metabolic profile and α-glucosidase-, α-amylase-, lipase-and acetylcholinesterase-inhibitory activities of eight peach varieties. *Molecules*, 26(14), 4183.

Morris, G. M., Huey, R., Lindstrom, W., Sanner, M. F., Belew, R. K., Goodsell, D. S., & Olson, A. J. (2009). AutoDock4 and AutoDockTools4: Automated docking with selective receptor flexibility. *Journal of Computational Chemistry*, 30(16), 2785–2791.

Mphahlele, M. J., Mmonwa, M. M., & Choong, Y. S. (2017). Synthesis and evaluation of N-(3-trifluoroacetyl-indol-7-yl) acetamides for potential *in vitro* antiplasmodial properties. *Molecules*, *22*(7), 1099.

Muhammad, N., Usmani, D., Tarique, M., Naz, H., Ashraf, M., Raliya, R., & Suhail, M. (2022). The role of natural products and their multitargeted approach to treat solid cancer. *Cells*, 11(14), 2209.

Murakami, M., Sato, H., & Taketomi, Y. (2023). Modulation of immunity by the secreted phospholipase A2 family. *Immunological Reviews*, 317(1),42-70.

Murphy, P. B. (2023). *Morphine*. In *StatPearls*. National Center for Biotechnology Information.

Najmi, A., Javed, S. A., Al Bratty, M., & Alhazmi, H. A. (2022). Modern approaches in the discovery and development of plant-based natural products and their analogues as potential therapeutic agents. *Molecules*, 27(2), 349.

Nisha, C. M., Kumar, A., Nair, P., Gupta, N., Silakari, C., Tripathi, T., & Kumar, A. (2016). [Title of the article]. *Bioinformatics Advances*, 2016, 9258578.

Nogueira, C. R., & Lopes, L. M. (2011). Antiplasmodial natural products. *Molecules*, 16(3), 2146-2190.

Okauchi, T., Ottoni, M., & Chiba, S. (2003). Acylation of N-p-toluenesulfonylpyrrole under Friedel–Crafts conditions: Comparison of classical and modified procedures. *Synthetic Communications*, 33(10), 1633–1638.

Olufunmilayo, E. O., Gerke-Duncan, M. B., & Holsinger, R. D. (2023). Oxidative Stress and Antioxidants in Neurodegenerative disorders. *Antioxidants*, 12(2), 517.

Onguéné, P. A., Ntie-Kang, F., Mbah, J. A., Lifongo, L. L., Ndom, J. C., Sippl, W., & Mbaze, L. M. A. (2014). The potential of anti-malarial compounds derived from African medicinal plants, part III: an *in-silico* evaluation of drug metabolism and pharmacokinetics profiling. *Organic and medicinal chemistry letters*, *4*(1), 6.

Orr, M. J., Islam, M. S., Tanaka, T., Shaw, C. A., & Christie, M. J. (2022). Discovery of highly potent serotonin 5-HT2 receptor agonists among tetrahydro-β-carbolines. *ACS Chemical Neuroscience*, 13(5), 657–667.

Parihar, A., Khan, R., Kumar, A., Kaushik, A. K., & Gohel, H. (2022). Absorption, distribution, metabolism, excretion and toxicity assessment of drugs using computational tools. In P. Sucharitha, K. R. Reddy, S. V. Satyanarayana, & T. Garg (Eds.), Computational approaches for novel therapeutic and diagnostic designing to mitigate SARS-CoV-2 infection (Chap. 5, pp. 335–355). Academic Press

Pereira, M. D., da Silva, T., Aguiar, A. C. C., Oliva, G., Guido, R. V., Yokoyama-Yasunaka, J. K., & Lopes, L. M. (2017). Chemical composition, antiprotozoal and cytotoxic activities of indole alkaloids and benzofuran neolignan of Aristolochia cordigera. *Planta medica*, 83(11), 912-920.

Pratihar, S. (2016). Triggering the approach of an arene or heteroarene towards an aldehyde via Lewis acid–aldehyde communication. *Organic & Biomolecular Chemistry*, 14(10), 2854–2865.

Preciado, D., Cardona-Galeano, W., Herrera-Ramírez, A., & Yepes, A. F. (2024). A potent therapeutic scaffold fusing quinazolinone/melatonin for future colorectal cancer interventions: Design, one-pot synthesis, biological and ADME-tox modeling studies. *Medicinal Chemistry Research*, 33(9), 1698–1713.

Rajput, A., Sharma, R., & Bharti, R. (2022). Pharmacological activities and toxicities of alkaloids on human health. Materials Today: Proceedings, 48, 1407–1415.

Ramachary, D. B., & Jain, S. (2011). Sequential one-pot combination of multi-component and multi-catalysis cascade reactions: An emerging technology in organic synthesis. *Organic & Biomolecular Chemistry*, 9, 1277–1300

Raval, K., & Ganatra, T. (2022). Basics, types and applications of molecular docking: A review. *IP International Journal of Comprehensive and Advanced Pharmacology*, *7*(1), 12-16.

Regassa, H., Sourirajan, A., Kumar, V., Pandey, S., Kumar, D., & Dev, K. (2022). A review of medicinal plants of the himalayas with anti-proliferative activity for the treatment of various cancers. *Cancers*, 14(16), 3898.

Richter, M. F., & Hergenrother, P. J. (2019). The challenge of converting Gram-positive-only compounds into broad-spectrum antibiotics. *Annals of the New York Academy of Sciences*, *1435*(1), 18-38.

Reichardt, C., & Welton, T. (2011). Solvents and solvent effects in organic chemistry (4th ed.). Wiley-VCH.

Roggero, C. M., Giulietti, J. M., & Mulcahy, S. P. (2014). Efficient synthesis of eudistomin U and evaluation of its cytotoxicity. *Bioorganic & medicinal chemistry letters*, 24(15), 3549-3551.

Saruengkhanphasit, R., Chanthasit, P., Hongsing, P., Wattanathorn, J., & Sritularak, B. (2025). Design, synthesis, *in silico* and *in vitro* evaluation of pyrrole–indole hybrids as dual tubulin and aromatase inhibitors with potent anticancer activities. *RSC Advances*, 15(22), 12345–12360

Sauleau, P., Martin, M.-T., Dau, M.-E. T., Youssef, D. T., & Bourguet-Kondracki, M.-L. (2006). Hyrtiazepine, an azepino-indole-type alkaloid from the red sea marine sponge *hyrtios erectus*. *Journal of Natural Products*, *69*(12), 1676–1679.

Salmoun, M., Devijver, C., Daloze, D., Braekman, J. C., & van Soest, R. W. (2002). 5-Hydroxytryptamine-derived alkaloids from two marine sponges of the genus Hyrtios. *Journal of natural products*, 65(8), 1173-1176.

Sharifi-Rad, J., Ozleyen, A., Tumer, T. B., Adetunji, C. O., El Omari, N., Balahbib, A., Taheri, Y., Bouyahya, A., Martorell, M., Martins, N., & Cho, W. C. (2019). Natural products and synthetic analogs as a source of antitumor drugs. *Biomolecules*, 9(11), Article 679.

Singu, B., & Verbeeck, R. K. (2021). Should codeine still be considered a WHO essential medicine?. *Journal of Pharmacy & Pharmaceutical Sciences*, *24*, 329-335.

Soni, J. P., Yeole, Y., & Shankaraiah, N. (2021). β-Carboline-based molecular hybrids as anticancer agents: A brief sketch. *RSC Medicinal Chemistry*, *12*(5), 730-750.

Soni, J. P., Nikitha Reddy, G., Rahman, Z., Sharma, A., Spandana, A., Phanindranath, R., Dandekar, M. P., Nagesh, N., & Shankaraiah, N. (2023). Synthesis and cytotoxicity evaluation of DNA-interactive β-carboline indolyl-3-glyoxamide derivatives: Topo-II inhibition and in silico modelling studies. *Bioorganic Chemistry*, 131, 106313.

Soni, J. P., Devi, P., Chemitikanti, S., Sharma, A., Swamy, C. V. D., Phanindranath, R. & Shankaraiah, N. (2023). Design, synthesis and in vitro cytotoxic evaluation of β-carboline tethered quinoline-4-carboxamide conjugates as DNA-interactive Topo II inhibitors. *Journal of Molecular Structure*, *1291*, 136001.

Stoeckigt, J., Antonchick, A. P., Wu, F., & Waldmann, H. (2011). Cheminform abstract: The Pictet-Spengler reaction in nature and in Organic Chemistry. *ChemInform*, 42(51).

Sun, D., Gao, W., Hu, H., & Zhou, S. (2022). Why 90% of clinical drug development fails and how to improve it?. *Acta Pharmaceutica Sinica B*, 12(7), 3049-3062.

Sung, H., Ferlay, J., Siegel, R. L., Laversanne, M., Soerjomataram, I., Jemal, A., & Bray, F. (2021). Global cancer statistics 2020: GLOBOCAN estimates of incidence and mortality worldwide for 36 cancers in 185 countries. CA: A Cancer Journal for Clinicians, 71(3), 209–249.

Szabó, T., Dancsó, A., Volk, B., & Milen, M. (2021). First total synthesis of β-carboline alkaloid trigonostemine G and its derivatives. *Natural product research*, *35*(1), 72-79.

Szabó, T., Volk, B., & Milen, M. (2021). Recent advances in the synthesis of β-carboline alkaloids. *Molecules*, 26(3), 663.

Takshak, S., & Agrawal, S. B. (2019). Defence potential of secondary metabolites in medicinal plants under UV-B stress. *Journal of Photochemistry and Photobiology B: Biology*, *193*, 51-88.

Taviano, M. F., Filocamo, A., Ragusa, S., Cacciola, F., Dugo, P., Mondello, L., & Miceli, N. (2018). Phenolic profile, antioxidant, and cytotoxic properties of polar extracts from leaves and flowers of Isatis tinctoria L. (Brassicaceae) growing in Sicily. *Plant Biosystems-An International Journal Dealing with all Aspects of Plant Biology*, *152*(4), 795-803.

Tietze, L. F. (1996). Domino reactions in organic synthesis. *Chemical Reviews*, 96(1), 115–136

Tokala, R., Sana, S., Lakshmi, U. J., Sankarana, P., Sigalapalli, D. K., Gadewal, N., Kode, J., & Shankaraiah, N. (2020). Design and synthesis of thiadiazolo-carboxamide bridged β-carboline-indole hybrids: DNA intercalative topo-iiα inhibition with promising antiproliferative activity. *Bioorganic Chemistry*, *105*, 104357.

Tshikhudo, P. P., Mabhaudhi, T., Koorbanally, N. A., Mudau, F. N., Avendaño Caceres, E. O., Popa, D., Calina, D., & Sharifi-Rad, J. (2024). Anticancer potential of β-carboline alkaloids: An updated mechanistic overview. *Chemistry & Biodiversity*, 21(2), e202301263.

Serdyuk, V., & Kolodina, A. (2018). Eudistomin u, Isoeudistomin u, and related indole compounds: Synthesis and biological activity. *Heterocycles*, 96(7), 1171.

Veeresham, C. (2012). Natural products derived from plants as a source of drugs. *Journal of Advanced Pharmaceutical Technology and Research*, *3*(4), 200-201.

Vericel Corporation. (2024). FDA approval of NexoBrid for eschar removal in burn patients.

Wang, T., Jones, D. P., Whittal, R. M., Rachid, M., & Shonhai, A. (2016). Inhibition of *Plasmodium falciparum* Hsp90 contributes to the antimalarial activities of aminoalcohol-carbazoles. *Journal of Medicinal Chemistry*, 59(13), 6348–6362.

Wang, Y., Wang, P., Kong, F.-D., Wang, J., Zuo, W.-J., Wang, H., Dai, H.-F., & Mei, W.-L. (2017). Two new alkaloids from the twigs of *trigonostemon filipes*. *Journal of Asian Natural Products Research*, *20*(3), 270–276.

Wang, X.-Z., Wu, F.-H., Qu, W., & Liang, J.-Y. (2013). A new β-carboline alkaloid from the seeds of *Griffonia simplicifolia*. *Chinese Journal of Natural Medicines*, *11*(4), 401–405.

World Health Organization. (2023). World malaria report 2023. Geneva: *World Health Organization.*

World Health Organization. (2014). Severe malaria. *Tropical Medicine & International Health*, 19(Suppl. 1), 7–131

Xiao, H., Pan, H., Liao, K., Yang, M., & Huang, C. (2017). Snake venom PLA2, a promising target for broad-spectrum antivenom drug development. *BioMed research international*, *2017*, 6592820–6592810.

Yu, X., Liu, Y., Xie, X., Zheng, X. D., & Li, S. M. (2012). Biochemical characterization of indole prenyltransferases: Filling the last gap of prenylation positions by a 5-dimethylallyltryptophan synthase from Aspergillus clavatus. *Journal of Biological Chemistry*, 287, 1371–1380

Zhang, P. Y., Wan, S. B., Ren, S. M., & Jiang, T. (2010). First total synthesis of marine alkaloid hyrtiosulawesine. *Chinese Chemical Letters*, *21*(11), 1307–1309.

Zhang, P., Sun, X., Xu, B., Bijian, K., Wan, S., Li, G., Alaoui-Jamali, M., & Jiang, T. (2011). Total synthesis and bioactivity of the marine alkaloid pityriacitrin and some of its derivatives. *European Journal of Medicinal Chemistry*, *46*(12), 6089–6097.

Zhao, C., Tao, M., Xu, L., Fan, N., Shu, Y., Xiao, Z., & Wang, Z. (2023). Silica-based nanodelivery systems loaded with matrine for the brown planthopper green control and rice growth promotion. *ACS Sustainable Chemistry & Engineering*, 11(49), 17299–17309.

Zhao, Y**.**, Shi, K., Wang, L., Liang, X., Chen, D., & Liu, J. (2025). Integrating machine learning, docking analysis, molecular dynamics, and experimental validation for accelerated discovery of novel FLT3 inhibitors against acute myeloid leukemia. *Journal of Molecular Modeling*, 31(2), Article 1183.

Zheng, X., & Polli, J. E. (2010, May 27). Identification of inhibitor concentrations to efficiently screen and measure inhibition Ki values against solute carrier transporters. *European Journal of Pharmaceutical Sciences*, 41(1), 43–52.

Zhdankin, V. V. (2013). Hypervalent iodine chemistry: Preparation, structure, and synthetic applications of polyvalent iodine compounds. Wiley.

Zhu, L.-H., Chen, C., Wang, H., Ye, W. C., & Zhou, G. X. (2012). Indole alkaloids from Alocasia macrorrhiza. *Chemical and Pharmaceutical Bulletin*, 60(5), 670–673.

Zong, N., Smith, J. T., Lee, H. R., Khan, M. A., Patel, R. S., Chen, Y., Garcia, M., Thompson, L. K., Huang, W., Li, D., Nguyen, T., Wilson, C. J., Martinez, P., Kim, S. Y., Roberts, J. D., Wang, X., Lopez, G., Clark, M., & Anderson, B. R. (2025). Advanced simulation methods using AI for drug efficacy, safety, and toxicity prediction improve lead optimization and candidate selection. *Mayo Clinic Proceedings*, 100(10), 2200–2212.

APPENDICES

APPENDIX 1

IR Spectrum of Compound 1

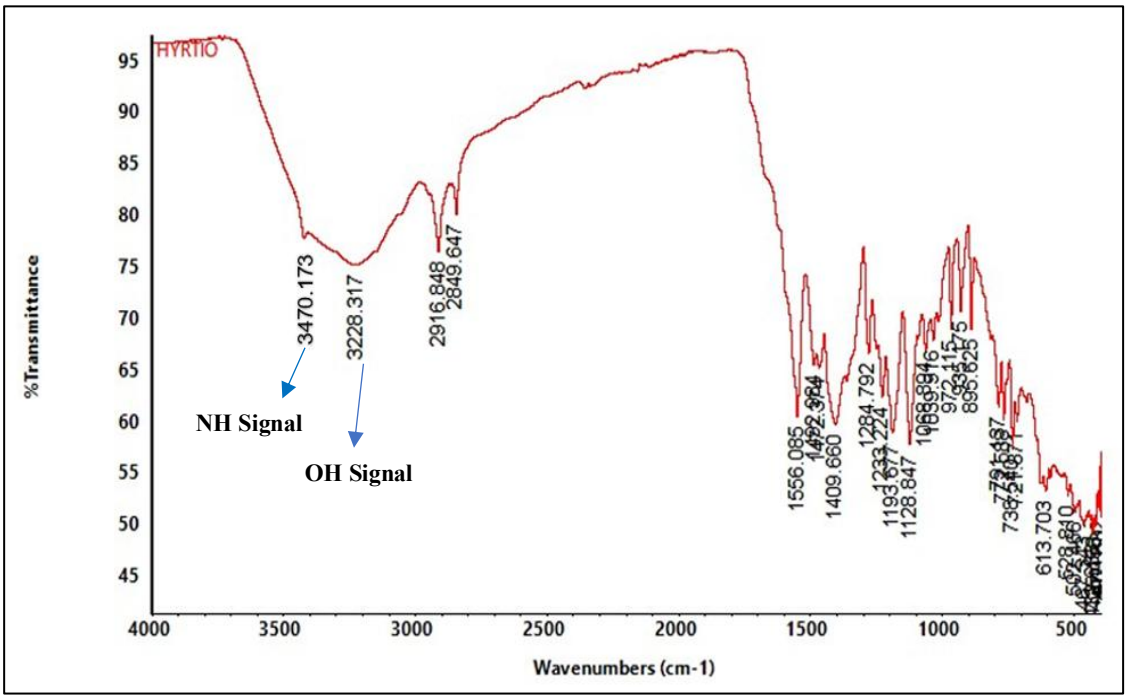

Mass Spectrum of Compound 1

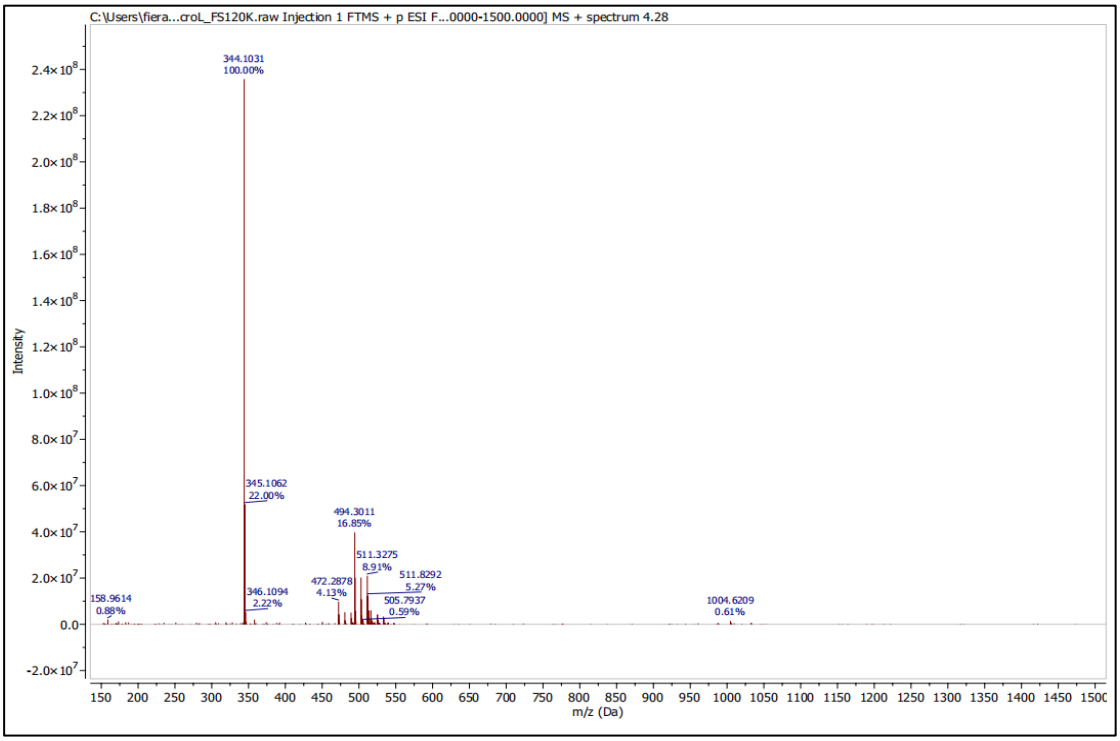

APPENDIX 2

^{1}H NMR Compound 18

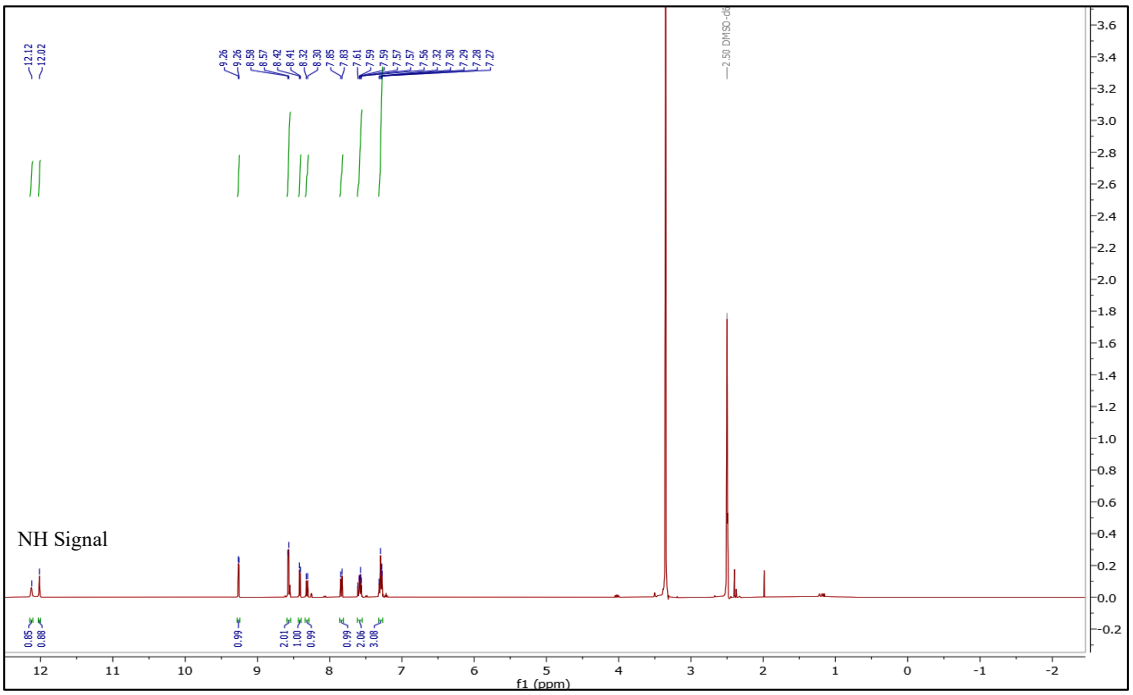

APT-NMR Compound 18

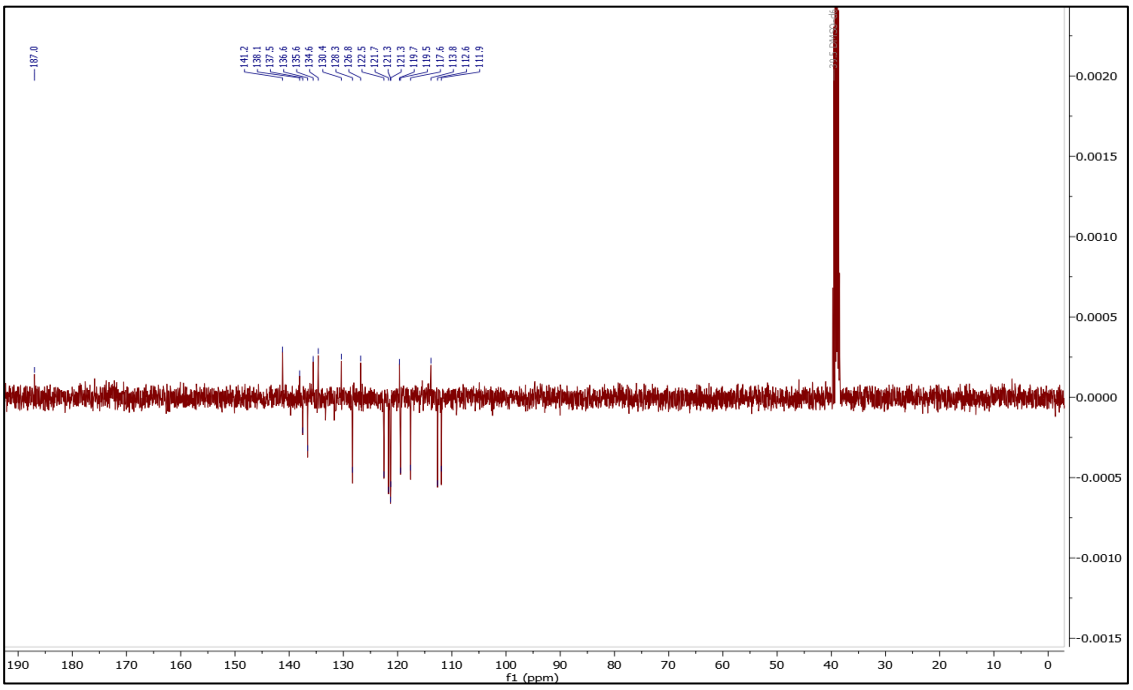

APPENDIX 3

^{1}H NMR Compound 109

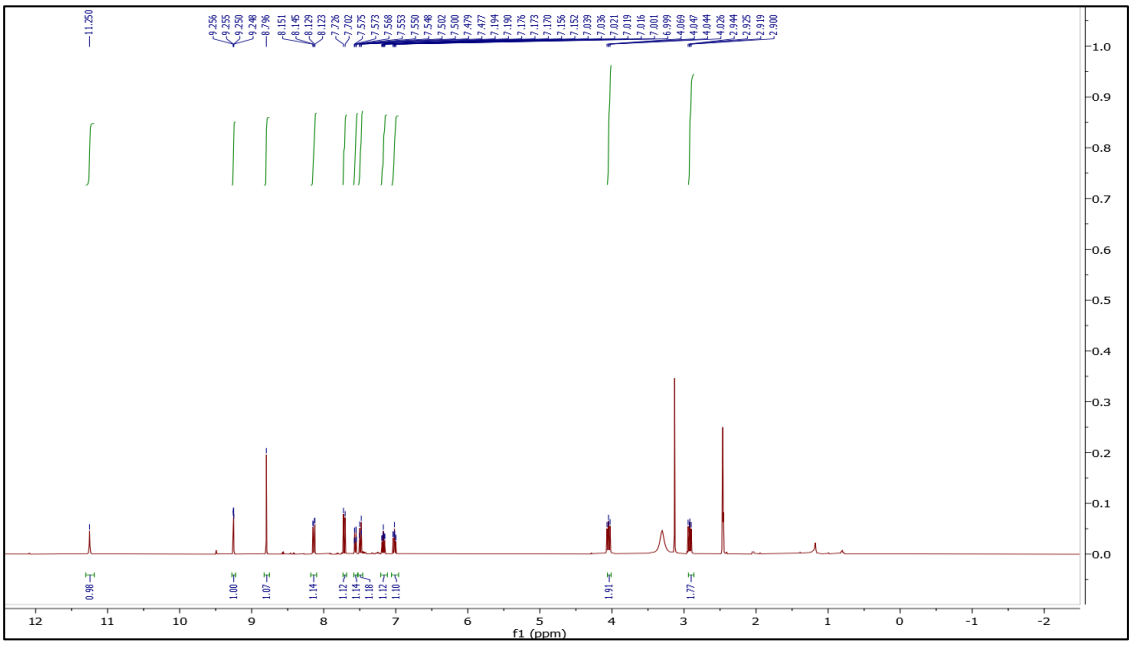

APT-NMR Compound 109

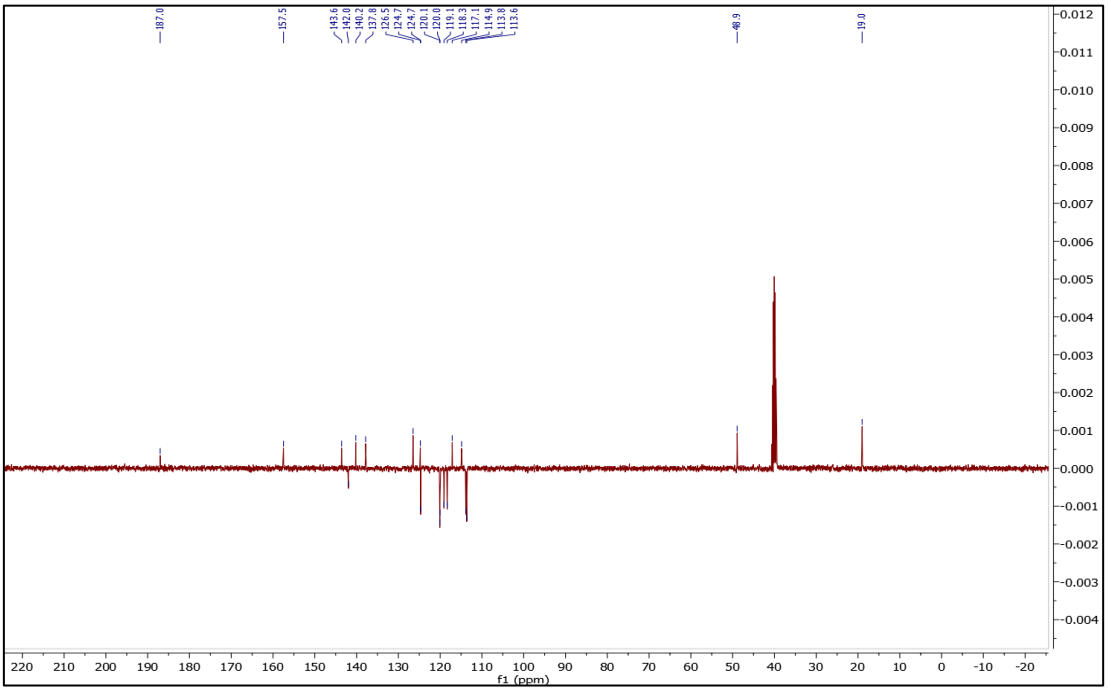

APPENDIX 4

^{1}H NMR Compound 117

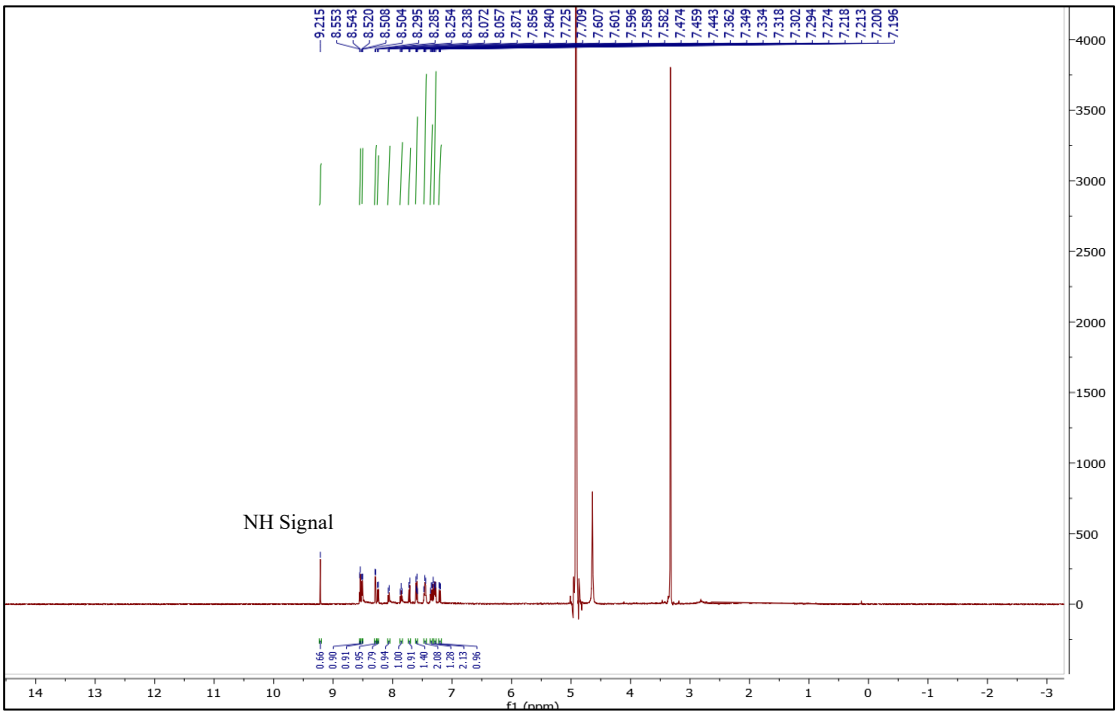

APT-NMR Compound 117

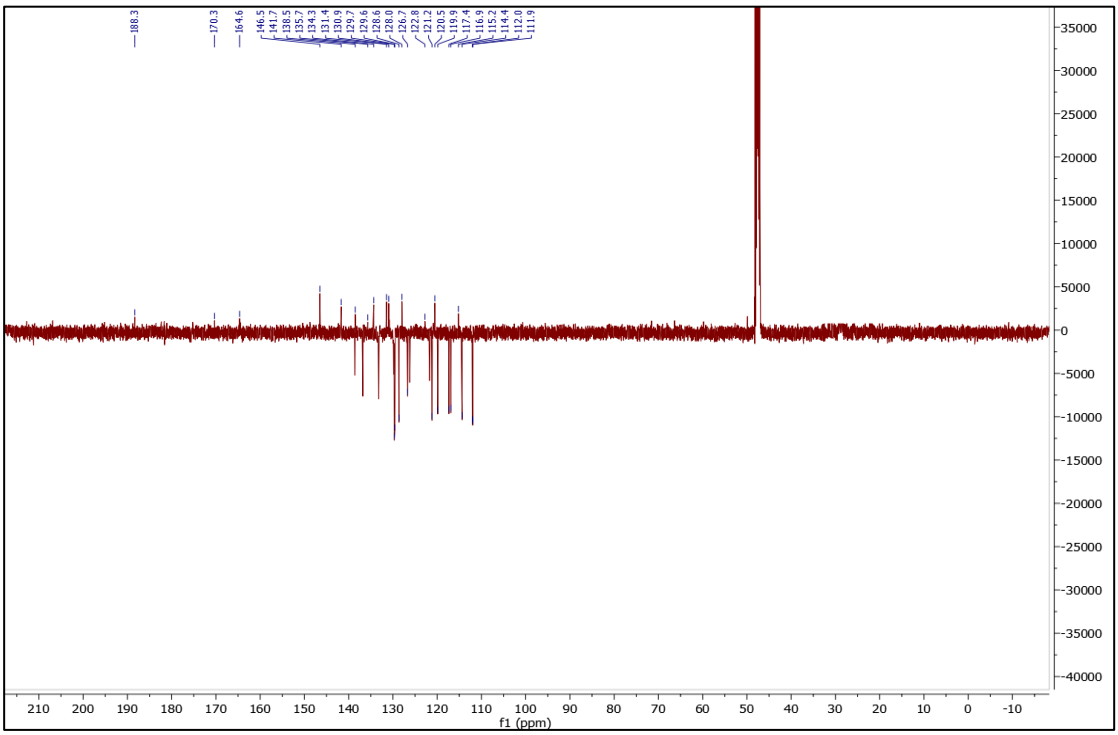

APPENDIX 5

^{1}H NMR Compound 126

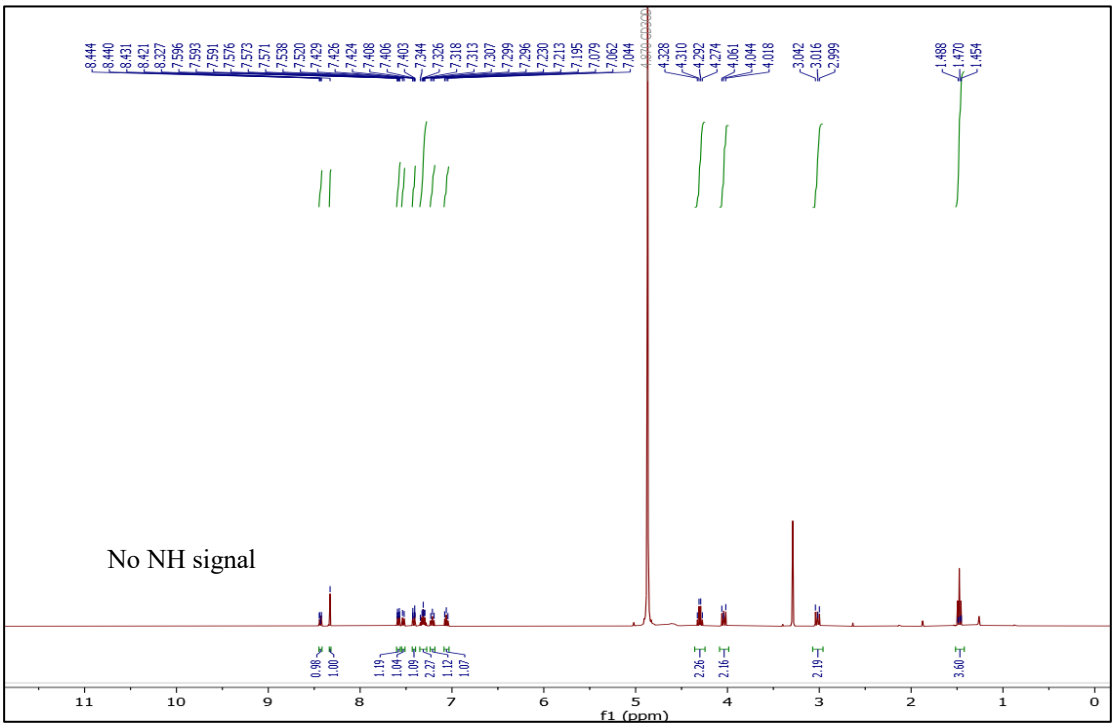

APT-NMR Compound 126

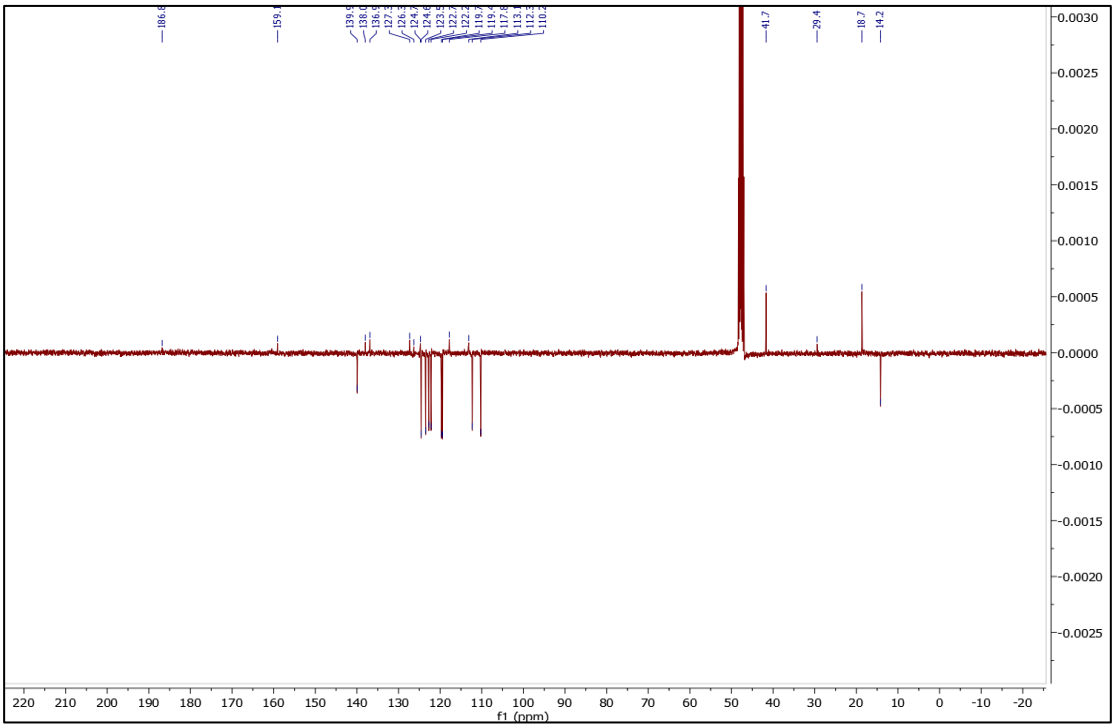

APPENDIX 6

IR Spectrum of Compound 126

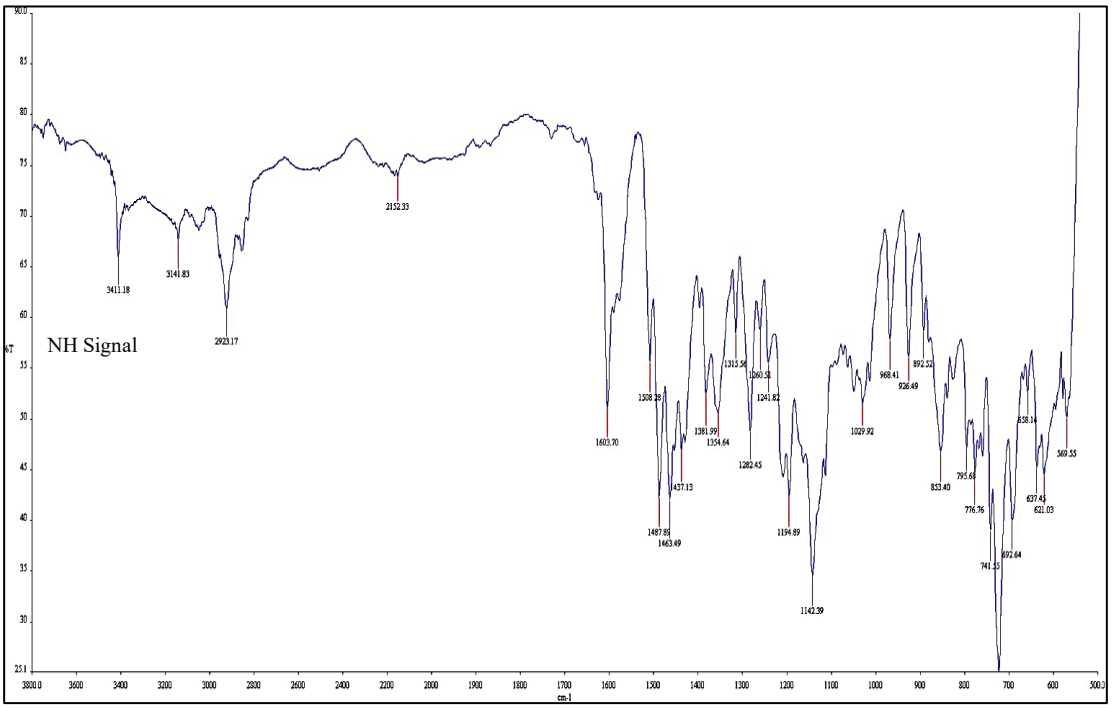

^{1}H NMR Compound 133

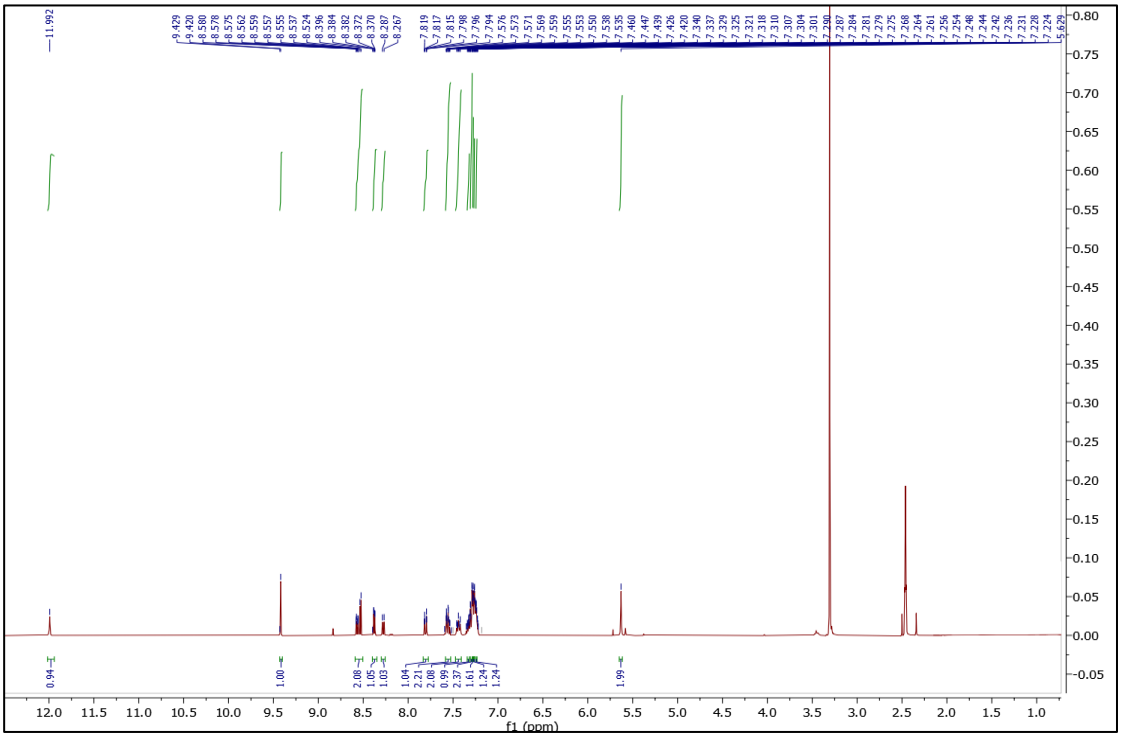

APPENDIX 7

APT NMR Spectrum of Compound 133

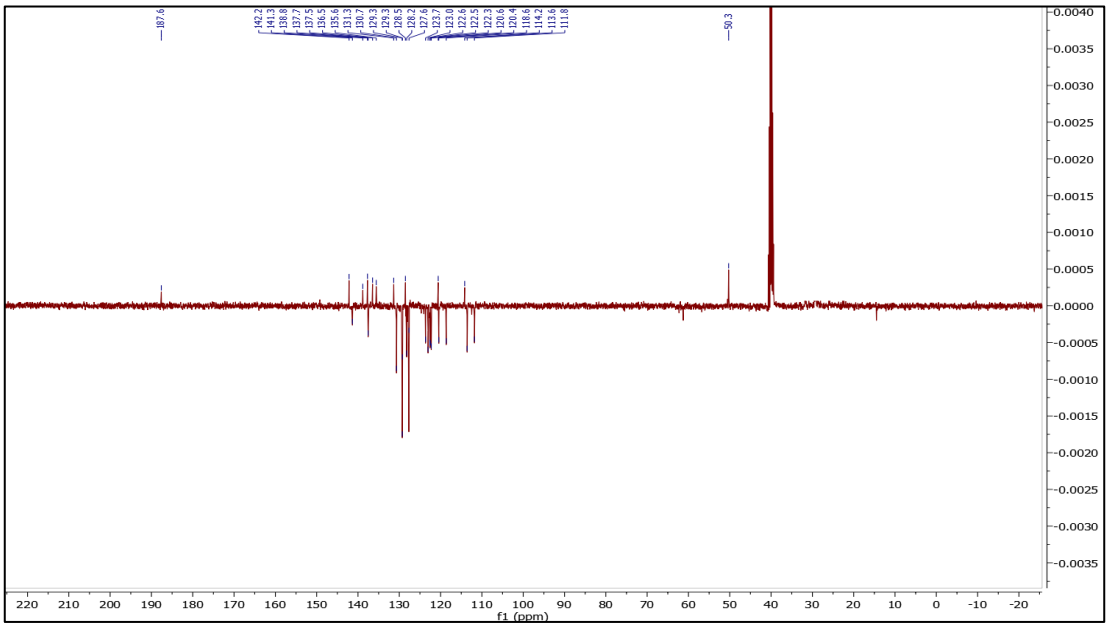

IC_{50} curve of compound (a) 53, (b) 113, and (c) 114

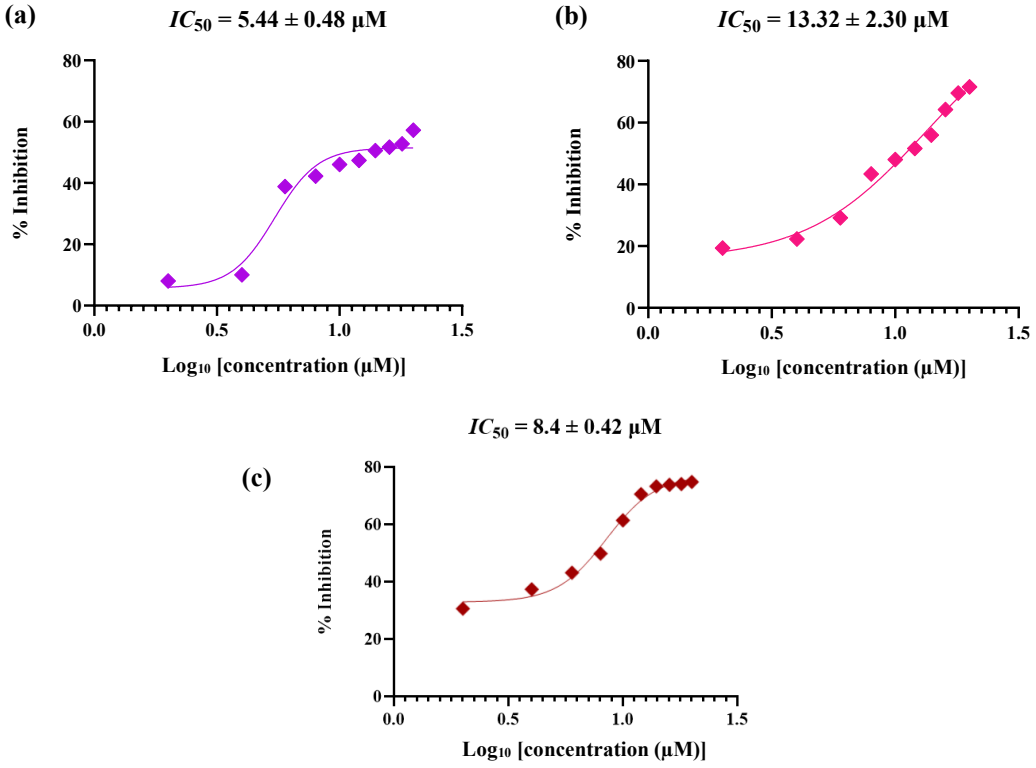

APPENDIX 8

Representative 96-Well Plates Showing the Inhibitory Effects of (A) Compound 53, (B) Compound 113, (C) Compound 114, And (D) Oxamate against *Plasmodium Falciparum* Lactate Dehydrogenase (*Pf*ldh)

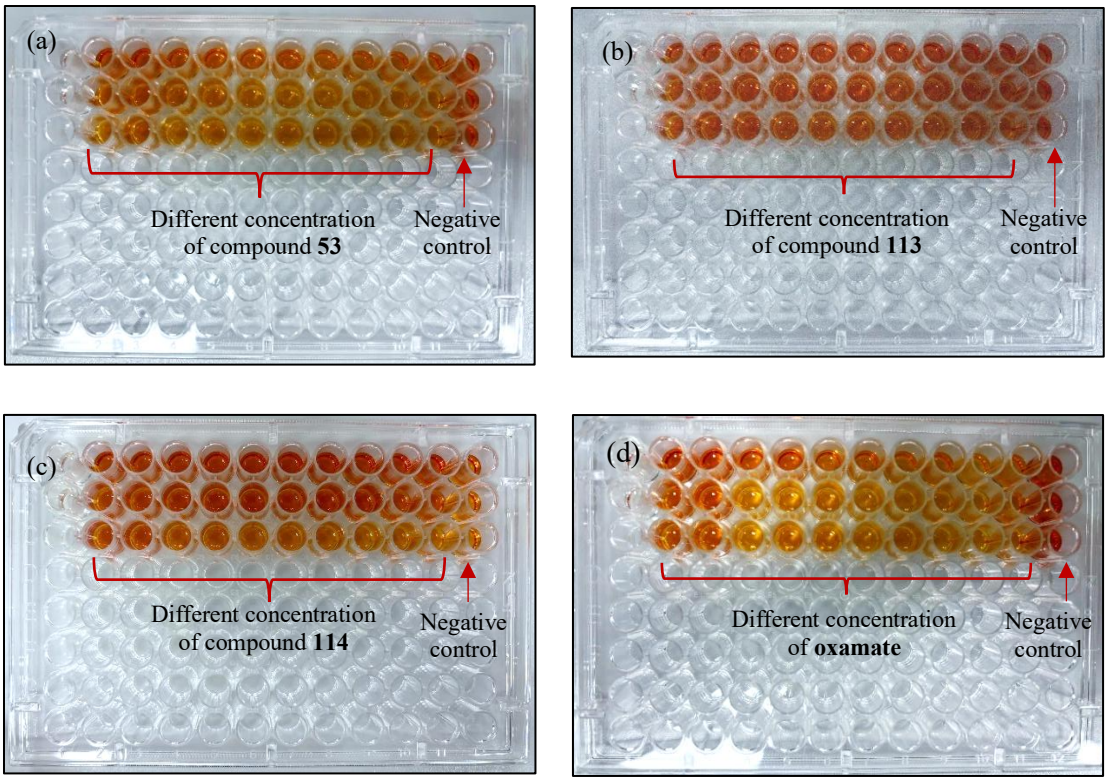

APPENDIX 8

Cytotoxicity IC_{50} Curve of Active Compounds Against (a) Triple Negative Breast Cancer Cell (MDA-MB-231) and (b) Human Colon Adenocarcinoma Cell (HT-29)

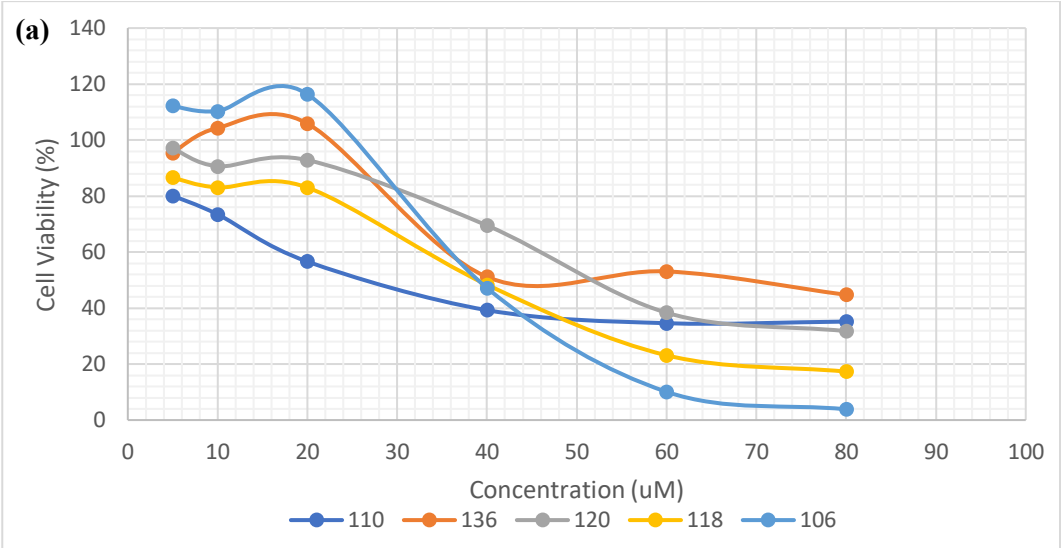

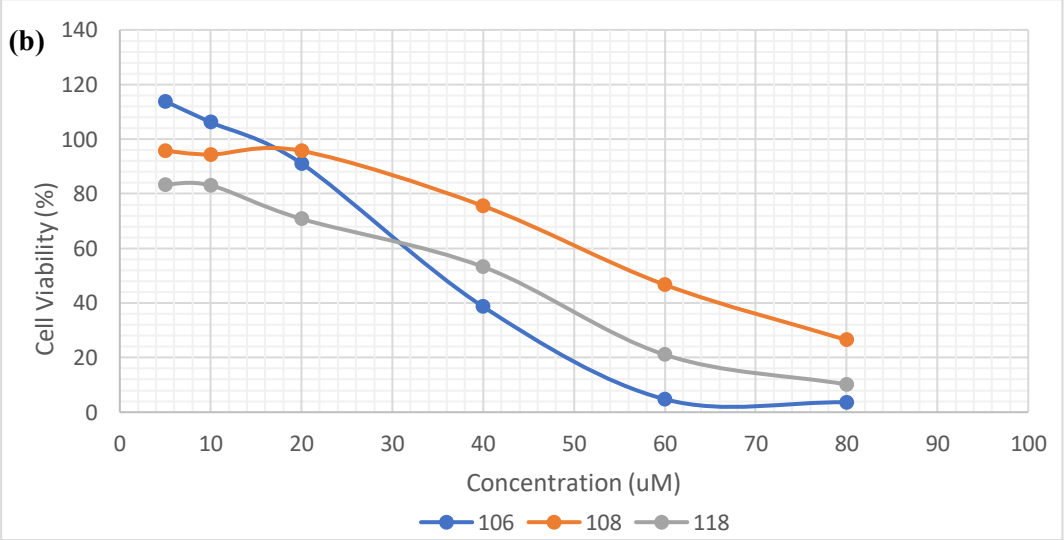

AUTHOR'S PROFILE



Siti Zafirah binti Zulkifli earned her Diploma in Science from the Faculty of Applied Sciences, Universiti Teknologi MARA, achieving a CGPA of 3.87. She received her Bachelor of Science (Hons) in Chemistry (Forensic Analysis) at the Faculty of Applied Sciences, Universiti Teknologi MARA with CGPA of 3.63 (First Class Honours). She later completed her Master of Science in Chemistry (Natural Products) at the same institution. She undertook her practical training as a QC Chemist at Model Tech Sdn. Bhd. (R&D), Melaka. She worked as a QC Chemist (Method Development) at Xepa-Soul Pattinson, a pharmaceutical company based in Melaka. She is skilled in handling and operating various instruments such as UHPLC, MPLC, RHPLC, GCMS, FTIR and NMR. During her PhD, her research focused on organic synthesis, bioactivity evaluation, and computational chemistry, particularly involving the synthesis and assessment of antimalarial and cytotoxic compounds through *in vitro* studies, as well as *in silico* molecular docking and molecular dynamics analysis. She has participated in several international conferences, innovations and published multiple research papers related to her field of study.

PUBLISHED ARTICLE

Zulkifli, S. Z., Pungot, N. H., Saaidin, A. S., Jani, N. A., & Mohammat, M. F. (2024). Synthesis and diverse biological activities of substituted indole β-carbolines: A review. *Natural Product Research*, 38(21), 3793–3806.

Sulaiman, N. F., **Zulkifli, S. Z.**, Saaidin, A. S., Lekkala, R., Hassan, N. I., & Pungot, N. H. (2025). Exploring β-carboline hybrids and their derivatives: A review on synthesis and anticancer efficiency. *European Journal of Medicinal Chemistry*, 288, 117412.

Zulkifli, S. Z., Afendy, A. A. A. B., Saaidin, A. S., & Pungot, N. H. (2025). Study of Friedel-Crafts acylation of 5-substituted indoles to access 3-acylindole derivatives. *Malaysian Journal of Chemistry*, 27(1).

Zulkifli, S. Z., Izzwan, P. H. M., & Pungot, N. H. (2025). A short review on the synthesis of 3,9-disubstituted β-carbolines: Unveiling potent anticancer and antibacterial properties. *Mini-Reviews in Organic Chemistry*.

Zulkifli, S. Z., Asha'ari, N. A. N., Aziz, A. F. A., & Pungot, N. H. (2024). Anti-inflammatory activity of 1-substituted glyoxal β-carboline derivatives. *Malaysian Journal of Fundamental and Applied Sciences*, 20(5), 1228–1234.

Zulkifli, S. Z., Abdul Aziz, A. A., Saaidin, A. S., Hamzah, N. H., & Pungot, N. (2025). Molecular docking and ADME profiles of hyrtiosulawesine derivatives targeting *Pf*LDH: Exploring potential as antimalarial agents. *Asian Journal of Chemistry*, 36, 2475–2484.

Pungot, N. H., Tarmizi, N. H. M., & **Zulkifli, S. Z.** (2023). Synthesis of 4-aryl substituted canthin-6-one with β-carboline skeleton via Pictet–Spengler condensation and cyclization reaction. *Malaysian Journal of Analytical Sciences*, 27(6), 1183–1191.

Pungot, N. H., Rahman, S. W. A. A., Syafawi, N. I., Ariff, P. N. A. M., **Zulkifli, S. Z.** et al. (2025). Recent advances in the synthesis and biological activities of quinolactacin and its derivatives: A comprehensive review. *Current Organic Synthesis*.

Pungot, N. H., Ash'ari, N. A. N., & **Zulkifli, S. Z.** (2025). A short review of Daibucarboline A and its derivatives: Exploring tetrahydro-β-carboline intermediates for anti-inflammatory potential. *Malaysian Journal of Chemistry*, 27(1).